Face Recognition:

Two-Dimensional and

Three-Dimensional Techniques

Thomas David Heseltine BSc. Hons.

The University of York

Department of Computer Science

- For the Qualification of PhD. -

- September 2005 -

ABSTRACT

We explore the field of automated face recognition. Beginning with a survey of existing methods applied to two-dimensional (2D) and three-dimensional (3D) face data, we focus on subspace techniques, investigating the use of image pre-processing applied as a preliminary step in order to reduce error rates. We implement the eigenface and Fisherface methods of face recognition, computing False Acceptance Rates (FAR) and False Rejection Rates (FRR) on a standard test set of images that pose typical difficulties for recognition. Applying a range of image processing techniques we demonstrate that performance is highly dependant on the type of pre-processing used and that Equal Error Rates (EER) of the eigenface and Fisherface methods can be reduced from 25.5% to 20.4% and 20.1% to 17.8% respectively, using our own specialised methods of image processing. However, with error rates still too high for use in many proposed applications we identify the use of 3D face models as a potential solution to the problems associated with lighting conditions and head orientation. Adapting the appearance-based subspace methods previously examined, for application to 3D face surfaces, introducing the necessary orientation normalisation and format conversion procedures, we show that low error rates can be achieved using surface shape alone, despite variations in head orientation and expression. In addition, these techniques are invariant to lighting conditions as no colour or texture information is used in the recognition process.

We introduce a 3D face database providing 3D texture mapped face models, as well as 2D images captured at the same instant. This database facilitates a direct comparison of 3D and 2D techniques, which has not previously been possible. Contrasting the range of face recognition systems we explore methods of combining multiple systems in order to exploit the advantage of several methods in a single unified system. Various methods of system combination are tested, including combination by dimensional accumulation, elimination and genetic selection. This research leads to an innovative multi-subspace face recognition method capable of combining 2D and 3D data, producing state-of-the-art error rates, with a clear advantage over single subspace systems: The lowest EER achieved using 2D, 3D and 2D Projection methods are 9.55%, 10.41% and 7.86% respectively, yet multi-subspace combination reduces this error down to 4.50% on the same test data.

Abstract

Continuing research into the use of 3D face models we develop an additional novel method of recognition, based on the correlation of isoradius contour signal ensembles, which possesses significant advantages over other methods in that orientation normalisation is encapsulated within the recognition process and hence not required as a preliminary alignment procedure. It is also able to simultaneously utilise information from many data modalities, such as colour, texture, shape and temperature, giving great potential as an aid to facial orientation normalisation or as a separate 3D object recognition technique in its own right.

TABLE OF CONTENT

LIST OF FIGURES

LIST OF TABLES

ACKNOWLEDGMENTS

Firstly I would like to thank my PhD supervisor Dr. Nick Pears. His guidance and encouragement have been central to the success of our research, while his experience and knowledge have provided a source of inspiration, without which few of our discoveries would have come to fruition.

I would also like to thank Prof. Jim Austin, head of the Advanced Computer Architecture Group, for his faith in my ability and providing the opportunities to apply my work in real applications. I wish him the best of luck with all his future endeavours.

The Advanced Computer Architecture Group and Cybula team have provided me with an interesting, stimulating and above all, friendly environment in which to work. Their support has been invaluable throughout my PhD, making my time in York both enjoyable and memorable. Their capabilities are second to none and they deserve great success in everything they take on.

I extend my appreciation to my parents, for their advice, understanding and patience during my studies. Without their support I would not have been able to achieve any of the goals I set out to complete.

Finally, I would like to thank the University of York Jiu Jitsu club, for providing the necessary relief outside of the academic world. My experience of university life would not have been the same, were it not for the dedication of the club and its instructors.

AUTHOR'S DECLARATION

Many of the findings resulting from the investigations described throughout this thesis have previously been presented at academic conferences and documented in the accompanying proceedings. As a result, various sections of this thesis share substantial content with our previously published work. Specifically, the following papers feature much of the work described here:

- Evaluation of image pre-processing techniques for eigenface-based face recognition [**14**]
- Face Recognition: A Comparison of Appearance-based Approaches[**15**]
- Three-Dimensional Face Recognition: An Eigensurface Approach [**16**]
- Combining multiple face recognition systems using Fisher's linear discriminant [**35**]
- Three-Dimensional Face Recognition: A Fishersurface Approach [**17**]
- Three-Dimensional Face Recognition Using Surface Space Combinations [**21**]

In addition, some content is also shared with one of our research papers currently under review, entitled 'Three-Dimensional Face Recognition Using Combinations of Multi-Feature Surface Subspace Components,' submitted to Image and Vision Computing 2005. Finally, extracts have been taken from our Literature Review, Qualifying Dissertation and Thesis Proposal documents previously submitted to the University of York Computer Science Department at intervals during our research project. All work included is our own.

1 Introduction

In the early years of the 21st century, we find ourselves continually moving further away from the necessity of physical human interaction playing a major part of menial everyday tasks. Striding ever closer to an automated society, we interact more frequently with mechanical agents, anonymous users and the electronic information sources of the World Wide Web, than with our human counterparts. It is therefore perhaps ironic that identity has become such an important issue in the 21st century. It would seem that in an age where fraud is costing the public billions of pounds every year and even the most powerful nations are powerless against a few extremists with a flight ticket, it is not who we are that is important, but rather, that we are who we claim to be. For these reasons, biometric authentication has already begun a rapid growth in a wide range of market sectors and will undoubtedly continue to do so, until biometric scans are as commonplace as swiping a credit card or scrawling a signature.

Face recognition has been described as the Holy Grail of biometric identification systems, due to a number of significant advantages over other methods of identification (as well as the difficulties encountered in the quest to obtain a practical working system). However, with the current state of the art, these advantages do not include operating performance in terms of recognition accuracy. When compared with other identification technologies, face recognition cannot compete with the low error rates achieved using iris or fingerprint systems. However, no other biometric technology can match face recognition for its convenience of identification 'at-a-glance' or the advantages offered in being analogous to our own method of identification, used by humans from the moment we first glance upon our parents' faces.

In this thesis we explore research carried out in the field of automated face recognition, identifying the problems encountered and the most promising methods of overcoming these difficulties. Taking this knowledgebase as a starting point, we strive to improve the current start of the art, with the ultimate aim of producing a highly effective face recognition algorithm, for use in such application areas as secure site access, suspect identification and surveillance. It is likely that the techniques developed throughout this thesis will have several potential areas of application other than those already mentioned. These would include such topics as image compression, video encoding,

image and shape reconstruction and image archiving. Although all worthy of study, each additional application area would entail additional tests and evaluation procedures, so in the interest of time we limit ourselves to the two applications of identification and verification.

1.1 Face Recognition as a Biometric

Strictly, the term biometrics describes the quantifiable characteristics used in measuring features of biological organisms. However, recently the term is more commonly used to describe the variation in biological characteristics of humans, used to differentiate between people. Some such measurements are now finding a use in automated security and surveillance systems, which use biometrics to verify an individual's identity against some claimed persona at a secure site access terminal or searching a database of known subjects to identify an individual from some previously captured biometric data. Interest in biometrics has grown as the technology has become more readily available and error rates have decreased.

Throughout this thesis we refer to a system's ability to recognise a given subject. We define recognition, in the context of biometric systems, as the capability to perform verification and identification. Verification is the process of comparing one biometric pattern with another biometric pattern, resulting in either a rejection or acceptance decision. Whereas identification is the process of comparing one biometric pattern with a set of two or more biometric patterns in order to determine the most likely match.

Over time, the need for passwords, swipe cards and pin numbers is slowly being replaced by uniquely identifying biometrics. Although public acceptance and the general understanding of the capabilities of this new technology hinder the switch from legacy systems, there are still great incentives to use biometrics:

- *Increased security.* Swipe cards and PIN numbers can easily be obtained by potential intruders, whereas acquiring a subject's biometric requires specialist knowledge and equipment, and in most cases would not be possible without alerting the subject's attention.
- *Reduced fraud.* It becomes extremely difficult for somebody to willingly give up his or her biometric data, so sharing identities (for "buddy punching" in time and attendance systems) is virtually impossible. In

addition, because it becomes necessary to expose one's own biometric data (i.e. your own face), potential fraudsters are reluctant to attempt false verification.

- *Cost reduction.* By replacing plastic swipe cards, all cost associated with producing, distributing and replacing a lost card is completely eliminated.

In addition to the advantages mentioned above, once a biometric identification system is in place, other advantages begin to emerge. For example, there are known cases of large corporations discovering several of their employees were in fact the same person, having managed to obtain numerous identities on the company payroll system: something easily identified when several employees appear to have the same facial biometric. What's more, without the biometric system in place, any intentional misleading could have been difficult to prove, putting the incident down to a clerical error, but the ability to view the same face logged in as multiple people is extremely convincing evidence.

These incentives have lead to several biometric options emerging over the last few years. The most common being fingerprint, face and iris recognition but other examples included the retina, voice, skin texture, ear shape, gait (walking stride), hand geometry, vein pattern, thermal signature and hand-written signature. Each has its own advantages and may be particularly suited towards specific applications. For example, fingerprint scanners are small, light and relatively cheap, allowing for integration into a wide range of mobile devices. The iris pattern is so complex and diverse that a false match is unlikely to occur even between millions of subjects (although there are reports of high enrolment failure rates), whereas the less accurate thermal signature can be taken in the dark from a distance: ideal for covert operation.

Face recognition, although not necessarily suitable for all applications, does have several key advantages over the other biometrics mentioned above, which we now discuss in detail:

Non-intrusive. Whereas most biometrics require some degree of user interaction in order to acquire biometric data, such as looking into an eye scanner or placing a finger on a fingerprint reader, accurate face recognition can be performed by simply glancing at a camera from a distance. This non-contact biometric acquisition is highly desirable

when subjects being scanned are customers, that may have some reluctance due to the big-brother stigma or associated criminality-surrounding acquisition of personal data and therefore the whole process needs to be kept as convenient as possible. This capability can be taken a step further, using strategic camera placement to perform recognition even without the subject's knowledge. An obvious example would be CCTV cameras monitoring an area for known criminals or tracking a suspected terrorist from one location to another.

Public acceptance. It has become apparent that face recognition systems generally receive a higher level of public acceptance than most other biometrics. This is perhaps partly due to the non-intrusive nature of face recognition as described above, but may also be the result of greater understanding and empathy of how the technology is capable of recognising a face; it is well known that the public fear what they do not understand. Another factor is the association that other biometrics have with crime (i.e. fingerprints). Whatever the reason, people have become accustomed to their facial image being required by numerous organisations and few people now object to looking at a camera for the purpose of biometric recognition. It is another thing entirely to require a more committed action on behalf of the subject, such as leaning into an eye scanner or making contact with some other scanning device. With many obvious benefits of integrating biometrics into governmental organisations (such as the NHS, welfare system or national ID cards), public acceptance is an important factor if these systems are to be implemented nationwide.

Existing databases. One key hold-up for any large organisation considering implementation of a biometric system is the amount of time required in collection of a biometric database. Consider a police force using an iris recognition system. It would take a number of years before the database was of sufficient size to be useful in identifying suspects. Whereas large databases of high quality face images are already in place, so the benefits of installing a face recognition system are gained immediately after installation.

Analogy to human perception. Perhaps the greatest advantage, (which is also often the most ignored) is that the biometric data required for face recognition (an image of a face) is recognisable by humans. This allows for an additional level of backup, should the system fail. A human reviewing the same biometric source (the reference image and live query image) can always manually check any identification or verification result.

Whereas any decision made by other biometric recognition systems, such as iris or fingerprint, would require an expert to provide any reliable confirmation. A second product of this duality with the human method of recognition is that the biometric data can be distributed to other organisations (from a police department to the airport authorities for example) and still be useful even if the other organisations do not have a face recognition system in operation.

A complete biometric face recognition system encompasses three main procedures. The preliminary step of face detection (which may include some feature localisation) is often necessary if no manual (human) intervention is to be employed. This involves the extraction of a face image from a larger scene. Many methods have been applied to this problem: template-based techniques, motion detection, skin tone segmentation, principal component analysis, and classification by neural networks to name but a few. All of which present the difficult task of classifying "non-face" images from those areas of a complex scene that do contain a face. This procedure is greatly aided if the conditions under which image acquisition is performed can be controlled. Therefore, it is not surprising that many algorithms currently available are only applicable to specific situations. Assumptions are made regarding the orientation and size of the face in the image, lighting conditions, background and subject co-operation.

The next procedure is that of searching and matching, often termed identification. This stage takes the probe image extracted from the scene during the face detection stage, and compares it with a database of known people (previously enrolled), searching for the closest matching images, thus identifying the most likely matching people. An important point regarding this process is that it does not produce a definitive 'yes' or 'no' decision as to whether any two images are of the same person or not. Instead the process simply indicates which images match the probe image more closely than the others do.

The final procedure is verification. This describes the process by which two face images are compared, producing a 'yes' or 'no' decision as to whether the images are of the same person. The process requires a query image (usually the live captured image) and a single pre-selected gallery image (also referred to as the target image). This pre-selection can take place in a number of ways: a swipe card or pin number indicating the appropriate gallery image; an automated identification procedure as described above, selecting the most likely match from an image set; a manually selected image offered as

a potential match. The two images in question are then compared producing a "same person" or "different people" classification. This decision is often made by application of a threshold to a similarity (or dissimilarity) score, such as that produced in the identification process. By adjusting this threshold value, one can change the balance between the number of false acceptances and false rejections.

1.2 Thesis Rationale

Face recognition has recently become a very active research area, partly because of the increased interest in biometric security systems in general, but also because of recent advances that have taken the state-of-the-art far beyond the initial attempts of using direct image comparison. However, perhaps one of the main driving forces behind the exploration of face recognition technologies is because the human vision system is capable of recognising faces to such a high degree of accuracy, under conditions that put current systems to shame. Not wanting to be beaten by human evolution, the computer vision community has applied a great deal of resources to improving face recognition such that it has now arisen as a separate field in its own right. Obviously, face recognition has strong links to the more general area of pattern recognition and it is from this research field that many face recognition methods were originally derived. Although the restricted variance between different face patterns, well known operating difficulties and target applications has meant that what may have begun as standard pattern recognition methods have been refined to such an extent that they become specialised face recognition techniques in their own right.

Despite significant advances having been made in two-dimensional face recognition technology, it has yet to be put to wide use in commerce or industry. Notwithstanding the range of advantages offered by face recognition, other biometrics are often chosen for applications in which a face recognition system would have seemed ideal. This is primarily because the error rates of current face recognition systems are still too high for many of the applications in mind. These high error rates stem from the consistent problem that face recognition systems are highly sensitive to the environmental circumstances under which face images are acquired. For example, head orientation, partial occlusion, expression and lighting conditions can all adversely affect recognition performance. Using standard 2D intensity images captured using a digital camera, in order to reduce error rates, it is necessary to maintain a consistent facial orientation for

both the query and gallery image. Even small changes in facial orientation can greatly reduce system effectiveness. This situation is worsened by the fact that facial expressions change from one image to another, as can light direction and intensity, increasing the chance of a false rejection or false acceptance (when both the enrolment image and live image are subject to the same extreme conditions).

The Face Recognition Vender Tests [1] and Face Recognition Grand Challenge [2] identify a number of particular areas in which further advancement is required in order to expand the number of successful applications. These include the general need to lower FARs and FRRs, the capability to operate in sunlight and at various non-frontal poses, but also to improve our understanding of the effects of demographic factors, the ability to predict performance on very large gallery sets and why using multiple images from video footage did not improve performance. Our research addresses the first three of these points, improving general FAR/FRR performance of 2D and 3D systems, the use of 3D shape data to improve robustness to lighting conditions and correcting orientation of facial pose.

In an attempt to overcome these problems, biometrics integrators have devised increasingly creative methods of controlling the acquisition environment in the various application scenarios. For example, LCD displays forcing the user to manoeuvre their head into specific positions, carefully placed cameras and artificial lighting are often employed to create consistent capture conditions. However, facial expression has proved to be much harder to control and in order to reduce error rates for such applications as secure site access, it is necessary to specify a required facial expression (usually neutral). Unfortunately, these approaches remove one of the key advantages of facial recognition i.e. no need for subject co-operation, rendering such systems less suitable for surveillance applications. Therefore, any improvement in the ability of face recognition systems to operate under a range of lighting conditions, facial expressions and head orientations will allow for a much wider application of the technology. In particular, automated surveillance of known criminals and terrorists in high-security areas would be of great value, but is not yet feasible using current face recognition methods. Any improvement allowing operation in such applications would also benefit less critical systems, such as time and attendance and site access programs. If error rates could be reduced to match those of other biometrics, then the other advantages of face recognition can be exploited without the cost of reduced overall accuracy.

We suggest that three-dimensional (3D) facial surface data could be used to combat some of the problems mentioned above. Firstly, when dealing with purely geometrical data, rather than the intensity information presented in two-dimensional images, lighting conditions do not effect the biometric data being compared (providing that the 3D facial surface can still be constructed accurately by the 3D capture device). The problem of facial orientation can also be compensated for, as the facial surface can be rotated in 3D space such that the orientation of the query model matches that of the gallery model. Changes in facial expressions, however, are still likely to cause degradation in performance. Although, the additional light-invariant geometrical measurements, together with the colour and texture data, may be sufficiently information rich to allow variability in facial expression, while still maintaining a low error rate.

Compared to the wealth of research carried out into 2D face recognition, there has been relatively little research into 3D facial recognition. There appears to be three main reasons for this:

- *Availability of data.* 2D images of faces are readily available on-line and easily created with use of a standard camera. 3D facial surface data, however, is scarcely available, if at all, and creation of such data can be a complex and expensive process.
- *Range of applications.* 3D recognition limits the possible applications to time and attendance, surveillance (in a highly controlled environment) and security applications, due to the need for specially dedicated equipment. This can be seen as particularly limiting, when compared to 2D methods, which could be applied to searching, indexing and sorting the existing image archives of legacy systems.
- *Human analogy.* Humans are capable of recognising a face in a photograph (a 2D image) to a high degree of accuracy. This has lead to the notion that a 2D image is all that is necessary for a machine to recognise a face.

Methods for comparing and matching 3D surfaces are plentiful [75] [76] [77] [78] (including graph matching approaches [79] [80] [81]: a typical representation for surface structure) and well documented, but few have been applied to the problem of 3D face recognition. It is also possible that existing 2D face recognition methods may be

applicable to the 3D data (particularly the appearance-based approaches), and be able to take advantage of the extra depth information. Therefore, initial development of 3D face recognition systems will be relatively straightforward, allowing comparison between current methods of face recognition, augmented to three dimensions.

Until recently, methods of 3D capture have usually required the use of laser scanning equipment. Such equipment, although highly accurate, may not be safe for human facial capture as the laser may damage the eye. Also, a scan can take significant time to complete, requiring the subject to remain perfectly still during this time, which would be unsuitable for some of the application scenarios in mind. Stereovision systems are able to capture at a faster rate, without the need of a laser. However, such systems require identification of areas of high contrast and distinctive local patterns; something that cheeks and forehead lack. For these reasons 3D facial recognition has remained relatively unexplored. The research that has been carried out in this area has had to rely on a very limited amount of facial surface data [3] [4][5][6][7][8] or made use of a single generic facial surface to enhance two-dimensional approaches by correcting pose or predicting lighting conditions [9] [10][11].

The emergence of new 3D capture equipment, such as the enhanced stereo vision system by Camera Metrix and Vision RT, InSpeck's illumination projection system and the Geometrix FaceVision200 has meant that population of a large database of 3D facial surfaces has now become viable. As the cost of this equipment falls, its use in application areas such as site access and surveillance becomes a distinct possibility.

In summary, the large amount of research that has already gone into two-dimensional face recognition provides a solid, well-documented background from which to begin, with the remaining problems of lighting conditions, facial orientation and expression presenting an initial set of suitably challenging goals, whereas the largely unexplored area of 3D face recognition, held back by lack of suitable 3D-capture technology, provides an area of research with high potential for significant advancement.

1.3 Research Goals

This thesis aims to cover a wide range of face recognition techniques, including the technical background, ideas, concepts and some of the more practical issues involved. The emphasis will be on research into methods of improving existing systems, while introducing new approaches and investigating unexplored areas of research. Although

the focus will tend towards the theoretical, we will prototype the algorithms as verification and identification applications applied to real-world data. We will also touch upon some of the more practical implementation issues that arise when using such systems in the real world, highlighting any additional work or technology that must be realised before a final application is implemented. The ultimate aim will be to produce a fully functional face recognition engine (providing the core verification and identification functions), which is not impaired by some of the shortcomings of existing face recognition systems.

More specifically, we aim to address the following issues:

- Give an overview of existing face recognition systems and the current state of research in this field.
- Identify the problems associated with existing face recognition systems and possible avenues of research that may help to address these issues.
- Improve the effectiveness of existing face recognition algorithms, by introduction of additional processing steps or adaptation of the method.
- Design and implement novel face recognition approaches, taking advantage of the newly emerging 3D-capture technology.
- Analyse and evaluate a range of face recognition systems applied to both two-dimensional and 3D data, in order to identify the advantages and disadvantages offered by the various approaches.
- Determine the most effective method of combining methodologies from the range of face recognition techniques, in order to achieve a more effective face recognition system.
- Evaluate this final face recognition system and present results in a standard format that may be compared with other existing face recognition systems.
- Identify limitations of the final face recognition system and propose a line of further research to combat these limitations.

2 Thesis Structure

The structure of this thesis is directly based around the collection of investigations that took place as part of the larger scale research project working towards 3D face recognition and understanding of how this performs when compared to 2D face recognition. We began with the motivation that significant improvements in face recognition technology could be achieved by exploiting the emerging technology of 3D scanning devices. However, the path to achieving this covered a number of sub-goals that separated nicely into smaller investigations, each uncovering new elements of knowledge that would aid us in our quest for the final system, but also worthy investigations in their own right.

Many of these investigations were presented at academic conferences and published in the accompanying proceedings. Therefore, each chapter of this thesis often shares a substantial amount of content with a corresponding published research paper. Details of these publications are provided for each chapter below. This approach does mean that some duplication occurs across multiple sections of the thesis. However, rather than attempt to dissect and merge sections, which would otherwise form a neat and complete account of the experiment carried out, we have left these chapters whole. The benefit of this approach is that each main chapter can be read as a single unit, together with overviews of the previous work necessary to fully understand the methods discussed. The reader can then refer to previous chapters for a more in-depth discussion, should they require a more thorough explanation.

It should also be noted that a number of earlier investigations are carried out on different data sets, preventing a direct comparison of the results obtained. The reason for this is that much of the research was being completed as data slowly became available throughout the research project (particularly for the 3D face models, which we gathered ourselves over a prolonged period). Rather than delay experimentation until a standard fixed dataset could be established, we commenced with each investigation at the earliest opportunity. It is only for this reason that we were able to progress as far as we have, resulting in the completion of fully functional 3D face recognition system. However, we recognised that the problem of incomparable results must be addressed in order to maximise the value of the research completed. Therefore in section 8 we carry

out a final comparative evaluation of the different systems, when applied to a fixed standard dataset.

Chapter 3 - Literature review

We separate the literature review into three distinctive sections, focussing on Two-Dimensional Face Recognition in section 3.1, 3D Face Recognition in section 3.2 and other related research in sections 3.3 and 3.4.

Chapter 4 - Two-dimensional face recognition

As a preliminary project we implemented three appearance-based face recognition systems: the direct correlation approach described in section 4.2; the eigenface method introduced by Turk and Pentland [48], detailed in section 4.3; and the Fisherface method discussed in section 4.4. We tested the performance on a number of test sets and attempted to reduce error rates using the standard image processing methods described in section 4.5. Our improvements to the eigenface and Fisherface systems were documented and presented at the International Conference on Image and Graphics and the International Conference on Digital Image Computing: Techniques and Applications respectively and published in the conference proceedings [14][15].

In these investigations we were able to show that the pre-processing methods we designed (specifically for difficult capture conditions), were able to improve the capability of standard face recognition systems, from a level at which they would not have been useful in a real world environment, to a point where they could be successfully applied in some commercial applications.

Chapter 5 - Three-dimensional Face Recognition

In this chapter we follow a similar line of research to that applied to two-dimensional approaches in exploring methods of 3D face recognition. However, it was thought that due to the unfamiliar nature, an additional section was required discussing the intricacies of 3D face models. These facial surfaces are discussed in section 5.1, followed by the alignment procedure in section 5.2. We then present work investigating three 3D face recognition methods: a direct correlation method in section 5.4; the application of Principal Component Analysis (PCA), termed the eigensurface method is described in section 5.5; and the LDA extension leading to the Fishersurface method described in section 5.6. Our eigensurface method has been presented at the

International Conference on Image Processing in Singapore in 2004 and later published in the conference proceedings [16]. Likewise, the Fishersurface investigations were documented and published in the Proceedings of the International Conference on Image Analysis and Recognition [17] .

As with the two-dimensional systems, a range of image processing techniques has been applied in an attempt to improve recognition accuracy. These are discussed in detail in section 5.3. Finally, we introduce a fourth novel approach to 3D face recognition in section 5.7, derived from the knowledge and experience gained in production of those methods described in previous sections. We term this technique the Iso-radius method.

The investigations in this chapter have made a significant contribution to the relatively small area of 3D face recognition, showing that PCA based methods in 2D systems can also be applied to 3D face data. Since our initial findings, other researchers have carried out similar investigations [6], drawing similar conclusions. In addition to this adaptation of 2D appearance-based approaches to 3D data, we have also introduced an innovative method using Iso-radius contours.

Chapter 6 - 2D-3D Face Recognition

In this chapter we address an issue that has arisen from the introduction of 3D face recognition systems. Due to the extent and availability of two-dimensional images currently in use within industry, there are significant advantages in being able to process two-dimensional images. In section 6, we discuss an innovation that bridges the gap between two-dimensional and 3D systems, allowing two-dimensional images to be matched against 3D models.

Chapter 7 - Combining Methods of Face Recognition

Here we introduce a novel method of combining multiple face recognition systems. The concept being that the benefits offered by numerous image sub-spaces could be amalgamated into a unified composite subspace system with a reduced error rate. Combinations are computed post-PCA and LDA, avoiding the polynomial space-time complexity in training on multiple image representations.

We begin by applying this combination algorithm to two-dimensional face recognition systems in section 7.1, before applying similar techniques to 3D systems in section 7.2, the results of which have been published in [21]. In section 7.3 we then go on to

discuss improvements over the combination method, by using a genetic algorithm. Finally, we apply this improved algorithm to the combination of two-dimensional and 3D systems, creating a recognition methods based on shape and texture.

In this chapter we were able to demonstrate that this combination method not only improves 2D and 3D face recognition systems, far beyond previous levels of performance, but may also be applied across 2D and 3D data together, producing error rates that are state-of-the-art.

Chapter 8 - Final Comparative Evaluation

As mentioned earlier, one problem that has arisen due to the unavailability of data on which to test face recognition systems, is the continual adjustment of our test sets from one investigation to another. In this chapter we reconcile this issue by carrying out a final evaluation of the best systems from each chapter, compared on a common dataset.

Therefore, this chapter provides a direct comparison of 2D, 3D and multi-subspace systems on a level which has not previously been possible: the various data types were captured in the same instant and therefore all results are a true comparison of performance across systems.

Chapter 9 – Final Conclusions and Future Work

In the final chapter we summarise the discoveries made throughout the research presented in this thesis. We draw conclusions from the results obtained and predict their impact on the research field, before suggesting the most promising avenues of future research.

3 Literature Review

In this section we explore some of the existing face recognition literature relevant to our own investigations. Research in automated methods of face recognition are said to have begun in the 1960s with the pioneering work of Bledsoe [18], although the first fully functional implementation of an automated face recognition system was not produced until Kanade's paper [19] in 1977. Since then, the huge majority of face recognition research has focused on 2D images, with relatively little work exploring the possibilities offered by 3D data. Although, as we near the completion of our thesis this area has become substantially more active, with some papers becoming available showing strong parallels to the work presented here and further reinforcing our own findings.

Many of the methods of 3D facial surface recognition that do exist have been developed along very different lines of research to that of 2D images. For these reasons, we explore 2D and 3D face recognition in two separate sections (3.1, and 3.2), before discussing the problems these systems must overcome in section 3.3, if any significant improvement is to be achieved and what steps have already been taken to combat these limitations. In section 3.4 we then discuss some of the research carried out by Hancock, Burton and Bruce [12] [13] that relate some of these 2D methods to the human visual system.

3.1 2D Approaches

We give a brief overview of 2D face recognition methods, including feature analysis, neural networks, graph matching and Support Vector Machines, as well as some of the more recent Bayesian approaches and Active Appearance Models. For each category we discuss some of the most relevant papers and specific techniques used. However, most focus is applied to the subspace methods because of the relatively simple implementation, which could be adapted to work with either 2D or 3D data. For a more detailed insight into alternative methods of 2D face recognition we refer the reader to Zhao et al. who provide a very comprehensive literature survey in the ACM Computing Surveys [20] with additional elaboration regarding some key issues in face recognition by Zhao and Chellappa in their paper 'Image-based Face Recognition: Issues and Methods'.

Feature analysis techniques involve the localisation of facial features, followed by measurements of these features' characteristics and relative positions. Brunelli and Poggio [30] describe a face recognition system that uses the following 22 geometrical features to distinguish between faces.

- Eyebrow thickness and vertical position.
- Nose vertical position and width.
- Mouth vertical position, width and height.
- Eleven radii describing the chin shape.
- Bigonial breadth (width of the jaw).
- Zygomatic breadth (face width across the cheek-bone)

Figure 3-1 - The 22 geometrical features used by Brunelli and Poggio [30] to distinguish faces.

Horizontal gradient maps are used to detect the left and right boundaries of the face and nose, while vertical gradient maps are more useful for detecting the top of the head, eyes, nose base and mouth. A template matching technique is used to locate the eyes. After which, knowledge of the average face structure (described by Brunelli and Poggio as anthropometric standards) is used to refine the search area for the remaining features. Once all the features have been detected and a 22-dimensional vector created to represent the face, recognition is carried out by means of a nearest neighbour classifier.

Brunelli and Poggio conclude that this method of geometrical feature recognition is effective only when used to distinguish between a small number of people, or as a

preliminary screening step, before further classification is performed by another recognition algorithm. By itself, there does not appear to be enough information within these 22 geometrical features to classify a large number of people.

Localisation and analysis of these multiple facial features bares some similarity to a graph matching approaches, which require the construction of a face image graph representation. Such graphs may encode information based on colour, texture, edge maps or feature location, but does not necessarily attempt localisation of a specific facial feature, instead relying on detection of more generic image features such as edge boundaries, corners and certain texture patterns. The graphs should attempt to collapse any variance between images of the same person, while emphasising differences between different people. Recognition is then performed using standard graph-matching techniques. There are two main difficulties encountered with graph matching approaches. Firstly, deciding how to generate the nodes of the graph. There are a limited number of robustly detected features on the face and too few nodes will cause different graphs to be indistinguishable. Whereas trying to use too many features, some of which may vary in location size and colour, may cause two graphs of the same face to have very different structures. Secondly, if the graph is being constructed from a 2D image of a face, a model may be required to predict the variations in graph structure caused by varying orientations of the face.

Wiskott et al [37] present a face recognition method using 'elastic bunch graphs'. An attempt is made to recognise faces from a large database containing single images of people, despite differences in facial expression and head orientation. These variances are collapsed by extraction of face descriptions in the form of image graphs. The N nodes of an image graph are made up of a set of fiducial points defined on a face. Some of which are easily located (e.g. pupils, corners of mouth, tip of nose etc.), while others are defined as the centre of gravity of these points (e.g. forehead, cheeks, chin etc.). Each of these nodes is labelled with a jet. A jet being defined as a set of 40 complex coefficients describing a small patch of grey values around a single pixel, based on a Gabor wavelet transform. The arcs of image graphs are labelled with two-dimensional distance vectors, describing the relative locations of the pixels described by the jets at the graph nodes.

Wiskott et al represents the general face structure in the form of a face bunch graph. This structure is effectively a collection of image graphs as described above, taken from

a wide variety of face images (the training set). Each node of a face bunch graph is defined as a set of jets (a bunch comprised of the jets from the various image graphs of the training set) and the arcs are labelled with the average distance vectors of the image graphs. The problem of varying head orientation is tackled by providing a different face bunch graph for each possible orientation, with a set of pointers to indicate which nodes correspond to each other. Matching is then performed by creating image graphs for the two face images being compared and applying a similarity function to these two image graphs. Image graphs are generated by adaptation of the face bunch graph to suit the face in the given image. Initially the averages of the jets in each bunch (each node of the face bunch graph) are used to estimate an area of the image that contains a face. The face bunch graph is then translated, scaled and distorted to find the best matching jets between the face image and the face bunch graph. The best jets are selected according to a similarity function which takes into account both the similarity of the jets themselves and the level of distortion (variation in graph arcs) of the face bunch graph. These jets (one jet per graph node) are then taken to represent the face as an image graph. The similarity of two image graphs is simply a measure of the difference between corresponding jets.

Performing 250 identification operations against databases of 250 people evaluates the elastic bunch graph matching technique. The results of which are impressive when comparing two frontal images or two side-profile images. With 98% and 84% achieving rank 1 respectively. However, the system has more difficulty in comparing half profile images or a front profile with a side profile image, scoring 57% and 18% respectively.

Unfortunately, Wiskott et al do not tackle the problem of varying lighting conditions directly. Although jets are fairly robust against changes in the brightness of an image, they could still be affected by changes in lighting direction and colour and as the algorithm relies heavily on comparing these jets, such conditions could cause a significant detrimental effect on the system. However, no results are presented to test the system's performance under varying lighting conditions. From this paper, we can see that texture information alone is sufficient to produce a substantial level of classification.

Neural network approaches use a training set of face images to create a neural network based classifier. In the case of face verification or identification, the neural network is

used to classify a face as belonging to a specific person, whereas for face detection an image must be classified as either a face or non-face.

Lawrence et al [36] describe a neural network approach for identification and verification of facial images. A hybrid neural network system is implemented, comprised of local image sampling, a self-organising map (SOM) and a convolutional neural network. The SOM neural network is used as a means of dimensionality reduction (as well as instilling some invariance to minor changes in the test image), prior to classification by the convolutional neural network, which is partially invariant to translation, rotation, scale, and deformation. The local image sampling procedure is simply a matter of scanning the image with a local window and creating a vector of the pixel intensity values taken from the window. As the window is passed over the image these vectors are built up to create a vector representation of the entire image.

Each node of the SOM is assigned to a reference vector, m_i, from the input space (a vector representation of an example image). The SOM is trained by comparing each vector, x, of an input image in the training set to each of the node reference vectors, m_i. The closest match is selected and the nodes updated according to the following equation.

$$m_i(t+1) = m_i(t) + h_{ci}(t)[x(t) - m_i(t)]$$

Equ. 3-1

Where t is the training iteration and h is a form of smoothing kernel, the neighbourhood function, for which the local neighbourhood region in the SOM is reduced over time t. The result is a topologically ordered set of nodes, in a much lower dimensional space (the optimum being three dimensions in these experiments). Each dimension of the SOM can be thought of as a holistic feature, similar to the eigenfaces of principal component analysis (see section 4.3) and likewise can be represented as an image. Each image in the training set is processed by the SOM, and hence represented as 3 images (feature maps), which are subsequently used to train the convolutional network using a back propagation gradient-descent learning algorithm. The network is formulated with one output for each class in the training set (each output identifies a specific person), preceded by multiple hidden layers of manually connected nodes.

The system is tested using a database of 40 individuals (ten images per person, 5 for training and 5 for testing), which includes images captured from various viewing angles

and lighting conditions. Some impressive error rates are achieved, of just 3.8% (incorrect classifications for the 40 people queried), which compares to an error rate of 10.5% for the eigenface system applied to the same database.

By manually localising a set of facial landmarks on a training set of face images, Cootes et al [72] use PCA to generate a statistical model of shape and texture variation. These active appearance models can then be used to predict face orientation accurately to within five degrees. Once pose angle has been estimated and the best-fit model determined, Cootes et al are then able to use the same appearance model to synthesise predicted appearance at different viewing angles.

Support Vector Machines use a training set of images to compute the Optimal Separating Hyperplane (OSH), minimising the risk of mis-classification between two classes of image in some feature space. Guo et al [22] apply this method to face recognition, using a binary tree classification technique in which a face image is iteratively classified as belonging to one of two classes, propagating up a binary tree structure until the two classes denote individual subjects and a final classification decision can be made. Testing this method on the ORL database of 400 images (40 subjects), they produce an average error rate of 3.0% compared with 5.25% error generated by the standard eigenface method. Jonsson et al [23] investigate a similar approach using client-specific support vectors, attempting to uncover the inherent reasons why SVM methods seem superior to PCA based approaches. The conclusion showed that when an LDA subspace representation is used, an SVM classifier in no more effective than simple Euclidean or normalised correlation metric.

Moghaddam et al use a probabilistic measure of similarity derived from a Bayesian analysis of the differences between face images [24]. Separating training data taken from the FERET database into intra-person and extra-person classes and computing probability functions using the difference of image intensity values in the two sets of data, leads to a similarity score derived from Bayes rule. This method was shown to produce greater match rates in the identification tests of the 1996 FERET competition than the other systems tested (including the eigenface method). Later work by Wechsler [25] creates a face recognition framework that unifies subspace approaches with a Bayesian classifier. The method hopes to minimise noise and enhance generalisation by application of PCA and LDA before a Maximum A Posteriori (MAP) decision rule is applied as the classifier in identification experiments on the FERET database. Again,

the Bayesien classification improves the eigenface and Fisherface methods by 5% to achieve 96% rank 1 recognition accuracy.

3.1.1 Appearance-Based Subspace Methods

In this section we investigate methods of face recognition that use image subspace projection in order to compare face images by calculating image separation in a reduced dimensionality coordinate space. Subspace methods use a training set of face images in order to compute a coordinate space in which face images are compressed to fewer dimensions, whilst maintaining maximum variance across each orthogonal subspace dimension. These methods typically use some form of PCA (Principal Component Analysis, also referred to as the Karhunen-Loeve expansion), as in the eigenface method described here, but also in such techniques as the Fisherface method, which uses Linear Discriminant Analysis (LDA) to produce a subspace projection matrix, the Independent Component Analysis method and Client Specific LDA. These techniques are powerful tools in the field of face recognition and PCA has become a de facto standard to which other systems are compared, as well as often being used as preliminary dimensional reduction in other methods of face recognition. Therefore much of our research will focus in this area.

Yambor [54] has published an in-depth analysis of the techniques applied in PCA and LDA recognition systems, providing useful mathematical examples for simple nine-pixel images and experimentation on the FERET database, which the reader would find useful in furthering an understanding of the underlying mathematical processes involved. Navarrete and Ruiz-Del-Solar [53] extends the comparison of appearance-based approaches to include not only PCA and FLD (Fisher's Linear Discriminant) methods but also an Evolutionary Pursuit method, in which a genetic algorithm is used to compute an optimal subspace. These three methods are tested with a range of distance metrics, including Euclidean, cosine, SOM clusters and a fuzzy feature contrast technique. Testing on the Yale and FERET databases, Navarrete and Ruiz-Del-Solar discover that FLD method has the highest recognition rate when used with the cosine distance metric (weighted such that moments are normalised).

The eigenface based method of face recognition, as proposed by Turk and Pentland uses Principal Component Analysis (PCA) to identify the image space axis with the highest variance in facial characteristics [48][49]. The large dimensionality of image space is

reduced to these principal components, on which recognition is then performed using a simple Euclidean distance measure. Here we give a brief overview of the concept of eigenface based face recognition. For a more in-depth discussion we refer the reader to section 4.1.

Figure 3-2 (left) shows how a 1x2 pixel image can be represented as a vector containing the two intensity values of the respective pixels. These vectors are used to describe coordinates (x and y) of a point within a graph. Hence, each image is mapped to a point within a two-dimensional image space as shown in Figure 3-2 (right). Notice how similar images appear close together within this image space, whereas different images appear far apart.

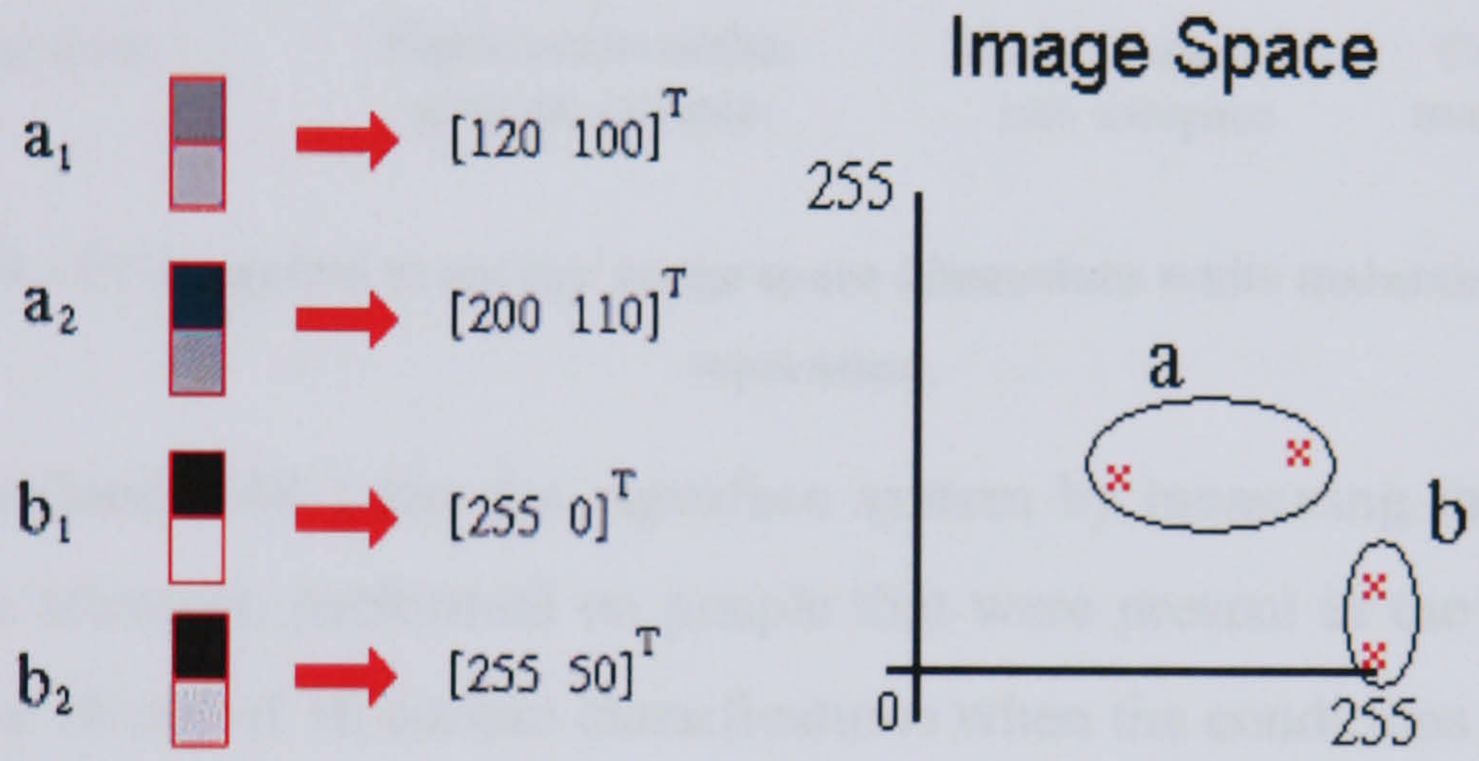

Figure 3-2 - Vector representations of images and there image space locations.

This same principle can be applied to larger images. A greyscale image of resolution 256x256 pixels can be represented by a single vector of length 65,536 (the number of pixels in the image), with each element of this vector containing the intensity value of the corresponding pixel. In the same way that a vector of length two describes a point in a two dimensional graph, the image vector describes a single point in 65,536-dimensional space, in other words one instance from the set of every possible image. Again, similar images map to points close together within this high dimensionality image space, and hence a class of images, such as faces, occupy a small region of the total image space, in which most deviation is along a specific number of dimensions or subspace.

However, the 65,536-dimensional space that represents all (256x256) images is too large to be of practical use. In order to reduce the dimensions of the image space, principal component analysis is used to identify the vectors that best describe this localised subspace (the face space), while maximising the spread of face images

throughout this new reduced dimensionality space. Computing the eigenvectors of the training set images extracts these characteristic elements of faces (the principal components) and ranks them in order of their eigenvalues. The eigenvectors with the highest eigenvalues are said to best describe the characteristics of a face and therefore we choose the top *k* eigenvectors to define face space.

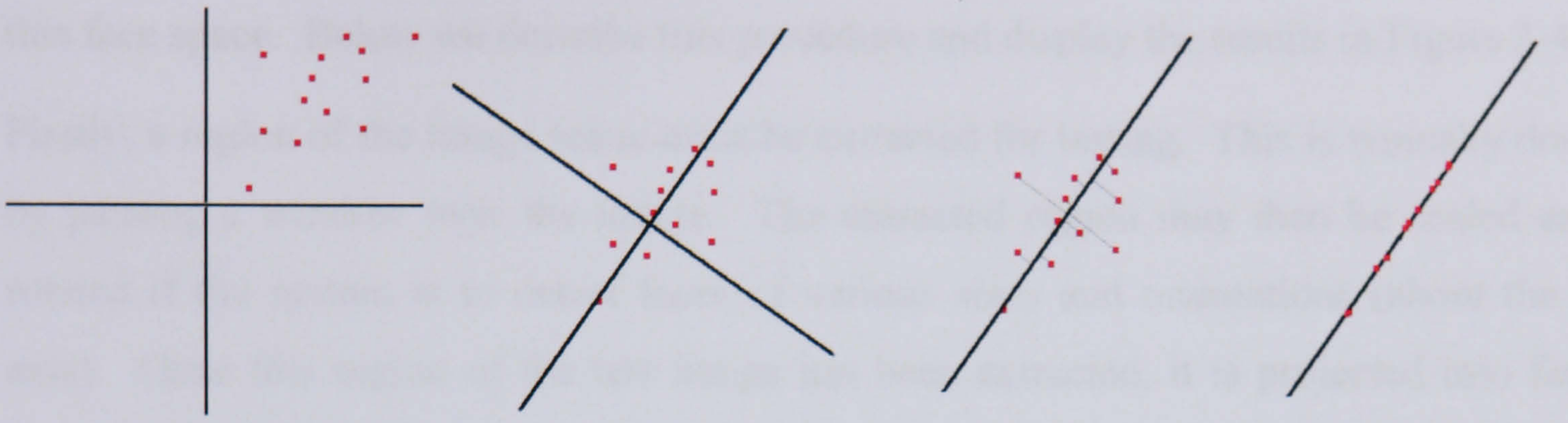

Figure 3-3 – PCA applied to reduce image space dimensions while maintaining high image seperation.

Turk and Pentland [48] test the eigenface system by measuring the accuracy on 16 classification attempts, performed on people that were present in the training set. The system scores 16 out of 16 correct classifications when the conditions are kept constant, but rapidly degrades to 15, 2, 12, 10 and 7 out of 16 when lighting, head size (scale), orientation, orientation and lighting, and size and lighting are varied, respectively.

Bartlett et al [60] propose that much of the discriminatory information required for recognition is contained within the higher order statistics of the face images. As PCA can only take into account second-order relationships between pixels, it is suggested that a generalised PCA algorithm such as Independent Component Analysis (ICA) could produce a more optimal subspace. Tested on the FERET dataset using the cosine distance metric, the ICA method was shown to recognise subjects to a greater level of accuracy than PCA methods, when images were taken on different days.

PCA may also be applied as a method of localising a face and eye positions for image alignment. Providing, the approximate position of the face in the image is known prior to eye localisation, this method can be applied with some success. However, for some applications it may be necessary to extract a facial image from a much larger scene, in which case a more reliable approach is to first detect the entire face, before limiting the search space for the eye locations. In this section we describe a method of face

detection, as introduced by Turk and Pentland [48], which uses an a similar technique to the PCA face recognition approach described above.

As well as each person's face occupying a different region of face space, images of faces generally occupy a local sub region of image space, which we term face space. Therefore, we can determine if an image is a face or not by measuring its distance from this face space. Below we describe this procedure and display the results in Figure 3-4.

Firstly, a region of the image scene must be extracted for testing. This is typically done by passing a window over the image. The extracted region may then be scaled and rotated if the system is to detect faces of various sizes and orientations (about the Z axis). Once this region of the test image has been extracted, it is projected into face space as described in section 4.3, to produce a face key. The face-key is then mapped back to the original image space, to reconstruct a facial image. If this reconstruction is similar to the original image region, it means that the original image has a suitable representation in face space and hence is likely to contain a face.

We therefore determine the likeness of an image region to a face, by calculating the mean squared error between the reconstructed face image and the original image region. This likeness value is assigned to the centre pixel of the region. The result is a face map of the original image scene, with darker areas indicating regions containing faces.

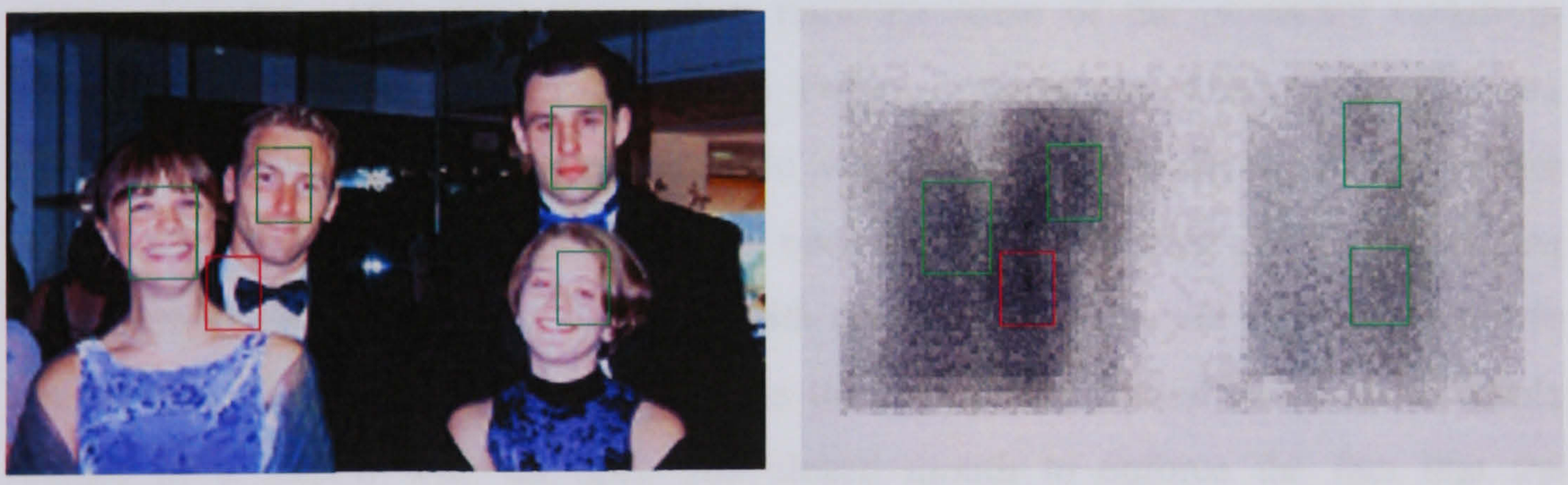

Figure 3-4 - Faces detected (left) by using the eigenface face-map (right).

The likelihood of an image being a face can be determined by examining its position within the image space. That is, its distance from the sub region containing images of faces. If the point in image space represented by an image lies within face space, it is likely to be a face. What's more, face space can be sub divided further into classifications of faces (individual people). The idea being that images of one person's face will occupy one small area of face space, whereas another person's face would occupy an entirely different area. This allows identification to be made by calculating

the distance between image locations in face space with a known person's location in face space.

The Fisherface based method of face recognition as described by Belhumeur et al [27], uses both PCA and LDA to produce a linear projection into a low dimensional subspace, similar to that used in the eigenface method. However, the Fisherface method is able to take advantage of 'within-class' information to maximise class separation. This means that the training set for the Fisherface method can utilise multiple images of each person to determine within-class variation (whereas eigenface typically uses only one image per person), allowing any variation between images of the same person to be minimised in the classification process. This is the Fisherface method's main advantage over the eigenface method. We are able to specify (by providing examples in the training set) how a person's face may change from one image to another, due to variations in lighting conditions facial expression and even small changes in orientation. The idea being, that by providing a set of images of each person taken under various lighting conditions and facial expressions, this method becomes more immune to such changes.

Belhumeur et al [27] point out that the eigenface method maximises the total scatter across all faces within face space, thus retaining some of the unwanted variations (caused by lighting and facial expression). For example, if one of the faces within the training set had an open mouth, this 'feature' would contribute to the scatter of the face images within face space, meaning that an open mouth is identified as a discriminating characteristic between people. Anyone with an open mouth would therefore begin to look similar (within face space). Whereas the Fisherface method could use multiple images of a person with an open and closed mouth to enforce the fact that the appearance of a mouth can change from one image to another, in which case it will have little influence in the classification process.

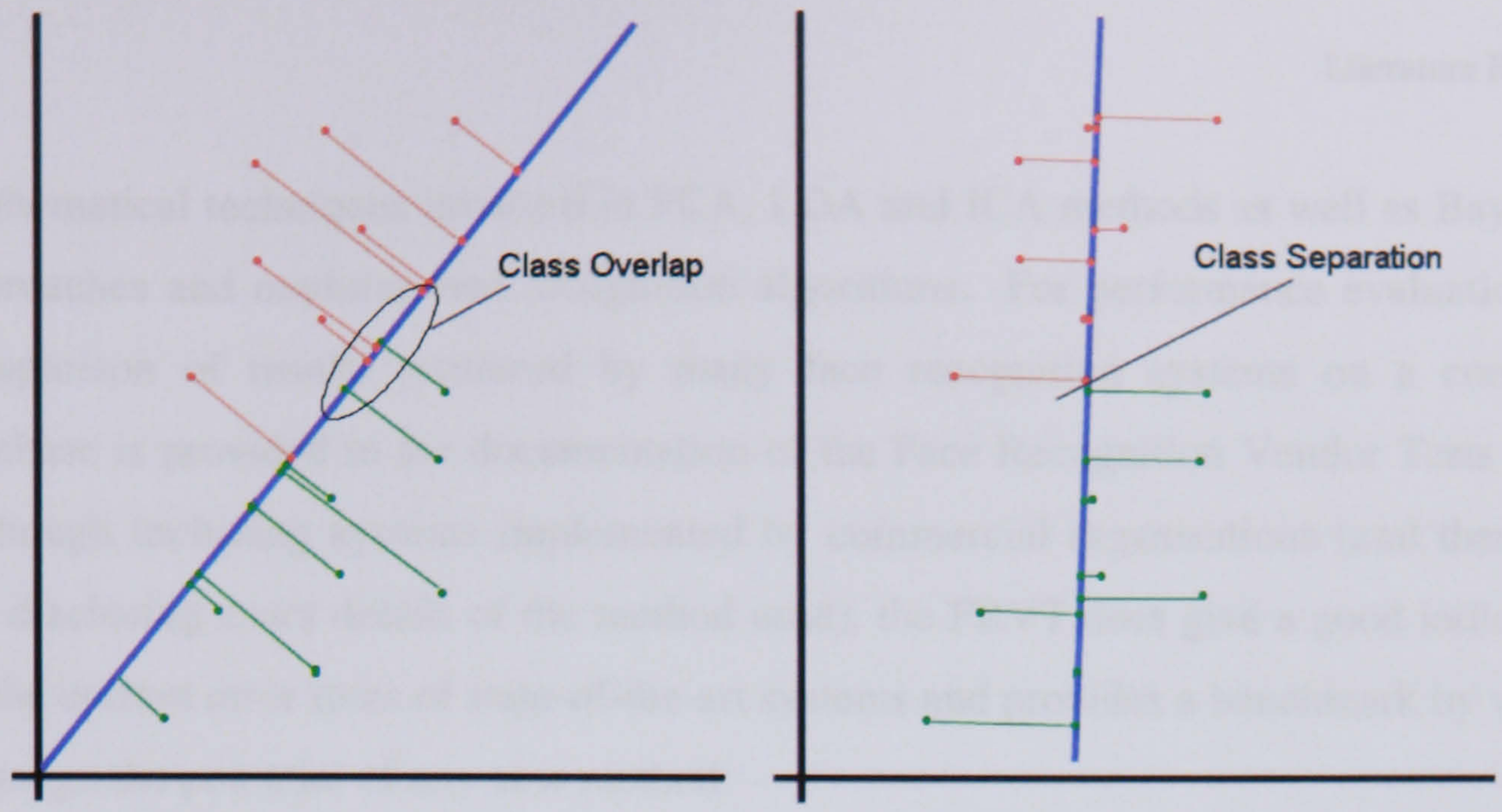

Figure 3-5 - Two examples of dimensionality reduction. On the left the projection causes the two classes to overlap, whereas the projection used on the right maintains the class separation.

In the graphs shown in Figure 3-5, we can see that although some dimensionality reductions may maximise spread, they do not necessarily maximise class separation. In the graph on the left, the two classes can be linearly separated in two dimensional space, whereas once they have been reduced to a single dimension, they become merged. A better projection is shown on the right, where the instances of each class have a clear division, even after dimensionality reduction. The matrix is formulated such that it will project any image of a face into a face space in which the ratio of between-class scatter to within-class scatter is maximised for all classes i.e. different people look very different and images of the same people look very similar.

Martinez and Kak have uncovered an interesting phenomenon [55] regarding the performance of LDA and PCA systems and its dependency on adequate training data. Testing standard PCA and LDA face recognition on the AR face database [39], they were able to show that PCA can outperform LDA, if the training set is particularly small and present intuitive reasons for these results. They suggest that if the training set is not representative of the image space regions occupied by individual subjects, then overall image variance can be a better discriminator than optimising the ratio of between-class and within-class variance. We have witnessed similar results, when the training set for the 2D Fisherface method did not adequately represent the test set.

For more detailed descriptions of the range of subspace approaches the reader would find that Shakhnarovich and Moghaddam [71] provide an excellent overview and comparative study of subspace approaches, with detailed explanations of the

mathematical techniques involved in PCA, LDA and ICA methods as well as Bayesian approaches and modular face recognition algorithms. For performance evaluations, a comparison of results produced by many face recognition systems on a common database is provided in the documentation of the Face Recognition Vendor Tests [1]. Although including systems implemented by commercial organisations (and therefore not disclosing exact details of the method used), the FRVT does give a good indication of the current error rates of state-of-the-art systems and provides a benchmark by which to gauge the potential of any new method.

3.2 3D Approaches

Although limited when compared with the wealth of research applied to 2D face recognition, there are a number of investigations that demonstrate how geometric facial structure can be used to aid recognition. Zhao and Chellappa [9] use a generic 3D face model to normalise facial orientation and lighting direction prior to recognition, increasing accuracy from approximately 81% (correct match within rank of 25) to 100% when applied to the Weizmann database. A generic 3D face model is scaled and aligned to match a 2D target image. If the head is not orientated appropriately (frontal profile), Zhao and Chellappa use the generic 3D face model, together with light source direction and pose estimations, to compensate by producing a prototype image of the frontal pose equivalent. Face recognition is then performed on this prototype image.

Similar improvements are witnessed in the Face Recognition Vendor Test [1], showing that pose correction using Romdhani et al's 3D morphable model technique [10] reduces error rates when applied to the FERET database. This method is analysed and discussed in more detail by Blanz et al [11], using a 3D morphable face model to aid in identification of 2D face images. Beginning with an initial estimate of lighting direction and face shape, Blanz et al iteratively alters shape and texture parameters of the morphable face model, minimising difference to the two-dimensional image. These parameters are then taken as features for identification, resulting in 82.6% correct identifications on a test set of 68 people.

This same technique of generating 3D morphable models from 2D images has been utilised in other experiments, such as Huang et al's component based face recognition approach using 3D morphable models to improve recognition accuracy when pose and illumination are unknown [56]. Taking a Support Vector Machine (SVM) approach developed in previous work [58], in which a face image is decomposed into smaller components interconnected by a flexible geometric model, Huang et al tackle the problem of a large training set requisite by synthesising many 2D training images from 3D face models under varying pose and virtual lighting conditions. The 3D morphable model is initially generated from three 2D images as described in Blanz and Vetter's earlier research [57], before numerous face images are synthesised. These images are then separated into components and used to train a second-degree polynomial SVM

classifier. Recognition accuracy is reported at 90%, compared with a comparable global face recognition method achieving 40%.

Bronstein et al [59] uses photometric stereo techniques to compute facial surface shape from numerous 2D images, acquired under varying lighting conditions. Surface gradient is used by a Fast Marching on Triangulated Domains (FMTD) algorithm to produce a map of geodesic distances across the facial surface without the need to reconstruct an actual 3D face model. Moments of a cononical form of this geodesic map are extracted as a face signature and compared using the Euclidean distance metric. Taking images of seven subjects from the Yale Face Database, Bronstein et al were able to show that within-class and between-class standard deviations were improved by an order of magnitude, compared with the direct comparison of facial surface gradients.

Although these methods show that knowledge of 3D face shape can aid normalisation for two-dimensional face recognition systems, none of the methods mentioned so far use actual geometric structure to perform recognition. However, the research does demonstrate that 3D facial information can be used extremely effectively to eliminate some of the problems encountered with 2D recognition (i.e. pose and illumination), even when only a generic 3D model is used. It is likely that if the actual geometric shape information of a subjects face contributed to the recognition process further improvements could be made.

To test the use of geometric shape data for recognition a preliminary investigation was carried out at the University of York by Turner and Austin [46] exploring the possibilities of using AURA (Advanced Uncertain Reasoning Architecture) [46][47] technology in conjunction with a graph-matching algorithm to perform face recognition. AURA is an architecture based on a pattern-matching concept utilising correlation matrix memories, with the key advantage of an extremely efficient hardware implementation, in the form of the Presence PCI card (or more recently the Presence II card) [62]. These devices are able to search onboard memory extremely quickly for matching patterns. What's more, because these devices are able to operate in parallel, a large database of face models may be distributed between several Presence II cards. The matching algorithm used the Relaxation By Elimination (RBE) graph matching techniques. This algorithm has several properties that make it particularly suitable for face recognition. Firstly, the neural network architecture (Correlation Matrix Memories) of the AURA system means that even noisy or incomplete data (e.g. caused

by wearing glasses, non-frontal head orientation or bright specula reflection) can still result in a successful match. Anomalies are effectively ignored and performance degrades gracefully in the presence of increasing noise and occlusion.

Although limited in terms of test data, the investigation demonstrated that the AURA graph matcher is capable of distinguishing between facial surfaces based on 3D geometry alone. However, the research was not pursued much further, as error rates remained relatively high compared to the more promising avenues of the eigensurface and Fishersurface methods (see sections 5.5 and 5.6). Despite this, because AURA architecture is able to operate independently of the CPU, it could be used to search a database of face models, pruning the most unlikely matches from the search space as an initial screening step. A large database could then be reduced to a small set of possible matches before a more rigorous algorithm is applied. Hence, allowing matching techniques that may not scale well to be applied to large databases. We supply the results of this investigation in Appendix II.

Beumier and Acheroy also make use of 3D surface information, by performing face recognition using a surface matching approach on the 3D facial structure [5][3]. These 3D facial surfaces are generated from a single image taken of a person's face, onto which structured light (stripes) are projected. The 3D structure of the face is computed by measuring the deformation of the stripes across the face. Some orientation normalisation is then required to ensure a consistent fronto-parallel view. This normalisation is performed by generating some initial parameters for the three angles of rotation and three directions of translation (based on nose detection, forehead and cheek angle), before refining the search until the minimum distance is found between the two facial surfaces being compared.

The paper describes various methods of matching the 3D facial surfaces. However, few methods were successful due to the nature of the 3D data obtained (which often contained high levels of noise). Curvature analysis proved ineffective, (again due to the noise present in the 3D surface). Feature extraction also proved difficult, probably due to the lack of detail in the model, resulting in the nose being the only reliably located feature. Despite this, they still managed to produce some good results using two methods of surface matching by means of comparing profiles extracted from the 3D facial surface. The first method extracts 15 profiles, by taking the intersection of the facial surface with evenly spaced vertical planes. These profile curves are compared by

dividing the area between the curves by the arc length, giving a distance measure. Beumier and Acheroy carry out verification tests on a database of 30 people, giving an EER between 9% and 13% when using automatic alignment, but dropping to between 3.25% and 6% if manual alignment is used.

The second method is to take one central profile and two lateral profiles, which are converted into one-dimensional vectors of local curvature values. The left and right lateral profiles are averaged to give a mean lateral profile. Facial surfaces are then compared by calculating the difference between these curvature values of the central and mean lateral profile. This method gives improved EERs of between 7.25% and 9% on the automatically aligned surfaces and between 6.25% and 9.5% on the manually aligned surfaces.

Although the database used is too small to make any firm conclusions, Beumier and Acheroy's research does suggest that:

- There is enough information to achieve a high level of face recognition accuracy in the facial 3D geometrical structure alone.
- A high level of accuracy (low levels of noise, missing data, spikes etc.) and precision (depth resolution) of the 3D data is essential for good performance.
- Few features can be reliably localised based on the geometrical structure alone. Therefore, a system that relies heavily on locating many features and measuring distances between them is likely to produce poor results.
- The performance of the orientation normalisation procedure has a significant influence on the overall system performance.

Another approach is taken by Chua et al [8], using point signature as a non-rigid object representation, on which recognition can then be performed. Chua et al treats the face recognition problem as a 3D recognition problem of non-rigid surfaces. By observing range data of various facial expressions, it is noted that certain areas of the face remain rigid while other areas are able to deform significantly. An attempt is made to extract these rigid areas of the face for recognition, thus creating a system that is invariant to facial expression. It is also hoped that by ignoring large areas of the face that are

unstable, the size of the models used for comparison will be greatly reduced, leading to a decrease in recognition time and space complexity.

The characteristic used to identify these rigid areas of faces and ultimately to distinguish between faces is the point signature, which describes the depth values surrounding the local region of a specific point on the facial surface. The point signature for any point p on a facial surface, is defined as a discrete set of values $d(\theta_i)$ where $0 < \theta_i < 360$ and $\Delta\theta = 10$. Each value $d(\theta_i)$ is the distance from a point at angle θ_i on a 3D curve C (defined as the intersection of a sphere of radius r, centred at point p, with the facial surface) to the corresponding point on the perpendicular projection of the 3D curve C`. The comparison of two point signatures $d_s(\theta_i)$ and $d_m(\theta_i)$ is performed using the following equation.

$$\left|d_s(\theta_i) - d_m(\theta_i)\right| < \varepsilon_{tol}(\theta_i) \forall i = 1,\ldots,n_\theta$$

Equ. 3-2

Where $\varepsilon_{tol}(\theta_i)$ is a set of tolerance values configured to produce the best acceptance and rejection rates. For a more in-depth discussion of point signature generation and comparison, we refer the reader to Chua et al's paper [8]. The first stage of point signature based recognition is the registration of 3D faces: performed by finding 3 points on each of two facial surfaces for which the following constraints hold:

- The point signatures of corresponding points match.
- The distances between the 3 points on one face, and the 3 points on the other face are within an error tolerance (possibly under various scales).

Once the three corresponding points on each face have been found the two facial surfaces can be aligned. Distances between the two facial surfaces are then measured according to a Gaussian distribution model and areas with a low distance measure are extracted as rigid areas. Two facial surfaces are compared by extracting the rigid areas of the face then generating point signatures for all points on the remaining facial surface. This set is reduced to a set of unique point signatures, which are then compared to the corresponding point signatures on the other facial surface.

Chua et al gather results from a set of range images taken from 6 different people. A total of 30 range images are used (four different expressions for each person, plus one probe image). The probe image is identified correctly for all six people. However, the

separation of scores is not particularly large. With the correct scores ranging from 93.75 % to 78.85% and the highest incorrect score being 76.92%.

Coombes et al [32] present a method of mathematically describing facial surface shape, based on differential geometry. Curvature analysis is performed on a depth map of the facial surface, to produce segmentation into one of eight fundamental surface types. Coombes et al stress the need for the depth map of a facial surface to be created from a specific viewpoint, therefore giving the prerequisite of some 3D facial alignment. They also describes several methods of computing the curvature of the facial surface and describe the advantages of a method developed by Coombes and Richards, which takes into account the possible error due to lack of detail when surfaces are at a sharp angle to the viewpoint.

The facial surface can be segmented into the eight surface types, based on the sign of the curvature: peak, ridge, saddle ridge, minimal, pit, valley, saddle valley and flat. Coombes et al suggest that two faces may be distinguished by comparing which regions of the two faces are classified as the various surface types. Prior to two facial surfaces being compared, they must first be registered. This is done by manually selecting several corresponding feature locations on each face, which are then used to scale, translate and rotate, such that two facial surfaces are aligned. Using this method, 3D facial surfaces have been produced for the average female and average male face, showing distinct differences in chin structure, nose shape, forehead shape and cheek bone position. A quantitative analysis of the average male and average female facial surfaces shows that the main differences are of prominence or retrusion in specific areas of the face.

Hesher et al [6] use PCA of depth maps and a Euclidean distance metric to perform identification with 94% accuracy on 37 face models (when training is performed on the gallery set). Our own investigations of a similar method are presented in section 5.5 (also published by Heseltine et al [16]), showing how different surface representations and distance measures affect recognition, reducing the EER from 19.1% to 12.7% when applied to a test set of 290 face models acquired under difficult capture conditions such as variations in head angle and expressions.

Gordon [4] takes a feature based approach, based on both depth and curvature information. It is stated that curvature data is easily derived from the range data, and

has substantial advantages. It has the potential for higher accuracy in describing surface based events and it is better suited to describing properties around facial regions such as the cheeks, forehead and chin. It is also viewpoint invariant. Gordon uses facial feature localisation and absolute measurements (millimetres rather than pixels) to calculate a set of feature descriptors from the 3D data.

The usefulness of a feature for the purpose of classification is dependent on its ability to discriminate between people. To evaluate the set of features, a value is calculated indicating the level of discrimination for each feature, this property is Fishers linear discriminant (FLD), as shown in the equation below.

$$d = \frac{\sum_{i=1}^{c}(m_i - m)^2}{\sum_{i=1}^{c}\frac{1}{n_i}\sum_{x\in\Phi_i}(x - m_i)^2}$$

Equ. 3-3

Where d describes the discriminating power of a feature Φ, between c different classes (people). Φ_i is the set (size n_i) of feature values of class i, and m_i and m are the means of Φ_i and feature values of all classes respectively. The features tested by Gordon are shown in Table 3-1.

Gordon continues to create a face recognition system by means of a simple Euclidean distance measure in feature space. Several combinations of features are tested using a database of 24 facial surfaces (8 different people), defining a correct recognition if the subject was selected as the top match from the database (lowest distance measure). Results range from 70.8% to 100% correct recognition, with the best score achieved by using the first 6 features of Table 3-1. A linear degradation was observed when using greater or fewer features.

Bronstein et al have investigated the use of texture mapped 3D face models focusing on expression invariant face recognition [61] using geometric invariants of the face extracted from 3D face data for non-rigid surface comparisons. By using isometric surface signatures known as bending-invariant cononical forms, generated by dimensionality reduction through multidimensional scaling. Bronstein et al compare signatures by a weighted Euclidean distance metric. Testing the method on a database

of 147 subjects, the method was shown to outperform eigen-decomposition methods for 10 identification operations.

Feature	Discriminating power
Head width	24.9
Nose height	16.6
Nose depth	9.6
Nose width	9.2
Distance between the eyes	6.6
Maximum curvature on nose ridge	6.2
Average minimum curvature on nose ridge	4.4
Total width of eyes (span)	4.2
Curvature at nose bridge	3.3
Right eye width	2.4
Curvature at nose base	2.1
Left eye width	1.3

Table 3-1 Evaluation of the discriminating ability of features extracted from 3D facial data, as presented in Gordon's paper [4].

The Face Recognition Grand Challenge (FRGC) [2] has recently been launched, in which multiple face recognition systems are compared under a similar framework to that of the FRVT. The test database provided with the FRGC includes a substantial amount of 3D face data with corresponding 2D texture images. This initiative is likely to intensify research into 3D face recognition and greatly improve the ability to compare and contrast various 3D face recognition methods. However. as the high resolution 3D models were acquired using the Minolta laser scanner any results presented are unlikely to be reproduced in a real-world environment where large laser scanning devices are not appropriate. Chang et al have already made use of this multi-modal data [73] showing how both 2D and 3D data can be utilised to greater effect than using either sets of data separately.

3.3 Recognition Difficulties

The problems caused by changes in lighting conditions have been well researched. Adini, Moses and Ullman suggest that the difference (mean square intensity difference on a pixel basis) between images of one face under different illumination conditions are greater than the differences between images of different faces under the same illumination conditions [26]. It has been attempted, with some success, to identify and compensate for the effect of lighting conditions in various face recognition systems. Zhao and Chellappa use a generic 3D surface of a face, together with a varying albedo reflectance model and a Lambertian physical reflectance model to compensate for both the lighting and head orientation [9], before applying a recognition system based on LDA.

Much research has also been carried out to improve eigenface recognition systems. Cutler has shown that it can successfully be applied to infrared images [7], resulting in a much decreased error rate. This shows that an artificial infrared light source could be used to reduce the effect of external light sources, producing an accurate system for use in security applications such as site access. However, the use of such a light source is not always practical, particularly if the camera is far from the subject.

Pentland, Moghaddam and Starner extended their eigenface system to include multiple viewing angles of a person's face [40], improving the system performance when applied to faces of various orientations. This was done by gathering several training sets, each containing images of people's faces from a specific angle. When recognition is performed, the face image is projected into the appropriate face space (depending on the orientation of the face in the image determined according to the distance from face space). Although this method does expand the systems capabilities, as the angle of orientation deviates from the fronto-parallel view, the system's performance degrades.

Pentland et al also incorporate a modular eigenface system [40], which significantly improves the overall performance, although it does not tackle the lighting problem directly. Belhumeur, Hespanha and Kreigman use Fisher's linear discriminant to capture similarities between multiple images in each class (per person) [27], hoping to discount variations due to lighting from the defined subspace. Their results show a significant improvement over the standard eigenface approach (from 20% to less than

2% error rate). However, it does not overcome the problem of changes in lighting conditions.

3.4 Human Facial Perception

In this section we take a slight deviation from the computer science perspective and review some literature that focuses on the ability of the human visual system to perform face recognition. Whether or not this line of investigation will prove useful in the quest to design an improved automatic face recognition technique remains to be seen, however we must remember that one of the main driving forces behind automated face recognition research is that we (humans) recognise people by a similar means. Automatic face recognition systems will always have this analogy to human perception, meaning a systems decision can easily be verified by a human operator. In addition, this concept provides some comfort in that we are not trying to tackle an impossible problem, a system has already been created that can perform this task: the human brain. However, we must be cautious regarding this statement. We are all aware of our impressive ability to recognise a close friend in a blurred image, partially occluded with dark glasses, at a glance across a crowded room, even if we have not seen them for several years (something that is far beyond the capability of any existing face recognition system). On the other hand, our face recognition ability can be surprisingly poor, given just a single photograph of somebody we have never met we often fail to recognise another image if a small change in lighting has occurred, conversely we can easily misidentify somebody because of a similar moustache, hairstyle or other features. If we relate this to our expectation of an automated face recognition system (instant recognition from a single reference image when compared against thousands of images in unknown conditions), perhaps automated systems have already surpassed human recognition. If so, this is a persuasive argument for adoption of a face recognition system in any scenario where identification is currently carried out by a human operator. For these reasons, this topic is worthy of some attention, in particular with regard to the following questions:

- How do humans recognise faces?
- Is there any correlation between human perception and automatic methods of recognition?

- Is there any value in attempting to emulate methods of human face recognition in order to improve existing systems?
- How good is human face recognition and at what point does an automated method become more effective than a human operator?

Burton et al [70] shows that familiarity of faces is very important for human facial recognition, especially when image quality is poor. By testing the ability of humans to recognise faces in poor quality security videos it was shown that if a person is familiar with a subject they can be recognised to a high degree of success (even in very poor conditions), compared to people who were unfamiliar with the subject (including police officers experienced in forensic identification). By performing two experiments, either obscuring the body of the subject (to eliminate cues from gait and clothing) or just the face region, Burton et al demonstrates that the face is by far the primary cue for recognition.

Another paper by Burton et al [69] has shown that a cognitive model of face recognition in combination with PCA can be used to simulate computation of familiarity, perhaps suggesting some commonality between the holistic appearance-based PCA methods of face recognition and the feature extraction of human facial perception. Hancock, Bruce and Burton [12][13] extend this comparison, contrasting the capabilities of the human visual system to that of PCA methods of face recognition, focusing on the psychological plausibility of the approach. They state that although PCA alone is not a plausible model of the processes involved in the human visual system, it does have many strong similarities due to its inherent global representation and the holistic nature of human facial perception. It is also noted that a human's ability to recognise faces does not rely on individual measurements of internal features, as we are still capable of recognising line drawings of faces, although it becomes significantly harder without the additional texture and shading information. Likewise, our own research has demonstrated that it becomes extremely difficult to recognise people using geometric structure alone (see Figure 5-3 in which all 3D models are of the same person). The human visual system also appears to be strongly adapted to distinguishing between (natural) faces to a much higher accuracy than other objects. Error rates increase when trying to recognise faces from photographic negatives, even though all the structural and texture information is still present. This suggests that a human's

ability to recognise faces is heavily influenced by knowledge of the generic structure, orientation, colour and texture of faces. This is reinforced by the illusion in Figure 3-6.

Figure 3-6 - When faces are not viewed in their natural state, the ability of the human visual system to distinguish between them is reduced. The modifications to the image on the right are scarcely noticeable, until the images are rotated by 180°.

In Hancock, Bruce and Burtons work, human participants are used to assign similarity and distinctiveness ratings to a database of facial images, by means of computer controlled questionnaires and recollection tests. These ratings are then compared to the principal component values, reconstruction error and identification error of an eigenface based face recognition system [48][14]. If any correlation exists, it is assumed that faces appearing similar to humans should occupy near positions in PCA space and hence produce low distance measures. The results show that PCA based identification does correlate, to some extent, with the human notion of similarity, giving average Kendall rank correlation values ranging from 0.12 to 0.22 for a number of different PCA systems [12]. Another interesting observation is that an increase in the performance of the PCA systems (Hancock et al experiment with various shape-free pre-processing and image filters) is accompanied by an increase in correlation to the human visual system. Hancock et al also show a correlation with the most principal component (first eigenface) and false acceptance rate, suggesting a link between 'familiarity' (resulting in the subject's mistaken belief that they have encountered a face before) and the most discriminating holistic feature [13]. The research also shows that finer scales of face images relate to this notion of familiarity, while the more coarse scales contribute to distinctiveness and memorability.

Another investigation into the correlation between human face recognition and automated systems is carried out by Coombes et al [32], this time focusing on the relationship between 3D facial surface information and the psychological

distinctiveness of a face. Ten human judges were used to rate faces according to how distinctive the facial image appeared to them. By comparing these distinctiveness ratings with the 3D facial surface data, it was discovered (as one may have assumed) that the more distinctive the face, the more the 3D facial surface deviated from the average facial surface. In particular, the more distinctive faces were composed of fewer flat surfaces in the lower regions of the facial surface.

3.5 Summary of Performance

From the various papers described above, it is apparent that 2D face recognition has achieved a reasonably high level of performance, particularly using the eigenface and Fisherface appearance-based approaches. However, the error rates still being produced by these systems do not seem to compare to the level that the human visual system is able to discriminate between faces (although this statement is quite subjective). The error rates are also still too high to be considered for many of the potential applications of face recognition. We see that neural network approaches are well suited towards face detection, which is a critical preliminary step to successful face recognition, but no system has been presented which utilises the benefits offered by such a system prior to any further verification or identification procedures. On a similar note, we have also seen how feature analysis, although not accurate enough to perform a high level of recognition of its own, could be used as a preliminary screening step.

Many researchers suggest that the main problem to be overcome by 2D face recognition systems is that of lighting conditions. If this were to be achieved, face recognition would become a much more attractive biometric for the purposes of verification for site access. However, for face recognition to be used in a surveillance application, the problem of facial expression and facial orientation must also be solved. Some attempts have been made to combat both of these problems, with limited success. It is surprising that image pre-processing, colour normalisation and lighting correction as used with photo processing systems has not been applied more readily as a preliminary step to appearance-based approaches (at most those explored use simple histogram equalisation or brightness and contrast adjustment), as it is likely that such additional processing could improve both the eigenface and Fisherface methods. Although Adini, Moses and Ullman point out that there is no image representation that can be completely invariant to lighting conditions, they do show that different representations of images, on which

lighting has less of an affect, can significantly reduce the difference between two images of the same face [26].

3D facial recognition has been identified as a viable biometric, with the potential for high performance classification. However, very few 3D facial recognition systems have been implemented and those that have been tested have only been applied to small databases. Nevertheless, the results have all been promising. It is also evident that subspace approaches could be equally applicable to 3D facial surface information, although a large database of 3D face models is required to facilitate further research in this area. The need for a common test database has been a recurring factor in many of the papers discussed here and although the FRVT [1] and FERET database [44] have gone some way to addressing these issues they are more often utilised in commercial tests rather than adopted in research investigations and this makes cross-method comparison very subjective. Some of the more common databases currently used for 2D face recognition are:

- The FERET database [41]
- The AR Face Database [39]
- The XM2VTS database. [66]
- The Psychological Image Collections at Sterling (PICS) [64]
- The UMIST Face Database [65]
- The Yale Face Database [67]

Although more researchers are beginning to make use of such databases for 2D face recognition, the same problem can now be seen arising in the 3D field. Further complicated by the greater variety of 3D data formats and the need for simultaneously acquired 2D images. The Face Recognition Grand Challenge (FRGC) [2] does look set to address some of these points, providing a defined testing methodology and 3D face data with accompanying 2D images, although the database will not be available in sufficient time for our own investigations and therefore we have had to address this problem ourselves (see section 5.1).

4 Two-dimensional Face Recognition

In this chapter we investigate and compare three well-known methods of 2D face recognition, namely the direct correlation, eigenface and Fisherface methods. The investigations documented serve as a necessary preface to the novel advances introduced in later chapters (particularly sections 7.1 and 7.4). We begin in section 4.1 with a brief description of face detection and feature localisation techniques used, before detailed descriptions of the three face recognition methods in sections 4.2, 4.3 and 4.4. In section 4.5 we introduce a range of image pre-processing methods used throughout this thesis, presenting the results of incorporating these techniques into the three face recognition systems in section 4.6.

All three methods discussed in this chapter are considered to be 'appearance-based', in that the image pixel data is used as a whole to perform recognition, rather than detecting and analysing relationships between individual facial features. Direct correlation is the term we use to describe a simple direct comparison of two facial images, producing a similarity score. This differs from the two subspace methods (eigenface and Fisherface) in that the face images are compared directly, in the original image space, rather than attempting to reduce a facial image down to the few most discriminating components. The purpose of investigating the direct correlation method is primarily to provide an initial baseline comparison by which to gauge any advantage offered by the subspace methods and whether any additional improvement using image pre-processing techniques is applicable to all three systems.

Two-dimensional face recognition systems use a standard 2D image (either colour or grey scale), often captured by means of a camera and frame-grabber, web-cam or scanned photograph, to perform recognition. Such systems have been in use for a number of years; incorporated into biometric access systems in airports, used in identification procedures in police departments and CCTV surveillance systems. However, these two-dimensional approaches are held back by a few critical problems. Firstly, such systems are extremely sensitive to head orientation, meaning that in order to achieve a positive verification the subject must be facing directly towards the camera (fronto-parallel orientation). The result is that throughput of site access systems is considerably reduced (subjects often have to attempt several verifications to achieve the

correct orientation) and surveillance systems rely on luck that the subject will face the camera. The second major problem is lighting conditions. If the subject is enrolled in an environment with different lighting conditions (including direction, intensity and colour) to that when verification is performed, the subject is often falsely rejected.

In this chapter we explore three two-dimensional appearance-based methods of face recognition, describing the theory and mathematical concepts behind each in sections 4.2, 4.3 and 4.4. We perform some preliminary experimentation using each of the three methods on a small test set of facial images, providing an initial baseline indication of how each system performs and the level of results that may be expected from such experimentation. A more thorough comparison of the three systems on a common data set is provided in section 4.6. For completeness sake, we also briefly cover the necessary preliminary requirements of feature localisation in section 4.1. However, we do not spend significant time researching or improving the method described, considering it to be another topic worthy of further study in a separate project.

4.1 Feature Localization

Before discussing the methods of comparing two facial images we now take a brief look at some at the preliminary processes of facial feature alignment. This process typically consists of two stages: face detection and eye localisation. Depending on the application, if the position of the face within the image is known beforehand (for a cooperative subject in a door access system for example) then the face detection stage can often be skipped, as the region of interest is already known. Therefore, we discuss eye localisation here, with a brief discussion of face detection in the literature review (section 3.1.1).

The eye localisation method is used to align the 2D face images of the various test sets used throughout this section. However, to ensure that all results presented are representative of the face recognition accuracy and not a product of the performance of the eye localisation routine, all image alignments are manually checked and any errors corrected, prior to testing and evaluation.

We detect the position of the eyes within an image using a simple template based method. A training set of manually pre-aligned images of faces is taken, and each image cropped to an area around both eyes. The average image is calculated and used as a template.

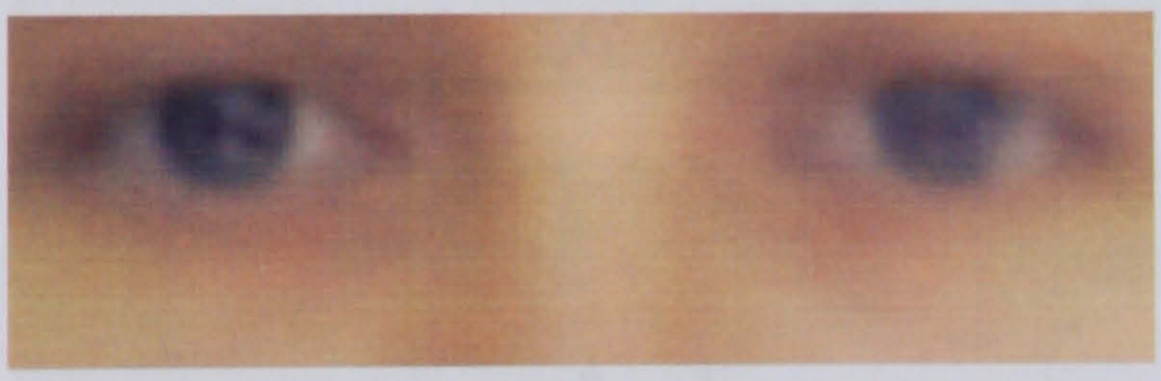

Figure 4-1 - The average eyes. Used as a template for eye detection.

Both eyes are included in a single template, rather than individually searching for each eye in turn, as the characteristic symmetry of the eyes either side of the nose, provides a useful feature that helps distinguish between the eyes and other false positives that may be picked up in the background. Although this method is highly susceptible to scale (i.e. subject distance from the camera) and also introduces the assumption that eyes in the image appear near horizontal. Some preliminary experimentation also reveals that it is advantageous to include the area of skin just beneath the eyes. The reason being that in some cases the eyebrows can closely match the template, particularly if there are shadows in the eye-sockets, but the area of skin below the eyes helps to distinguish the

eyes from eyebrows (the area just below the eyebrows contain eyes, whereas the area below the eyes contains only plain skin).

A window is passed over the test images and the absolute difference taken to that of the average eye image shown above. The area of the image with the lowest difference is taken as the region of interest containing the eyes. Applying the same procedure using a smaller template of the individual left and right eyes then refines each eye position. This basic template-based method of eye localisation, although providing fairly precise localisations, often fails to locate the eyes completely. However, we are able to improve performance by including a weighting scheme.

Eye localisation is performed on the set of training images, which is then separated into two sets: those in which eye detection was successful; and those in which eye detection failed. Taking the set of successful localisations we compute the average distance from the eye template (Figure 4-2 top). Note that the image is quite dark, indicating that the detected eyes correlate closely to the eye template, as we would expect. However, bright points do occur near the whites of the eye, suggesting that this area is often inconsistent, varying greatly from the average eye template.

Figure 4-2 – Distance to the eye template for successful detections (top) indicating variance due to noise and failed detections (bottom) showing credible variance due to miss-detected features.

In the lower image (Figure 4-2 bottom), we have taken the set of failed localisations (images of the forehead, nose, cheeks, background etc. falsely detected by the localisation routine) and once again computed the average distance from the eye template. The bright pupils surrounded by darker areas indicate that a failed match is often due to the high correlation of the nose and cheekbone regions overwhelming the poorly correlated pupils. Wanting to emphasise the difference of the pupil regions for these failed matches and minimise the variance of the whites of the eyes for successful

matches, we divide the lower image values by the upper image to produce a weights vector as shown in Figure 4-3. When applied to the difference image before summing a total error, this weighting scheme provides a much improved detection rate.

Figure 4-3 - Eye template weights used to give higher priority to those pixels that best represent the eyes.

4.2 The Direct Correlation Approach

We begin our investigation into face recognition with perhaps the simplest approach, known as the direct correlation method (also referred to as template matching by Brunelli and Poggio [29]) involving the direct comparison of pixel intensity values taken from facial images. We use the term 'Direct Correlation' to encompass all techniques in which face images are compared directly, without any form of image space analysis, weighting schemes or feature extraction, regardless of the distance metric used. Therefore, we do not infer that Pearson's correlation is applied as the similarity function (although such an approach would obviously come under our definition of direct correlation). We typically use the Euclidean distance as our metric in these investigations (inversely related to Pearson's correlation and can be considered as a scale and translation sensitive form of image correlation), as this persists with the contrast made between image space and subspace approaches in later sections.

Firstly, all facial images must be aligned such that the eye centres are located at two specified pixel coordinates and the image cropped to remove any background information. These images are stored as greyscale bitmaps of 65 by 82 pixels and prior to recognition converted into a vector of 5330 elements (each element containing the corresponding pixel intensity value). Each corresponding vector can be thought of as describing a point within a 5330 dimensional image space. This simple principle can easily be extended to much larger images: a 256 by 256 pixel image occupies a single point in 65,536-dimensional image space and again, similar images occupy close points within that space. Likewise, similar faces are located close together within the image space, while dissimilar faces are spaced far apart. Calculating the Euclidean distance *d*,

between two facial image vectors (often referred to as the query image q, and gallery image g), we get an indication of similarity. A threshold is then applied to make the final verification decision.

$$d = \|q - g\| \quad (d \leq threshold \Rightarrow accept) \wedge (d > threshold \Rightarrow reject) \ .$$

Equ. 4-1

4.2.1 Verification Tests

The primary concern in any face recognition system is its ability to correctly verify a claimed identity or determine a person's most likely identity from a set of potential matches in a database. In order to assess a given system's ability to perform these tasks, a variety of evaluation methodologies have arisen. Some of these analysis methods simulate a specific mode of operation (i.e. secure site access or surveillance), while others provide a more mathematical description of data distribution in some classification space. In addition, the results generated from each analysis method may be presented in a variety of formats.

Throughout the experimentations in this thesis, we primarily use the verification test as our method of analysis and comparison, although we also use Fisher's Linear Discriminant to analyse individual subspace components in section 7 and the identification test for the final evaluations described in section 8.

The verification test measures a system's ability to correctly accept or reject the proposed identity of an individual. At a functional level, this reduces to two images being presented for comparison, for which the system must return either an acceptance (the two images are of the same person) or rejection (the two images are of different people). The test is designed to simulate the application area of secure site access. In this scenario, a subject will present some form of identification at a point of entry, perhaps as a swipe card, proximity chip or PIN number. This number is then used to retrieve a stored image from a database of known subjects (often referred to as the target or gallery image) and compared with a live image captured at the point of entry (the query image). Access is then granted depending on the acceptance/rejection decision. The results of the test are calculated according to how many times the accept/reject decision is made correctly.

In order to execute this test we must first define our test set of face images. Although the number of images in the test set does not affect the results produced (as the error rates are specified as percentages of image comparisons). it is important to ensure that the test set is sufficiently large such that statistical anomalies become insignificant (for example, a couple of badly aligned images matching well). Also, the type of images (high variation in lighting, partial occlusions etc.) will significantly alter the results of the test. Therefore, in order to compare multiple face recognition systems, they must be applied to the same test set. However, it should also be noted that if the results are to be representative of system performance in a real world situation. then the test data should be captured under precisely the same circumstances as in the application environment. On the other hand, if the purpose of the experimentation is to evaluate and improve a method of face recognition, which may be applied to a range of application environments, then the test data should present the range of difficulties that are to be overcome. This may mean including a greater percentage of 'difficult' images than would be expected in the perceived operating conditions and hence higher error rates in the results produced.

Below we provide the algorithm for executing the verification test. The algorithm is applied to a single test set of face images, using a single function call to the face recognition algorithm: CompareFaces(FaceA, FaceB). This call is used to compare two facial images, returning a distance score indicating how dissimilar the two face images are: the lower the score the more similar the two face images. Ideally, images of the same face should produce low scores, while images of different faces should produce high scores.

Every image is compared with every other image, no image is compared with itself and no pair is compared more than once (we assume that the relationship is symmetrical). Once two images have been compared, producing a similarity score, the ground-truth is used to determine if the images are of the same person or different people. In practical tests this information is often encapsulated as part of the image filename (by means of a unique person identifier). Scores are then stored in one of two lists: a list containing scores produced by comparing images of different people and a list containing scores produced by comparing images of the same person. The final acceptance/rejection decision is made by application of a threshold. Any incorrect decision is recorded as either a false acceptance or false rejection. The false rejection rate (FRR) is calculated

as the percentage of scores from the same people that were classified as rejections. The false acceptance rate (FAR) is calculated as the percentage of scores from different people that were classified as acceptances.

```
For IndexA = 0 to length(TestSet)
   For IndexB = IndexA+1 to length(TestSet)
      Score = CompareFaces(TestSet[IndexA], TestSet[IndexB])
      If IndexA and IndexB are the same person
         Append Score to AcceptScoresList
      Else
         Append Score to RejectScoresList

For Threshold = Minimum Score to Maximum Score:
   FalseAcceptCount, FalseRejectCount = 0
   For each Score in RejectScoresList
      If Score <= Threshold
         Increase FalseAcceptCount
      For each Score in AcceptScoresList
         If Score > Threshold
            Increase FalseRejectCount
   FalseAcceptRate = FalseAcceptCount / Length(AcceptScoresList)
   FalseRejectRate = FalseRejectCount / length(RejectScoresList)
   Add plot to error curve at (FalseRejectRate, FalseAcceptRate)
```

Figure 4-4 Algorithm for computing false acceptance rates and false rejection rates for a typical one-to-one verification application.

These two error rates express the inadequacies of the system when operating at a specific threshold value. Ideally, both these figures should be zero, but in reality reducing either the FAR or FRR (by altering the threshold value) will inevitably result in increasing the other. Therefore, in order to describe the full operating range of a particular system, we vary the threshold value through the entire range of scores produced. The application of each threshold value produces an additional FAR, FRR pair, which when plotted on a graph produces the error rate curve shown below.

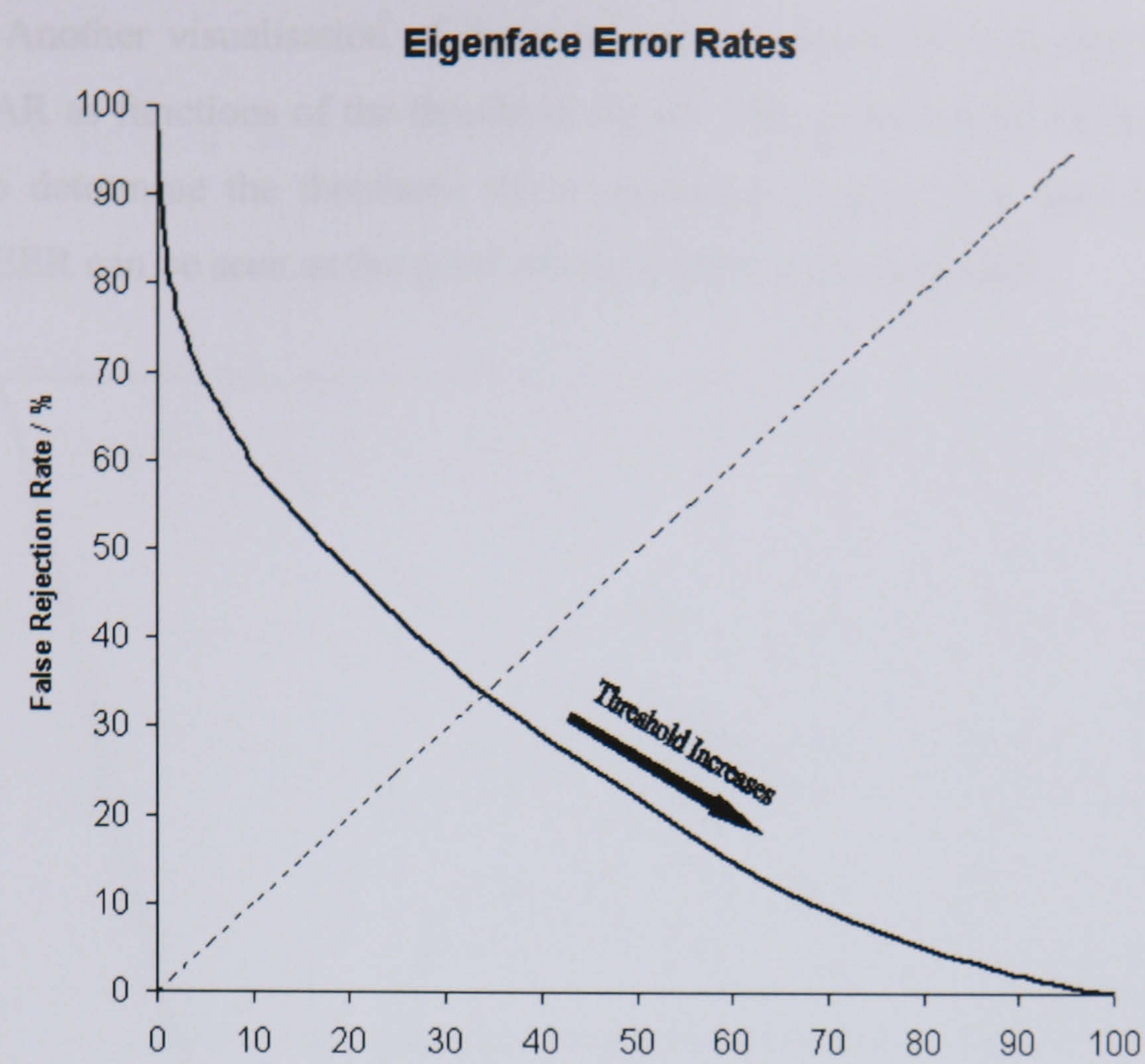

Figure 4-5 - Example Error Rate Curve produced by the verification test.

The equal error rate (EER) can be seen as the point at which FAR is equal to FRR. This EER value is often used as a single figure representing the general recognition performance of a biometric system and allows for easy visual comparison of multiple methods. However, it is important to note that the EER does not indicate the level of error that would be expected in a real world application. It is unlikely that any real system would use a threshold value such that the percentage of false acceptances were equal to the percentage of false rejections. Secure site access systems would typically set the threshold such that false acceptances were significantly lower than false rejections: unwilling to tolerate intruders at the cost of inconvenient access denials. Surveillance systems on the other hand would require low false rejection rates to successfully identify people in a less controlled environment. Therefore we should bear in mind that a system with a lower EER might not necessarily be the better performer towards the extremes of its operating capability.

There is a strong connection between the above graph and the receiver operating characteristic (ROC) curves, also used in such experiments. Both graphs are simply two visualisations of the same results, in that the ROC format uses the True Acceptance Rate(TAR), where TAR = 1.0 – FRR in place of the FRR, effectively flipping the graph

vertically. Another visualisation of the verification test results is to display both the FRR and FAR as functions of the threshold value. This presentation format provides a reference to determine the threshold value necessary to achieve a specific FRR and FAR. The EER can be seen as the point where the two curves intersect.

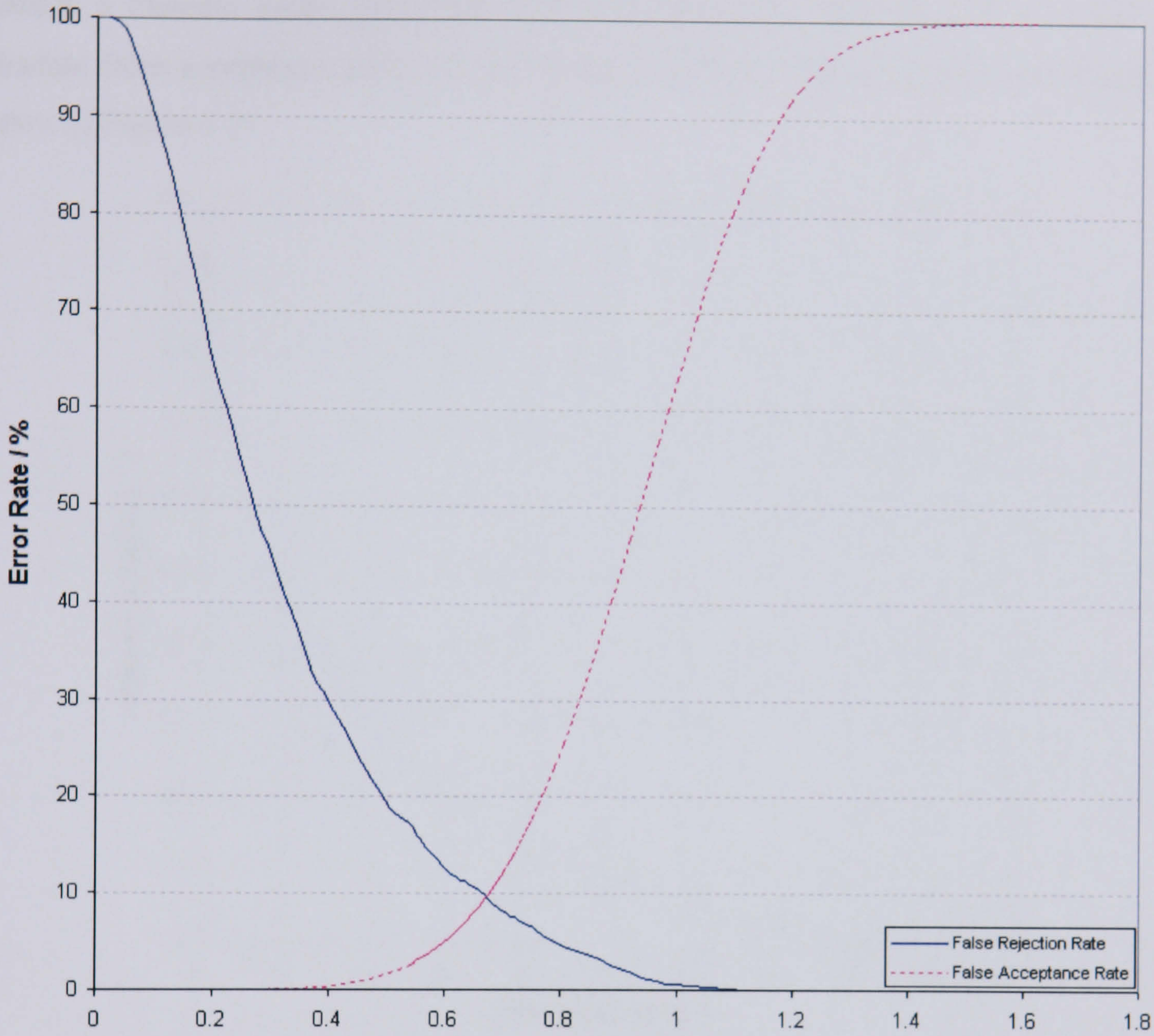

Figure 4-6 - Example error rate curve as a function of the score threshold.

The fluctuation of these error curves due to noise and other errors is dependant on the number of face image comparisons made to generate the data. A small dataset that only allows for a small number of comparisons will results in a jagged curve, in which large steps correspond to the influence of a single image on a high proportion of the comparisons made. A typical dataset of 720 images (as used in section 4.2.2) provides 258,840 verification operations, hence a drop of 1% EER represents an additional 2588 correct decisions, whereas the quality of a single image could cause the EER to fluctuate by up to 0.28.

4.2.2 Results

As a simple experiment to test the direct correlation method, we apply the technique described above to a test set of 720 images of 60 different people, taken from the AR Face Database [39]. Every image is compared with every other image in the test set to produce a likeness score, providing 258,840 verification operations from which to calculate false acceptance rates and false rejection rates. The error curve produced is shown in Figure 4-7.

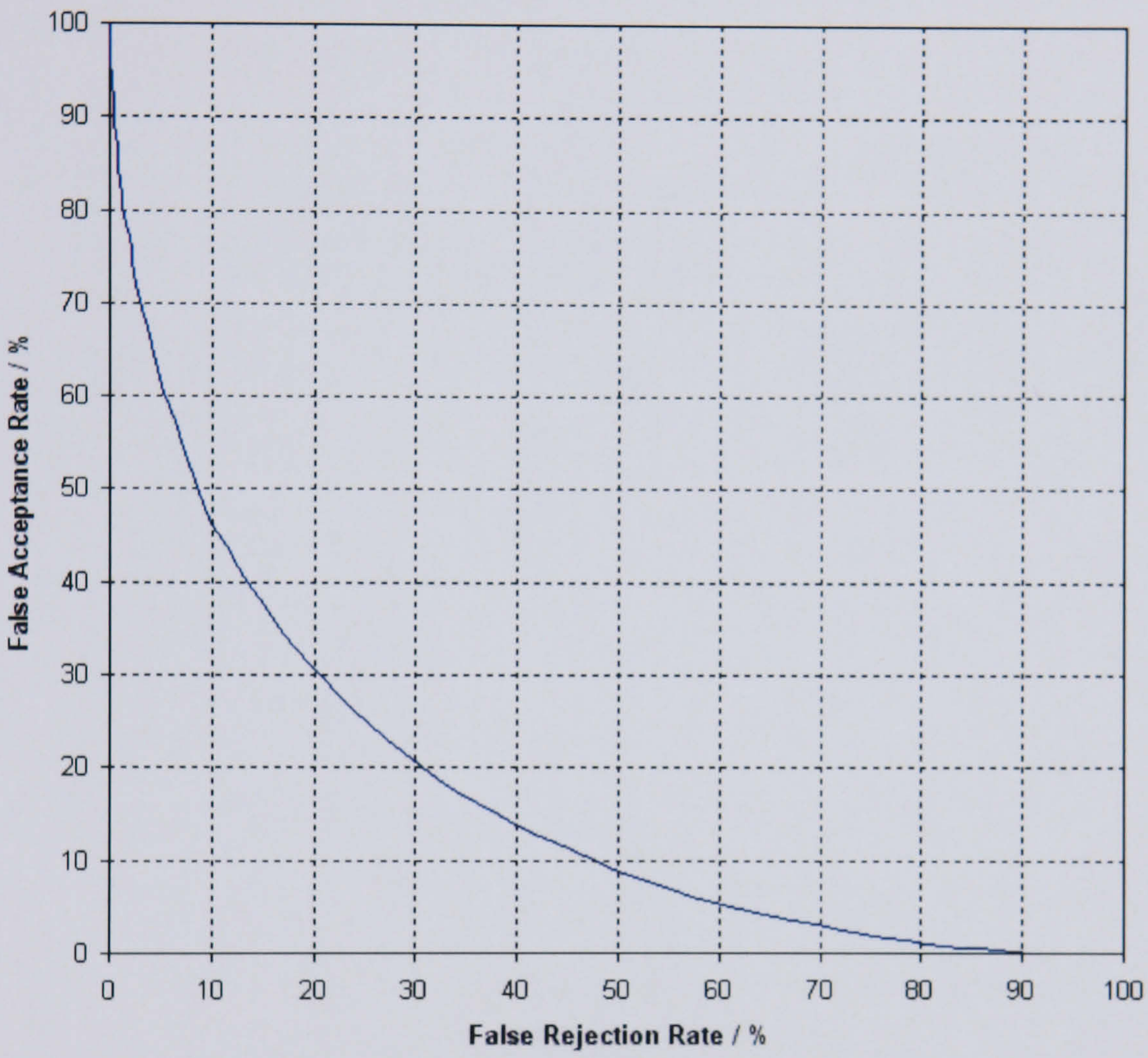

Figure 4-7 - Error rate curve produced by the direct correlation method using no image pre-processing.

We see that an EER of 25.1% is produced, meaning that at the EER threshold approximately one quarter of all verification operations carried out resulted in an incorrect classification. There are a number of well-known reasons for this poor level of accuracy. Tiny changes in lighting, expression or head orientation cause the location in image space to change dramatically. Images in face space are moved far apart due to these image capture conditions, despite being of the same person's face. The distance between images of different people becomes smaller than the area of face space covered by images of the same person and hence false acceptances and false rejections occur frequently. Other disadvantages include the large amount of storage necessary for

holding many face images and the intensive processing required for each comparison, making this method unsuitable for applications applied to a large database. In section 4.3 we explore the eigenface method, which attempts to address some of these issues.

4.3 The Eigenface Approach

We now turn our attention to the eigenface method of face recognition as introduced by Turk and Pentland [48]. This method has become one of the most well known methods of face recognition due to it relatively simple nature, strong mathematical foundation and reasonably successful results. The method attempts to reduce a facial image down to the most variant features, such that recognition can be performed in a substantially reduced image space than that of the direct correlation method. However, rather that detecting and measuring a set of specific features on a facial image, the method maintains a holistic representation, discarding any need for feature detection other than that required for the initial image alignment. It requires the application of Principal Component Analysis (PCA), also known as the Karhunen- Loeve transform, to a training set of facial images. For the purpose of these experiments we take a training set of 60 images.

Consider our training set of images of 75 by 112 pixels. These images could be represented as two-dimensional (75 by 112) arrays of pixel intensity data. Similarly, vectors of 8400 (75x112) dimensions could represent the images. Interpreting these vectors as describing a point within 8400 dimensional space means that every possible image (of 75 by 112 pixels) occupies a single point within this image space. What's more, similar images (for example images of faces) should occupy points within a fairly localised region of this image space. Taking this idea a step further, we assume that different images of the same face map to nearby points in image space and images of different faces map to far apart points. Ideally, we wish to extract the region of image space that contains faces, reduce the dimensionality to a practical value, yet maximise the spread of different faces within the image subspace. Here we apply Principal Component Analysis to define a space with the properties mentioned above.

We take the set of M training images (in our case M = 60): $\{\Gamma_1, \Gamma_2, \Gamma_3, \ldots \Gamma_M\}$ and compute the average image $\Psi = \frac{1}{M}\sum_{n=1}^{M} \Gamma_n$, followed by the difference of each image from the average image $\Phi_n = \Gamma_n - \Psi$. Thus we construct the covariance matrix as,

$$C = \frac{1}{M}\sum_{n=1}^{M} \Phi_n \Phi_n^T \qquad \textit{where}$$
$$= AA^T \qquad A = [\Phi_1 \Phi_2 \Phi_3 \ldots \Phi_M]$$

Equ. 4-2

The eigenvectors and eigenvalues of this covariance matrix are calculated using standard linear methods. These eigenvectors describe a set of mutually orthogonal axes within the image space, along which there is the most variance in the face images and the corresponding eigenvalues represent the degree of variance along these axes. The M eigenvectors are sorted in order of descending eigenvalues and the M` greatest eigenvectors (in our system M` = 30) are chosen to represent face space. The effect is that we have reduced the dimensionality of the space to M`, yet maintained a high level of variance between face images throughout the image subspace. Each eigenvector contains 8400 elements (the number of pixels in the original bitmap) and can be displayed as images, as shown in Figure 4-8.

Figure 4-8 - Average face image and the first 5 eigenfaces defining a face space with no image pre-processing.

Due to the likeness to faces, Turk and Pentland to refer to these vectors as eigenfaces, and the space they define, face space. Once face space has been defined, we can project any image into face space by a simple matrix multiplication:

$$\omega_k = u_k^T (\Gamma - \Psi) \qquad for \quad k = 1,...M`$$

Equ. 4-3

where u_k is the kth eigenvector and ω_k is the kth weight in the vector $\Omega^T = [\omega_1, \omega_2, \omega_3, \ldots \omega_{M`}]$. Each element of the vector $\Omega$, describes the magnitude of the respective principal component (in other words the coordinate placement of the face image along that eigenvector dimension). Therefore, these M` weights represent the contribution of each respective eigenface and by multiplying the eigenfaces by their weight and summing, we can view the face image as mapped into face space (shown in Figure 4-9).

The vector, Ω, is taken as the 'face-key' for a person's image projected into face space. We compare any two 'face-keys' by a simple Euclidean distance measure, $\varepsilon = \|\Omega_a - \Omega_b\|$. An acceptance (the two face images match) or rejection (the two

images do not match) is determined by applying a threshold. Any comparison producing a distance below the threshold is a match.

Figure 4-9 - Test images and their face space projections.

4.3.1 Preliminary Experimentation

We conduct experiments using a database of 960 bitmap images of 120 individuals (60 male, 60 female), extracted from the AR Face Database provided by Martinez and Benavente [39]. We separate the database into two disjoint sets: i) The training set, containing 60 images of different people of various gender, race and age taken under natural lighting conditions with neutral expression; ii) the test set containing 900 images (15 images of 60 people of various gender, race and age). Each of the 15 images were taken under the conditions described in Table 4-1.

Expression \ Covering	**Lighting**			
	Natural	**From the left**	**From the right**	**From left and right**
Neutral expression	Day 1, Day 2	Day 1, Day 2	Day 1, Day 2	Day 1, Day 2
Happy expression	Day 1, Day 2			
Angry expression	Day 1, Day 2			
Mouth covered	Day 1	Day 1	Day 1	

Table 4-1 - Image capture conditions.

All the images are stored as bitmaps (converted into vectors for PCA). After initial investigations to determine an appropriate resolution, we find there is no significant change in the EER for resolutions of 100 pixels between the eyes down to just 15 pixels. As a compromise between test execution time and some pre-processing techniques possibly working better with higher resolutions, we select 25 pixels distance between

the eyes to conduct further experiments. All images are scaled and rotated such that the centres of the eyes are aligned 25 pixels apart, using our eye detection algorithm (not described here). Each image is cropped to a width and height of 75 and 112 pixels respectively.

Figure 4-10 - Example test set images for a single person (first 6 repeated on two days).

To gather results for the False Rejection Rate, each of the 15 images for a single person, is compared with every other image of their face. No image is compared with itself and each pair is only compared once (the relationship is symmetric), giving $n_c = \frac{1}{2} n_p (n_i^2 - n_i) = 6300$ comparisons to test false rejection, where n_p is the number of people and n_i is the number of face images per person.

False acceptance results are gathered using only images of the type "Day1, neutral expression, natural lighting" and "Day 2, neutral expression, natural lighting." Other comparisons are unlikely to produce false acceptances (due to the combination of different lighting, expression and obscuring), resulting in an initial low ERR, hence any effect of image processing on the more problematic comparisons would be seemingly reduced. Using these images, every person is compared with every other person. This gives 4 comparisons per pair of people, with no person compared to themselves and each pair only compared once. Thus, a total of $n_c = 2(n_p^2 - n_p) = 7080$ comparisons are made between different people to test false acceptance, where n_p is the number of people (60).

Hence, each equal error rate is based on 13380 verification attempts, using a set of comparisons under a range of conditions, such that the FRR and the FAR are maximised. For each threshold value we produce a FAR and a FRR. By applying a range of threshold values we produce a range of FAR and FRR pairs that are plotted on

a graph. The results for our benchmark system (no pre-processing) can be seen below. The EER of 34.0% can be seen as the point where FAR equals FRR (Figure 4-11).

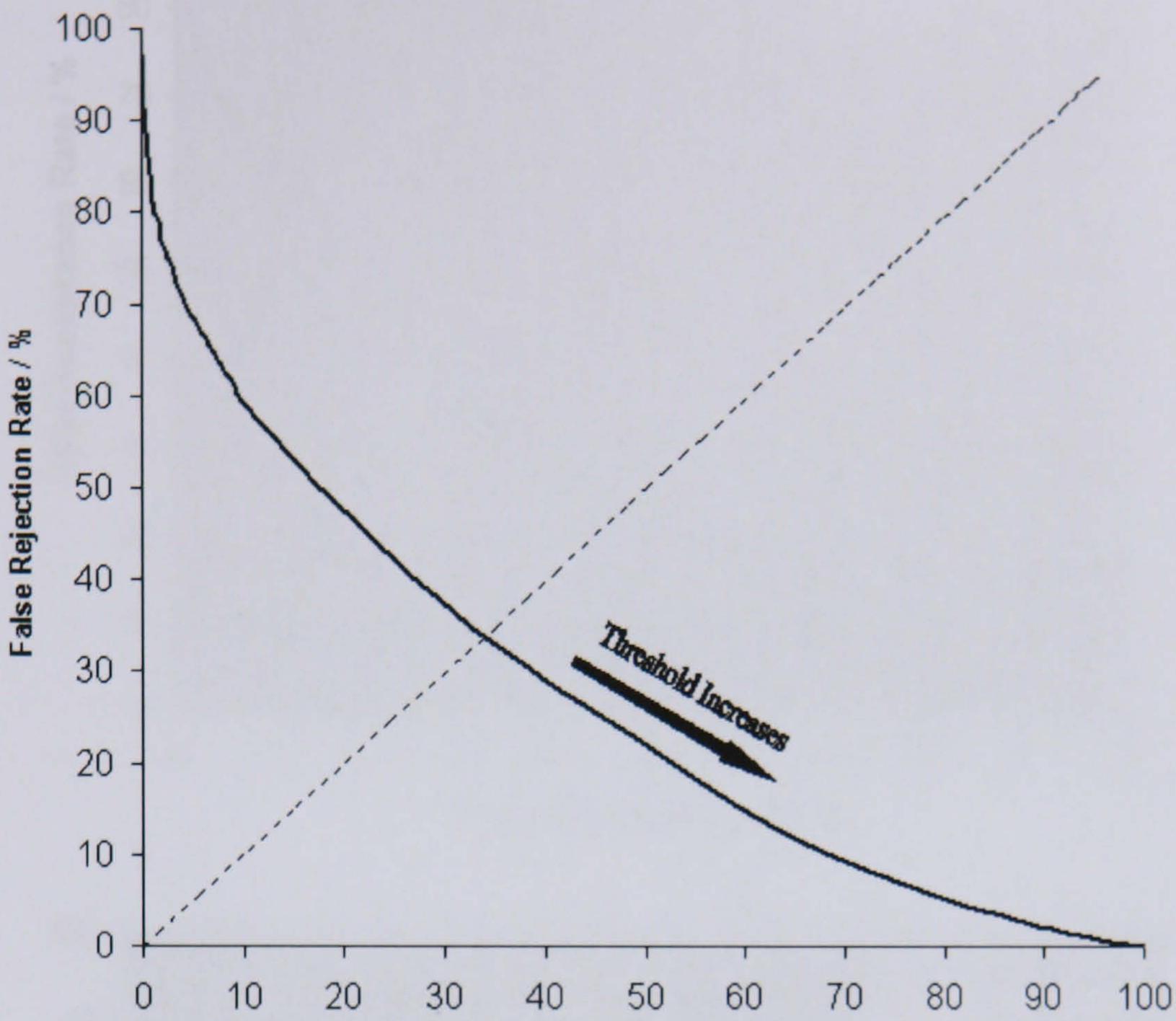

Figure 4-11 - Error rates from various thresholds using an eigenface system with no image pre-processing.

4.3.2 Image Resolution and Crop Region Investigation

It is known that the image resolution and crop region can have a significant effect on the performance of a face recognition system. In this section, we perform a series of investigations to determine an appropriate resolution and image crop for further investigations regarding other image processing techniques. We expect there to be a trade-off between image size (resolution and crop) and performance of the eigenface system (in terms of both processing time and recognition accuracy). Using the same evaluation method as described in section 4.3.1, we produce error rate curves at various image resolutions and image crops.

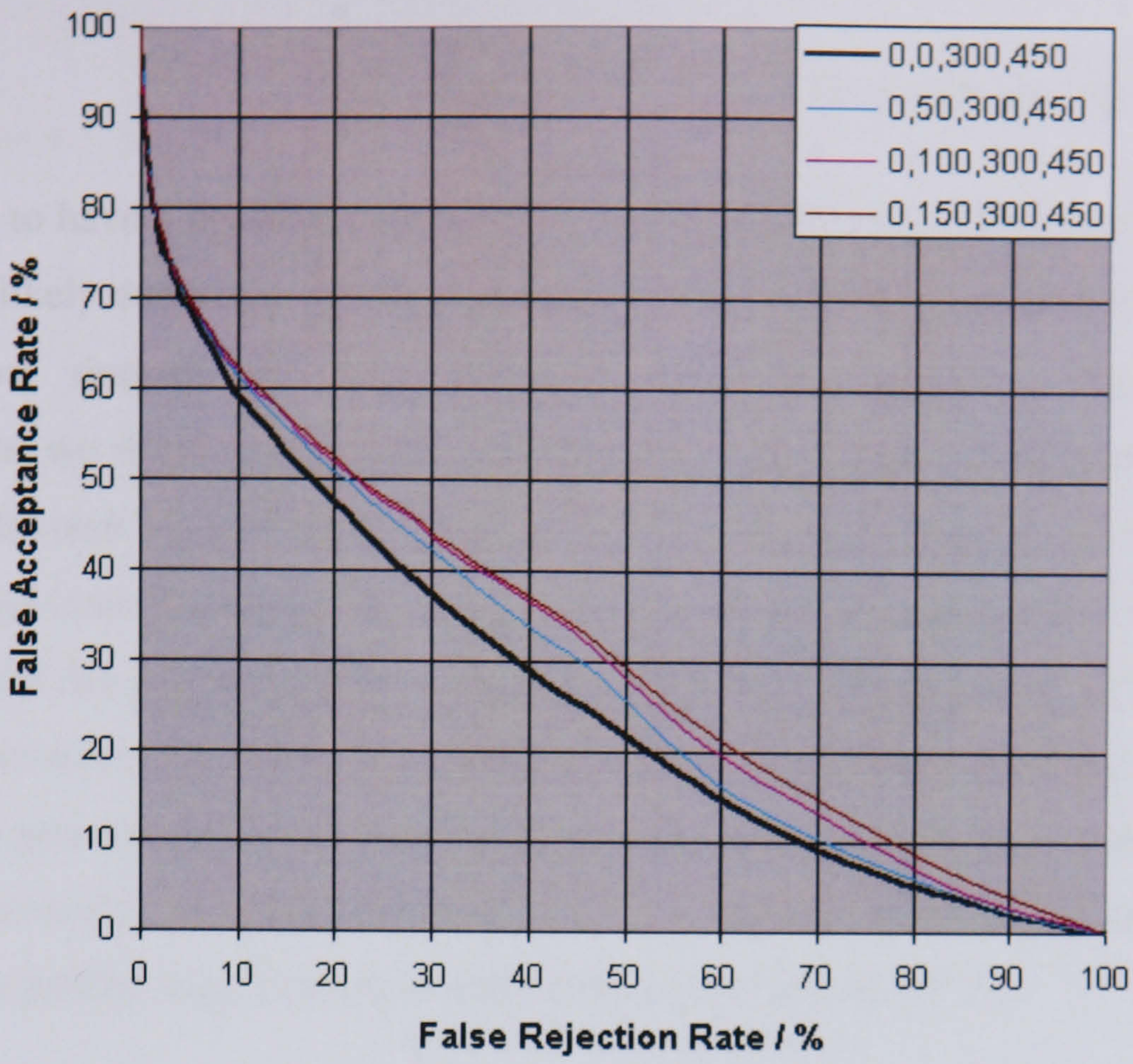

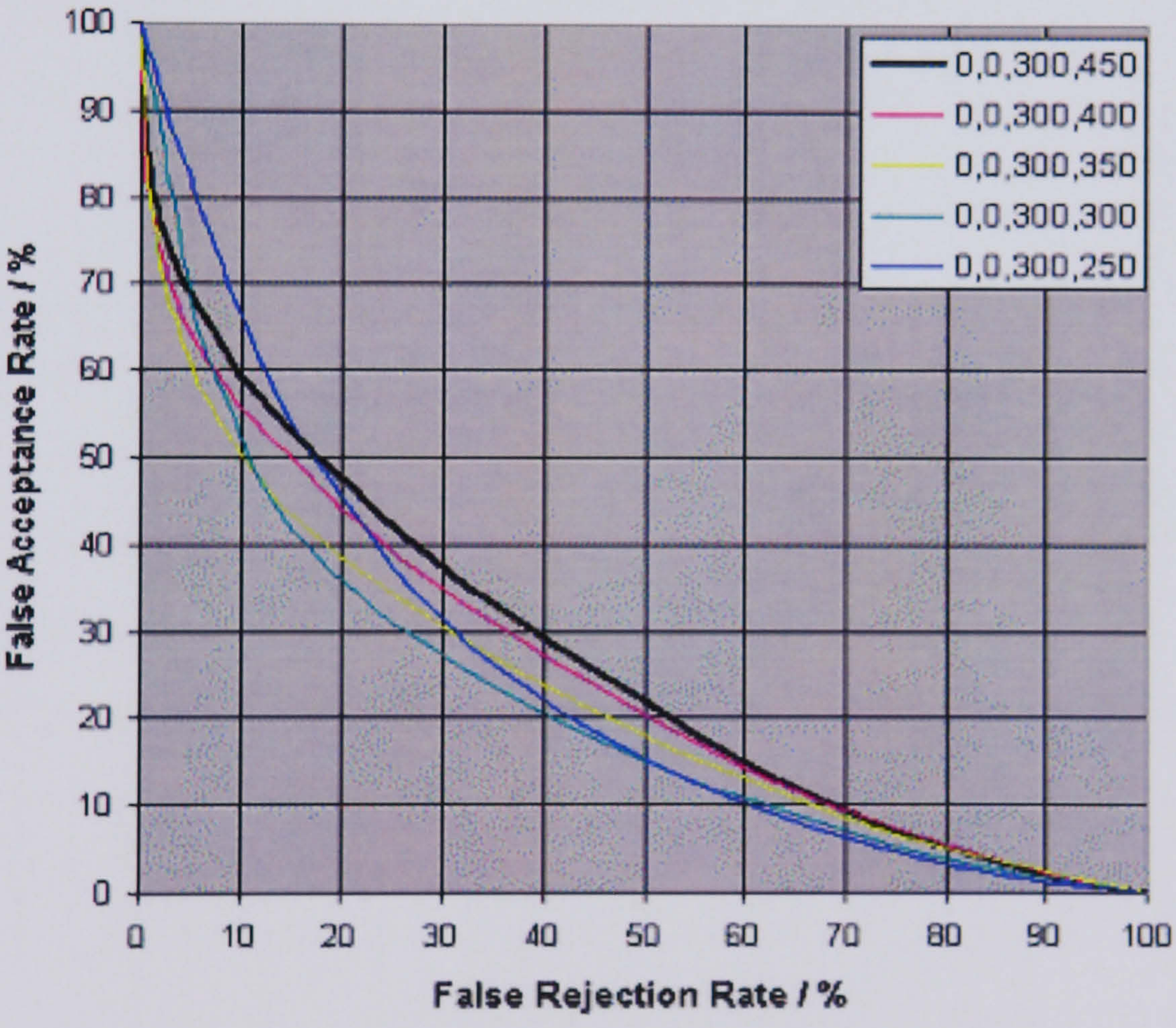

Figure 4-12 - Error rate curves for the 2D eigenface system, when applied to faces images of various crop regions. The legends indicate the upper-left and lower-right coordinates of the crop regions, relative to the original image size.

We see that cropping areas off the top of the image results in a reduction of the system's performance (Figure 4-12 top). This may be due to the discriminating properties of the hairline, forehead shape and head size. Whereas removing the lower regions of the

image seems to have a positive impact on the systems error rates (Figure 4-12 bottom). This is most likely due to the mouth area being the most flexible part of the face, which changes most dramatically with different facial expressions. Despite these improvements, we decide to keep the original area of the image, without applying any cropping. Although we have demonstrated that the crop region significantly affects the error rates, and indeed the error rate could be improved by removing the lower regions of the face, it is our goal to overcome these problems by creating a more discriminating image representation. If such a representation is found, the lower regions of the face may begin to provide a positive contribution to the system performance. Once the best image pre-processing method has been found, we can then test various crop regions again, for any further improvement in performance (see section 5.1.2).

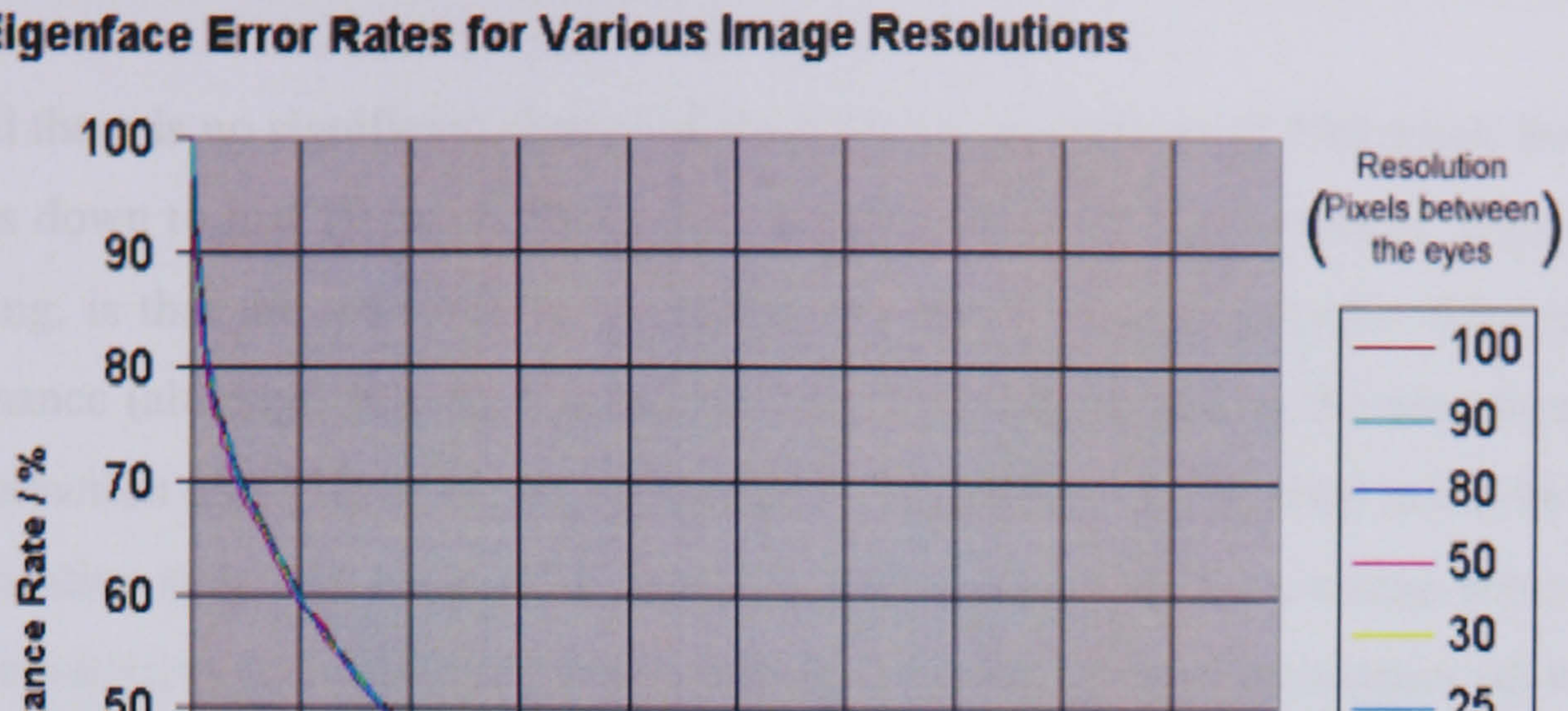

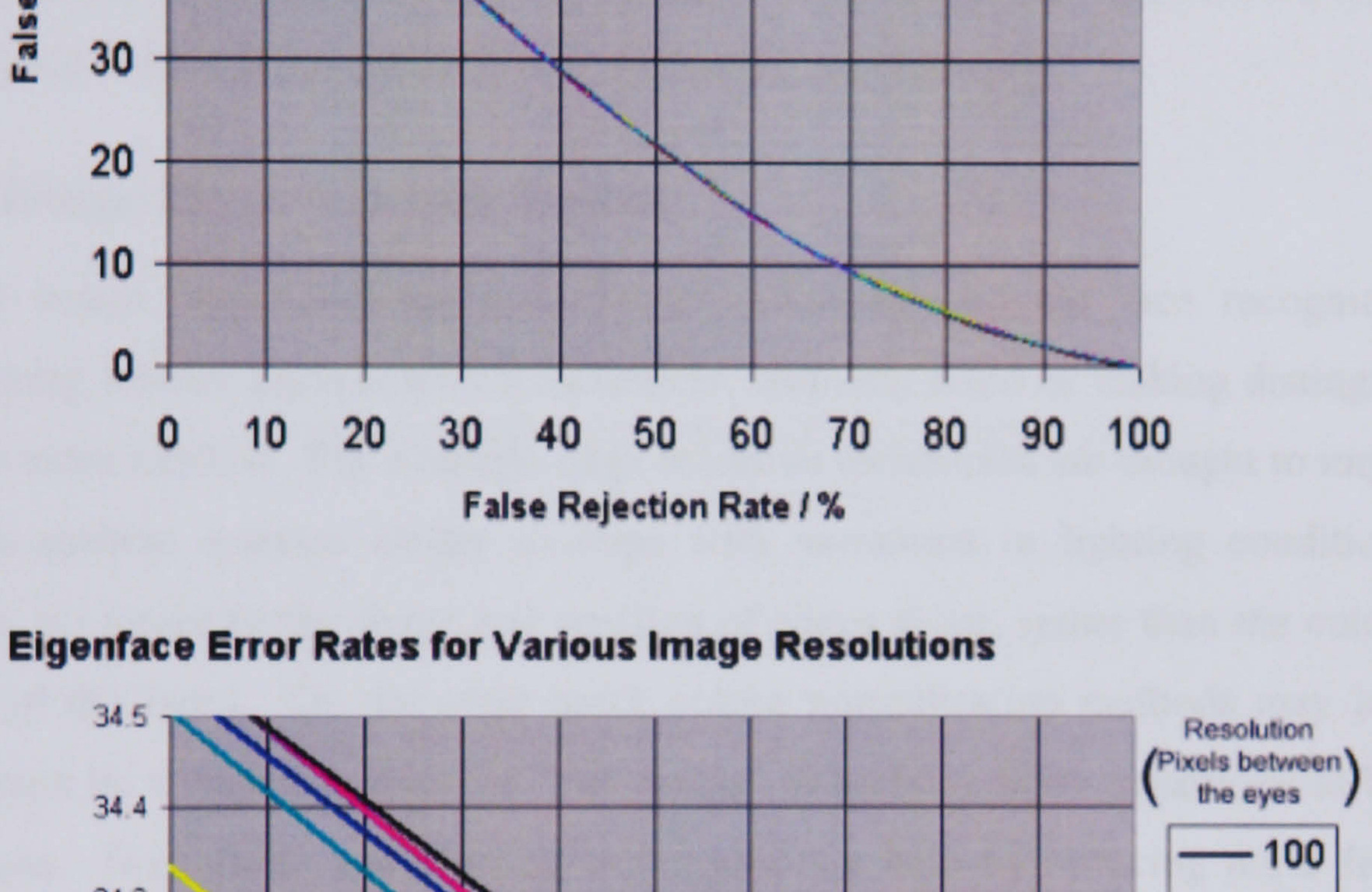

Figure 4-13 - Error rate curves for the 2D eigenface system, when applied to faces images of various resolutions. The graph on the right shows the region between 33.5% and 34.5% error rates of the graph on the left.

We find there is no significant change in the EER for resolutions of 100 pixels between the eyes down to just 10 pixels (from 34.1 percent, down to 33.9 percent). Even more surprising, is that the reduction in resolution appears to actually improve the system's performance (although only by a small degree). This may be due to the smoothing and noise reduction side effects of the sub-sampling algorithm. As a compromise between test execution time and some pre-processing techniques possibly working better with higher resolutions, we select 25 pixels distance between the eyes to conduct all further experiments. All images are scaled and rotated such that the centres of the eyes are aligned 25 pixels apart, using our eye detection algorithm (see section 4.1.1). Each image has a width and height of 75 and 112 pixels respectively.

4.3.3 Image Pre-processing Results

Various image pre-processing methods are often said to aid face recognition by normalising various environmental influences, reducing noise or making distinguishing features more explicit. For example edge detection techniques are thought to improve a face recognition systems ability to cope with variations in lighting conditions (by reducing an image to the shape and position of edges alone, rather than the colour and texture of the face). On the other hand, colour normalisation methods may improve recognition by trying to extract the 'true colour' of facial regions, regardless of lighting conditions. Smoothing and blurring techniques can help by reducing noise from the camera CCD and may also offer some resistance to small movements, rotations and expression changes.

All of these image pre-processing techniques produce very different effects on face images, and depending on the circumstances in which a system is expected to operate, may either help or hinder performance. What's more, there is surprisingly little literature exploring how image-processing effects differ across the three variations of appearance-based approaches discussed here. With such a variety of image processing methods and a variety of reasons why each may improve performance, we are motivated to test a large range of standard techniques.

Having tested the baseline eigenface system on raw image data and identified a suitable resolution at which to conduct further investigations, in order to ascertain the effects of image pre-processing, we now present results for a range of image processing

techniques, before applying PCA. Figure 4-14 shows the resulting images, after application of the various processing techniques described in detail in section 4.5.

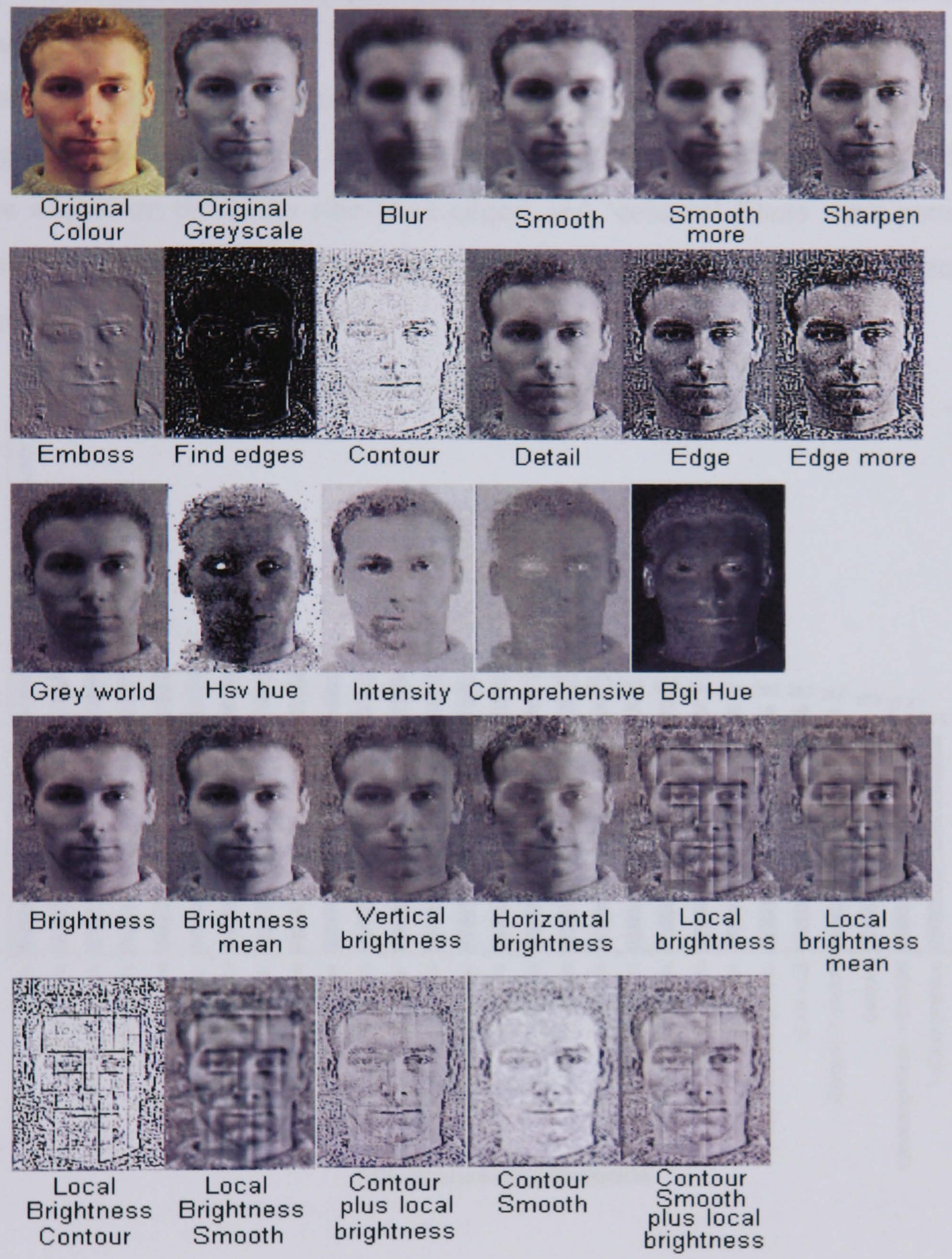

Figure 4-14 - Example results of the image pre-processing methods applied to a face image.

The recognition results produced by each system, using the range of processing methods, are presented as a bar chart of verification EERs (Figure 4-15). The baseline eigenface system (no image processing) is displayed in the chart as a dark red bar. It can be seen that the majority of image processing methods did produce some improvement to the eigenface system. However, what is surprising is the large increase

in error rates produce by some of the colour normalisation methods of image processing, most notably the BGI Hue introduced by Finlayson and Schaefer [33]. We believe that the reduction in effectiveness when using such methods is due to the loss of information during these procedures. Edges become less defined and some of the shading due to geometrical structure is lost (see Figure 4-14). An increase is also witnessed using the blurring filters, where one can easily see that structural information is being lost. It is therefore not surprising to see that the edge-enhancing methods had a positive impact on the EERs (the 'find edges' and 'contour' filters were particularly effective), as did the statistical methods, which normalise intensity moments (increasing the shading gradient in many areas).

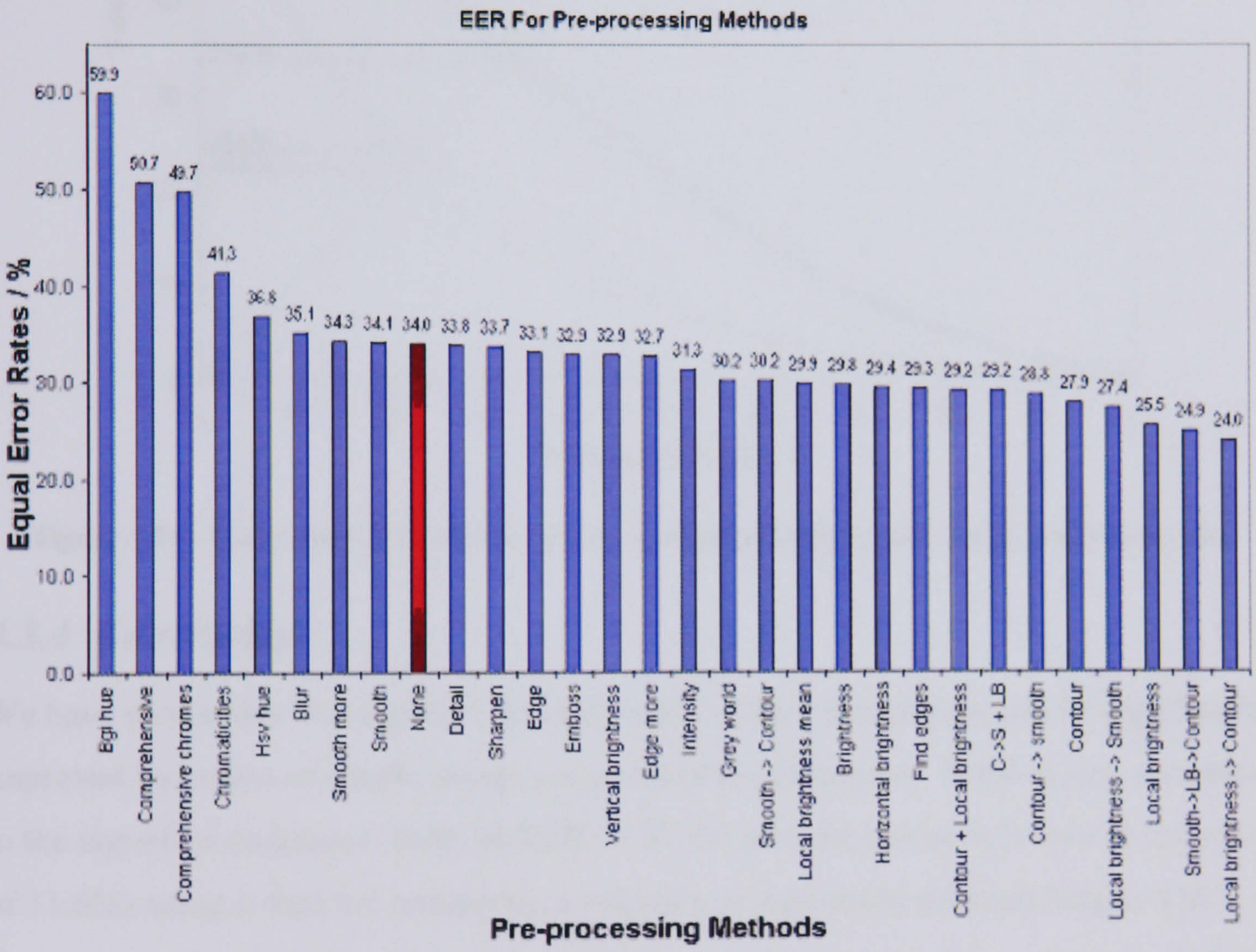

Figure 4-15 - EER Results for various image processing methods (13,380 verification operations).

Having identified the most successful image processing method of those evaluated, as normalising intensity moments within local regions of the image, then applying a convolution contour filter, we continue to improve the system by testing different cropping of images to find the optimum for this image processing method, reaching an EER of 22.4% (Figure 4-16).

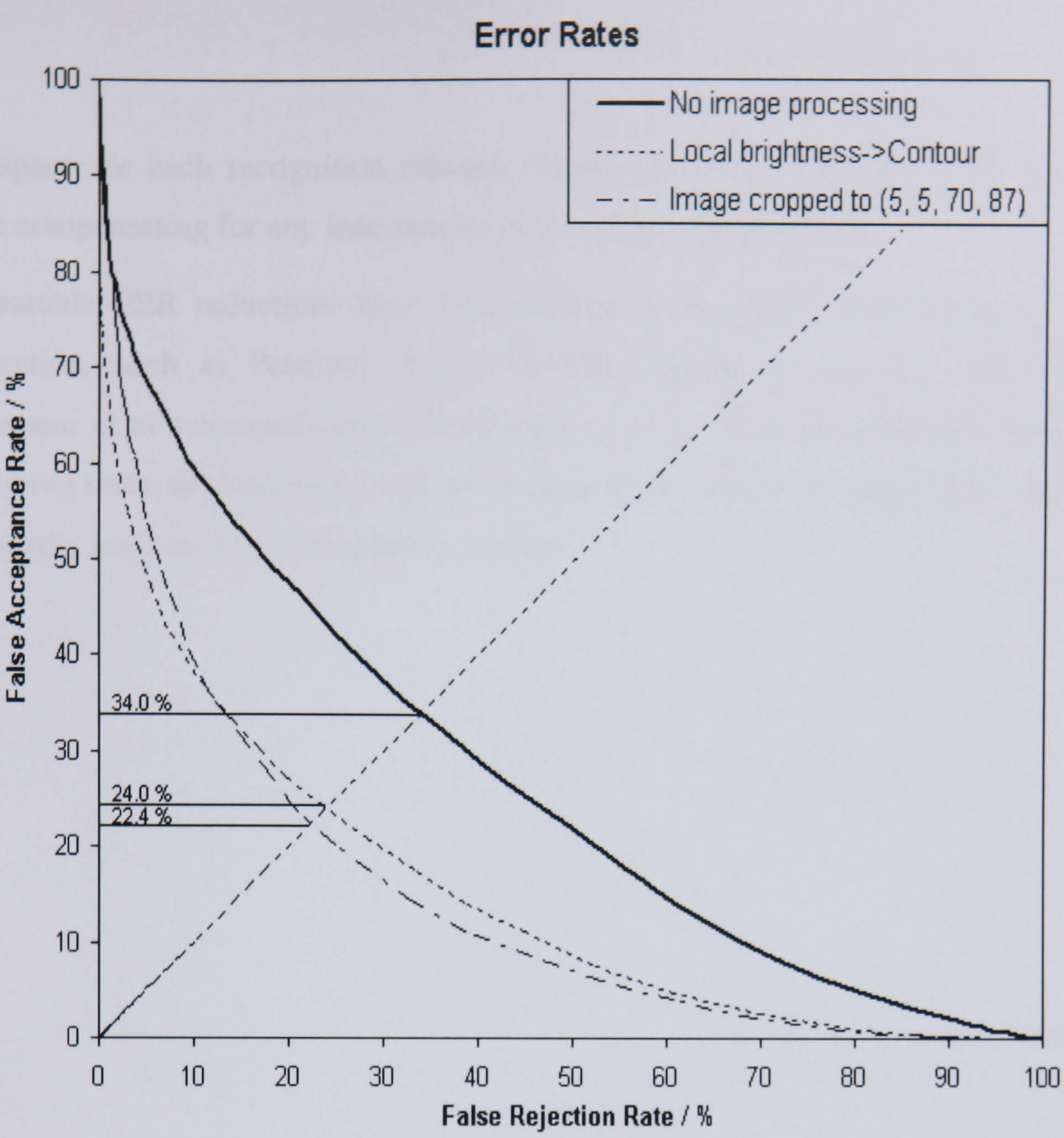

Figure 4-16 - Error rates for baseline system, most successful pre-processing and image crop

4.3.4 Conclusion

We have shown that the eigenface-based method of face recognition can be significantly improved by means of simple image pre-processing techniques. Without any alterations to the eigenface technique itself, an EER of 22.4% percent can be achieved (a reduction of 11.6%) using a data set containing a majority of extremely difficult images (20% of the images are partially obscured and 40% of the images have extreme lighting conditions).

There are some factors that may be the cause of the remaining 22.4% error, which were not compensated for by the image pre-processing techniques. Firstly, the eye detection algorithm was be no means perfect and although an attempt was made to manually correct any misaligned images, it is clear (from browsing the database) that some images are not aligned well. It would be relatively simple to implement a system in which several small translations and scales of the original image were projected into

face space for each recognition attempt (taking the lowest distance value returned), hence compensating for any inaccuracies in the alignment procedure.

Comparable EER reductions have been witnessed in similar PCA methods of face recognition, such as Pentland et al's modular eigenspace system [40] and in Belhumeur et al's comparison to Fisher faces [27]. It is likely that the image pre-processing methods described could be of similar benefit to these algorithms, and result in a greatly improved face recognition system.

4.4 The Fisherface Approach

The Fisherface method of face recognition as described by Belhumeur et al [27] uses both principal component analysis (PCA) and linear discriminant analysis (LDA) to compute an image subspace in which face image variance is maximised, similar to that used in the eigenface method. However, the Fisherface method is able to take advantage of 'within-class' information, minimising variation within each class relative to between-class class separation. To accomplish this we expand the training set to contain multiple images of each person, providing examples of how a person's face may change from one image to another due to variations in lighting conditions, facial expression and even small changes in orientation. We define the training set τ as,

$$\tau = \{X_1, X_2, ..., X_C\}$$
$$\text{where } X_n = \{\Gamma_1, \Gamma_2, \Gamma_3, ...\}$$

Equ. 4-4

Where Γ_i is a facial image and the training set is partitioned into c classes, such that all the images in each class X_i are of the same person and no single person is present in more than one class. We begin by computing three scatter matrices, representing the within-class (S_W), between-class (S_B) and total (S_T) distribution of the training set throughout image space.

$$S_T = \sum_{n=1}^{M} (\Gamma_n - \Psi)(\Gamma_n - \Psi)^T$$

$$S_B = \sum_{i=1}^{c} |X_i| (\Psi_i - \Psi)(\Psi_i - \Psi)^T \qquad S_W = \sum_{i=1}^{c} \sum_{x_k \in X_i} (x_k - \Psi_i)(x_k - \Psi_i)^T$$

Equ. 4-5

Where $\Psi = \frac{1}{M}\sum_{n=1}^{M}\Gamma_n$, is the average image vector of the entire training set, and $\Psi_i = \frac{1}{|X_i|}\sum_{\Gamma_i \in X_i}\Gamma_i$, the average of each individual class X_i (person). By performing PCA on the total scatter matrix S_t, and taking the top M-c principal components, we produce a projection matrix U_{pca}.

$$U_{pca} = \arg\max_{U} \left| U^T S_T U \right|$$

Equ. 4-6

This projection matrix is used to reduce the dimensionality of the within-class scatter matrix, ensuring it is non-singular, before computing the top *c-1* (in our case 59) eigenvectors of the reduced scatter matrices, U_{fld} as shown below.

$$U_{fld} = \arg\max_{U} \left(\frac{\left| U^T U_{pca}^T S_B U_{pca} U \right|}{\left| U^T U_{pca}^T S_W U_{pca} U \right|} \right) .$$

Equ. 4-7

Finally, the matrix U_{ff} is calculated as shown in Equ. 4-8, such that it will project a facial image into a reduced image space of *c-1* dimensions, in which the ratio of between-class scatter to within-class scatter is maximised for all *c* classes.

$$U_{ff} = U_{fld} U_{pca}$$

Equ. 4-8

Once the U_{ff} matrix has been constructed it is used in much the same way as the projection matrix in the eigenface system (see Equ. 4-3), reducing the dimensionality of the image vectors from 5330 to just 59 (*c-1*) elements. Again, like the eigenface system, the components of the projection matrix can be viewed as images, referred to as Fisherfaces.

Figure 4-17 - The first five Fisherfaces, defining a face space with no image pre-processing

4.5 Image Pre-processing Techniques

The problems caused by changes in lighting conditions have been well researched. Adini, Moses and Ullman suggest that often the differences between images of one face under different illumination conditions are greater than the differences between images of different faces under the same illumination conditions [26] . It has been attempted, with some success, to identify and compensate for the effect of lighting conditions in various face recognition systems. Zhao and Chellappa use a generic 3D surface of a face, together with a varying albedo reflectance model and a Lambertian physical reflectance model to compensate for both the lighting and head orientation [9], before applying a recognition system based on linear discriminant analysis. Much research has also been carried out to improve eigenface recognition systems. Cutler has shown that it can successfully be applied to infrared images [7], resulting in a much decreased error rate. This shows that an artificial infrared light source could be used to reduce the effect of external light sources, producing an accurate system for use in security applications such as site access. However, the use of such a light source is not always practical, particularly if the camera is far from the subject.

Pentland, Moghaddam and Starner extended their eigenface system to include multiple viewing angles of a persons face [40], improving the systems performance when applied to faces of various orientations. They also incorporate a modular eigenspace system [40], which significantly improves the overall performance, although it does not tackle the lighting problem directly. Belhumeur, Hespanha and Kreigman use Fisher's linear discriminant to capture the similarities between multiple images in each class (per person) [27], hoping to discount the variations due to lighting from the defined subspace. Their results show a significant improvement over the standard eigenface approach (from 20% to less than 2% error rate). However, as both the eigenface and Fisherface methods are both appearance-based approaches, it's likely that additional image processing could improve both methods. Although Adini, Moses and Ullman point out that there is no image representation that can be completely invariant to lighting conditions, they do show that different representations of images, on which lighting has less of an affect, can significantly reduce the difference between two images of the same face [26].

In this section we describe a range of image processing techniques that may affect the performance of the two-dimensional appearance-based methods of face recognition described in this chapter. The set of image processing techniques consist of well-known image manipulation routines, altering image brightness, contrast and colour. Note that the terms intensity, brightness and lightness are often used interchangeably, although intensity generally refers to the actual value of an individual pixel colour component, whereas brightness and lightness describe a more global characteristic of the whole image.

We separate the methods in four categories: Colour normalisation, statistical methods, convolution and method combinations. For each technique we present the average face image, a visual representation of the discriminant value for each pixel and the first five eigenvectors, as can be seen below for the original image with no pre-processing.

Figure 4-18 - No image processing

4.5.1 Colour Normalisation Methods

Intensity

We use a well-known image intensity normalisation method, in which we assume that, as the intensity of the lighting source increases by a factor, each RGB component of each pixel in the image is scaled by the same factor. We remove the effect of this intensity factor by dividing by the sum of the three colour components according to Equ. 4-9.

$$(r_{norm}, g_{norm}, b_{norm}) = \left(\frac{r}{r+g+b}, \frac{g}{r+g+b}, \frac{b}{r+g+b} \right)$$

Equ. 4-9

Since the pixels of the resulting image have equal intensity, summing the three colour channels would result in a blank image. Therefore, to create an image with single scalar values for each pixel (creating the one dimensional image vector as required by our

PCA and LDA systems) we can either take a single colour channel, or sum just the red and green components (the chromaticities, effectively the inversion of the blue component).

Figure 4-19 - Blue component of intensity normalisation (Intensity)

Figure 4-20 - Sum of red and green components (Chromaticities)

Grey world

Here we take a similar approach to the above normalisation, but compensating for the effect of variations in the colour of the light source. Different colours of light cause the RGB colour components of an image to scale apart, by factors α, β and γ respectively, $(r_{new}, g_{new}, b_{new}) = (\alpha r, \beta g, \gamma b)$, which can then be normalised using the equation below, where N is the number of pixels in the image and r, g and b are the intensity values of the red, green and blue colour components respectively.

$$(r_{norm}, g_{norm}, b_{norm}) = \left(\frac{Nr}{r_1 + r_2 + \ldots + r_N}, \frac{Ng}{g_1 + g_2 + \ldots + g_N}, \frac{Nb}{b_1 + b_2 + \ldots + b_N} \right)$$

Equ. 4-10

Figure 4-21 - Grey world normalisation

Comprehensive

We use an algorithm proposed by Finlayson [34], which normalises an image for variations in both lighting geometry and illumination colour. The method involves the repetition of intensity normalisation followed by grey world normalisation (as described above), until the resulting image reaches a stable state (i.e. the change in pixel values from one cycle to another is sufficiently small).

Figure 4-22 - Blue component of comprehensive normalisation (Comprehensive)

Figure 4-23 - Sum of the red and green components of a comprehensive normalised image (Comprehensive chromes)

Finlayson shows that any two images of a scene taken under varying light colours and intensities will iterate down to the same pixel values. In practice this usually occurs within five or six iterations. Again, to create a one-dimensional vector we either take the blue component or sum the red and green components.

Hsv hue

The hue of an image is calculated using the standard hue definition, such that each pixel is represented by a single scalar value *H*, as shown in Equ. 4-11.

$$H = \cos^{-1}\left(\frac{\frac{1}{2}\left[(r-g)+(r-b)\right]}{\sqrt{(r-g)(r-g)+(r-b)(g-b)}}\right)$$

Equ. 4-11

Hue is often described as perceptual colour irrespective of lightness or saturation. Therefore, this representation may have beneficial effects in normalising skin tone and hair colour.

Figure 4-24 - Image hue

Bgi hue

Finlayson and Schaefer introduce a definition of hue that is invariant to brightness (the scaling of each colour channel by a constant factor) and gamma (raising the colour channels to a constant power) [33] , which are often caused by variations in scene environment and capture equipment.

$$H = \tan^{-1} \frac{\log(r) - \log(g)}{\log(r) + \log(g) - 2\log(b)}$$

Equ. 4-12

Figure 4-25 - Brightness and gamma invariant hue

4.5.2 Statistical Methods

We introduce some statistical methods that apply transformations to the image intensity values in order to make the brightness and contrast constant for all images. The effect is that every image appears to be equally as bright (as a whole) and span across an equal range of brightness.

These statistical methods can be applied in a number of ways, mainly by varying the areas of the image from which the statistics are gathered. It is not necessarily the case that lighting conditions will be the same at all points on the face, as the face itself can cast shadows. Therefore, in order to compensate for the variations in lighting conditions across a single face, we can apply these methods to individual regions of the face. This means that, we are not only compensating for a difference in lighting conditions from one image to another, but also for different lighting conditions from one area of the face to another.

Brightness

Global transformation of brightness, such that intensity moments are normalised. The mean and standard deviation of pixel intensity is calculated. Each pixel is then multiplied and offset, such that the resultant mean and standard deviation become specific set values.

Figure 4-26 - Normalised intensity moments (Brightness)

Brightness mean

Global transformation of brightness, such that the intensity mean becomes a constant specified value. The difference between the average pixel intensity and a specific set brightness value is used as an offset to adjust image brightness, without altering the intensity deviation.

Figure 4-27 - Normalised image brightness (Brightness mean)

Horizontal brightness

Application of the brightness method to individual rows of pixels. Effectively normalising each horizontal row independently. This technique will help to compensate for variations in brightness levels between the upper and lower facial regions (caused by overhead lighting for example).

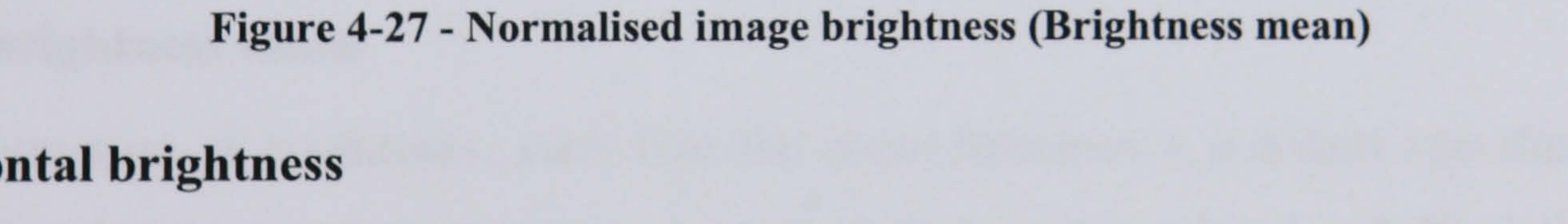

Figure 4-28 - Normalisation of intensity moments of pixel rows (Horizontal brightness)

Vertical brightness

Application of the brightness method to individual columns of pixels. Like the horizontal brightness technique, this method can account for varying lighting levels from the left to the right side of the face.

Figure 4-29 - Normalisation of intensity moments of pixel columns (Vertical brightness)

Local brightness

Application of brightness method to individual local regions of an image. Following a similar line of reasoning to the horizontal brightness and vertical brightness techniques, we apply brightness normalisation to smaller regions of the face. This allows for all regions to be normalised to mid-level intensity values with even deviation, regardless of the lighting levels incident on other areas of the facial surface.

Figure 4-30 - Normalisation of intensity moments of individual local regions (Local brightness)

Local brightness mean

Transformation of brightness, such that the mean becomes a constant specified value within local regions of the image. Again, similar to the reasoning behind the local brightness technique, but this method does not normalise the intensity deviation.

Figure 4-31 - Normalisation of pixel brightness for individual local regions (Local brightness mean)

4.5.3 Convolution Methods

Convolution methods involve the application of a small template to a window, moved step-by-step, over the original image. These templates can be configured to enhance or suppress features, reduce noise and extract edges. Each filtering techniques is described below, with the filter kernel template shown on the left of the example images for each technique.

Smooth

Standard low-pass filtering using a 3x3 pixel template, with an σ value of 0.788.

1 1 1

1 5 1

1 1 1

Figure 4-32 - Smooth filtering

Smooth more

Similar to the above, only with a larger 5x5 pixel neighbourhood and a σ value of 1.028.

1 1 1 1 1

1 5 5 5 1

1 5 44 5 1

1 5 5 5 1

1 1 1 1 1

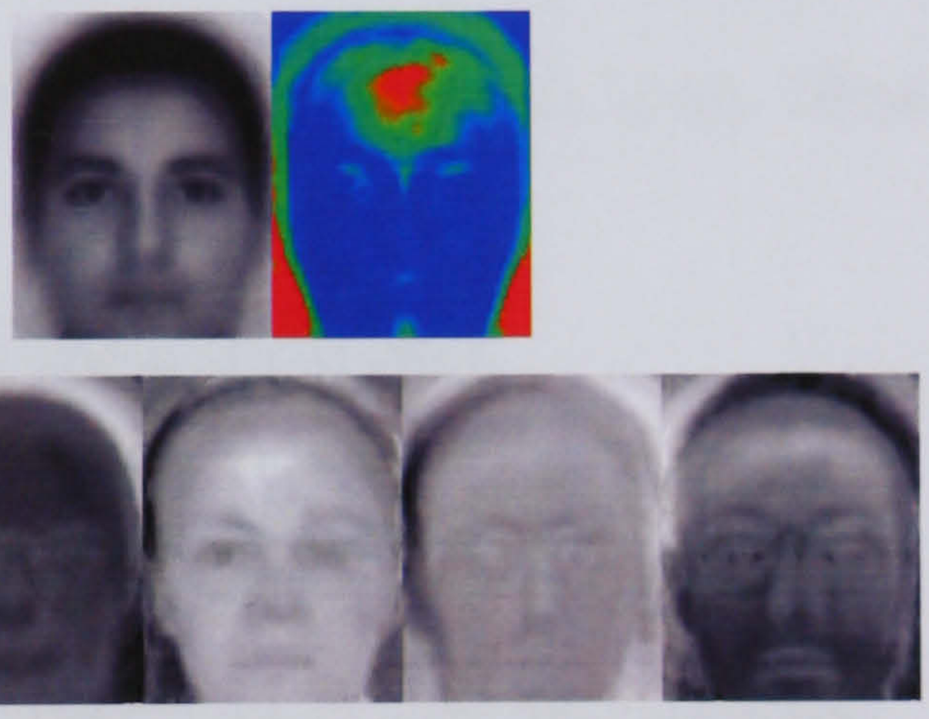

Figure 4-33 - Application of the 'smooth more' image filter

Blur

An extreme blurring effect using a large 5x5 template.

1 1 1 1 1

1 0 0 0 1

1 0 0 0 1

1 0 0 0 1

1 1 1 1 1

Figure 4-34 - Application of the 'blur' image filter

Edge

Enhances the edges of an image using a 3x3 template.

-1 -1 -1

-1 10 -1

-1 -1 -1

Figure 4-35 - Application of the 'edge' image filter

Edge more

Same as the above only with less prominence on the centre pixel, hence creating a greater amplification of edge boundaries.

-1 -1 -1

-1 9 -1

-1 -1 -1

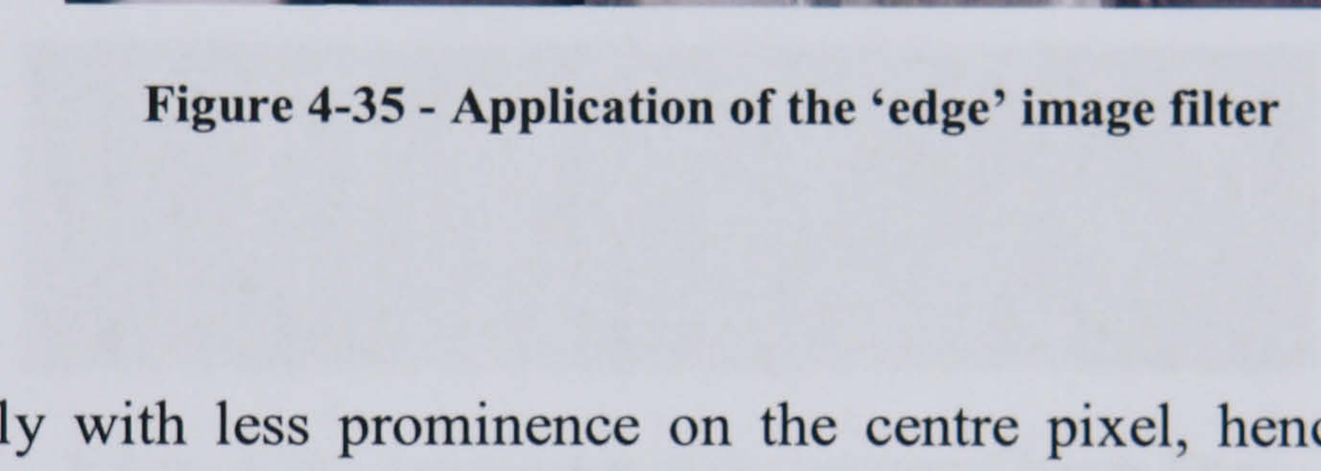

Figure 4-36 - Application of the 'Edge more' image filter

Find edges

Application of a 3x3 edge enhancement template, followed by a threshold to segment an image to include only those pixels that lie on strong edge boundaries.

-1 -1 -1

-1 8 -1

-1 -1 -1

Figure 4-37 - Application of the 'find edges' image filter

Contour

Similar to Find edges, only more sensitive to changes in contrast.

-1 -1 -1

-1 8 -1

-1 -1 -1

Figure 4-38 - Application of the 'contour' image filter

Detail

Enhance areas of high contrast using a 3x3 template.

0 -1 0

-1 10 -1

0 -1 0

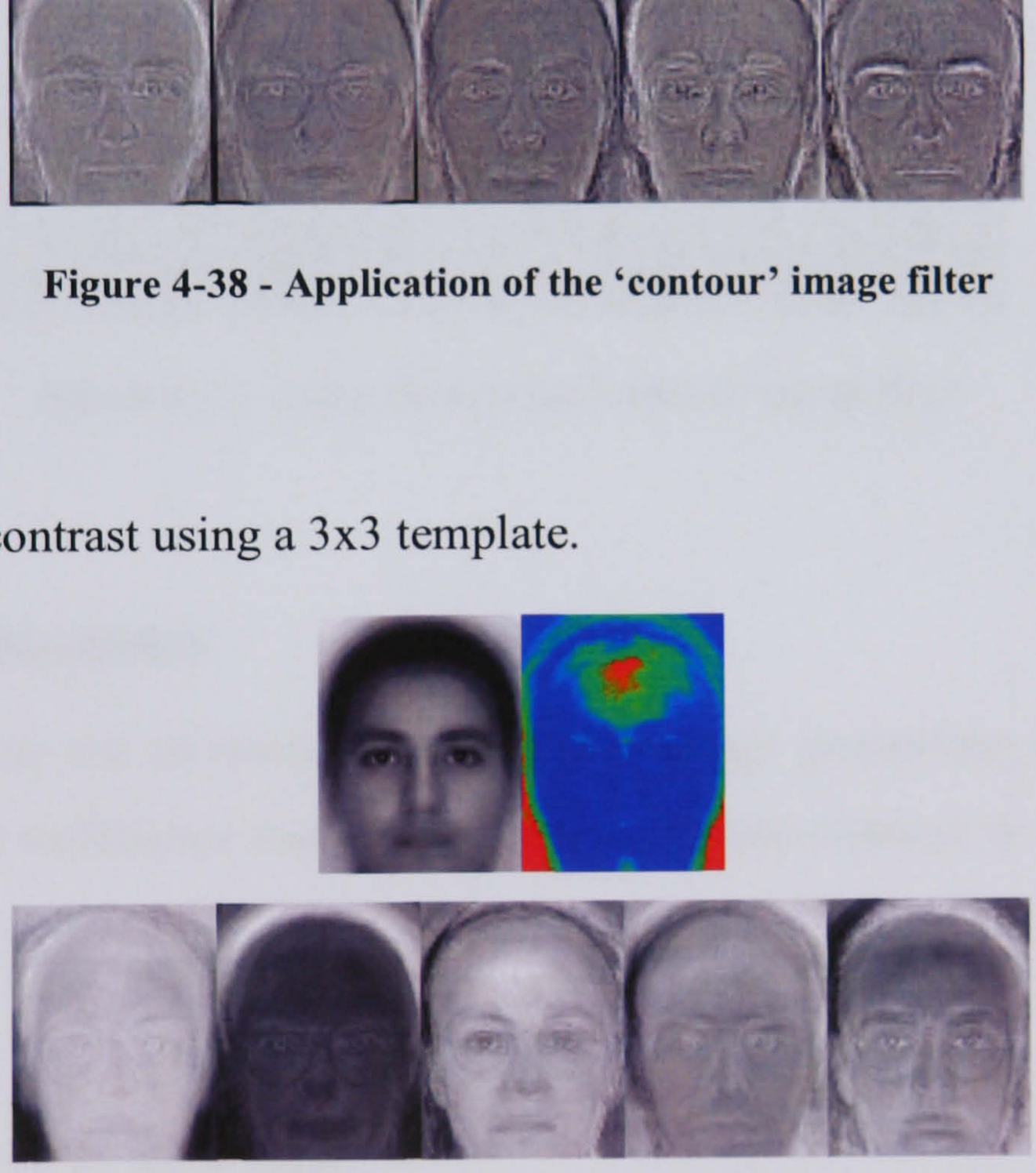

Figure 4-39 - Application of the 'detail' image filter

Sharpen

Reduces image blur by application of a 3x3 template.

-2 -2 -2

-2 32 -2

-2 -2 -2

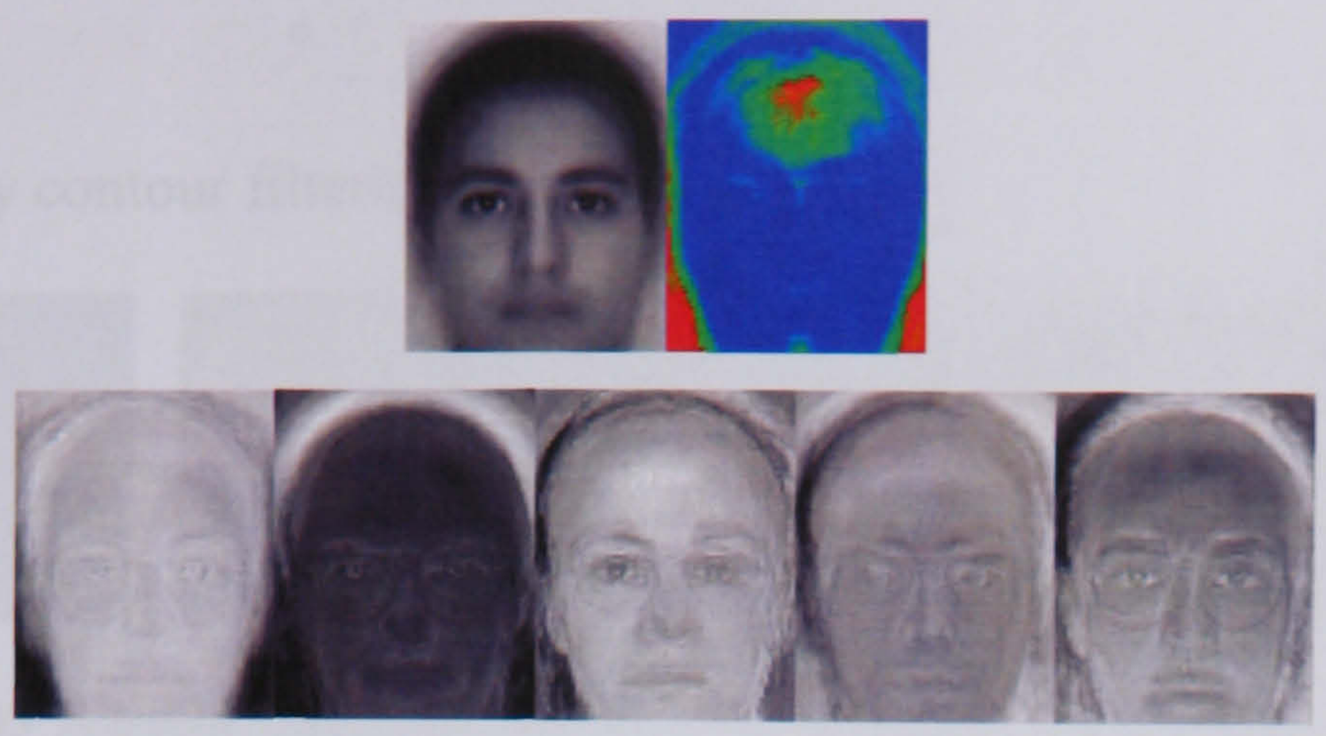

Figure 4-40 - Application of the 'sharpen' image filter

Emboss

A simple derivative filter that enhances edges with a shadow casting affect.

-1 0 0

0 1 0

0 0 0

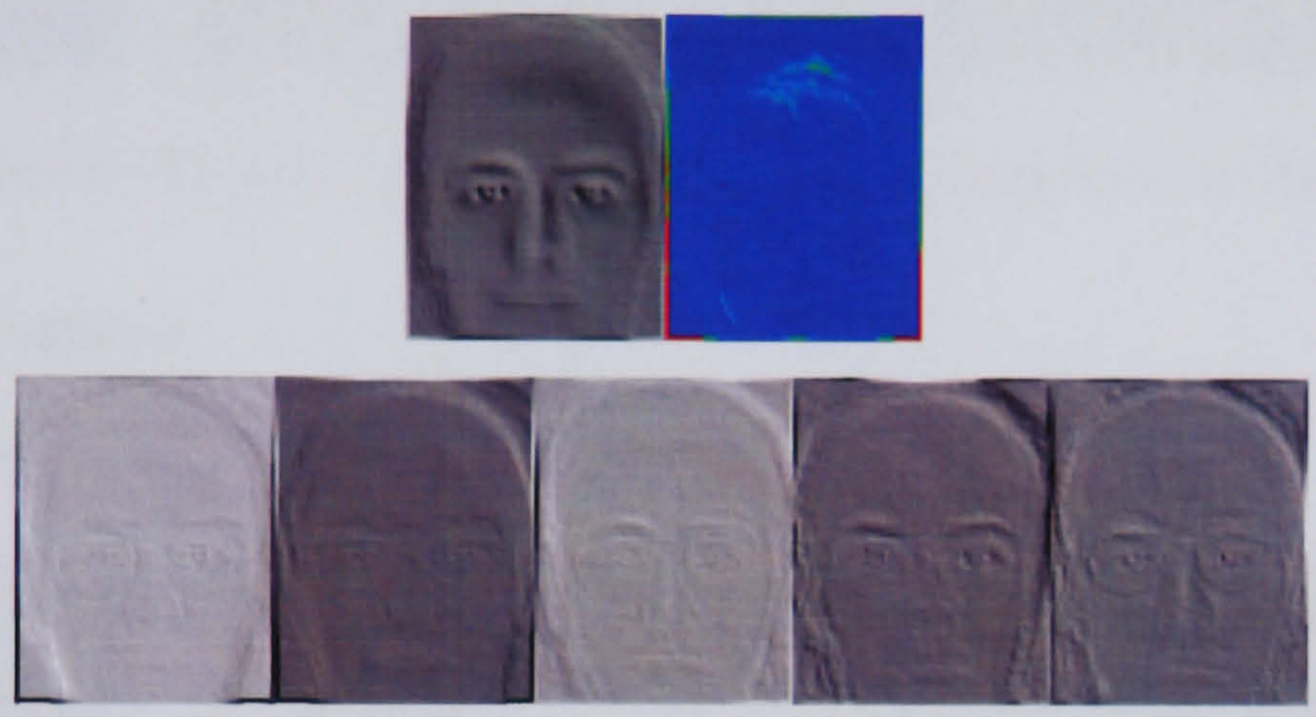

Figure 4-41- Application of the 'emboss' image filter

4.5.4 Method Combinations

In an attempt to capture the advantages of multiple image processing methods, we combine some of those techniques that produce the best improvement in EER (Figure 4-15).

Contour -> Smooth

Contour filtering followed by smoothing.

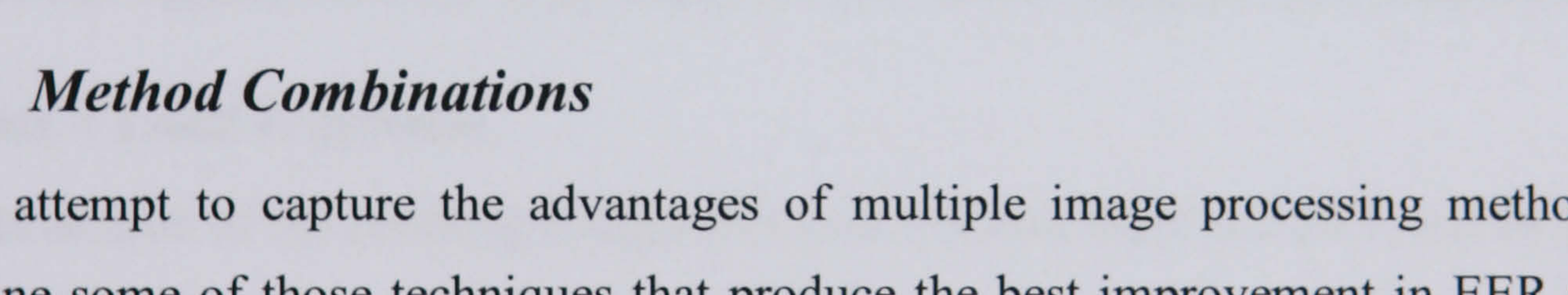

Figure 4-42 Application of the 'contour' and 'smooth' image filters

Smooth->Contour

Smoothing followed by contour filtering.

Figure 4-43 Application of the 'smooth' and 'contour' image filters.

Local brightness -> Smooth

Local brightness transformation followed by smoothing.

Figure 4-44 Application of the 'local brightness' and 'smooth' image processing techniques

Local brightness -> Contour

Local brightness transformation followed by contour filtering.

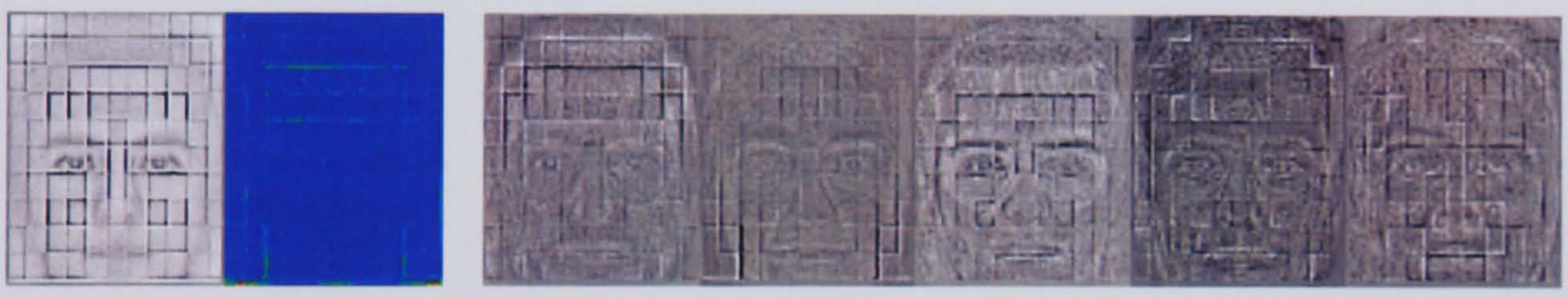

Figure 4-45 Application of the 'local brightness' and 'contour' image pre-processing techniques

Contour + Local brightness

The summation of the resulting images from the Contour filter and the Local Brightness transformation.

Figure 4-46 Summation of the 'contour' and 'local brightness' image pre-processing techniques

C->S + LB

Contour filtering followed by smoothing, summed with the Local Brightness transformation.

Figure 4-47 Application of the 'contour' and 'smooth' image filters summed with the 'local brightness' transformation

S->LB->C

Smoothing followed by the Local Brightness transformation, followed by Contour filtering.

Figure 4-48 Application of 'smooth', 'local brightness' and 'contour' image pre-processing

4.6 Improving and Comparing 2D Face Recognition

In this section we apply the three appearance-based face recognition methods described in sections 4.2, 4.3 and 4.4, to a common test set. We pre-process the images prior to training and testing using one of the image processing techniques described in section 4.5 and compare the resulting error rates with those produced by using no pre-processing.

We conduct experiments using a database of 960 bitmap images of 120 individuals (60 male, 60 female) of various race and age, extracted from the AR Face Database provided by Martinez and Benavente [39]. The database is separated into two disjoint sets: i) The training set, containing 240 images of 60 people under a range of lighting conditions and facial expressions; ii) the test set containing 720 images (60 people of various gender, race and age, 12 images each). The six examples shown in Table 4-2 were repeated on two days, making up the 12 images of each subject in the test set. All the images are pre-aligned with the centres of the eyes 25 pixels apart. Each image is cropped to a width and height of 65 and 82 pixels respectively.

Lighting	Natural	Left	Right	Both	Natural	Natural
Expression	Neutral	Neutral	Neutral	Neutral	Happy	Angry
Example						

Table 4-2. Image capture conditions included in the database test set.

4.6.1 Test Procedure

Effectiveness of the face recognition methods is evaluated using error rate curves (FRR against FAR) for the verification operation. The 720 images in the test set are compared with every other image using one of the face recognition methods, producing a distance value for each comparison. No image is compared with itself and each pair is compared only once (the relationship is symmetric). A threshold is applied in order to derive the rejection/acceptance decision. Hence, each FRR (percentage of incorrect rejections), and FAR (percentage of incorrect acceptances) pair is calculated from 258,840 verification operations. By varying the threshold we produce a set of FRR FAR plots,

forming the error rate curve, as shown in Figure 4-49. We then take the EER (point at which FRR equals FAR) as a single comparative value.

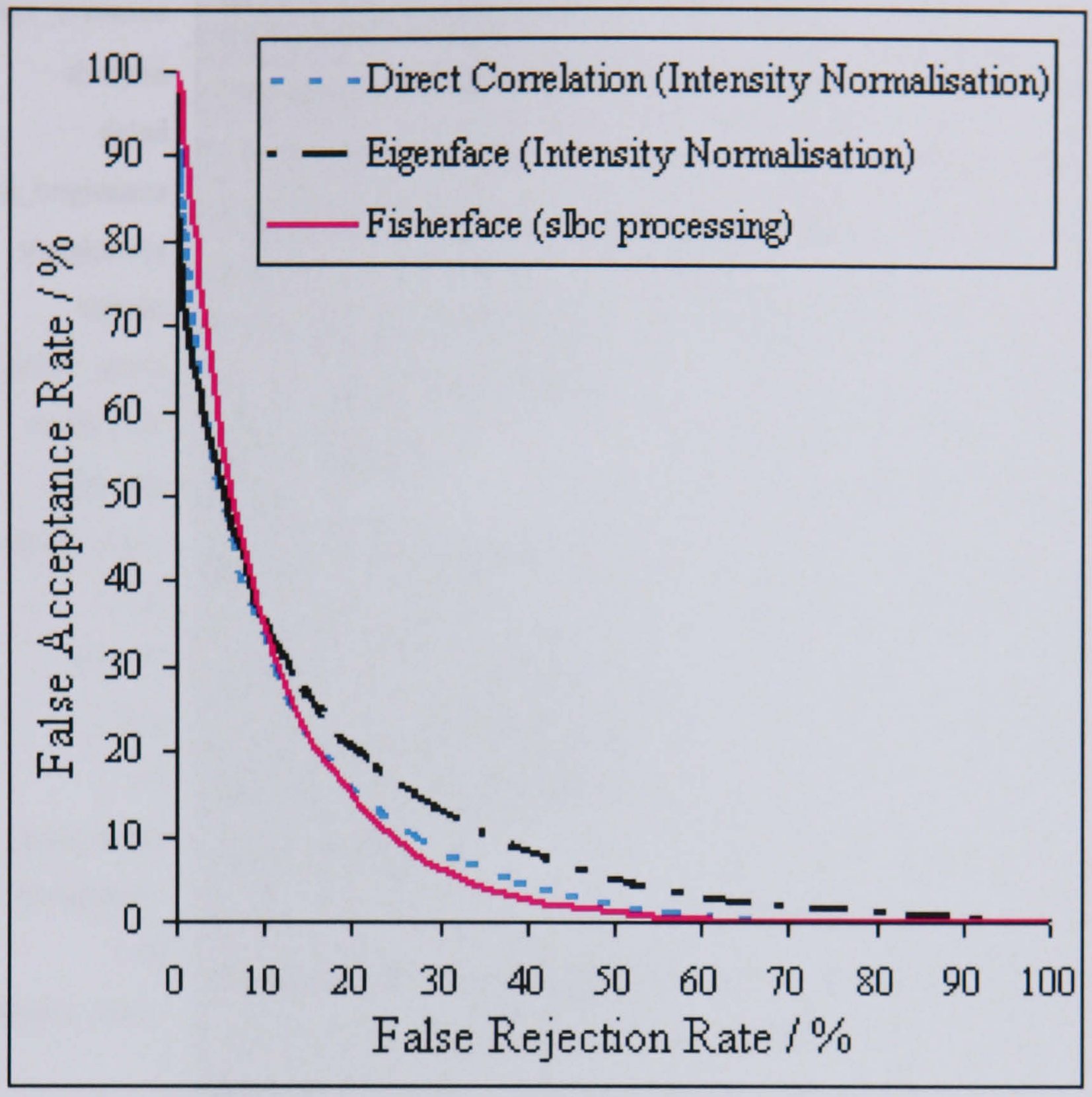

Figure 4-49 Error Rates of face recognition methods using the best performing image pre-processing techniques

Having tested the full range of image pre-processing techniques, we present the EERs in Figure 4-50, identifying the best performing image processing techniques for each of the three face recognition methods. Both the direct correlation and eigenface methods perform best when used with intensity normalisation, achieving an EER of 18.0% and 20.4% respectively. The Fisherface method achieves the lowest EER of 17.8%, when used with the "slbc" pre-processing technique.

We also see that only a slight improvement is gained by the Fisherface method, from 20.1% to 17.8% EER, whereas direct correlation has a much more significant improvement, from 25.1% down to 18.0%. In fact, when using the best image pre-processing technique the Fisherface method is only marginally better than direct correlation, although it still maintains the advantage of a reduced processing time, due to the shorter length of the projected image vectors.

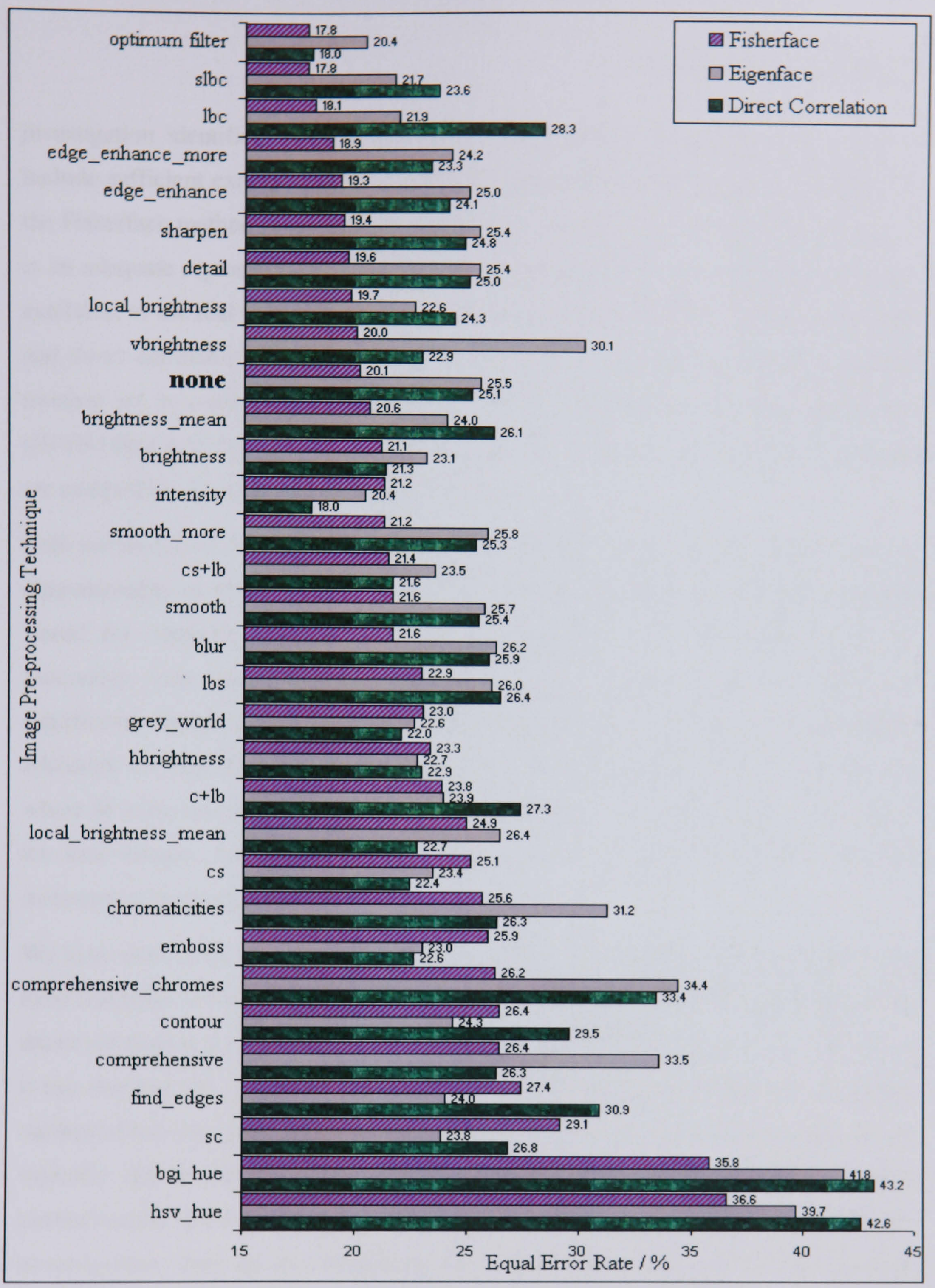

Figure 4-50 Equal Error Rates of face recognition methods used with a range of image pre-processing techniques

4.6.2 Conclusion

Initial comparison of the baseline systems produced results that are contradictory to other experiments carried out on the eigenface and Fisherface methods [27]. Further

investigation identified that the training set used for the Fisherface method did not include sufficient examples of all conditions represented in the test data. In order for the Fisherface method to perform recognition effectively, it is vital that the training set is an adequate representation of the real application data. If such training data is not available, or the real world image capture conditions cannot be predicted, the eigenface and direct correlation methods are a better alternative. However, providing a suitable training set is available, the Fisherface method has significantly lower error rates (20.1%) than both the eigenface (25.5%) and direct correlation methods (25.1%), which are comparable in terms of recognition accuracy.

Both methods have a space and time complexity of the same order, O(*ni*), where *n* is the dimensionality of the face key data (or pixels in the image) and *i* the number of images stored for comparison. However, with image vectors of 5330 elements (*n*), the processing time and storage requirements of the direct correlation method are significantly higher than the eigenface method, which uses vectors of only 59 elements. Although the eigenface method has the additional training time of PCA, $O(Mn^2+n^3)$, where *M* is the number of items in the training set and *n* the dimensionality (pixels) of the face images, the increased complexity at training is usually preferred over the increased recognition time.

We have shown that the use of image pre-processing is able to significantly improve all three methods of face recognition, reducing the EER of the eigenface, Fisherface and direct correlation methods by 2.3, 5.1 and 7.1 percentage points respectively. However, it has also become apparent that different image pre-processing techniques affect each method of face recognition differently. Although some image processing techniques are typically detrimental (blurring, smoothing, hue representations and comprehensive normalisation) and others are generally beneficial (slbc, sharpen, detail, edge enhance) to recognition, there are also techniques that will decrease error rates for some methods while increasing error rates for others. The most prominent example of this is intensity normalisation, which is evidently the best technique for both direct correlation and eigenface methods, yet increases the EER for the Fisherface method.

This result suggests that although intensity normalisation is able to improve system performance (supposedly by normalising lighting conditions), the LDA applied in the Fisherface method is able to make better use of the non-normalised data. Therefore, it must either be the case the intensity normalisation removes information that is useful for

recognition (and utilised by the Fisherface method) or that the Fisherface method is able to compensate for lighting variation more effectively than the intensity normalisation algorithm.

Taking the best image pre-processing technique shows that the Fisherface method has the lowest EER (17.8%), yet its lead over the other two methods is considerably reduced. In this case, although much more computationally efficient, it is only marginally better than direct correlation (EER 18.0%), but still maintains a significant improvement over the eigenface method (EER 20.4%).

Further experimentation is required in order to identify which specific features are enhanced by which pre-processing method and in what circumstances a given pre-processing method is most effective. In addition, it may be the case that using a different number of principal components will reduce error rates further, but this may also be dependent on the pre-processing method used.

5 Three-Dimensional Face Recognition

Despite significant advances in face recognition technology, it has yet to achieve the levels of accuracy required for many commercial and industrial applications. This is mainly due to the inaccuracies caused by the environmental circumstances under which images are captured. Variation in lighting, facial expression and orientation all significantly increase error rates, making it necessary to maintain consistent conditions between query and gallery images for the system to function adequately. However, this approach eliminates some of the key advantages offered by face recognition: a passive biometric in the sense that it does not require subject co-operation.

The use of 3D face models is motivated by a number of factors. Firstly, by relying purely on geometric shape, rather than colour and texture information, we render the system invariant to lighting conditions. Secondly, the ability to rotate a facial structure in 3D space, allowing for compensation of variations in pose, aids those methods requiring alignment prior to recognition. Finally, the additional discriminatory depth information in the facial surface structure, not available from two-dimensional images, provides supplementary cues for recognition. As an example, eye separation can be recovered from both sets of data, but nose depth can only easily be recovered from 3D data. We do recognise however, that two-dimensional colour-texture information provides a rich source of discriminatory information, which is forfeit if 3D data alone is used. Therefore, the focus here is to first determine the ability of 3D data alone to form the basis of a face recognition system, as compared to 2D systems. Additional research can then identify methods of reintroducing normalised two-dimensional texture data in order to reduce error rates further (see chapter 7.4).

We investigate the use of facial surface data, taken from 3D face models, as a substitute for the more familiar two-dimensional images. In section 5.1 and 5.2 we discuss the 3D face models used in systems development and how we achieve model alignment prior to analysis and recognition. We then begin to explore 3D face recognition as we began with 2D systems in section 4, using the simplest of recognition approaches: the direct correlation method. In section 5.5 we continue the research pattern applied to 2D face recognition, by taking the well-known eigenface method of face recognition, introduced

by Turk and Pentland [48] and adapt it for use on 3D data. Testing a range of surface representations and distance metrics, we identify the most effective methods of recognising faces using 3D surface structure. This experimentation is then extended to use Linear Discriminant Analysis in section 5.6, before introducing a completely novel approach (section 5.7), as a product of the experience gained from application of the previous methodologies.

5.1 3D Face Models

In order to evaluate and experiment with methods of 3D face recognition, we require a large database of 3D face models. However, until recently, 3D capture methods have been slow and cumbersome, requiring the subject to remain perfectly still. For these reasons, 3D face recognition has remained relatively unexplored, when compared to the wealth of research focusing on two-dimensional face recognition. Although some investigations have experimented with 3D data, [3] [4][5][6][7][8] they have had to rely on small test sets of 3D face models or used generic face models to enhance two-dimensional images prior to recognition [9][10][11]. However, this research demonstrates that the use of 3D information has the potential to improve face recognition well beyond the current state of the art. With the emergence of new 3D capture equipment, the population of a large 3D face database has now become viable. Therefore, we have undertaken a project at The University of York to provide a database of over five thousand 3D face models to facilitate research into 3D face recognition technology [50]. The following section contains extracts from the requirement specification used for acquisition of the 3D face database.

5.1.1 Data Acquisition

In this section we discuss the specifications of a database of 3D face models, intended for use by Cybula Ltd, The University of York Computer Science, Electronics and Psychology Departments. The University of York 3D Face Database (UOY3DFD) will be used to facilitate research into such fields as automated face recognition, facial image encoding and human facial perception. All data collected will be owned and managed by Cybula Ltd. and made freely available to the other participants (mentioned above) for academic research. It is intended that other researchers and companies will also be granted access to the data for free or otherwise, if agreed by Cybula Ltd.

Multiple 3D models of each person are captured and stored in the Wavefront OBJ file format [63] while corresponding texture images are stored in the bitmap file format. The database is separated into two disjoint subsets:

- Set A is included to provide fast and efficient database population, incorporating only the 15 most desired capture conditions.
- Set B is intended to provide some flexibility to the data acquisition procedure. It has the option of containing a fewer or greater number of models per person. This allows for more in-depth investigations or capture sessions that may arise at exhibitions and conferences, where we would be unable to capture all the models required in Set A, but could take the opportunity to capture just a couple of models per person.

Software was written to facilitate a highly automated acquisition procedure for data Set A. This software provides an electronic form to be filled out prior to each subject model set acquisition. The information gathered is stored in a text file alongside each 3D model and corresponding texture image. Face models are captured in a specific order (following a predetermined script of capture conditions), as prompted by the acquisition software. A consent agreement form was signed by each subject, prior to any image acquisition. Files are automatically named and stored according to the criteria described in Appendix I and II. The following information is stored about each subject:

- Gender
- Ethnicity
- Date of birth
- Age
- External features present
- Whether or not permission has been given by the subject to reproduce their image in publications.

5.1.2 Capture Conditions

The database represents a range of age, gender, race and external features under a range of controlled capture conditions, accepting the following limitations:

- The majority of subjects will be within the 18 to 60 years age range.
- We aim for an equal number of male and female subjects, although in the interest of data quantity, some majority will be acceptable.
- For diversity of race we will initially rely on the diversity of the natural population. However, should it be decided that a suitable representation has not been obtained additional capture sessions will be undertaken.
- To capture 3D models of subjects with beards, glasses and other external features, we will rely on the diversity of natural population and presence of these features will be recorded in the database.
- No effort will be made to control lighting conditions other than ensuring that lighting levels are within the operating capabilities of the 3D camera.

In order to generate face models at various head orientations, subjects were asked to face reference points positioned roughly 45° above, below, to the left and right of the camera, but no effort was made to enforce a precise angle of orientation.

Data Set A Standard data set. Specified to encourage consistency of useful capture conditions. Limited number of conditions to reduce capture time and increase throughput.	
ID	Description
01	Front facing, neutral expression, optimum distance from camera (1.7m from unit to nose tip)
02	Neutral expression, (whole body) facing roughly 45 degrees left
03	Neutral expression, (whole body) left side profile (90 degrees left)
04	Neutral expression, (whole body) facing roughly 45 degrees right.
05	Neutral expression, (whole body) right side profile (90 degrees right)
06	Neutral expression, facing roughly 45 degrees up.
07	Neutral expression, facing roughly 45 degrees down.
08	Front facing, smiling.

09	Front facing, eyes closed.
10	Front facing, angry expression.
11	Front facing, neutral expression.
12	Front facing, eyebrows raised.
13	Front facing, mouth slightly parted.
14	Front facing, neutral expression, no glasses.
15	Front facing, neutral expression, no glasses. further away from the camera (1.9m from unit to nose tip).

Table 5-1 All image capture conditions included in the UOY 3D Face Database.

Data Set B
Flexible data set. Specified to allow a broader range of capture conditions or data acquisition sessions with very limited time and resources.
Set B is comprised of any conditions described in Set A. At least two models of each person must be captured, but there is no limit on the maximum number of models per person. In addition to the conditions described in Set A, additional conditions may be included, in which case the condition details are recorded.

Table 5-2 Definition of data set B of the UOY 3D Face Database.

5.1.3 3D Face Data

In this section we now discuss the nature of the 3D face models being used in these experiments. We describe the 3D-face model structure, multiple representations and limitations in terms of resolution, noise and precision.

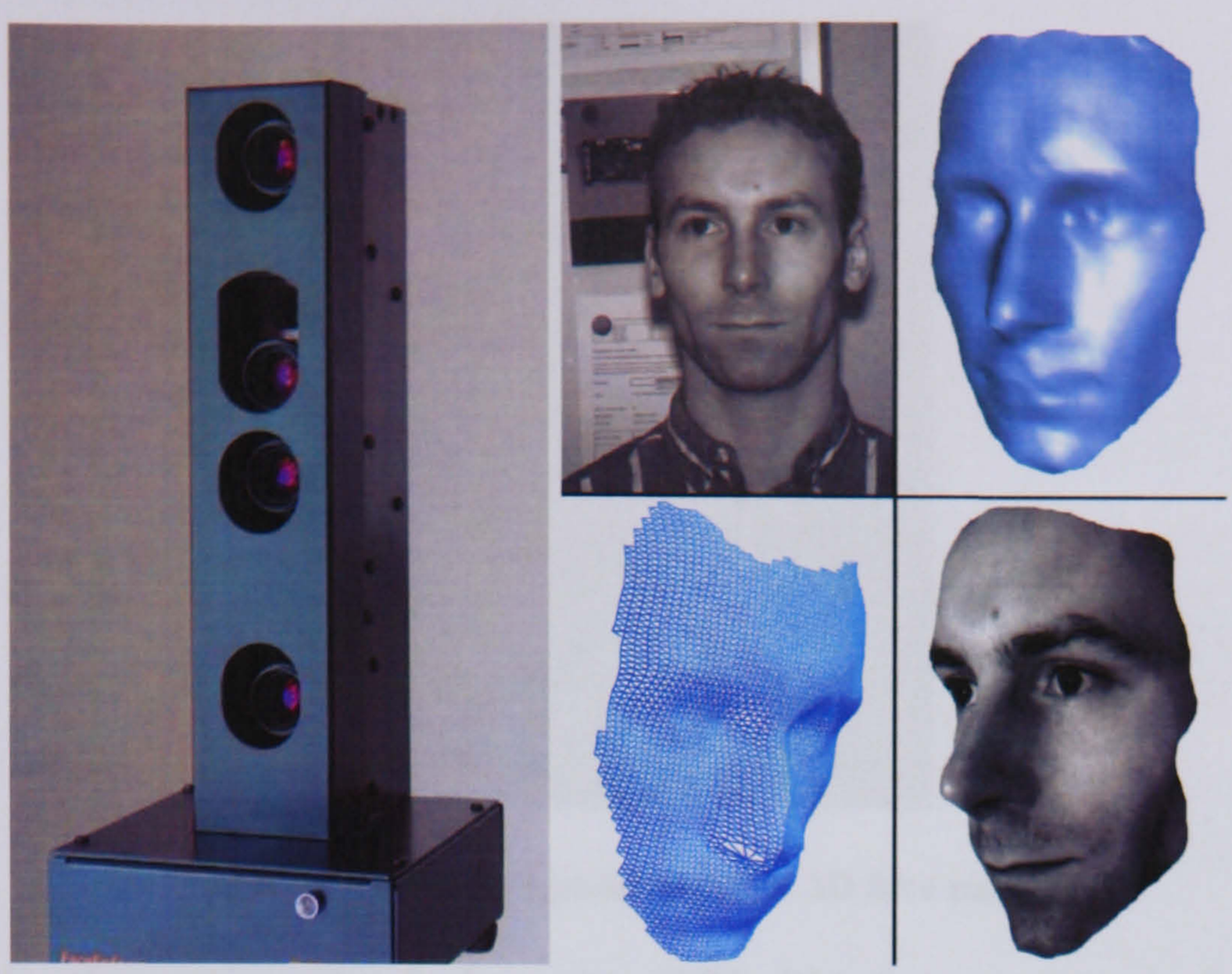

Figure 5-1 3D Camera and example 3D face data formats

The 3D models are generated in sub-second processing time from a single shot with a 3D camera, provided by Cybula Ltd., which operates on the basis of stereo disparity of a high-density projected light pattern. The unit consists of two monochrome progressive scan cameras, from which greyscale images are captured and used to produce a 3D point cloud of the facial surface. A third camera is used to capture texture information in the form of a greyscale bitmap image, which is subsequently mapped onto the model surface, as seen in Figure 5-1 (bottom right). Once all three cameras are permanently fixed into position, a calibration operation is performed to determine the relative angles of the three cameras. Corresponding points on each of the two greyscale images are found, allowing the position in 3D space to be calculated using triangulation. Each point in 3D space is also associated with a pixel in the colour texture image. The 3D facial surfaces are generated and output in the Wavefront OBJ file format.

In its simplest form, the 3D face model is merely a set of points in 3D space, with each point lying on some object surface visible in both of the stereo images. This means that the point cloud actually describes the nearest surface to the 3D camera. Any areas that are occluded from either of the cameras or projector will result in gaps in the point cloud, as can be seen in Figure 5-2 around the nostril and ear regions.

Figure 5-2 Example point cloud of 3D face model

In addition to this point cloud data the OBJ file format also includes polygon information. Each polygon is defined as a reference to three neighbouring points (or vertices), hence describing a 3D triangular faceted face. This data allows for production of smooth polygon visualisations (and ultimately full texture mapping) as well as wire-mesh representations, which become useful for navigating between locally connected vertices in surface processing techniques.

It is likely that the resolution of these 3D models is to have a significant effect on the performance of a 3D face recognition system, due to the level of detail represented in model. However, the resolution of such 3D models cannot be stated as a simple value as with 2D images and it is important to consider some of the factors that effect 3D point cloud resolution. Firstly, there is no simple relationship between the resolution of the stereo images and that of the point cloud. Rather, the stereo image resolution affects the precision of each point in the point cloud. It is not unless the stereo image resolution is increased sufficiently to expose additional features, that we introduce additional points to the 3D surface and hence increase the resolution. Therefore, it would seem that we are really interested in the point cloud density and its influence on recognition accuracy. However, using this measurement also has its problems. Firstly, the point density is not uniform across the 3D surface: it is dependent on the number of features detected in each area and the surface orientation relative to the camera (in Figure 5-2 we see a much lower density down the side of the nose than on the cheek areas). If we consider the average point density over the entire model, this figure can be greatly influenced by gaps due to nostrils, open mouths and glasses or additional surface areas such as the

shoulders, chest and neck. Therefore, we define the resolution of a face model simply in terms of the number of points on the surface of the face. This typically numbers in the five thousand to six thousand range, but should only be taken as a general guide to point resolution.

In these investigations we use the University of York 3D Face Database, recently made available as part of an ongoing project to provide a database of 3D face models [50]. As stated in section 5.1.2, the standard data set contains fifteen capture conditions per person, examples of which can be seen in Figure 5-3. The University of York 3D Face Database now consists of over 5000 models of over 350 people, making it the largest 3D face database currently available, although the Face Recognition Grand Challenge [2] has announced the imminent release of a 3D face database and the Max Planck Institute also provides a smaller database of high resolution 3D face models.

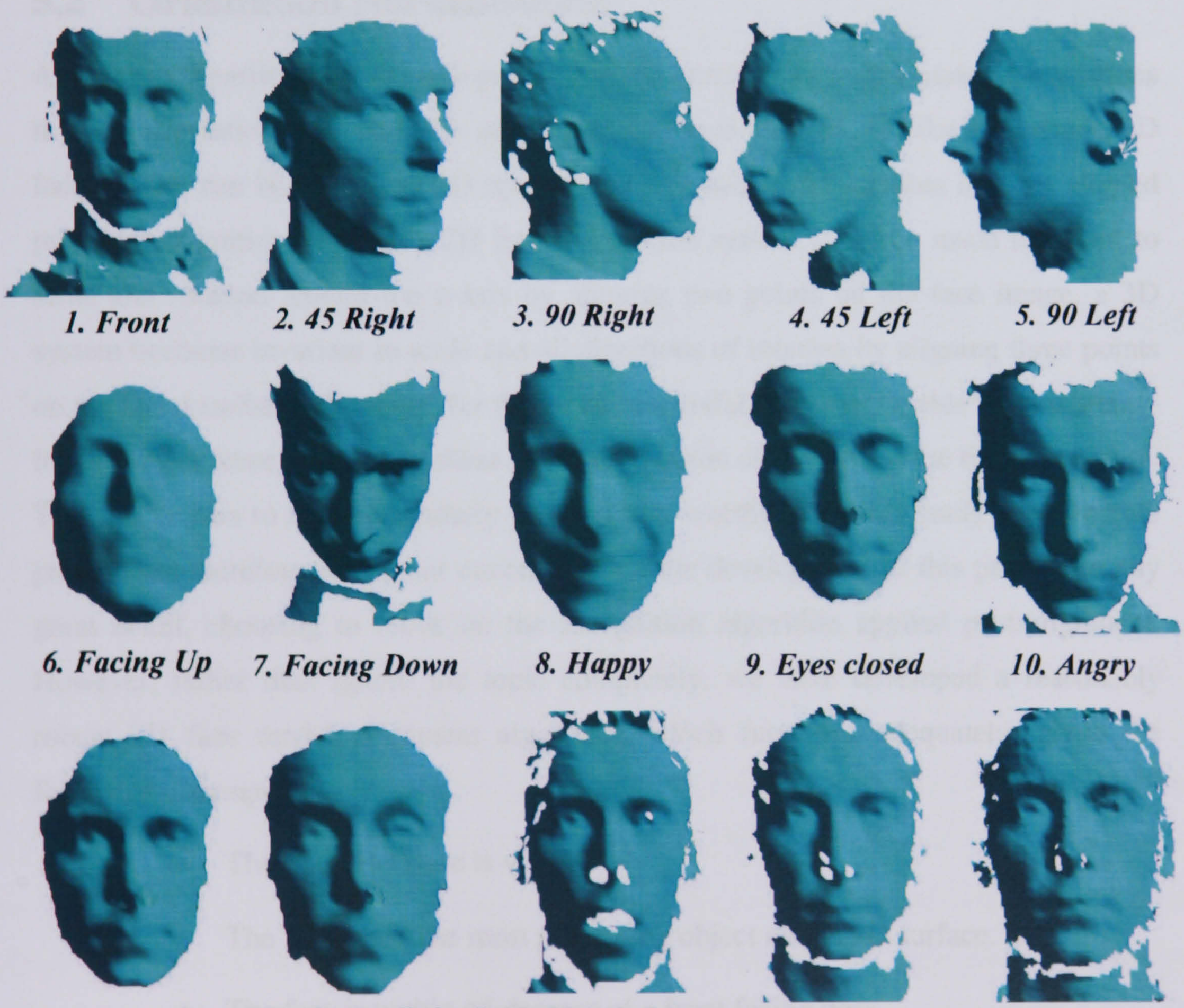

Figure 5-3 All capture conditions collected in the UOY 3D Face Database.

The research described in this thesis has been conducted as an ongoing series of sub-projects running alongside the data collection efforts for the University of York 3D Face Database. Because of this parallel progress, not all of the face data was available at the beginning of the research and therefore different training and test sets have been used in some of the experimentation. In particular, the earlier experiments were conducted using a smaller test set. Although these experiments can be compared on a qualitative basis, it does not provide the direct comparison necessary for a rigorous quantitative scientific evaluation. Therefore, we address this issue in chapter 8, by performing a final evaluation which compares the face recognition systems when applied to a consistent set of test data.

5.2 Orientation Normalisation

As discussed earlier, 3D face recognition has the potential to compensate for variations in head orientation from one face model acquisition to another. Unlike 2D images, 3D face models can be rotated in 3D space, such that two facial surfaces become aligned prior to recognition. Just as a 2D face recognition system could be made invariant to scale and rotation around the z-axis by aligning two points on the face image, a 3D system becomes invariant to scale and all directions of rotation by aligning three points on the facial surface. However, for this to be successful, we must be able to consistently localise these three points regardless of the orientation of the face at the time of capture. This has proven to be a particularly difficult task worthy of further study as a separate project and therefore we do not concentrate on the development of this process in any great detail, choosing to focus on the recognition algorithm applied post-alignment. However, rather than ignore the topic completely, we have developed a reasonably robust 3D face model alignment algorithm, which functions adequately, given the following assumptions:

- The tip of the nose is visible.
- The nose tip is the most protruding object on the 3D surface.
- The face is within 45 degrees of a front facing pose.

We apply the 3D orientation normalisation algorithm in a similar manner to the 2D image alignment used in 2D face recognition systems. After localising facial landmarks,

we translate and rotate all face models into a front-facing orientation prior to any training, enrolment, and verification and identification procedures. In 2D systems, localising the eye centres allows for image alignment. In terms of colour and texture, the eyes are well-defined, unique areas of the face with precise and easily detected centres (the pupils), but with the absence of texture information (when using purely geometric information) this is not the case. As seen in Figure 5-4, when texture information is not available, pinpointing the centre of the eyes is particularly difficult, even for the human vision system.

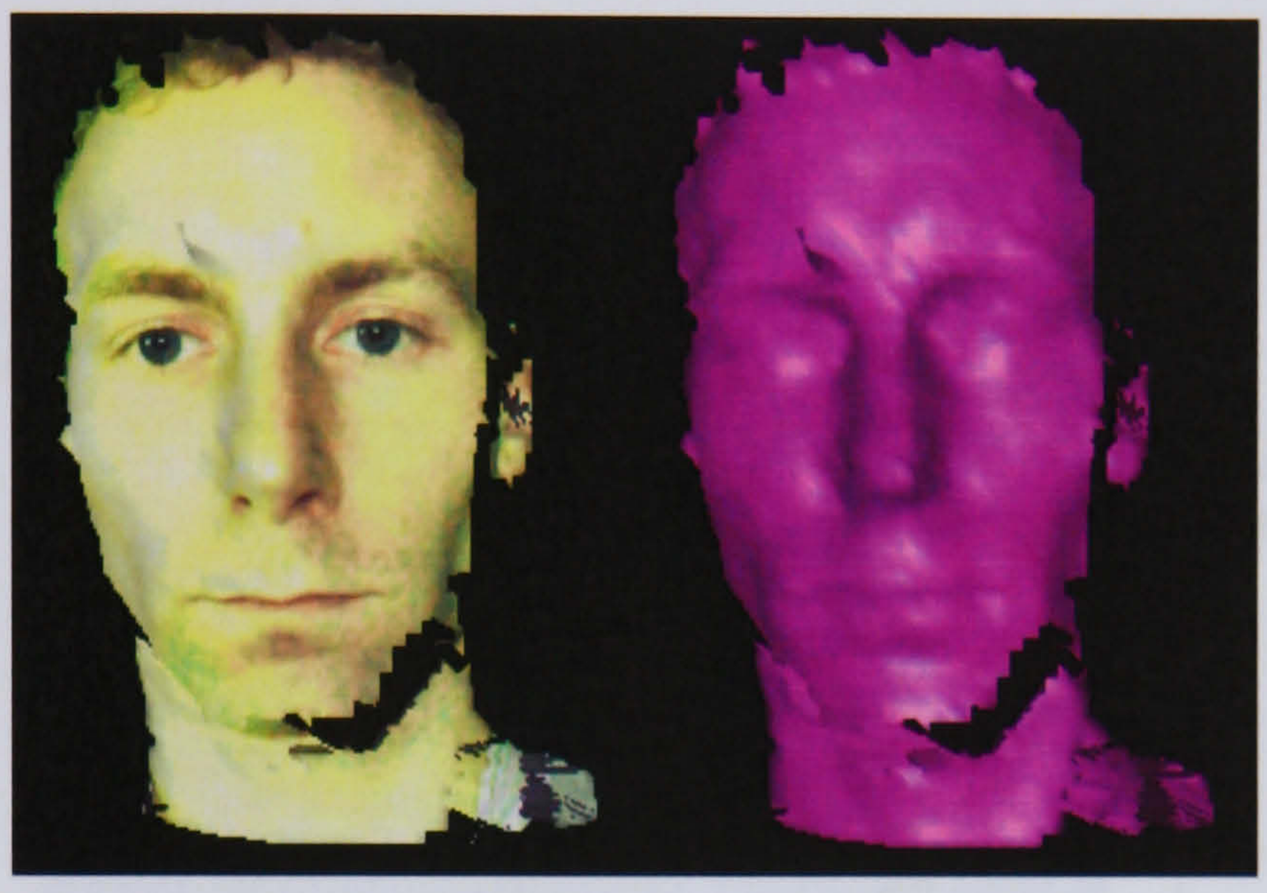

Figure 5-4 - 3D facial surface data viewed with and without texture mapping.

Theory suggests that we require a minimum of three points on the facial surface to align a 3D model. However, we are faced with the problem that there are few facial landmarks that are easily detected to a high degree of precision when using surface shape alone. Therefore, we have developed an algorithm that uses many more points, creating a more robust solution, relying on multiple redundancy and majority voting. The algorithm consists of four stages, which we now describe, in detail.

5.2.1 Nose Tip Localisation

Perhaps the most easily located facial feature is the nose tip, and it is for this reason that we begin orientation normalisation by locating this feature. Once it has been located, we can then use a-priori knowledge of local face shape to search for additional features. However, before locating the nose tip, we can gain some advantage by removing regions of the 3D surface that are unlikely to contain the nose. By assuming that the head is not rotated more than 45 degrees from a vertical alignment about the z-axis, we use a simple method of cropping the upper and lower regions of the 3D surface: removing the

forehead and chin regions. This is done by forming two horizontal cylinders of radius P and Q, centred about the uppermost vertex on the 3D model as shown in Figure 5-5. Any vertex falling within the smaller cylinder (radius P) is assumed to be part of the forehead, where as all vertices falling outside the larger cylinder (radius Q), are attributed to the chin, shoulders and neck. The radii P and Q are adjusted to accommodate various head sizes, rotation about the z-axis and the presence of headwear. Note that we do not crop regions to the left and right of the surface. This is to prevent cropping the nose, should the head be rotated about the y-axis to face left or right.

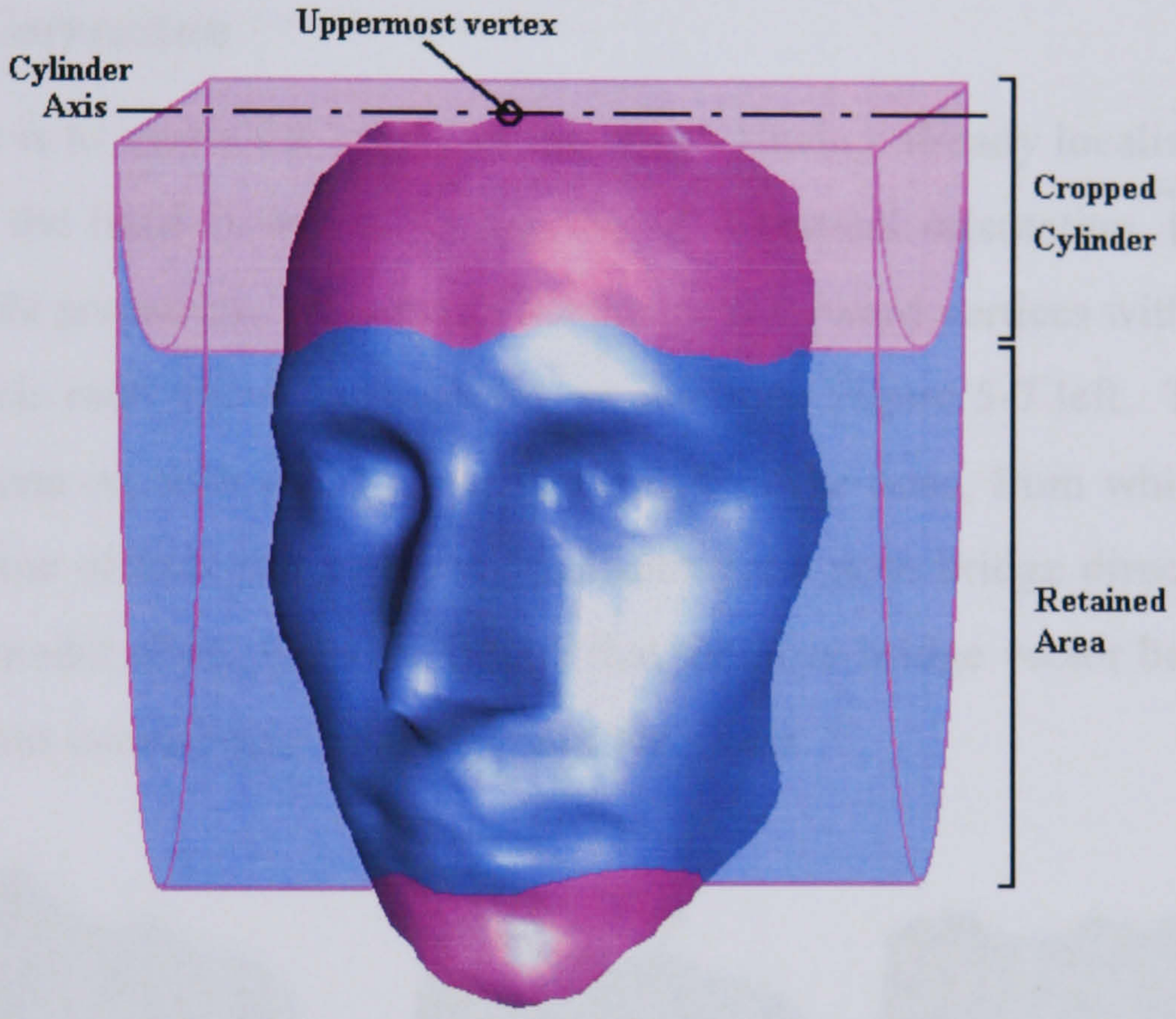

Figure 5-5 3D face cropping

Once the search space has been limited to the mid-region of the 3D surface we can begin locating the nose tip. The approach we take is to identify the most protruding point on the surface. If the head is in a fronto-parallel orientation, the nose can be identified as the most forward vertex (the vertex with the smallest z coordinate). However, as we don't know which way the subject will be facing, we must iteratively rotate the surface about the x and y axis, identifying the most forward vertex on each iteration. Providing each increment in rotation angle is sufficiently small, the result is that the nose tip has the smallest z coordinate on more occasions than any other vertex.

```
Centre of rotation = mean vertex
For x-rotation from -45 to 45, step 5:
      For y rotation from -45 to 45 step 5:
                  Flag most forward vertex
Nose tip = vertex with most flags
```

Figure 5-6 Nose tip localisation algorithm.

Having located the nose tip, we translate the 3D surface such that the nose tip is located at the origin of the coordinate space. Thus normalising the x, y and z position of the face in 3D space.

5.2.2 Roll Correction

The next stage is to locate the bridge of the nose. Having already localised the nose tip and assuming the head is within 45 degrees of a vertical orientation, this becomes a relatively simple procedure. We search for the most forward vertices within a 90-degree arc of concentric radii above the nose tip, as shown in Figure 5-7 left. This provides a set of points (one on each radii) along the bridge of the nose, from which we take the least squares line of best fit as a vector indicating the nose bridge direction. We then rotate the 3D model about the z-axis, such that the nose bridge vector becomes vertical in x-y plane, thus normalising rotation about the z-axis.

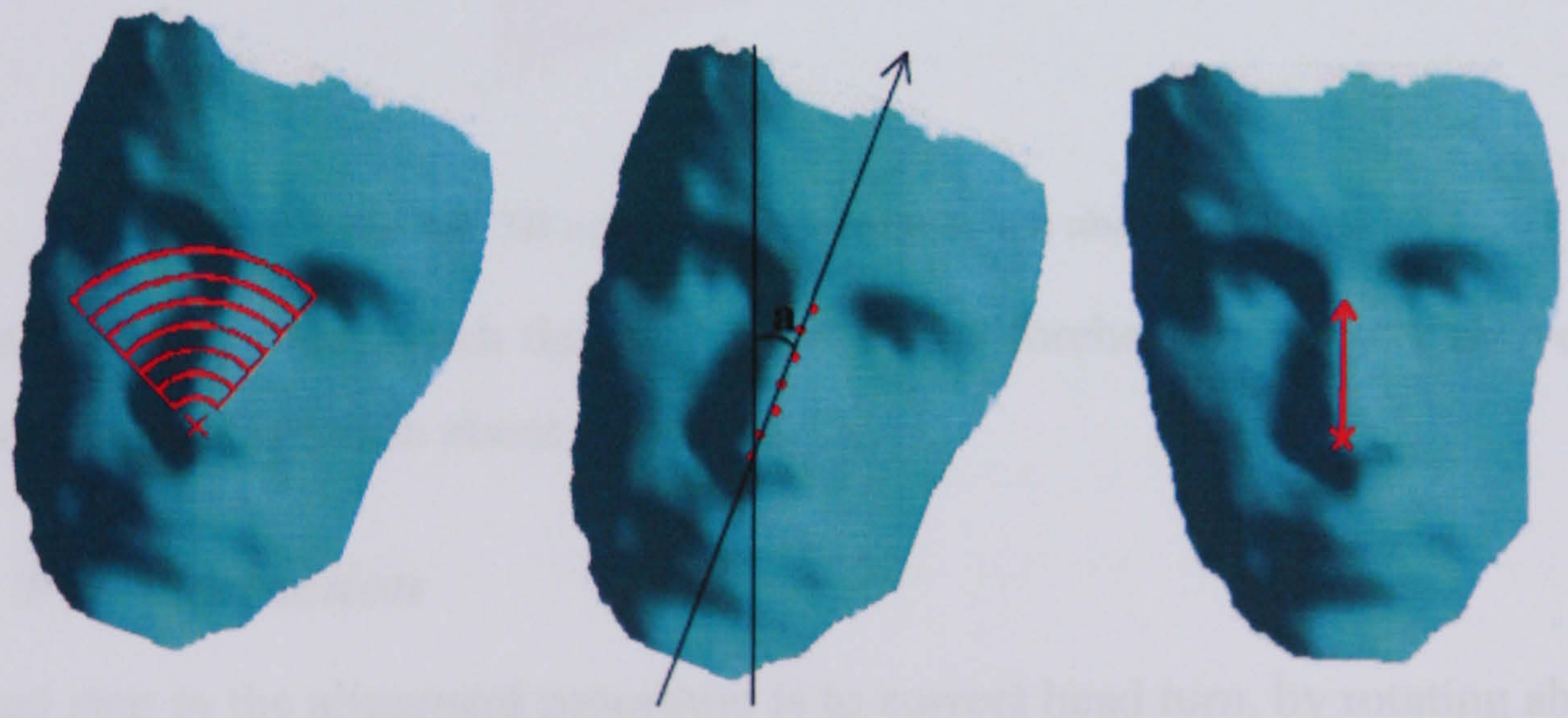

Figure 5-7 3D orientation normalisation about the z-axis

5.2.3 Tilt Correction

Initially, one may suggest that the bridge of the nose could also be used to normalise rotation about the x-axis (by ensuring that a point on the noise bridge is located directly above the nose tip. However, we have found this method to produce imprecise alignment, as just a small mis-localisation along the nose bridge can result in large discrepancies in the degree of corrective rotation applied. A much more suitable point to use in normalising tilt about the x-axis would be located on the forehead, due to the relatively flat surface structure (and hence little impact through mis-location). Therefore, the next step is to locate a point on the facial surface intersecting with the plane x = 0, at a distance *F* (typically 90mm) from the nose tip.

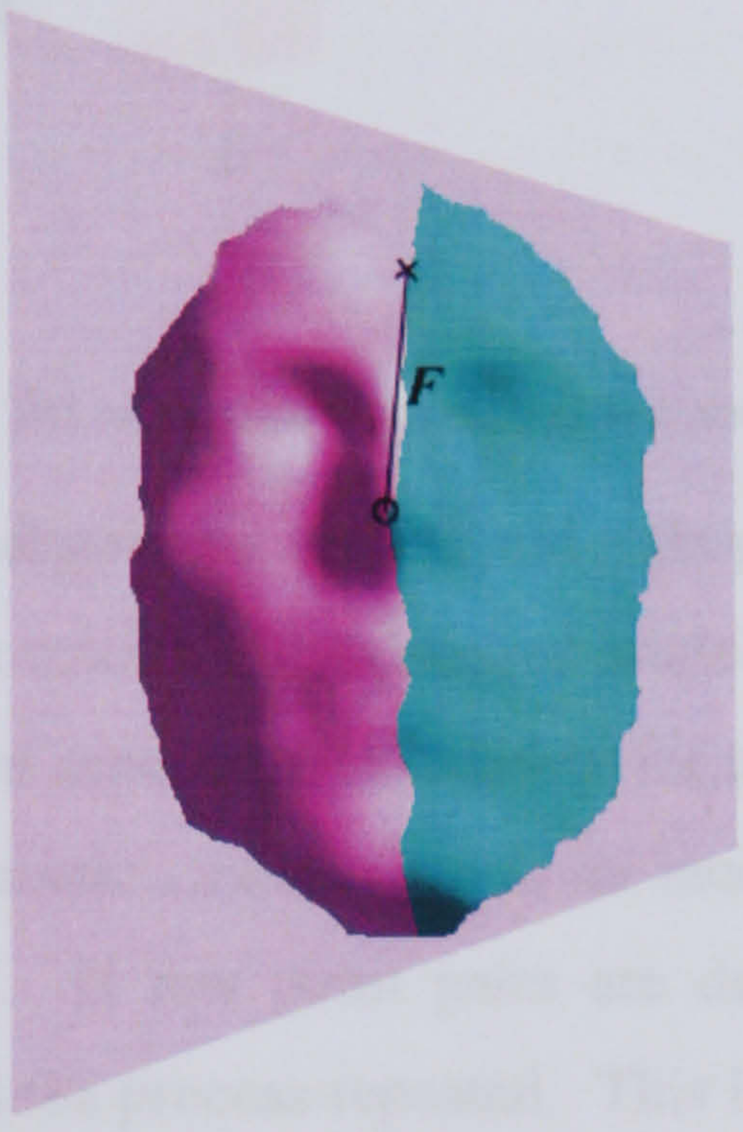

Figure 5-8 3D orientation normalisation about the x-axis

Rotating the 3D model, such that this point on the forehead is directly above the nose tip, normalises orientation about the x-axis.

5.2.4 Pan Correction

The final step in the alignment procedure is to correct head turn, by rotating about the y-axis. This is done by locating points of intersection between the facial surface, an arbitrary horizontal plane and a vertical cylinder, centred about the nose tip. For a given horizontal plane and cylinder of radius *W* there will be two points of intersection: one on the left side of the face and one on the right, as shown in Figure 5-9 (left). By adjusting

the y-coordinate of the horizontal plane, we produce a set of intersection point pairs on the facial surface (Figure 5-9, right).

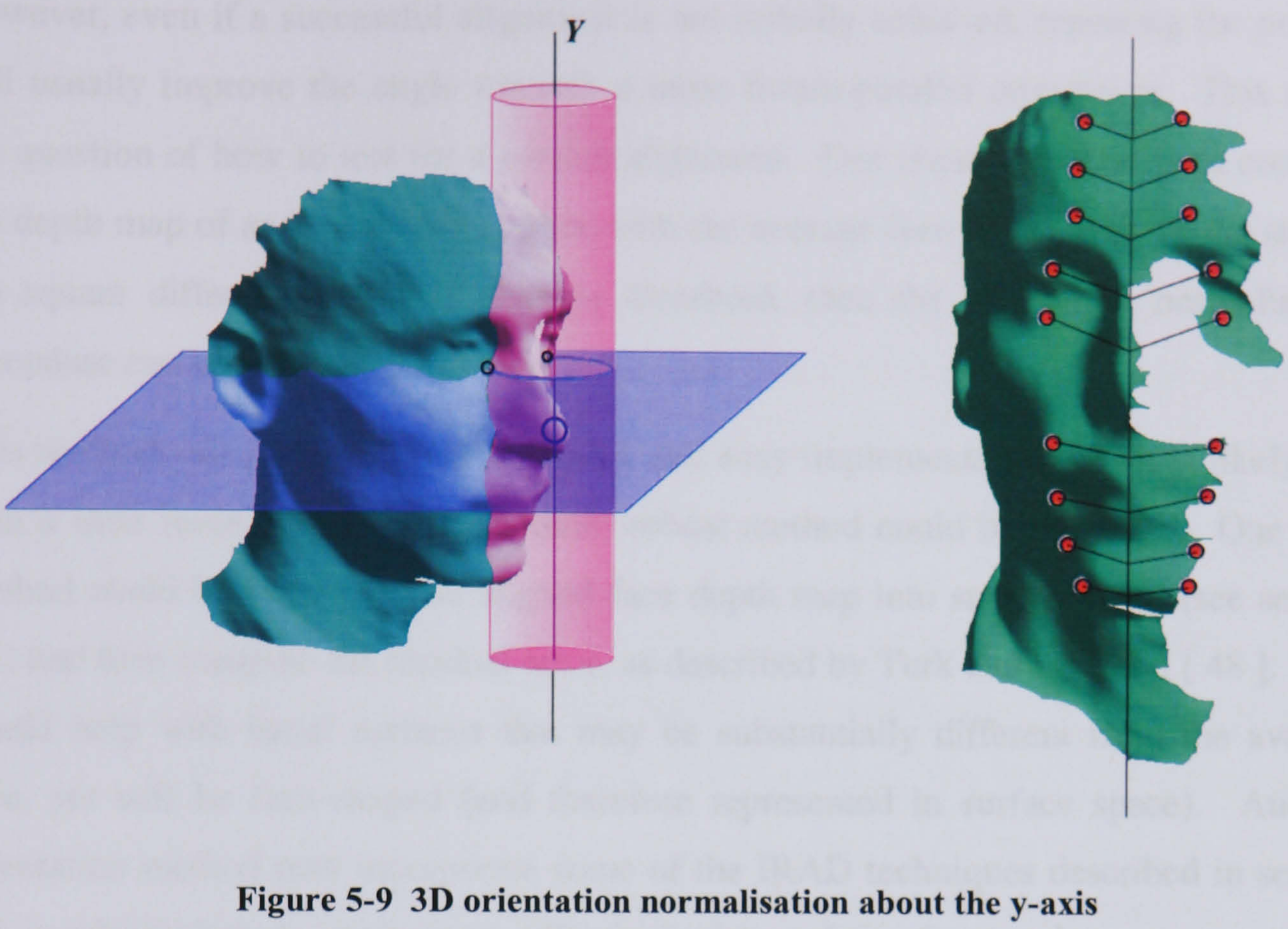

Figure 5-9 3D orientation normalisation about the y-axis

To achieve a fronto-parallel alignment, the left and right points of each pair should have the same z-coordinates. We calculate the required angle of rotation about the y-axis to achieve this balance and then repeat the calculation for a set of even spaced horizontal planes. If no point of intersection exists (due to an incomplete 3D surface), then that horizontal plane is ignored. If few point pairs are detected then the radius of the cylinder can be adjusted and the process repeated. This is often necessary if the head is particularly small (i.e. a child's head), meaning that the face is wholly contained within the cylinder.

The final degree of rotation (about the y-axis) is calculated as the average of all corrective angles for the point pairs. This averaging method helps to compensate for noise, facial distortion (due to expression) or small non-face protrusions (headwear).

5.2.5 Fine Tuning and Back-Checking

Certain steps in the orientation normalisation procedure are dependant on the initial angle of the head and it was found that repeating the process can result in a different final orientation. Experimentation has shown that the nearer the initial angle to a fronto-parallel orientation, the more successful the orientation procedure is likely to be.

However, even if a successful alignment is not initially achieved, repeating the process will usually improve the angle towards a more fronto-parallel orientation. This raises the question of how to test for a correct alignment. Our chosen method is to compare the depth map of an aligned 3D surface with the average face depth map. If the sum of the square difference exceeds a given threshold, then the orientation normalisation procedure can be repeated.

This method was chosen due to the quick and easy implementation and it is likely that with a little more thought a much more robust method could be produced. One such method could be to project the aligned face depth map into surface space (see section 4.1) and then compute the residual error, as described by Turk and Pentland [48]. This would help with facial surfaces that may be substantially different from the average face, yet still be face-shaped (and therefore represented in surface space). Another orientation method may incorporate some of the IRAD techniques described in section 5.7, in which all three rotations are effectively detected simultaneously.

5.3 3D Surface Representations

In this section we describe the various representations of 3D surfaces used throughout this thesis. We begin with a description of how depth maps are generated from the 3D face models in section 5.3.1, before discussing the pre-processing techniques used to generated other surface representations in section 5.3.2.

5.3.1 Depth Map Generation

3D surfaces can be stored in a variety of formats, including point clouds, meshes, polygons, curve-splines etc., but it is the depth map representation that we choose as our standard format for storage and processing. This is mainly due to its implementation as a one-dimensional array, to which we can directly apply the direct correlation, PCA and LDA algorithms used in the two-dimensional systems. Hence allowing a direct comparison of the two approaches with little adaptation of the algorithms themselves. In addition, the depth map representation can be conveniently stored as a greyscale bitmap image, allowing for thumbnail browsing, cropping, scaling and filtering using standard graphics packages and image processing libraries.

Prior to depth map generation it is often necessary to perform some form of smoothing and noise reduction on the original 3D face model. A slight ripple effect is often witnessed due to small inaccuracies in computation of point depth and areas of specula reflection can result in spikes and pits. Such anomalies are easily removed using a two-pass noise reduction procedure:

```
For each vertex in point cloud:
   spike = maximum difference in depth to neighbouring vertices
   If absolute(spike) > N:
      New vertex depth = average depth of neighbouring vertices
For each vertex in point cloud:
   New vertex depth = weighted average depth of neighbouring
   vertices, where weighting is inversely proportional to
   distance in the xy plane.
```

Figure 5-10 3D face model smoothing algorithm

After smoothing, conversion from the OBJ file format into a depth map is a relatively simple procedure that we now describe in detail.

```
Orientate 3D model
Scale 3D model
Translate 3D model (0.5*width, 0.5*height, 0)
For each vertex in point cloud:
      X, y, z = coordinates of vertex
      If x>=0 and x < width and y>= 0 and y < height:
      index = width*int(y) + int(x)
            Depth[index] += z
      Count[index]++
For index =0 to length(depth):
            Depth[index] /= count[index]
Interpolate missing depth values
```

Figure 5-11 OBJ to depth map conversion routine.

We begin by performing orientation normalisation, such that the 3D face model is facing forwards and centred about the origin (see section 5.2) and scaled by a fixed pre-defined value, such that the horizontal and vertical distances between vertices is approximately one unit. We then translate the model to centre in the middle of the depth map area. For each vertex in the point cloud we then use the x and y components of the coordinates to determine the index of the depth map array, before assigning the z coordinate as the depth value. If multiple vertices should fall within the same array index, the final depth value is calculated as an average. The initial scaling should have meant that few gaps are produced in the depth map array, but to ensure a smooth and complete surface we then interpolate any missing depth values. However, we do not interpolate across large holes (such as may be caused by glasses, open mouths or other occlusions) or beyond the outer edges of the facial surface.

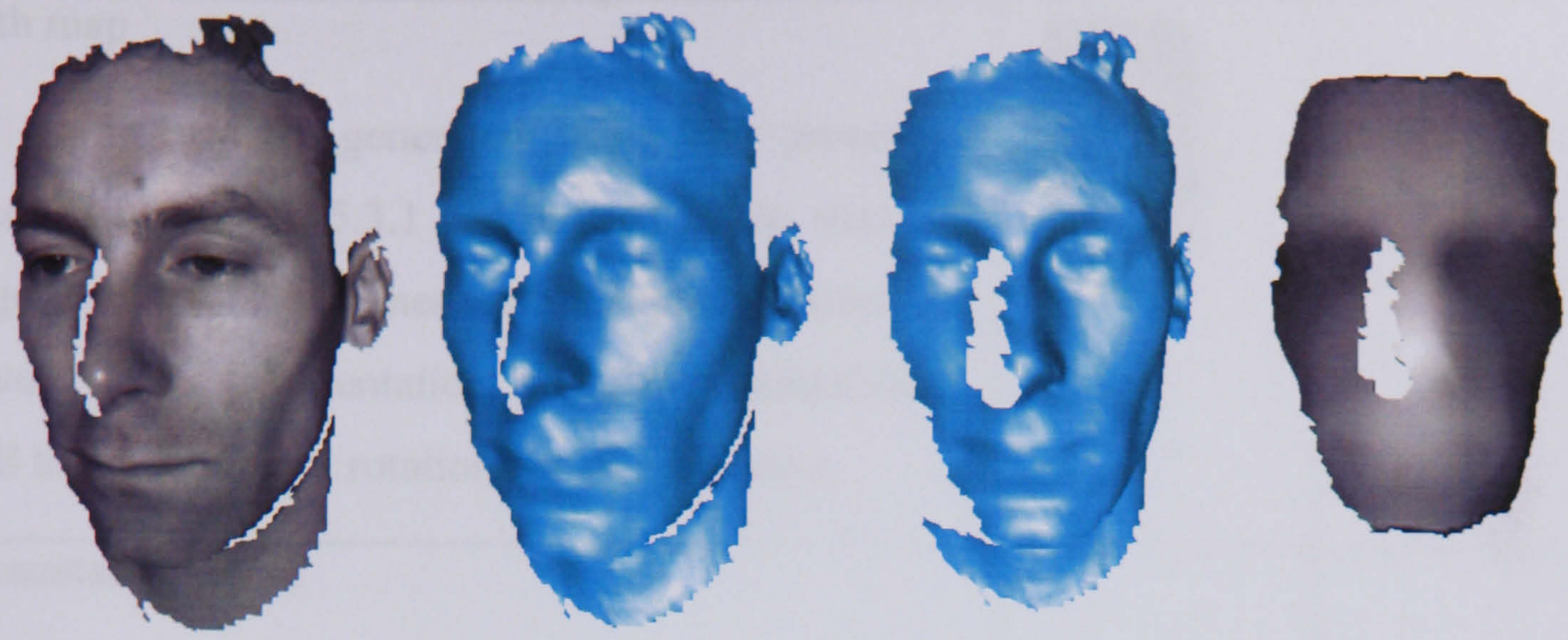

Figure 5-12 Original 3D face model (left two), orientation normalised 3D face model and depth map representation (right two).

5.3.2 3D Surface Processing

It is well known that the use of image processing techniques can significantly reduce error rates of pattern matching applications for two-dimensional images by removing unwanted effects caused by environmental capture conditions, as demonstrated in sections 4.3.3 and 4.6 experimenting with two-dimensional face recognition methods (published in [14][15]). Much of this environmental influence is not present in the 3D face models, but pre-processing may still aid recognition by making distinguishing features explicit and/or reducing noise content as shown in section 5.5 and 5.6 (published in [16]). In this section we discuss the pre-processing techniques used to produce alternative representations of the 3D surface structure. These methods are applied to depth map images prior to any further analysis in either the training or test procedures. Typically, pre-processing algorithms are applied to training and test sets as a batch process and the resulting images stored on disk, ready for eigenvector analysis or face space projection later, such that a separate surface space is generated for each surface representation and hence creates a separate face recognition system. We test a number of surface representations throughout the experiments described in this thesis, for which results can be found in sections 5.4, 5.5.3, 5.6.2 and the final evaluation in section 8. Below, we describe the variety of surface representations, derived from aligned 3D face models.

Depth map The depth map is generated using the procedure described in section 5.3.1 and is used as the standard image from which all other surface representations are derived. This representation is highly susceptible to small translations and rotations in all directions.		
Horizontal Gradient Applies the 2x1 kernel to compute the horizontal derivative describing the change in depth with respect to the x-axis. The resultant gradient map is invariant to translations along the z-axis and therefore also more stable with regard to small rotations about the x-axis. However, the small kernel size means surface noise is amplified.		-1 1
Vertical Gradient Applies the 1x2 kernel to compute the vertical derivative describing the change in depth with respect to the y-axis. Like the horizontal gradient it is invariant to translations along the z-axis, but still susceptible to noise.		-1 1
Horizontal Gradient Large To create this representation we apply a similar kernel to that of the horizontal gradient representation, but calculating the change in depth over a greater horizontal distance. Using a larger kernel size reduces the filters susceptibility to small amounts of noise, yet maintains the other advantages of gradient features.		-1 0 0 0 1

Vertical Gradient Large Another version of the vertical gradient, using a larger 1x4 kernel to reduce the influence of noise.		-1 0 0 1
Laplacian An isotropic measure of the second spatial derivative, calculating the depth change with respect to the x y plane. This surface representation is invariant to translation along the z-axis and may also offer improved stability regarding small rotations about the z-axis, as it is less reliant on the vertical and horizontal direction. However, this representation is likely to significantly amplify the surface noise, creating a highly speckled texture.		0 1 0 1–4 1 0 1 0
Sobel X Application of the horizontal Sobel derivative filter, calculating the horizontal gradient with the added benefit of local reinforcement, producing a much smoother (and potentially more robust) gradient map.		-1 0 1 -2 0 2 -1 0 1
Sobel Y Application of the vertical Sobel derivative filter, with similar advantages to the other gradient representations, plus greatly reduced noise.		1 2 1 0 0 0 -1 -2 -1
Sobel Magnitude The magnitude of Sobel X and Y combined, creating an absolute measure of gradient magnitude with no directional bias.		

Horizontal Curvature Applies the Sobel X kernel twice to calculate the second horizontal derivative, creating a curvature map of the 3D surface with respect to the x-axis. Any noise present on the surface will have been amplified by each application on the Sobel X filter, meaning this representation will have a high noise content.		
Vertical Curvature Applies the Sobel Y kernel twice to calculate the second vertical derivative, creating a curvature map of the 3D surface with respect to the y-axis. Again, this representation will have a high noise content, due to the cascaded noise amplification.		
Curvature Magnitude The magnitude of the vertical and horizontal curvature values, providing an absolute measure of curvature magnitude with no directional bias.		
Curve Type Segmentation of the surface into the eight discreet curvature types: peak, ridge, saddle ridge, minimal, pit, valley, saddle valley and flat.		
Min Curvature The minimum value of the horizontal & vertical curvature maps. This representation can be thought of as a measure of surface convexity: the more convex the surface point the darker the pixel.		

Max Curvature The maximum value of horizontal & vertical curvature maps. Hence, creating a representation of the surface concavity: the more concave the surface point, the brighter the image pixel.		
Abs Min Curvature The minimum value of the absolute horizontal & absolute vertical curvatures. The resulting representation highlights those areas that are highly curved with respect to both the x-axis and y-axis.		
Abs Max Curvature The maximum value of the absolute horizontal & absolute vertical curvatures. The resulting representation provides an indication of the magnitude of ridge curvature in either the horizontal or vertical directions.		

Table 5-3 3D face surface representations

5.4 Direct Correlation

The direct correlation approach is applied to 3D images (in the form of depth maps) as for two-dimensional images: a simple direct comparison of the query and target images, producing a difference value. However, in this case rather than using two-dimensional intensity images of surface texture, we use 3D depth maps of the facial surface. Firstly, 3D face models are orientated to face directly forwards using our orientation normalisation algorithm described in section 5.2, before being converted into a depth map representation and compared using some distance metric and verified by application of a threshold value. By altering this threshold value we are able to bias the system towards either a low FAR (with a high FRR) or a low FRR (with a high FAR). We experiment on a database of 290 depth maps, taken from the University of York 3D Face Database, consisting of subjects of various race, age and gender with varying pose and expression. No training set is required, as we do not perform any weighting or image space analysis. Instead, this experimentation will provide an indication of the effectiveness of a very rudimentary 3D face recognition system in its simplest form: direction comparison of facial depth maps. We also demonstrate how various surface representations result in different error rates, while referring the reading to section 5.3 for a detailed explanation of the various surface representations tested.

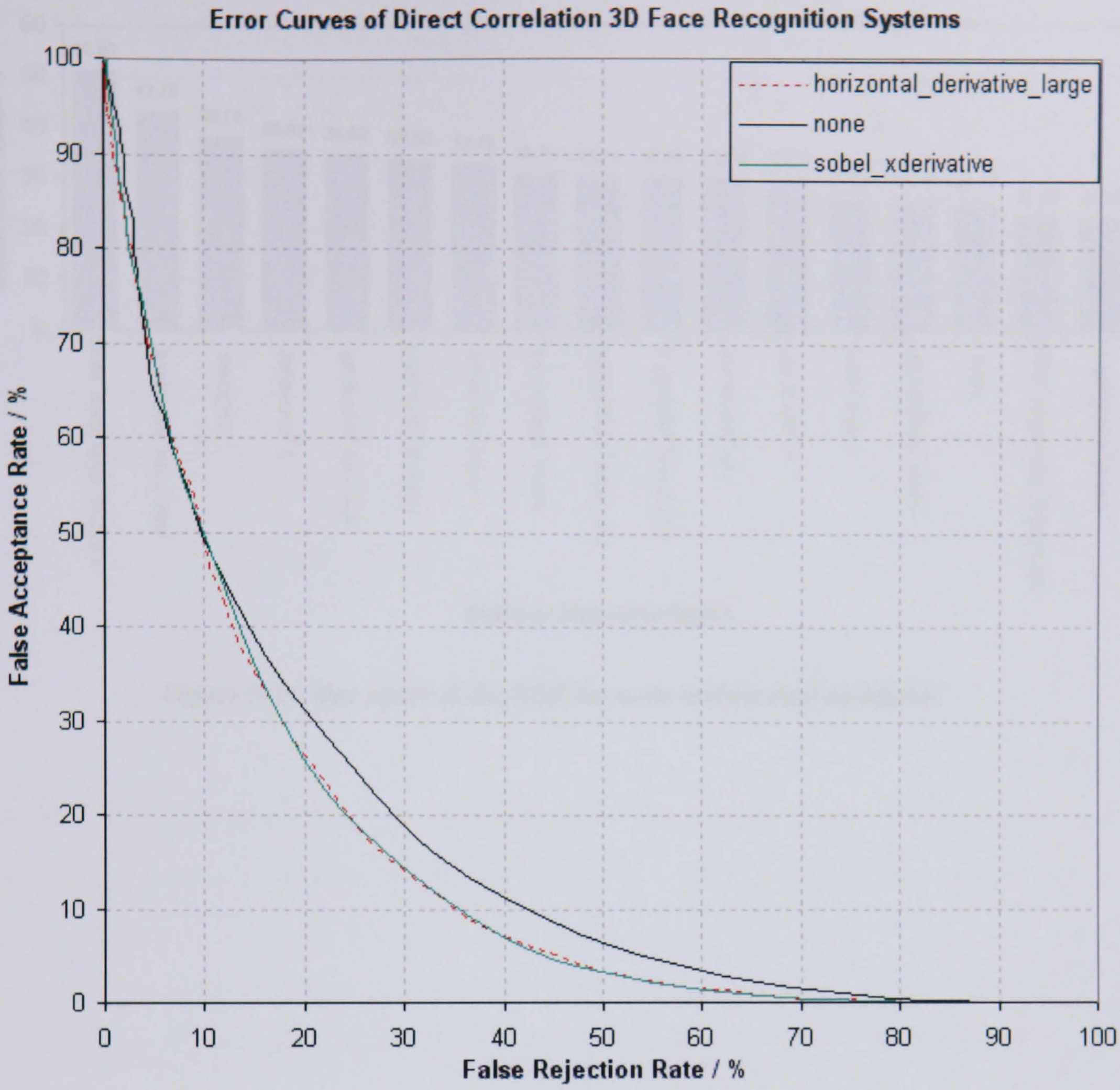

Figure 5-13 Error rate curves of the best three performing surface representations

Figure 5-13 above shows the error rate curve for the three best performing surface representations. Surprisingly, out of the seventeen surface representations tested the original depth map representation still features in the top three representations. Although some improvement is witnessed when derivatives relative to the x-axis of the depth map are compared. Figure 5-14 below shows the EER generated for each surface representation using the direct correlation method of three dimensional face recognition. It is interesting to note that the majority of representations degrade performance. This is most likely due to the noise amplification side effects of the first and second order derivatives.

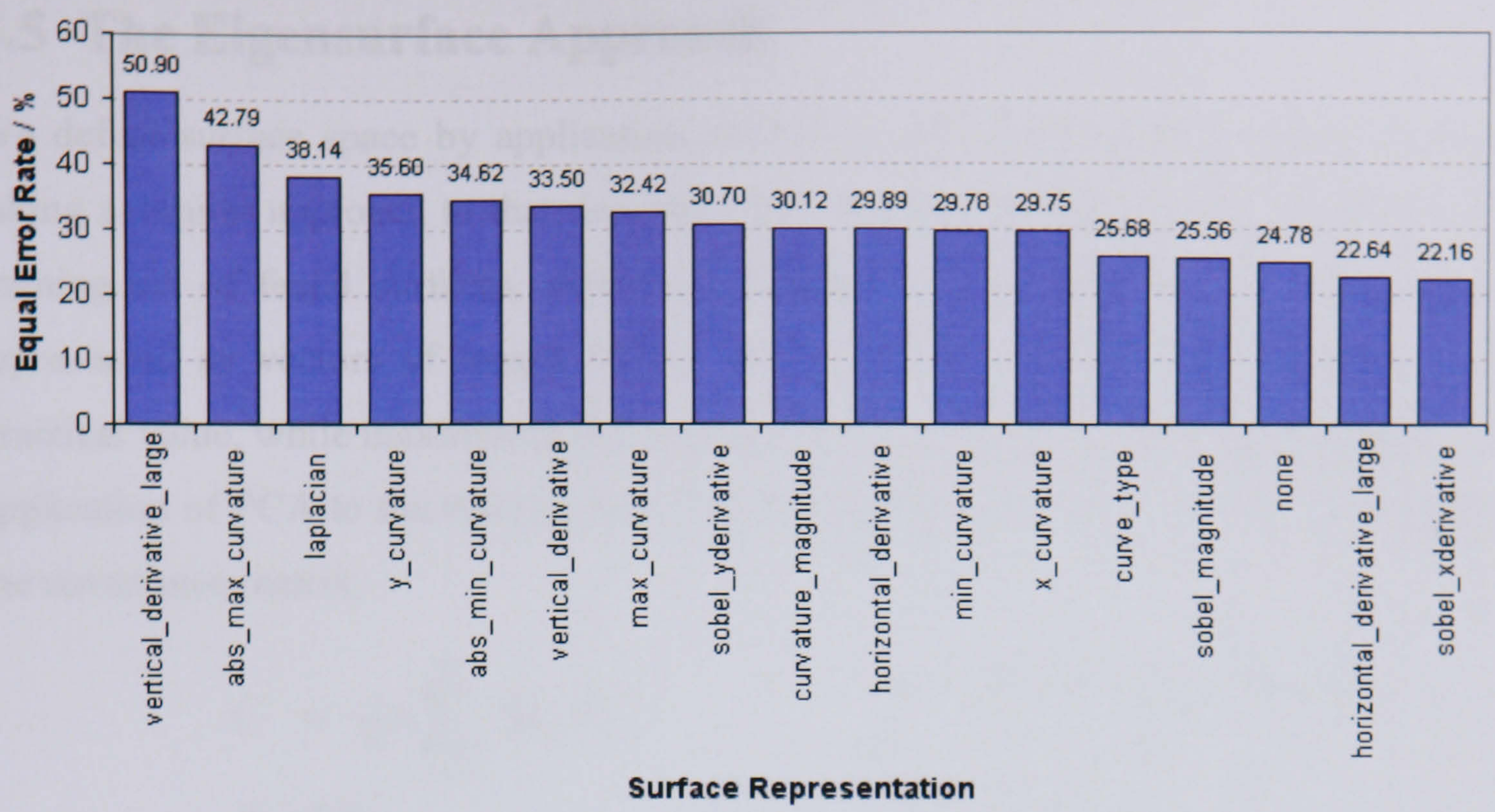

Figure 5-14 Bar chart of the EER for each surface representation

5.5 The Eigensurface Approach

We define surface space by application of PCA to the training set of facial surfaces, taking a similar approach to that described by Turk and Pentland [48]. Consider our training set of facial surfaces, stored as orientation normalised 60x105 depth maps, represented as vectors of length 6300. We begin by reducing dimensionality to a practical value, while maximising the variance of facial surfaces within the subspace, by application of PCA to the training set of M (40) depth maps $\{\Gamma_1, \Gamma_2, \ldots \Gamma_M\}$, computing the covariance matrix,

$$C = \frac{1}{M}\sum_{n=1}^{M} \Phi_n \Phi_n^T \qquad A = [\Phi_1 \Phi_2 \Phi_3 \ldots \Phi_M]$$
$$= AA^T \qquad \Phi_n = \Gamma_n - \Psi$$
$$\Psi = \frac{1}{M}\sum_{n=1}^{M} \Gamma_n$$

Equ. 5-1

Where Φ_n is the difference of the *nth* depth map from the average ψ. Eigenvectors and eigenvalues of the covariance matrix are calculated using standard linear methods. The resultant eigenvectors describe a set of axes within the depth map space, along which most variance occurs and the corresponding eigenvalues represent the degree of this variance along each axis. The M eigenvectors are sorted in order of descending eigenvalues and the M`(40) greatest eigenvectors chosen to represent surface space. We term each eigenvector an eigensurface, displayed as range images in Figure 5-15.

Figure 5-15 Average face surface depth map and first seven eigensurfaces

5.5.1 Verification of Facial Surfaces

Once surface space has been defined, we project any face into surface space by a simple matrix multiplication, using the eigenvectors calculated from covariance matrix *C*.

$$\omega_k = u_k^T (\Gamma - \Psi) \quad for\ k = 1 \ldots M`.$$

Equ. 5-2

Where u_k is the *kth* eigenvector and ω_k is the *kth* weight in the vector $\Omega^T = [\omega_1, \omega_2, \ldots \omega_M]$. The vector Ω is taken as the 'face-key' representing a person's facial structure in surface space and is compared by either Euclidean or cosine distance metrics.

$$d_{euclidean} = \|\Omega_a - \Omega_b\| \qquad d_{\cos ine} = 1 - \frac{\Omega_a^T \Omega_b}{\|\Omega_a\| \|\Omega_b\|}$$

Equ. 5-3

In addition, we can also divide each face-key by the vector of its respective eigenvalues λ, prior to distance calculation, removing any inherent dimensional bias and introducing two supplementary metrics, the Mahalanobis distance and weighted cosine distance.

$$d_{\text{mahalanobis}} = \left\| \frac{\Omega_a}{\lambda} - \frac{\Omega_b}{\lambda} \right\| \qquad d_{\text{wcosine}} = 1 - \frac{\frac{\Omega_a^T}{\lambda} \frac{\Omega_b}{\lambda}}{\left\| \frac{\Omega_a}{\lambda} \right\| \left\| \frac{\Omega_b}{\lambda} \right\|}$$

Equ. 5-4

An acceptance (facial surfaces match) or rejection (surfaces do not match) is determined by applying a threshold to the calculated distance.

5.5.2 Evaluation Procedure

For the purpose of these experiments, we will be using a subset of the 3D face database, acquired during preliminary data acquisition sessions. This set consists of 330 models taken from 100 people under the ten conditions shown in Figure 5-16.

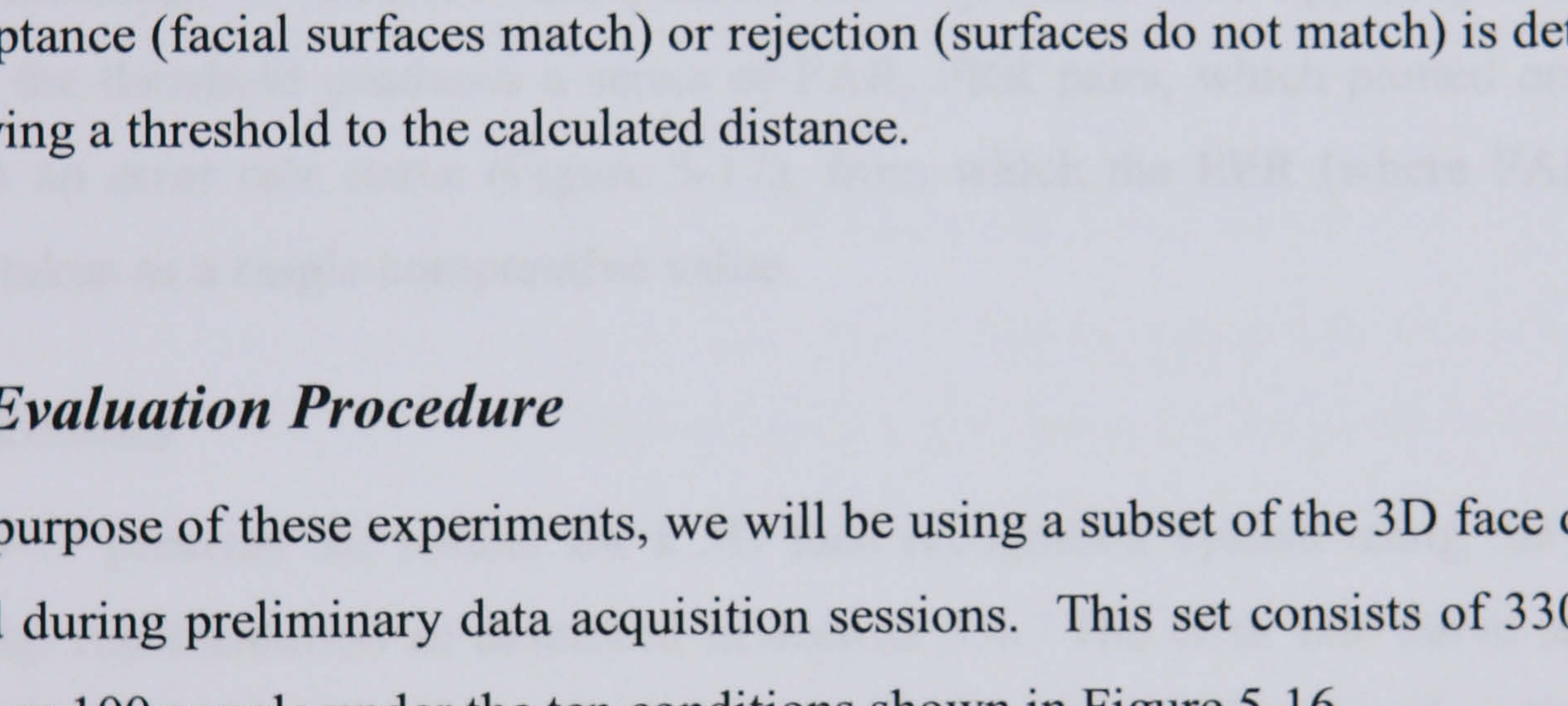

Figure 5-16. Face models taken from the UOY 3D face database

During capture no effort was made to control lighting conditions. In order to generate face models at various head orientations, subjects were asked to face reference points positioned roughly 45° above and below the camera, but no effort was made to enforce a precise angle of orientation.

3D face models are orientated to face directly forwards using our orientation normalisation algorithm (see section 5.2) before being converted into depth maps. The database is then separated into two disjoint sets: the training set consisting of 40 depth maps (type 1, Figure 5-16) and a test set of the remaining 290 depth maps. Both sets contain subjects of various race, age and gender and nobody is present in both the training and test sets.

In order to evaluate the effectiveness of the face recognition methods, we compare each of the 290 surfaces in the test set with every other surface (41,905 verification operations). False acceptance rates (FAR) and false rejection rates (FRR) are calculated as the percentage of incorrect acceptances and rejections after applying a threshold. Varying the threshold produces a series of FAR, FRR pairs, which plotted on a graph produces an error rate curve (Figure 5-17), from which the EER (where FAR equals FRR) is taken as a single comparative value.

5.5.3 Results

Figure 5-17 presents the results for a 3D face recognition system using the standard depth map representation as described in section 5.4. The error rate curve shows the FAR and FRR for a range of threshold values. The results clearly show that dividing by eigenvalues to normalise vector dimensions prior to distance calculations, significantly decreases error rates for both Euclidean and cosine distance, with the Mahalanobis metric providing the lowest EER for the depth map representation.

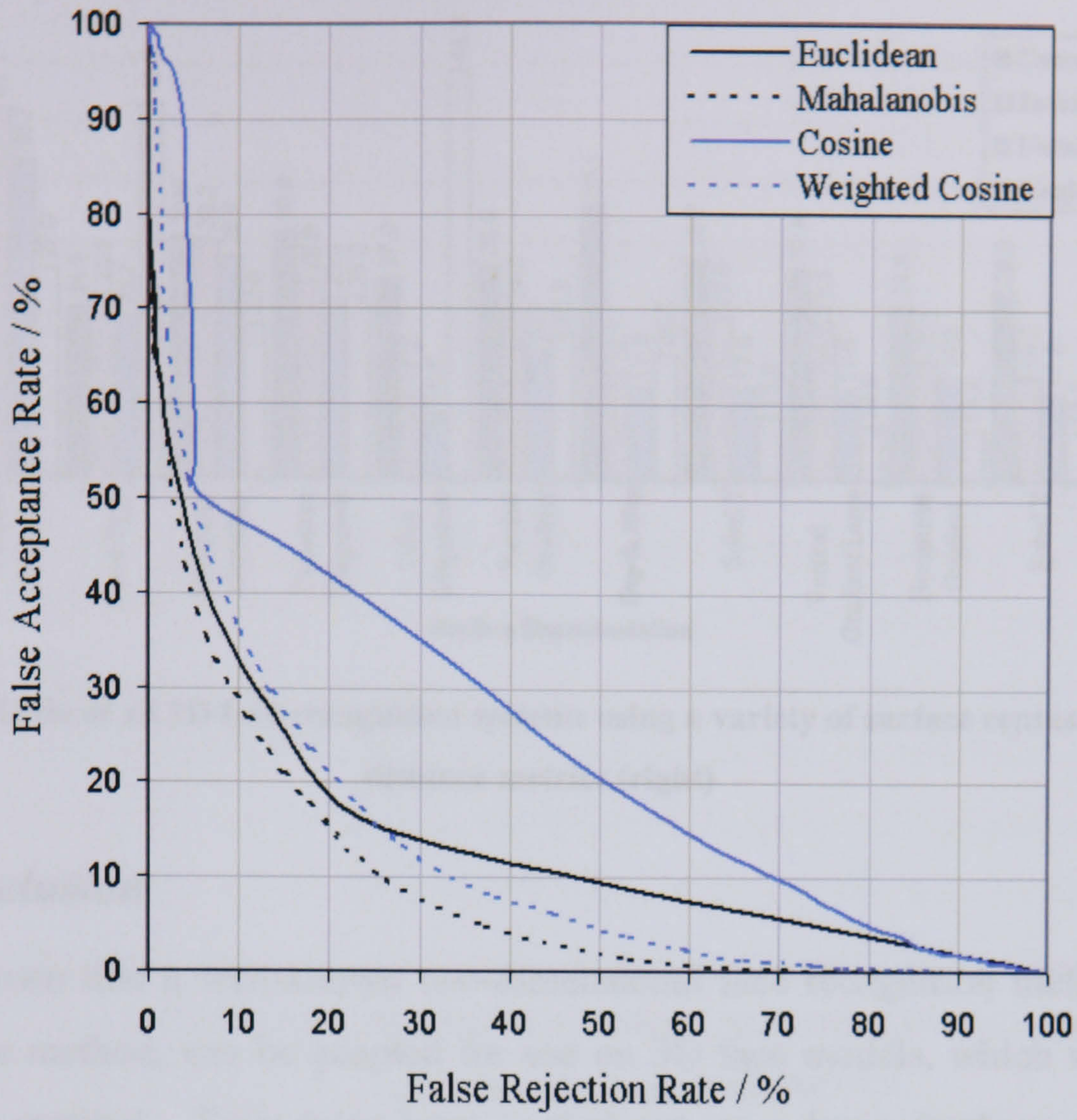

Figure 5-17. Error rate curves for the base line depth map system.

Repeating the experiment for each of the surface representations described in section 5.3, we produce a bar chart of EERs (Figure 5-18), taken as the point where FAR is equal to FRR on the error rate curve. The EERs produced show that surface gradient representations provide the most distinguishing information, with horizontal derivatives giving the lowest EERs of all, using the weighted cosine distance metric. In fact, the weighted cosine distance returns the lowest EER for the majority of surface representations. However, the most effective surface representation seems to be dependent on the distance metric used for comparison.

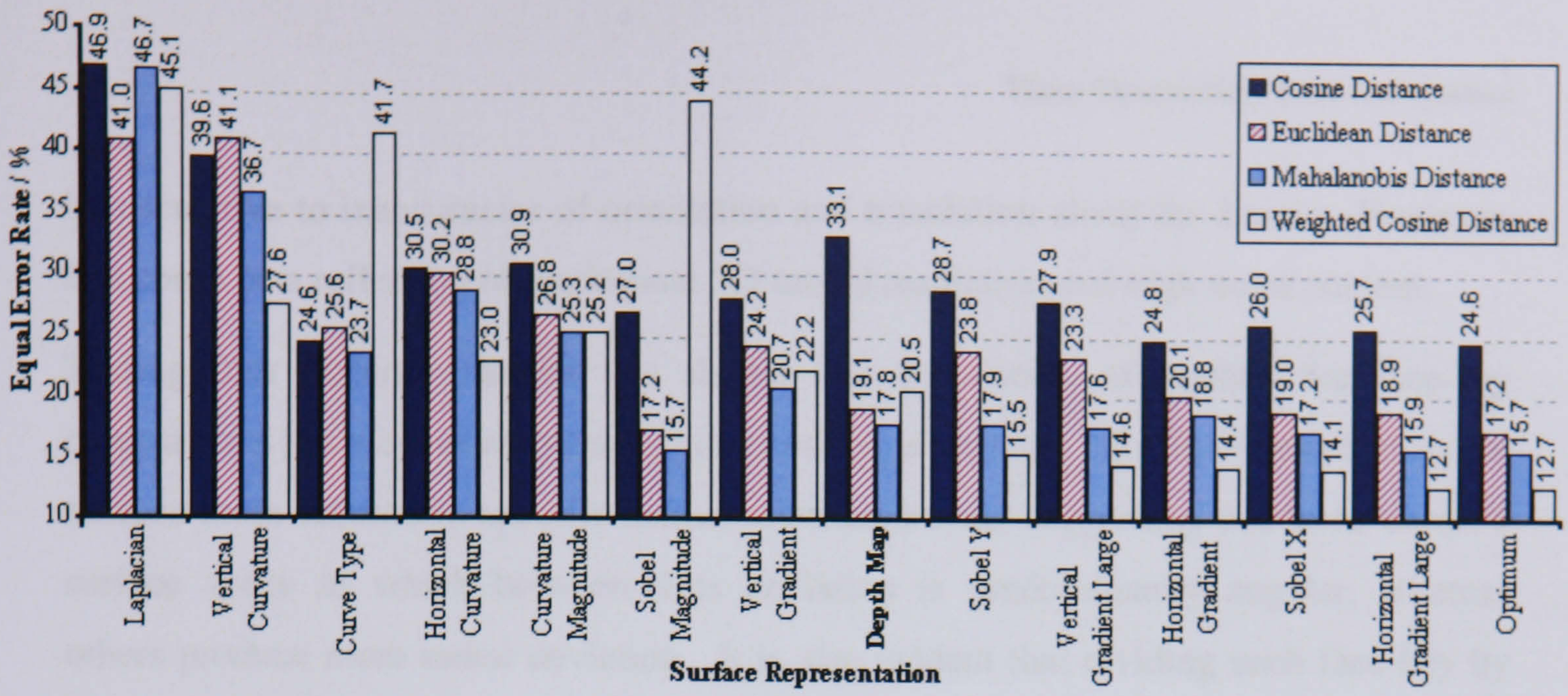

Figure 5-18. EERs of all 3D face recognition systems using a variety of surface representations and distance metrics (right)

5.5.4 Conclusion

We have shown that a well-known two-dimensional face recognition method, namely the eigenface method, can be adapted for use on 3D face models, which we name the eigensurface method. Tests have been carried out on a large database of 3D facial surfaces, captured under conditions that present typical difficulties when performing recognition. The error rates produced from the 3D baseline system (19.1% EER using Euclidean distance) are notably lower that those gathered in similar experiments using two-dimensional images (25.5% EER) [15]. Although a more direct comparison is required, using a common 2D/3D test database, in order to draw any quantitative conclusions, initial results suggest that 3D face recognition has distinct advantages over conventional two-dimensional approaches.

Experimenting with a number of surface representations, we have discovered that facial surface gradient is more effective for recognition than depth and curvature representations. In particular, horizontal gradients produce the lowest error rates, seeming to indicate that horizontal derivatives provide more discriminatory information than vertical. Another advantage is that gradients are likely to be more robust to inaccuracies in the alignment procedure, as the derivatives will be invariant to translations along the Z-axis.

Curvature representations do not seem to contain as much discriminatory information as other surface representations. We find this surprising, as second derivatives should be

less sensitive to inaccuracies of orientation and translation along the Z-axis. However, this could be a reflection of inadequate 3D model resolution and high noise content.

Testing four distance metrics has shown that the choice of method for face-key comparisons has a considerable affect on resulting error rates. The Euclidean and cosine metrics seem tailored to specific surface representations, suggesting that some create a surface space in which between-class deviation is predominantly angular, whereas others produce more radial deviation. It is also evident that dividing each face-key by respective eigenvalues, normalising dimensional distribution, usually improves results for both Euclidean and cosine distances. This indicates that the distribution along one surface space dimension is not necessarily proportional to its discriminating ability and that face-keys become more discriminative when all dimensions are weighted evenly. However, this is not the case for some surface representations with higher EERs, suggesting that these representations incorporate only a few dominant useful components, which become masked when weighted evenly with the majority of less discriminatory components.

Error rates of the best performing 3D eigensurface system (12.7% EER) are substantially lower than the best two-dimensional systems (20.4% EER and 17.8% EER) tested under similar circumstances in our previous investigations [14][15]. Although we recognise the differences between these experiments (most notably the lack of a common 3D/2D test set), the results do show that geometric face structure is useful for recognition when used independently from colour and texture and capable of achieving high levels of accuracy. Given that the data capture method produces models invariant to lighting conditions and provides the ability to recognise faces regardless of pose, makes this system particularly attractive for use in security and surveillance applications. However, more testing is required to identify the limitations of the eigensurface method, although one obvious issue is the system's reliance on accurate orientation normalisation. Improved orientation normalisation techniques would likely produce lower error rates or an alternative approach, in which an orientation invariant representation was produced (removing the need to normalise orientation) may lead to an improved recognition capability, as discussed in section 5.7.

5.6 The Fishersurface Approach

Having achieved reasonable success from the PCA-based eigensurface system [14], we now continue this line of research, experimenting with another well-known method of face recognition, namely the Fisherface approach as described by Belhumeur et al [27], adapted for use on 3D face data. Testing a range of surface representations and distance metrics, we identify the most effective methods of recognising faces using 3D surface structure.

We apply PCA and LDA to surface representations of 3D face models, producing a subspace projection matrix, as with Belhumier et al's Fisherface approach [27], taking advantage of 'within-class' information, minimising variation between multiple face models of the same person, yet maintaining high class separation. To accomplish this we use a training set containing several examples of each subject, describing facial structure variance (due to influences such as facial expression), from one model to another. From the training set we compute three scatter matrices, representing the within-class (S_W), between-class (S_B) and total (S_T) distribution from the average surface Ψ and classes averages Ψ_n, as shown in Equ. 5-5.

$$\begin{aligned}
&Training\ Set = \{X_1, X_2, \ldots X_c\} \\
&\quad where\ X_n = \{\Gamma_{n1}, \Gamma_{n2}, \Gamma_{n3}, \ldots\} \\
&\Psi = \frac{1}{\sum_{m=1}^{c}|X_m|}\sum_{n=1}^{c}\sum_{i=1}^{|X_n|}\Gamma_{ni} \\
&\Psi_n = \frac{1}{|X_n|}\sum_{i=1}^{|X_n|}\Gamma_{ni}
\end{aligned}
\qquad
\begin{aligned}
S_T &= \sum_{n=1}^{c}\sum_{i=1}^{|X_n|}(\Gamma_{ni} - \Psi)(\Gamma_{ni} - \Psi)^T \\
S_B &= \sum_{n=1}^{c}|X_n|(\Psi_n - \Psi)(\Psi_n - \Psi)^T \\
S_W &= \sum_{n=1}^{c}\sum_{i=1}^{|X_n|}(\Gamma_{ni} - \Psi_n)(\Gamma_{ni} - \Psi_n)^T
\end{aligned}$$

Equ. 5-5

The training set is partitioned into c classes, such that all surface vectors Γ_{ni} in a single class X_n are of the same person and no person is present in multiple classes. Calculating eigenvectors of the matrix S_T, and taking the top 250 (number of surfaces minus number of classes) principal components, we produce a projection matrix U_{pca}. This is then used to reduce dimensionality of the within-class and between-class scatter matrices (ensuring they are non-singular) before computing the top *c-1* eigenvectors of the reduced scatter matrix ratio, U_{fld}, as shown in Equ. 3-2.

$$U_{fld} = \arg\max_{U} \left(\frac{\left| U^T U_{pca}^T S_B U_{pca} U \right|}{\left| U^T U_{pca}^T S_W U_{pca} U \right|} \right) . \qquad U_{pca} = \arg\max_{U} \left(\left| U^T S_T U \right| \right) . \quad U_{ff} = U_{fld} U_{pca} .$$

Equ. 5-6

Finally, the matrix U_{ff} is calculated, such that it projects a face surface vector into a reduced space of *c-1* dimensions, in which the ratio of between-class scatter to within-class scatter is maximised for all *c* classes. Like the eigenface system, components of the projection matrix U_{ff} can be viewed as images, as shown in Figure 5-19 for the depth map surface space.

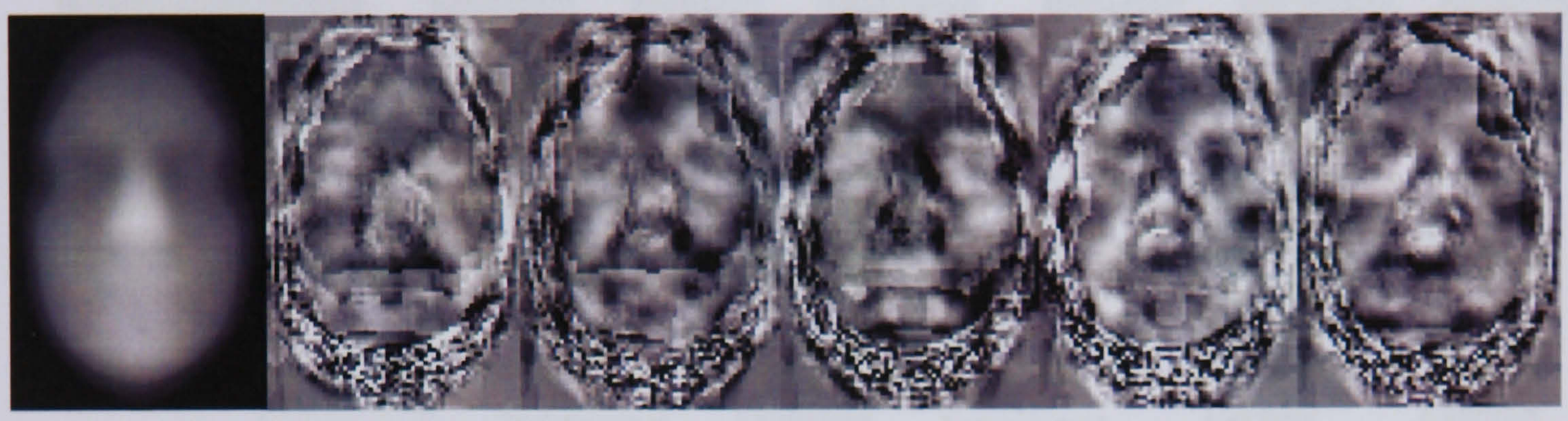

Figure 5-19 The average surface (*left*) and first five Fishersurfaces (*right*)

Once surface space has been defined, we project a facial surface into reduced surface space by a simple matrix multiplication, as shown in Equ. 5-7.

$$\Omega = (\Gamma - \Psi)^T U_{ff} .$$

Equ. 5-7

The vector $\Omega^T = [\omega_1, \omega_2, \ldots, \omega_{c-1}]$ is taken as a 'face-key' representing the facial structure in reduced dimensionality space. Face-keys are compared using either Euclidean or cosine distance measures as shown in Equ. 5-8.

$$d_{euclidean} = \left\| \Omega_a - \Omega_b \right\| . \qquad d_{cosine} = 1 - \frac{\Omega_a^T \Omega_b}{\left\| \Omega_a \right\| \left\| \Omega_b \right\|} .$$

Equ. 5-8

An acceptance (facial surfaces match) or rejection (surfaces do not match) is determined by applying a threshold to the distance calculated. Any comparison producing a distance value below the threshold is considered an acceptance.

5.6.1 Evaluation Procedure

For the purpose of these experiments we select a sample of 1770 face models (280 people), from the University of York 3D Face Database (UOY-3DFD) captured under the conditions shown in Figure 5-20. During data acquisition no effort was made to control lighting conditions. In order to generate face models at various head orientations, subjects were asked to face reference points positioned roughly 45° above and below the camera, but no effort was made to enforce precise orientation.

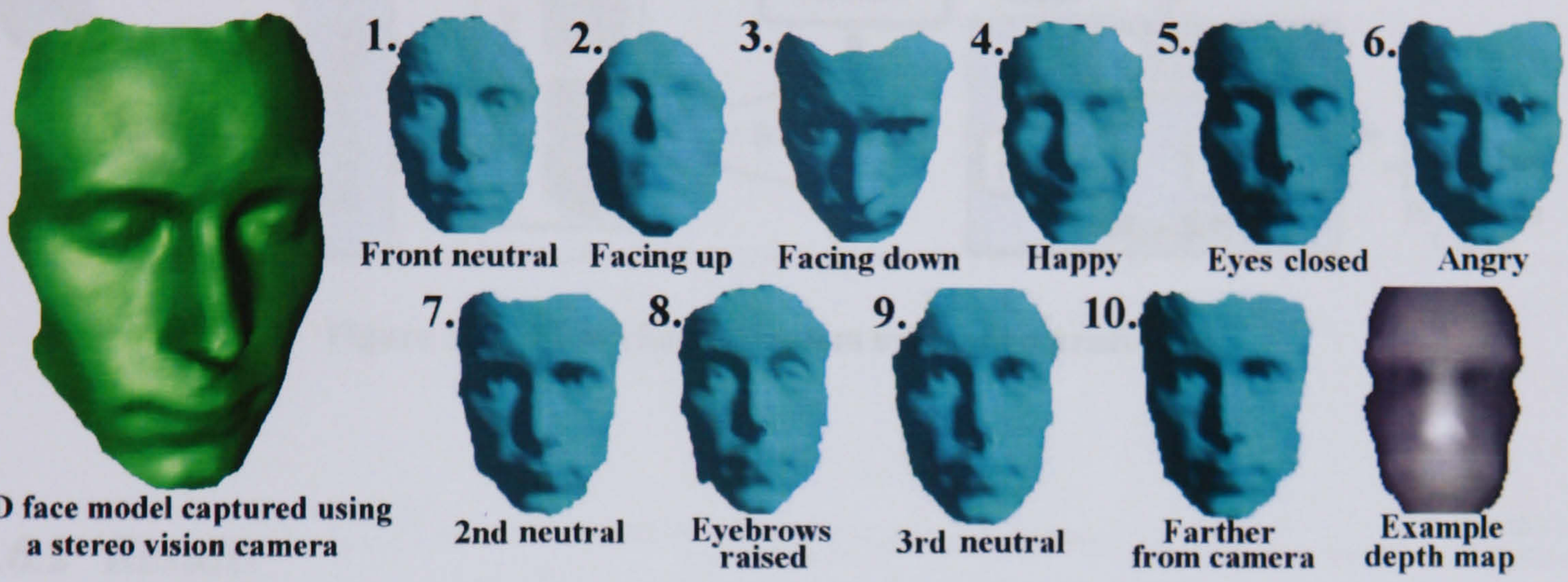

Figure 5-20 Example face models taken from The University of York 3D face database

3D models are aligned to face directly forwards before conversion into depth map representation. The database is then separated into two disjoint sets: the training set consisting of 300 depth maps (6 depth maps of 50 people) and a test set of the remaining 1470 depth maps (230 people), consisting of all capture conditions shown in Figure 5-20. Both the training and test set contain subjects of various race, age and gender and nobody is present in both the training and test sets. The training set of 300 surfaces is then used to calculate the projection matrices as described in section 5.6.

In order to evaluate the effectiveness of a surface space, we project and compare the 1470 face surfaces with every other surface in the test set, no surface is compared with itself and each pair is compared only once (1,079,715 verification operations). The false acceptance rate (FAR) and false rejection rate (FRR) are then calculated as the percentage of incorrect acceptances and incorrect rejections after applying a threshold. Varying the threshold produces a series of FAR FRR pairs, which plotted on a graph produce an error curve as seen in Figure 5-23. The equal error rate (EER, the point at which FAR equals FRR) can then be taken as a single comparative value.

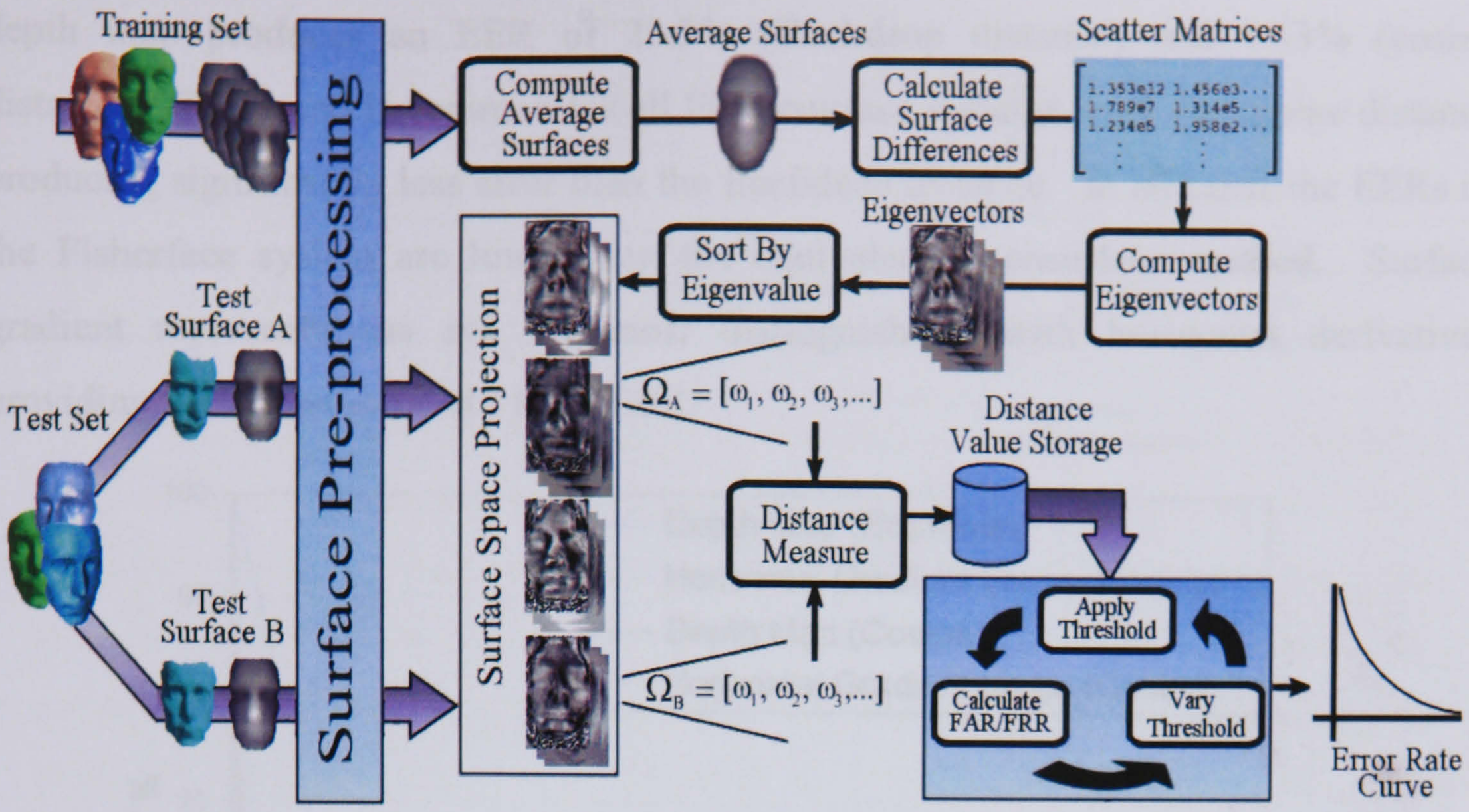

Figure 5-21 Flow chart of system evaluation procedure

5.6.2 Results

In this section we present results gathered from performing 1,079,715 verification operations on the test set of 1470 face models, using the surface representations described in section 3. Systems are tested separately using Euclidean and cosine distance measures. In addition we provide a direct comparison to the eigensurface method [16] trained and tested using the same face models, distance metrics and the same number of (c-1) principal components.

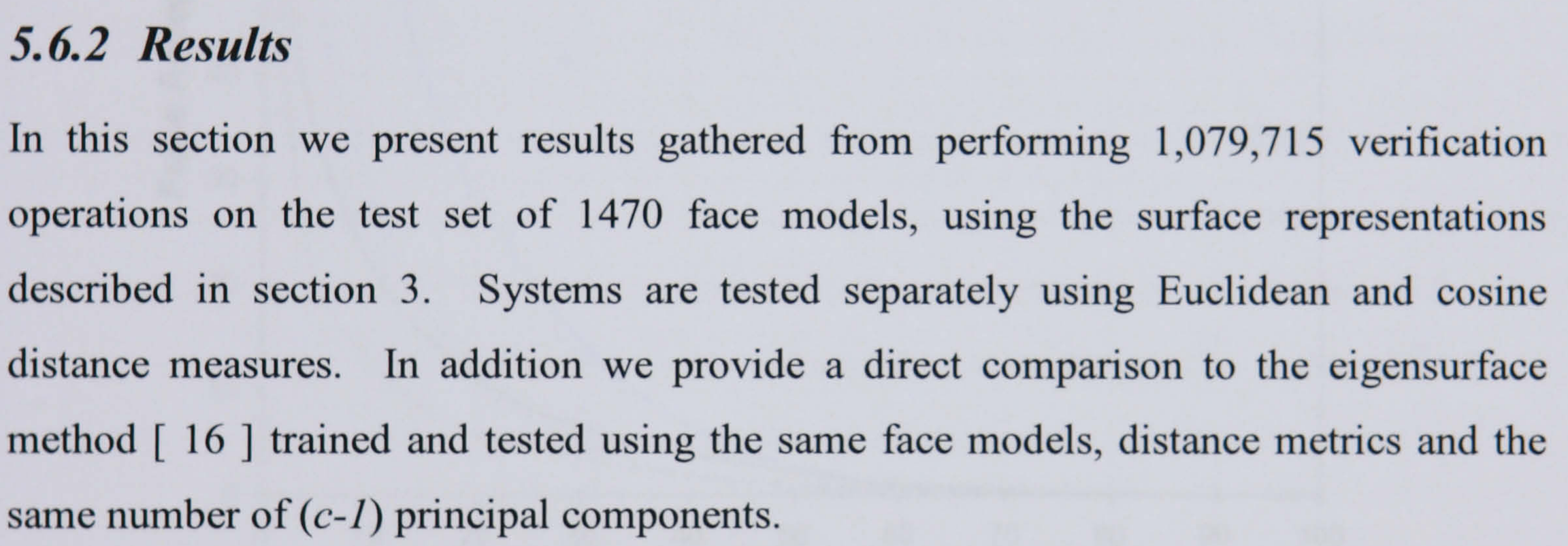

Figure 5-22 EERs of Fishersurface and eigensurface systems using two distance metrics

Figure 5-22 shows the diversity of error for eigensurface and Fishersurface methods, using cosine and Euclidean metrics for the range of surface representations. The initial

depth map produces an EER of 23.3% (Euclidean distance) and 15.3% (cosine distance). This trend is common for all Fishersurface systems, with the cosine distance producing significantly less error than the Euclidean distance. In all cases the EERs of the Fisherface system are lower than the equivalent eigensurface method. Surface gradient representations are the most distinguishing, with horizontal derivatives providing the lowest error of 11.3% EER.

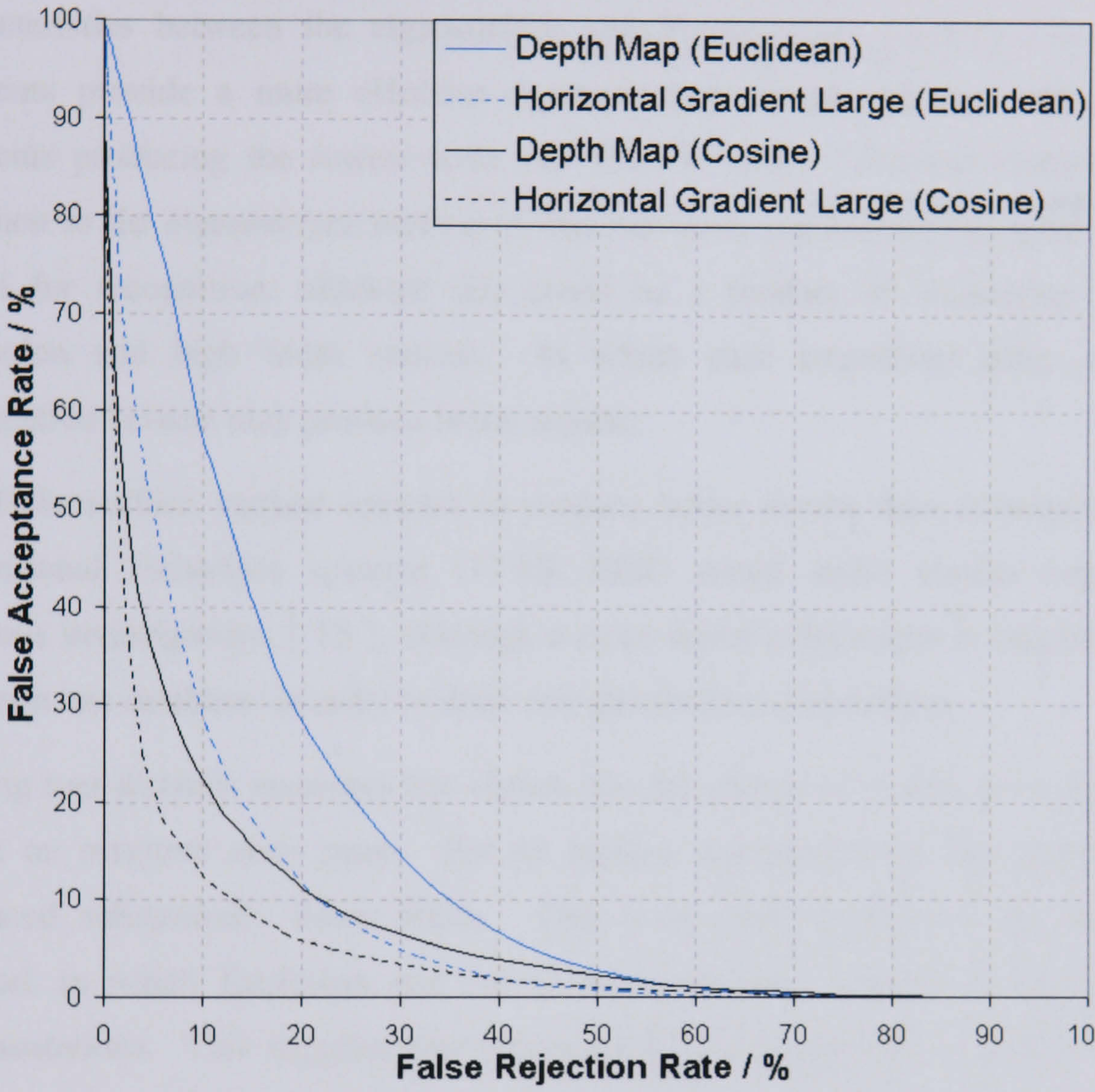

Figure 5-23 Fishersurface system error curves using two distance metrics and surface representations

5.6.3 Conclusion

We have applied a well-known method of two-dimensional face recognition, namely the Fisherface method, to 3D face models using a variety of facial surface representations, which we name the Fishersurface method. The error rates produced using the initial depth map representation (15.3% and 23.3% EER) show a distinct advantage over the previously developed eigensurface method (32.2% and 24.5% EER). This is also the case for the best surface representations, producing 11.3% EER for the Fishersurface system and 24.5% EER for the eigensurface method. We also note an increase in the

eigensurface EERs compared to those reported in section 5.5 (published in [16]). This could be attributed to the different training and test data, or possibly the different number of principal components used.

Experimenting with a number of surface representations, we have discovered common characteristics between the eigensurface and Fishersurface methods: facial surface gradients provide a more effective representation for recognition, with horizontal gradients producing the lowest error rate (11.3% EER). Another observation, also common to the eigensurface method is that curvature representations seem to be least useful for recognition, although this could be a product of inadequate 3D model resolution and high noise content. In which case smoothing filters and larger convolution kernels may produce better results.

The Fishersurface method appears to produce better results than corresponding two-dimensional Fisherface systems (17.8% EER) tested under similar conditions in previous investigations [15], although a more direct comparison is required, using a common test database, in order to draw any quantitative conclusions.

Testing two distance measures has shown that the choice of metric has a considerable effect on resultant error rates. For all surface representations, the cosine distance produced substantially lower EERs. This is in stark contrast to the eigensurface method, in which Euclidean and cosine measures seem tailored to specific surface representations. This suggests that incorporating LDA produces a surface space with predominantly radial between-class variance, regardless of the surface representation, whereas when using PCA alone, this relationship is dependant on the type of surface representation used.

In summary, we have managed to reduce error rates from 15.3% EER using initial depth maps, to an EER of 11.3% using a horizontal gradient representation. This improvement over the best eigensurface system shows that incorporation of LDA improves performance in 3D as well as two-dimensional face recognition approaches. Given that the 3D capture method produces face models invariant to lighting conditions and provides the ability to recognise faces regardless of pose, this system is particularly suited for use in security and surveillance applications.

5.7 IRAD Face Contours

In this section we propose a new technique for comparing 3D face models, which is distinct from the appearance-based subspace methods discussed throughout the rest of this thesis. This new approach is fuelled by our appreciation that subspace methods require accurate alignment prior to recognition and the incentive to obviate this requirement.

The goal was to create a representation of the face, capable of storing both geometric shape and colour information, that is invariant to rotation and translation in 3D space, requiring as little feature localisation and pre-registration as possible. In working towards this goal we have produced a technique capable of recognising not only faces, but any 3D object with at least one easily located feature. We call this technique the Isoradius contours method, and we abbreviated this to the IRAD method.

The method is most effective when there is a distinctive and easily identified feature on the surface of a 3D object that can be localised with high precision. In the case of the human face, one such feature is the tip of the nose. We have already discussed techniques for localising this feature in section 5.2.1 and we use those same procedures to detect the required feature for the IRAD contours method. However, we will not require the subsequent steps of locating the nose bridge and forehead or balancing the left and right sides of the face (in other words orientation normalisation is not required) before performing recognition: the IRAD contours method reduces the orientation problem to a simple signal correlation at a later stage in the process.

Once the nose has been located we produce the IRAD contours. We define an IRAD contour as the intersection of a sphere (radius r, centred at the nose tip), with the facial surface. Hence, an IRAD contour forms a space curve, often in a closed loop on the 3D surface for which each point is a distance *r* from the nose tip. By altering the radius r of the intersecting sphere we are able to produce an IRAD contour passing through any point of the object surface. Therefore, it is possible to represent the entire facial surface as a set of IRAD contours, relative to the nose tip. By selecting several discreet radii, we produce a set of IRAD contours from which signals are extracted. There may be one signal from the IRAD contour, for example describing contour shape, or there may be many signals, describing shape, texture, colour etc.

We discuss the details of generating the IRAD contours in section 5.7.3, before describing the recognition component in terms of cross-correlating signal ensembles extracted from these contours in section 5.7.5.

The use of the sphere is an important concept, as the spheres infinite rotational symmetry means that the shape of the IRAD contour is independent of surface orientation and hence invariant to subject pose. We are able to perform pose invariant recognition, by reducing the alignment search space to a simple one-dimensional cross-correlation process, with the potential to incorporate both geometric structure as ell as colour and texture information. In addition there is also the potential for overcoming the problems associated with facial expression (although this is yet to be tested), which we discuss in section 5.7.7.

IRAD contours are not restricted to object recognition alone, but may also be used in the registration process of a 3D object (such as a face) by determining the orientation and facilitating alignment procedures prior to other methods of 3D face recognition as discussed in this thesis.

5.7.1 Previous Work

Many methods of analysing and encoding 3D structure have been presented in the literature. However, relatively little of this research has been applied to the problem of face recognition. Gordon's work [4], comprised the localisation of multiple 3D facial features, such as the bridge of the nose, eye corners etc. before a comparison is made based on the depth and curvature feature space. Other papers [61] [51] also use 3D surfaces combined with 2D intensity information, although again these required the localisation of multiple features before some form of registration takes place (i.e. image alignment and 3D orientation).

In this thesis we have used 3D model object files consisting of interconnected vertices as well as encoding this as normalised surface information in the form of depth maps. Beumier and Acheroy [3] take profile contours as 3D features, Coombes et al [32] extract segments based on curvature classification, whereas Heseltine [16] [17] (see section 5.5 and 5.6) and Hesher [6] use principal components of surface shape as features. The IRAD contour approach described here has some similarities to the splash representations of Stein and Medioni [68], in which normal deviation across a small

3D surface patch is used for 3D object recognition. Stein and Medioni liken the surface normal representation to the pattern produced by a 'milk splash' radiating out from a central point of collision, as normals radiate out respective to a central reference normal. Stenin and Medioni note that such representations are dependant on accurate localisation of the central reference point, in the same way that our IRAD contours method required the accurate localisation of the nose tip. However, the closest related work to the our approach is the research carried out by Chua et al [8], using a 3D point signature to recognise human faces. The concept of point signature was initially discussed by Chau and Jarvis [31], investigating new approaches of recognising 3D objects.

Chua et al produce a point signature for a point p on the 3D surface by intersecting a sphere of radius r (centred at point p) to form a curve C. A plane of best-fit P, is then approximated to this curve C, passing through point p. The signature is extracted as the orthogonal distance from plane P to curve C, sampled at regular intervals for the full range of 360 degrees about p. Because C is unlikely to be planar, the orthogonal distance varies around the circumference: being positive when C is above the plane and negative when below.

The approach taken by Chua et al varies from the IRAD contours method by two key factors:

- Firstly, Chua et al generate a single signature for a specific point on the facial surface. To perform recognition, many of these points are required and hence multiple features must be detected. In contrast the IRAD contours method generates multiple contours relative to a single point on the 3D surface.

- In the point-signature method, the signature is measured according to the orthogonal distance from the 3D surface to a best-fit plane. In contrast, the IRAD contours methods extracts a signal describing the surface normal variance across the surface contour.

Chua et al's method suffers from the problem that any missing or deformed parts of the surface can severely disrupt the signature extracted. This is because each signature is measured relative to a best-fit plane passing through the point of interest. Any noise,

such as spikes or holes will effect the orientation of the best-fit plane and hence alter the entire signature for that point. Such an effect will also occur due to changing surface shape due to facial expressions and ageing. In contrast, the signal generated for one area of the surface by the IRAD contours method, is not dependant on the surface shape of the rest of the face. For example, the signal extracted across the rigid forehead area will remain consistent, despite changes in the signal extracted from the same contour across the more malleable mouth and cheek areas.

5.7.2 The IRAD Contour Representation

In these investigations we use the University of York 3D face database as described in section 5.1.3. In particular we make use of the wire-mesh representation, in which each vertex in the point cloud is connected to a number of neighbouring vertices on the facial surface. We separate IRAD contour signal extraction into three conceptual stages:

- Nose tip detection.
- IRAD contour generation.
- Signal extraction.

We now discuss the contour generation and signal extraction stages in the sections below, while referring the reader to section 5.2.1 for a discussion on localizing the nose tip.

5.7.3 Isoradius Contour Generation

We define an 'Isoradius Contour' (or IRAD for short) as the locus across a 3D surface that is at a constant distance from some point of interest (typically the tip of the nose for face recognition) on the same 3D surface. One may think of this locus as the intersection of a sphere (radius r, cantered at a point of interest p) with the 3D surface. If the surface is planar, then this locus will be a circle in 3D space, also centred about p. However, a non-planar surface will generate an irregular contour that meanders across the surface at a constant distance r from p.

Figure 5-24 Contour generation using the intersection of a sphere on the face surface

By varying the radius r, we generate a series of concentric contours on the 3D surface, as shown in Figure 5-24. We may select any arbitrary density of IRADs on the surface, although a suitable density would be to increment the radius by a similar amount to the average inter-point distance in the 3D mesh representation.

Unless the 3D surface is of sufficiently high density, it is unlikely that many of the vertices in the 3D mesh will lie precisely on the surface of the sphere. Therefore, the points along the IRAD are generated according to the facets that straddle the surface of the sphere. For an IRAD of radius r, centred about point p, we generate IRAD points along the contour using the algorithm described Figure 5-26.

```
For each vertex v of the 3D surface:
      For each neighbouring vertex n:
            If (|| v - p || < r and || n - p || >= r):
                  Calculate IRAD point as intersecting
                  vector vn at a distance r from p
```

Figure 5-25 IRAD contour generation algorithm.

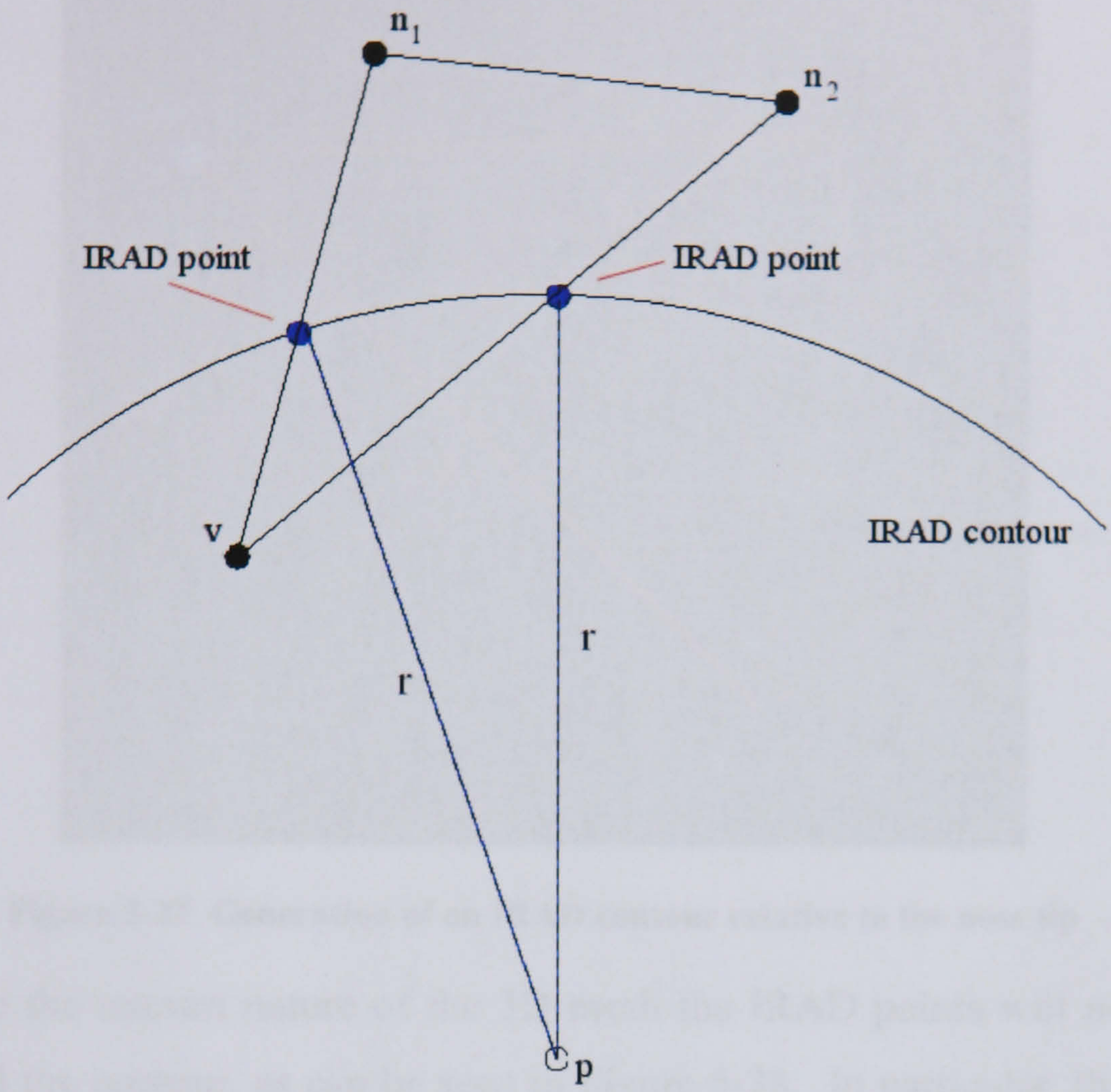

Figure 5-26 Interpolation of contour points between vertices in the original 3D point cloud

Note that the information as to which points are neighbouring is provided within the surface mesh data. Once these IRAD points are generated it is fairly simple to order the points according to their position around the contour by sorting them by the angle formed to the vertical axis through p. However, before a signal can be extracted there are a few more practical issues that need addressing.

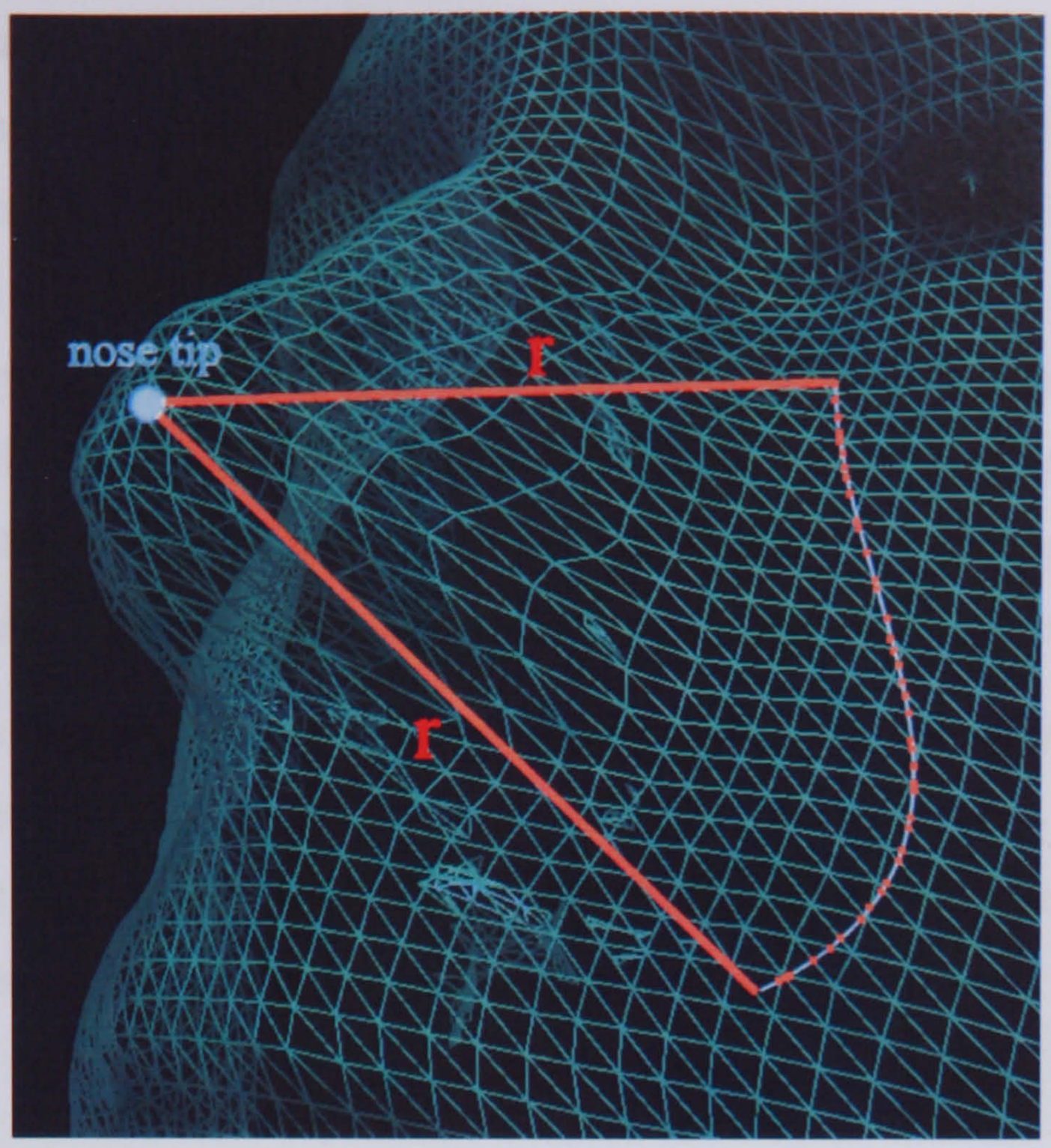

Figure 5-27 Generation of an IRAD contour relative to the nose tip

Firstly, due to the uneven nature of the 3D mesh the IRAD points will not be evenly spaced around the contour, as can be seen in Figure 5-28. In particular, the points will be sparse in areas where the surface is near orthogonal to the viewing plane of the 3D capture camera. This problem can be solved by simply interpolating points around the contour at specific increments along the circumference.

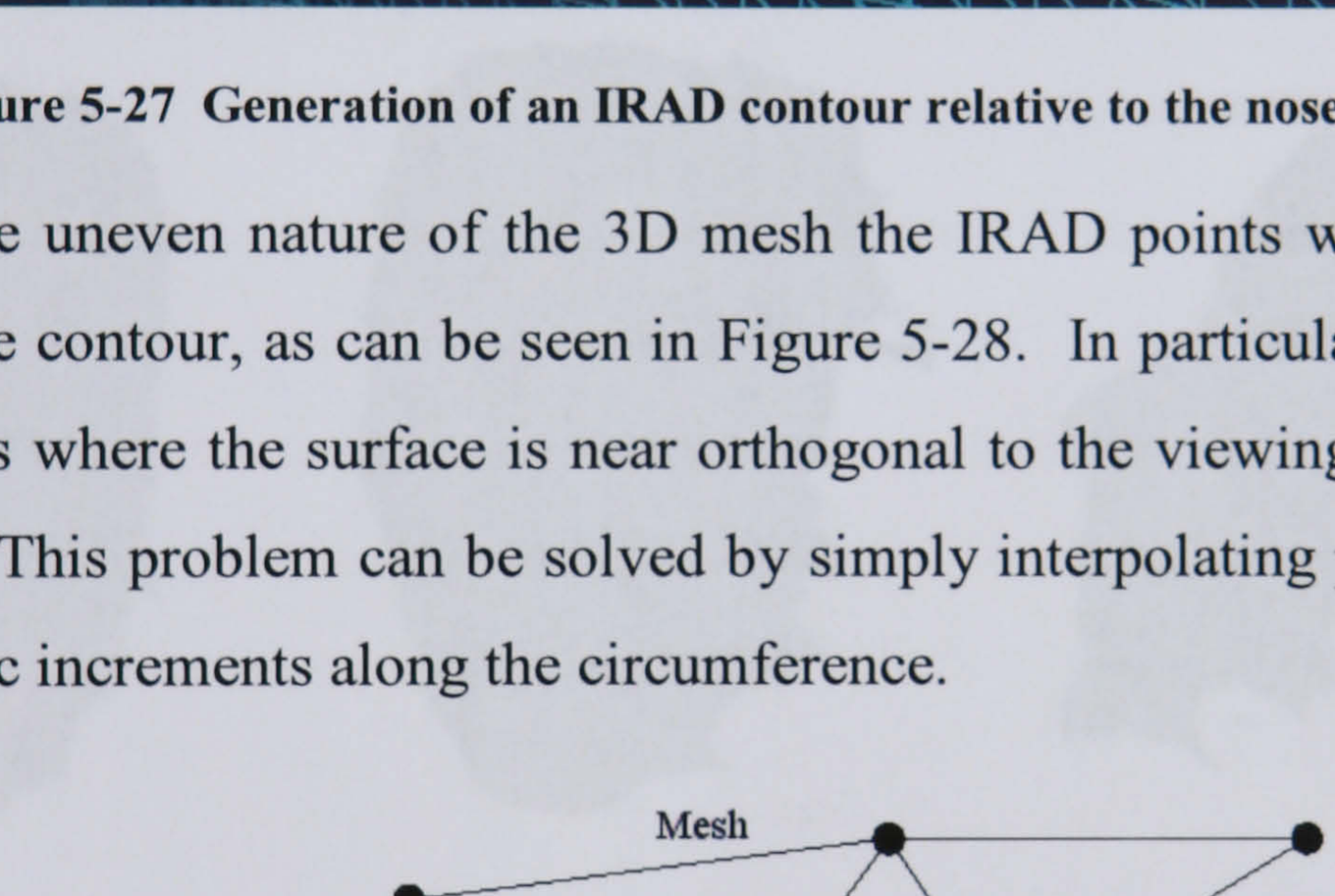

Figure 5-28 Irregular contour points interpolated from existing vertex mesh

The second issue of concern is that if there are holes in the 3D surface (due to occlusions or specular reflection causing problems with the 3D reconstruction algorithm) than this can result in a broken IRAD contour. We have two options for dealing with this problem. We could simply interpolate over the holes, just as we do in generating evenly spaced IRAD points or we can maintain a fragmented IRAD contour, sections of which must be recognised separately in the comparison stage. A sensible approach is to interpolate over any small holes, whilst allowing the larger holes to break the contour, leading to matching fragmented signals as described in section 5.7.6.

To conclude this section, we have devised a method of generating consistent loci on a 3D facial surface, relative to the nose tip, which we term IRADs. The shape and location of these surface contours are invariant to rotation and translation in 3D space, providing the nose tip can be detected accurately.

Figure 5-29 IRAD contours invariant to rotation in 3D space

5.7.4 Signal Extraction

We now described the signal extraction phase of the IRAD contour method of face recognition. Having generated the IRAD contours in the previous section we have identified areas of the 3D surface that can be consistently and accurately located, regardless of the orientation of the 3D facial surface. What remains is to extract some features from these contours that can be used for recognition. We have two sources of information from which to extract these features. Firstly, there is the shape of the 3D surface itself and secondly we have the texture information (in terms of greyscale

intensity) of the surface. Using the intensity information is relatively simple as this is an independent scalar value, which can simply be read for each point on the IRAD. However, as discussed in previous chapters, in order to maximise one of the key advantages of 3D face recognition we must rely on the 3D shape alone (thus making the system invariant to lighting conditions). Therefore, given that incorporation of the texture information would be a relatively simple process at a later stage, we now concentrate on extracting a signal to represent the surface shape alone.

Any shape information that we extract from the IRAD contour must be relative to the tip of the nose in order to maintain a representation that is invariant to translation and reduce the orientation problem to a cross-correlation of a one-dimensional signal. One such feature, which we can measure relative to the contour direction, is the curvature of the facial surface. The curvature of any point on an IRAD contour may be represented by the local variance of the surface normal, which can be computed by a simple difference operation between the normal of one IRAD point and the next IRAD point (or nth point along to measure the variance over a greater distance).

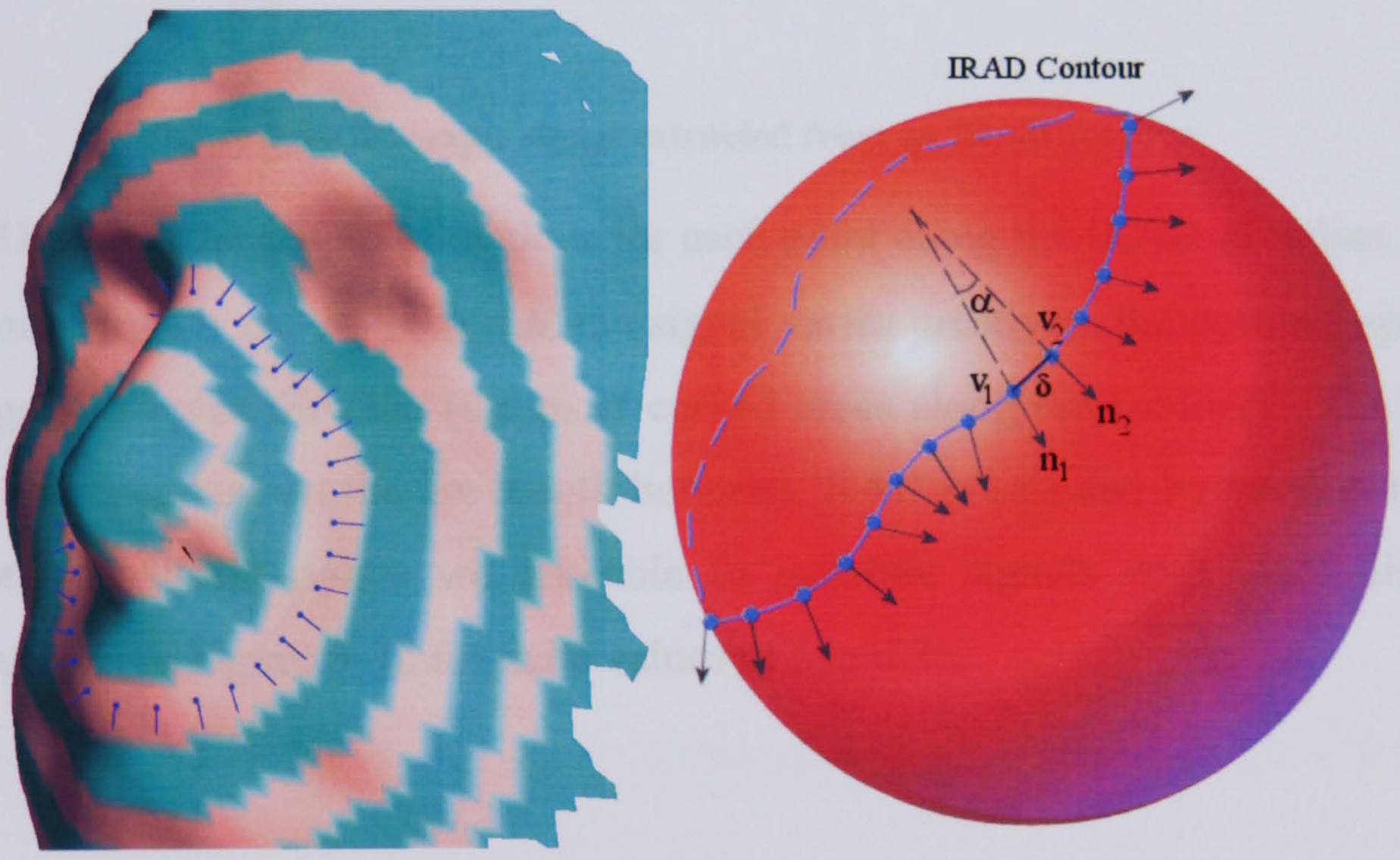

Figure 5-30 Surface normals used as an measurement of contour shape

Figure 5-30 above shows the normals of the facial surface for each point along the IRAD. A similar IRAD can be seen in the image on the right, represented on the sphere defining the IRAD radius, centred about p. Note that the shape of the contour itself could be encoded for recognition, but instead we take the difference between facial surface normals (*n1* and *n2* shown above). The signal extracted is the cosine of α, as

shown in Figure 5-31. Obviously, the difference between normals cannot be calculated over any holes in the surface, rather, such an occurrence is flagged as a break in the signal.

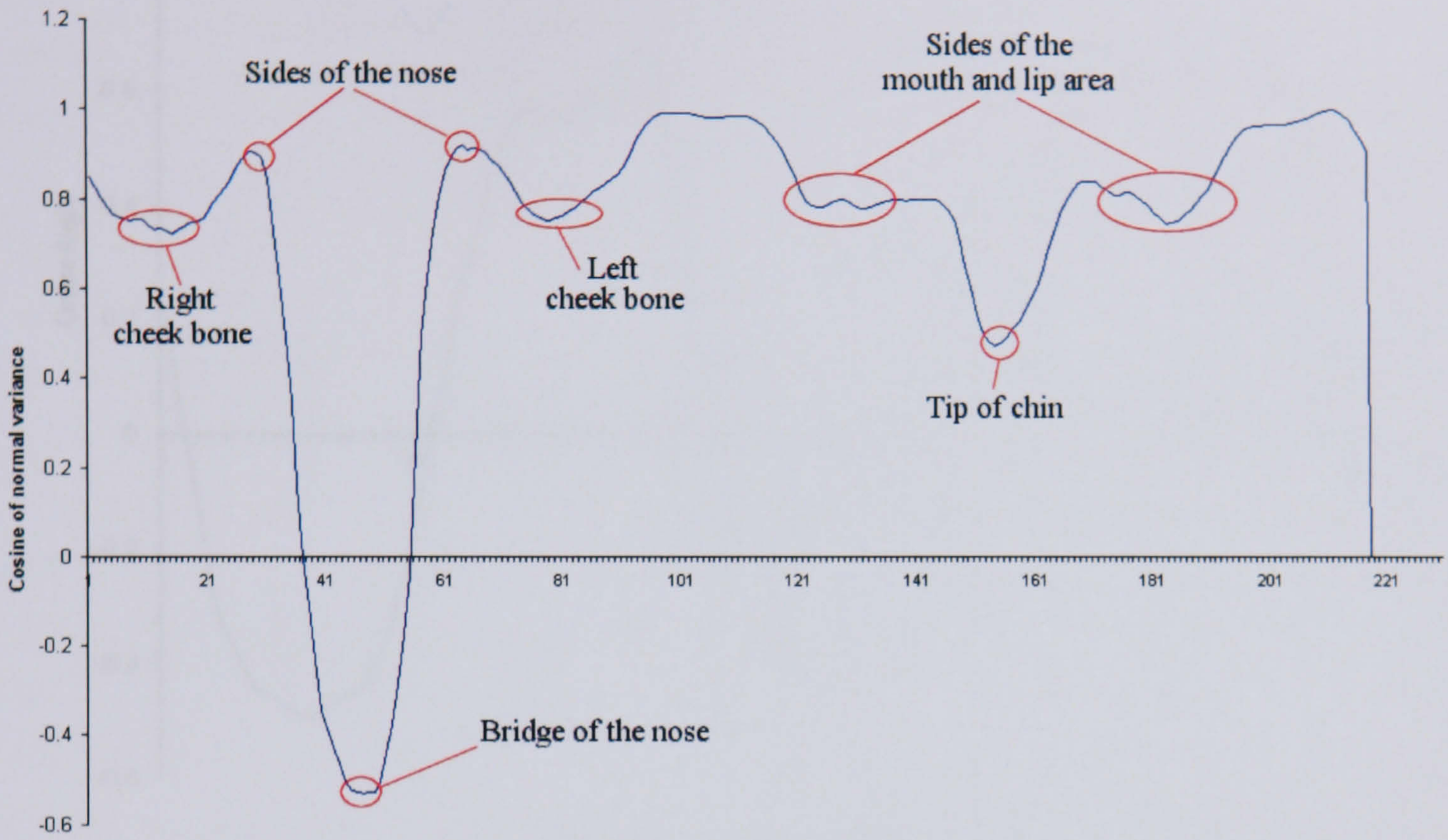

Figure 5-31 Example signal extracted from an IRAD contour

Figure 5-31 shows the cosine of angle α for each point along the IRAD of radius 21mm from the nose tip. It can be seen that the signal varies greatly as the normals span the nose bridge and tip of the chin (the most curved areas along the contour). The signal generated is dependant on the arc length between IRAD points and by varying the arc length between IRAD points we are able to generate signals with quite different features, as seen in Figure 5-32 for delta values of 5 and 25.

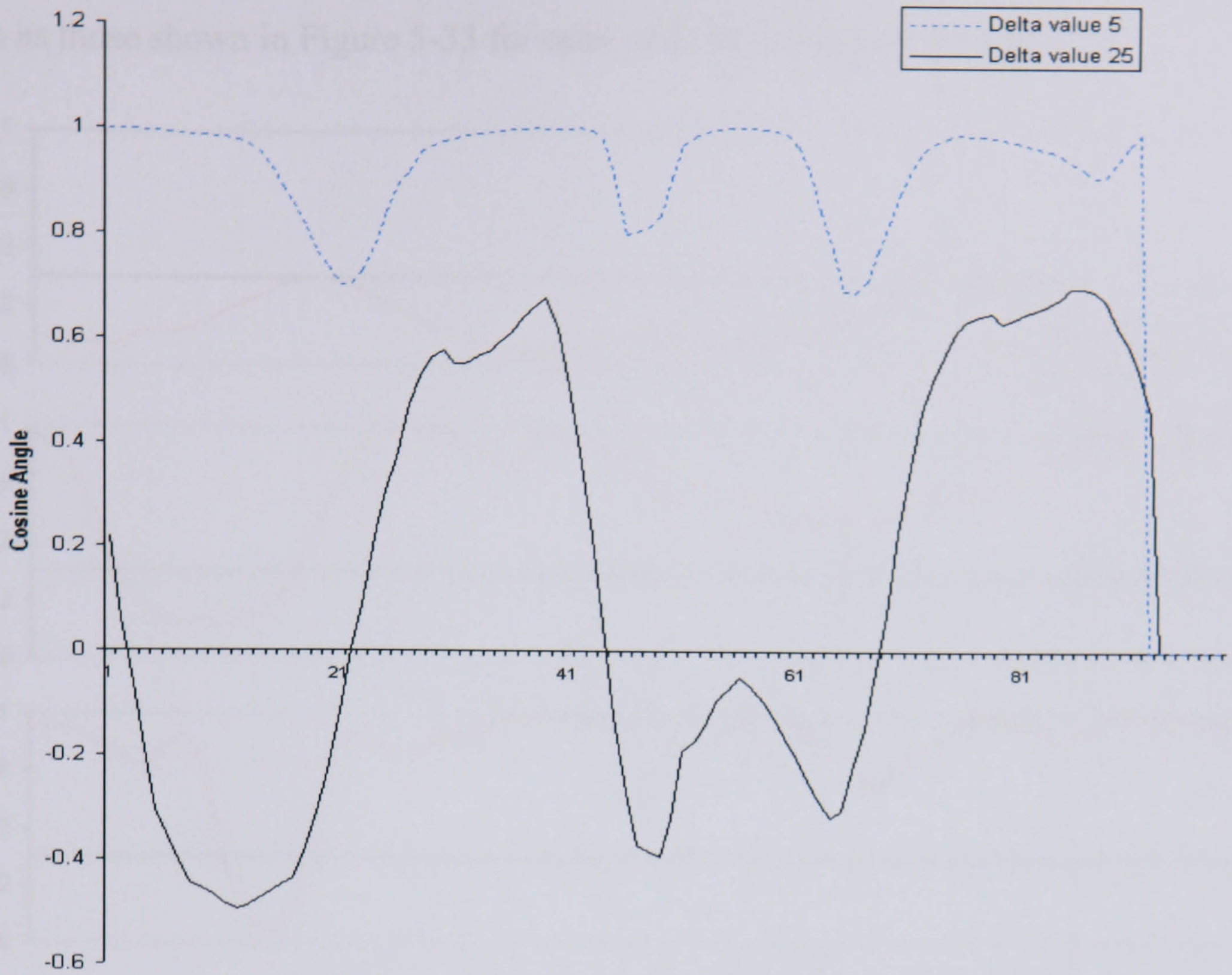

Figure 5-32 Two IRAD contour signals generated from the same contour using different delta (step) values

As alternative (or additional) cues we can also extract any of the following data from the IRAD:

- The contour shape itself encoded as the change in contour direction from one IRAD point to the next.
- The greyscale intensity of each IRAD point.
- The components of some (possibly normalised) colour space for each IRAD point.

Each of these signals can be used in unison, creating an ensemble of one-dimensional signals representing surface shape, contour shape, colour and texture of the 3D face, with each value associated with a specific IRAD point.

The next step is to extract multiple signals to describe a greater area of the 3D facial surface. Each IRAD only describes a single contour across the surface of the face, but

by generating multiple IRADs at various radii, we produce a larger ensemble of signals, such as those shown in Figure 5-33 for radii of 8, 16, 24 and 48 respectively.

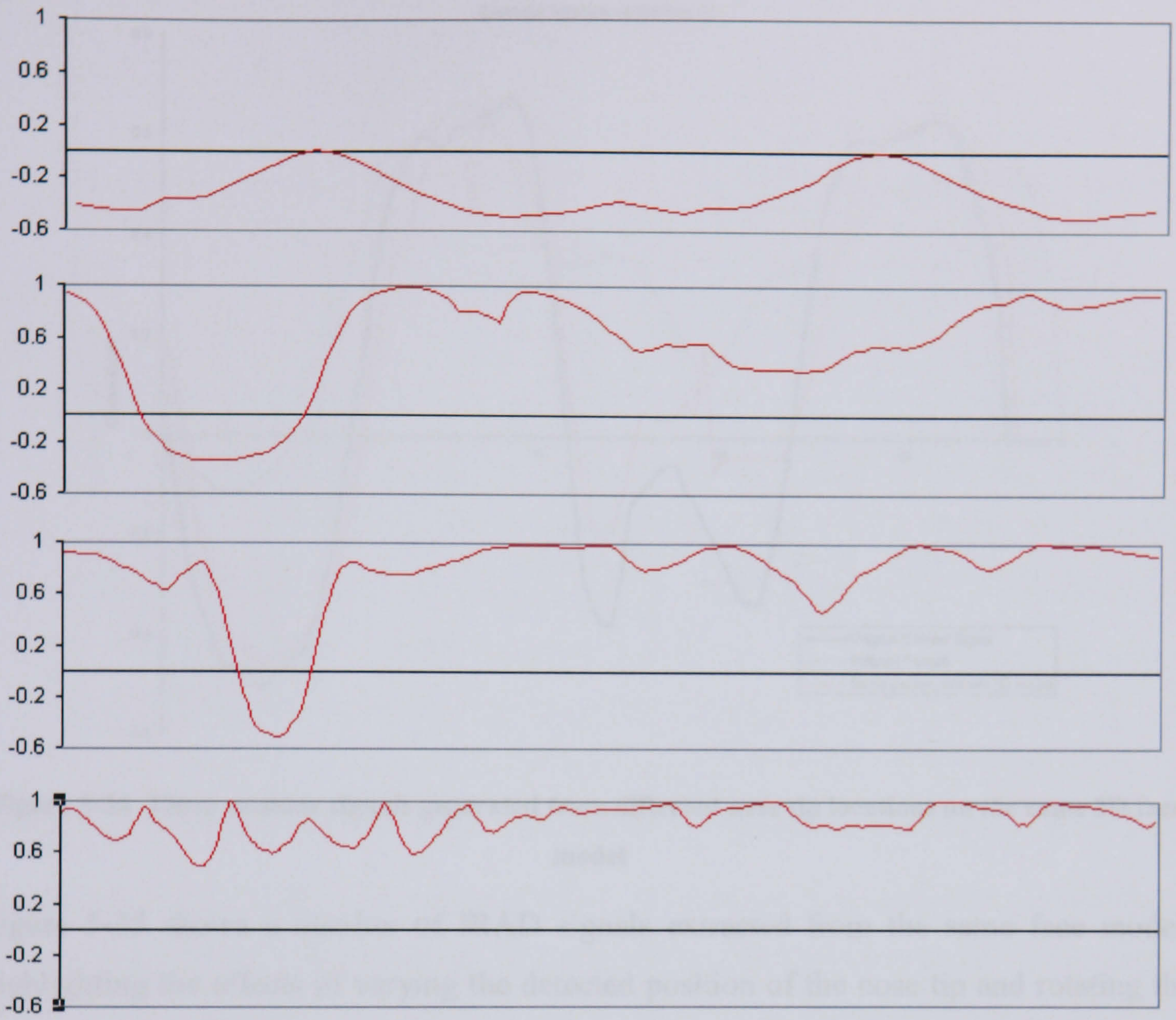

Figure 5-33 An IRAD contour signal ensemble, describing the shape of a 3D face surface

5.7.5 IRAD Comparison

In this section, we described how two 3D face models may be compared by correlating the IRAD signals extracted from each facial surface. Figure 5-34 shows three signals extracted from an IRAD of radius 21. The red and black signals are from two different models of the same person, whereas the dashed line is an IRAD signal of the same radius extracted from a 3D face model of a different person. Clearly the two different people have greatly differing face shapes as can be seen by the different signals in Figure 5-34. It is also clear that there are some small differences in the two signals from the same person. These are likely due to the variations introduced by changes in facial expression and perhaps slight variance in the localisation of nose tip. However,

the two signals from the same person correlate to a much higher degree than those from different people.

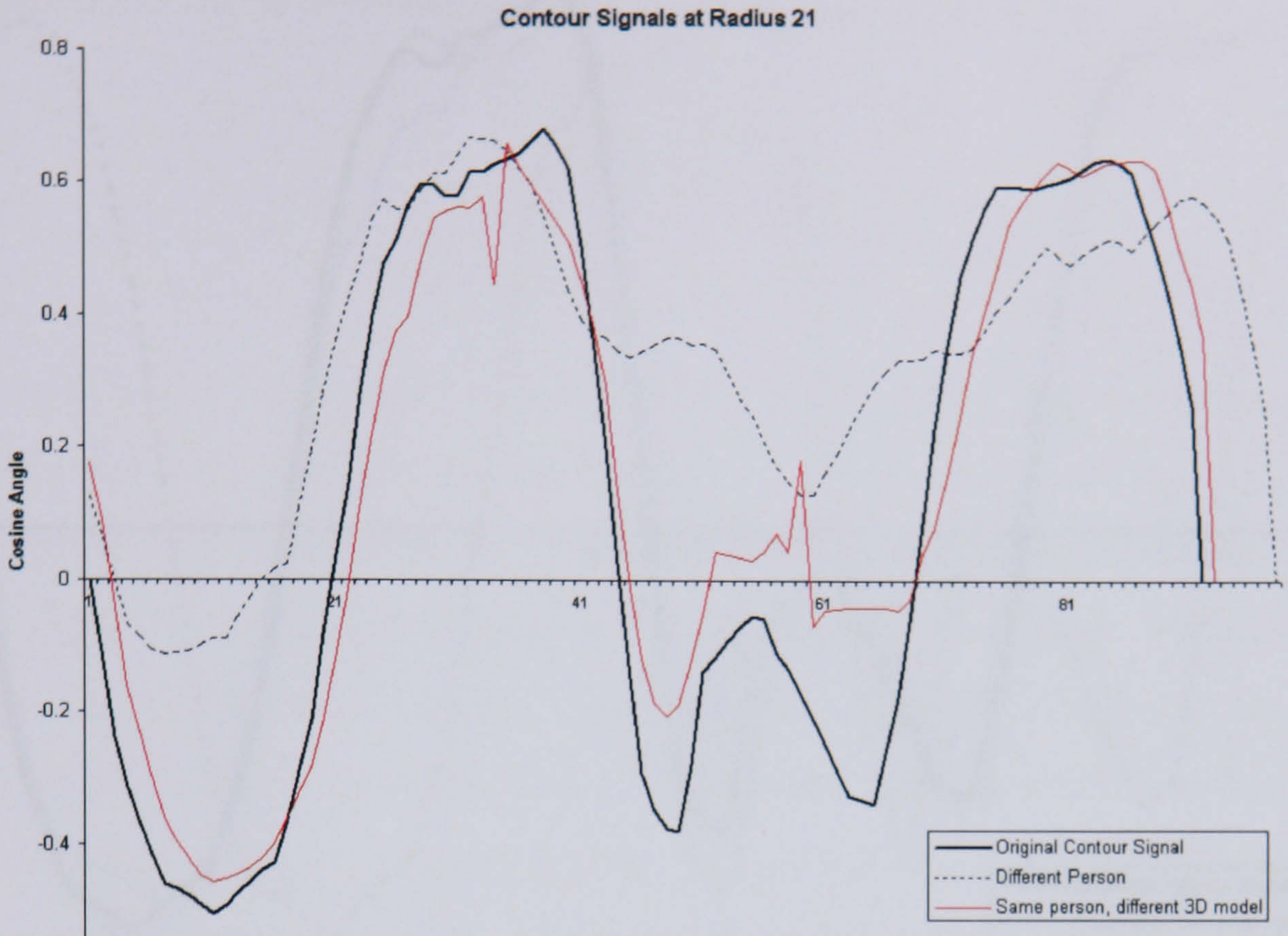

Figure 5-34 Three contour signals generated from different nose tip locations on the same 3D face model

Figure 5-35 shows a number of IRAD signals extracted from the same face model, highlighting the effects of varying the detected position of the nose tip and rotating the face model in 3D space. We see that varying the location of the nose tip results in minor deformation of the signal shape, whereas rotating the 3D model results in a phase shift of the signal along the x-axis.

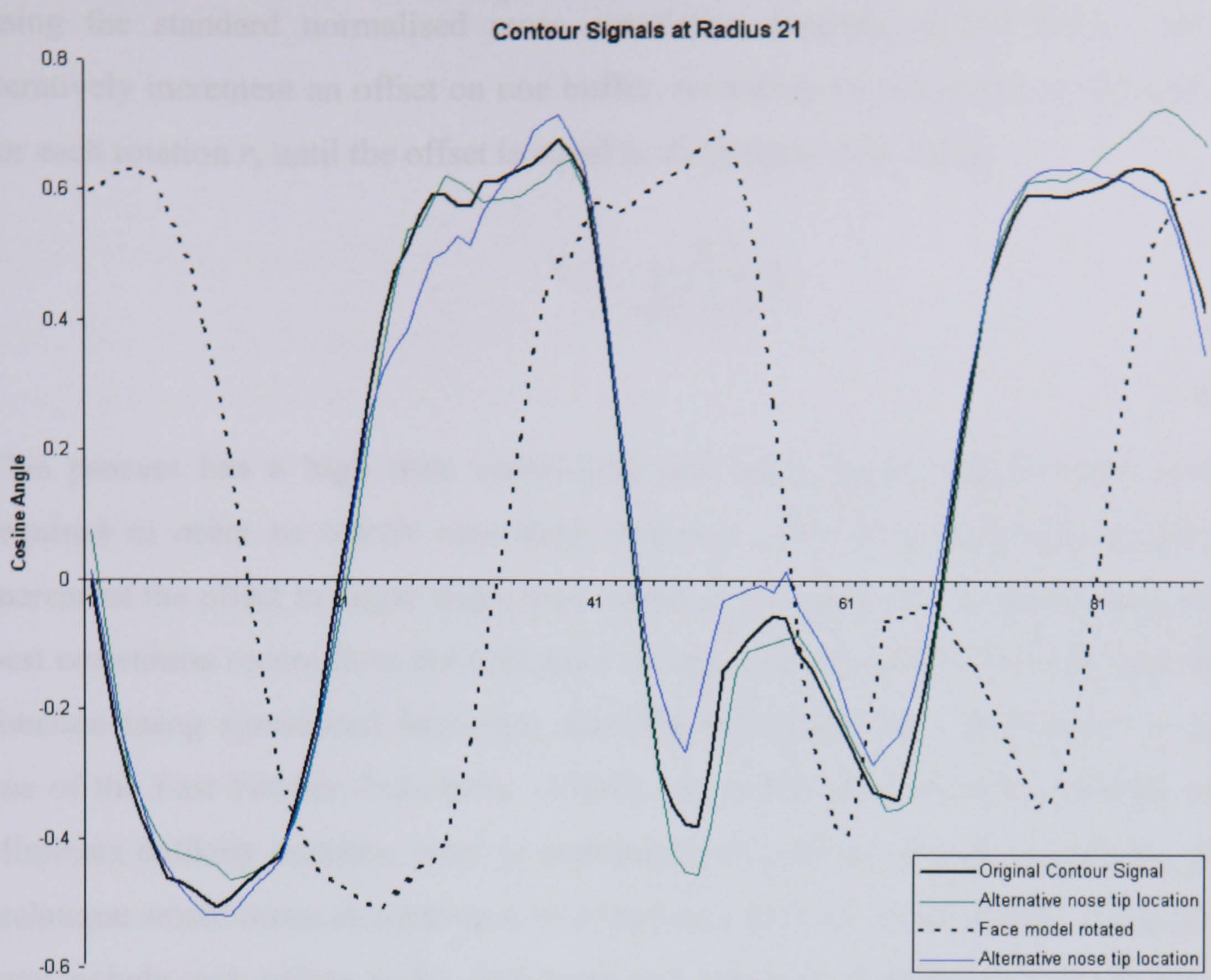

Figure 5-35 Variations in IRAD contour signal due to nose tip locations and rotations in 3D space

Signal comparison is done by a cross-correlation approach, measuring the correlation of any two signals across the full range of phase shifts. The highest correlation achieved is taken as the similarity score for that IRAD signal. The process of one dimensional signal correlation is well documented and it is this process that forms the final stage of the matching process. However, the power of the IRAD method is not in the cross-correlation itself, but in the method of signal extraction, which reduces the problem of translation and orientation in 3D space to a simple one-dimensional shift in the correlation process. What's more, because we are able to extract numerous signals from a 3D model (forming a signal ensemble) we are able to represent colour, texture and shape from all areas of the facial surface using the same method. Cross-correlation can then be repeated for each signal, and the correlation scores combined (by a weighted sum for example) to produce a final score. However, a more effective method would be to include a constraint to ensure that each signal in the ensemble could not correlate out of synchronisation with the other signals, thus enforcing the same shift (and hence the same rotational orientation) for each individual signal. We implement the correlation function by storing the query (q) and target (t) signals in two buffers for comparison

using the standard normalised cross correlation formula shown below, while we iteratively increment an offset on one buffer, recording the maximum correlation value for each rotation *r*, until the offset is equal to the length of the buffer.

$$C_r = \frac{q^T t}{\sqrt{q^T q + t^T t}}$$

Equ. 5-9

This process has a high time complexity and some speed optimisations would be required in order to search very large datasets. One such technique would be to increment the offset in larger steps, then repeat the calculation for offsets close to the N best correlation scores from the first pass. It may also be worthwhile implementing the function using specialised hardware, allowing extremely fast comparisons or making use of the Fast Fourier Transform. Finally, a number of pre-filters could be used to eliminate unlikely matches, prior to performing the full correlation procedure. Such a technique would mean computing a set of features from an IRAD signal. These features may include such values as the maximum and minimum amplitude of signal peaks and troughs, signal frequencies and surface path length, as well as using functions across multiple IRADs, such as the ratio of IRAD lengths. These pre-filtering criteria should be applied as weak constraints, before computing the full signal correlation. The tolerance thresholds on the criteria may be set according to the maximum expected within-class deviation, in order to ensure that no possible matches are eliminated.

The final step in computing some likeness score between to IRAD signal ensembles is to combine the correlation scores from multiple signals into a single unified score. In this chapter we investigate four of the simplest methods of combination:

- The sum of correlation scores from all IRADs.
- The sum of normalised (such that moments are equal) scores.
- The sum of scores from a subset of the most discriminatory IRADs.
- A weighed sum of scores (inversely proportional to the IRAD radius).

However, we do note that these combination functions are relatively unsophisticated and that much more effective methods of combination may be found with further investigation. Such methods may include a weighting based on the frequency and

amplitudes of the signal, or perhaps a discriminant analysis of the IRAD regions most useful for recognition. It may also be the case that other signals, such as those representing colour and texture are combined using another method.

5.7.6 Dealing with Noise

There are several common types of noise that are likely to be present in the IRAD signal ensembles. In this section we discuss some methods of coping with these unwanted artefacts, in order to improve recognition accuracy and increase operating capability. The types of noise we expect to encounter are:

- Spikes and pits on the 3D surface.
- Surface holes.
- Shape deformation.

Firstly, spikes and general surface noise can be eliminated using standard smoothing algorithms, such as Gaussian smoothing and point averaging. Selectively applying these techniques on a first pass to the large spikes (and pits), identified by measuring the distance along the z-axis to neighbouring points, can reduce these spikes before application of a more global smoothing to remove the lower amplitude surface noise.

Figure 5-36 Example effect of noise reduction on the 3D face surface using a simple local averaging technique

Small holes in the surface resulting from missing polygons (typically due to failure in finding a stereo correspondence) can easily be filled by computing an average central point and connecting the mesh. However, larger holes occurring on one side of the nose, because the subjects were facing to the left or right, or missing areas around the eyes and forehead due to hair or glasses require a different approach. Our signal matching procedure must be able to cope with partial signals, which do not complete a loop on the surface. In Figure 5-37 below it can be seen how a complete signal would be reduced to a partial signal as two unconnected surface areas. It is clear that the partial signal would not fully correlate with the original signal. However, by splitting the partial signal into two sub-signals at the point of the surface break, it is possible to match the two sub-signals to a larger complete signal by correlating each one individually. The rule applied in this scenario is to correlate partial signals in order of signal length. Once a correlation is achieved, further correlations are performed using any remaining sections of the signal not yet correlated.

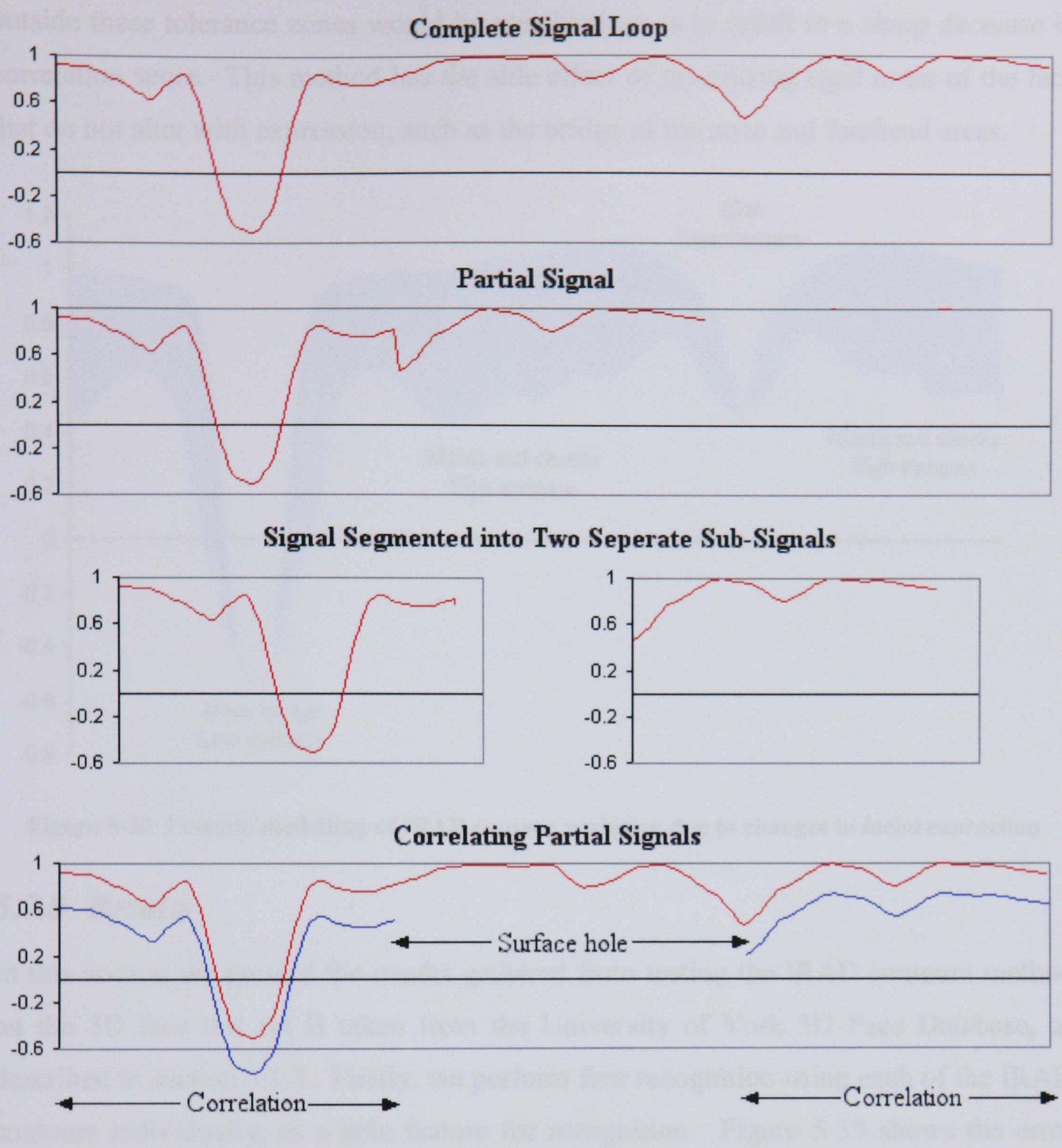

Figure 5-37 Method of combating the problem of partial IRAD contour signals

5.7.7 IRAD Variance Due to Facial Expression

One issue with the IRAD method that we have not yet touched upon is the ability to cope with variations in facial expression. The IRAD signal representation of the facial shape is susceptible to changes in facial expression and we have not incorporated any attempt to compensate for this in the results presented in section 5.7.8. However, it is possible to model variations in signal shape due to expression by modelling the variance in signal amplitude as expression changes. This would allow a tolerance 'buffer-zone' in which a signal correlation would be expected to vary. Any part of the signal falling

outside these tolerance zones would be weighted so as to result in a sharp decrease in correlation score. This method has the side effect of prioritising rigid areas of the face that do not alter with expression, such as the bridge of the nose and forehead areas.

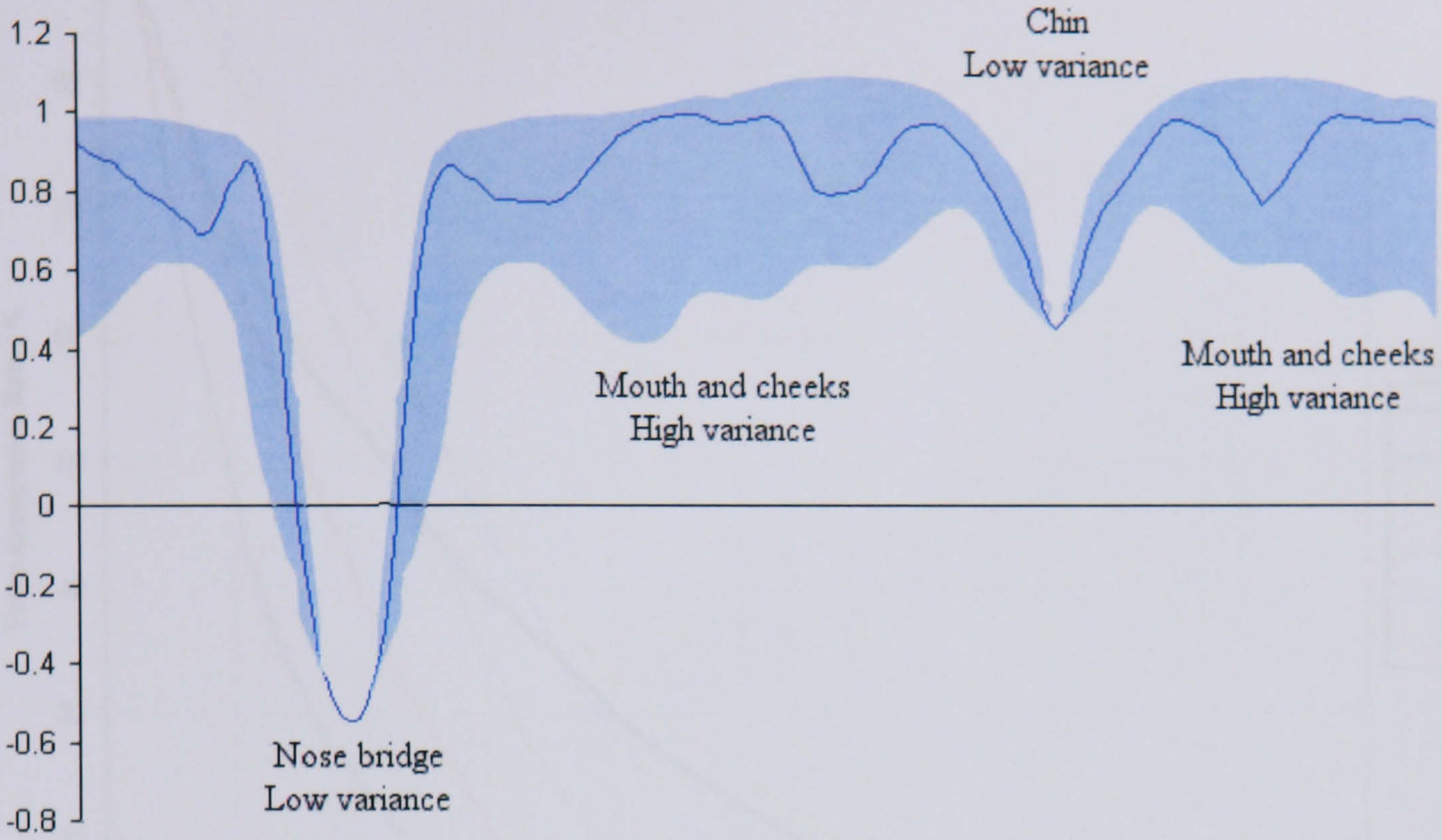

Figure 5-38 Possible modelling of IRAD contour variation due to changes in facial expression

5.7.8 Results

In this section we present the results gathered from testing the IRAD contours method on the 3D face test set B taken from the University of York 3D Face Database, as described in section 5.1.3. Firstly, we perform face recognition using each of the IRAD contours individually, as a sole feature for recognition. Figure 5-39 shows the error curves for six of the IRAD contours at a radius of 5, 21, 37, 53, 69 and 85 millimetres from the tip of the nose. We see that the EER varies from 21.91% for the IRAD contour of radius 21 millimetres, to 36.74% for the IRAD at a radius of 85 millimetres. Repeating this experiment for radii at increments of 2millimetres from 3 to 87 millimetres, we produce a bar chart of EERs comparing the effectiveness of each individual IRAD, as seen in Figure 5-40.

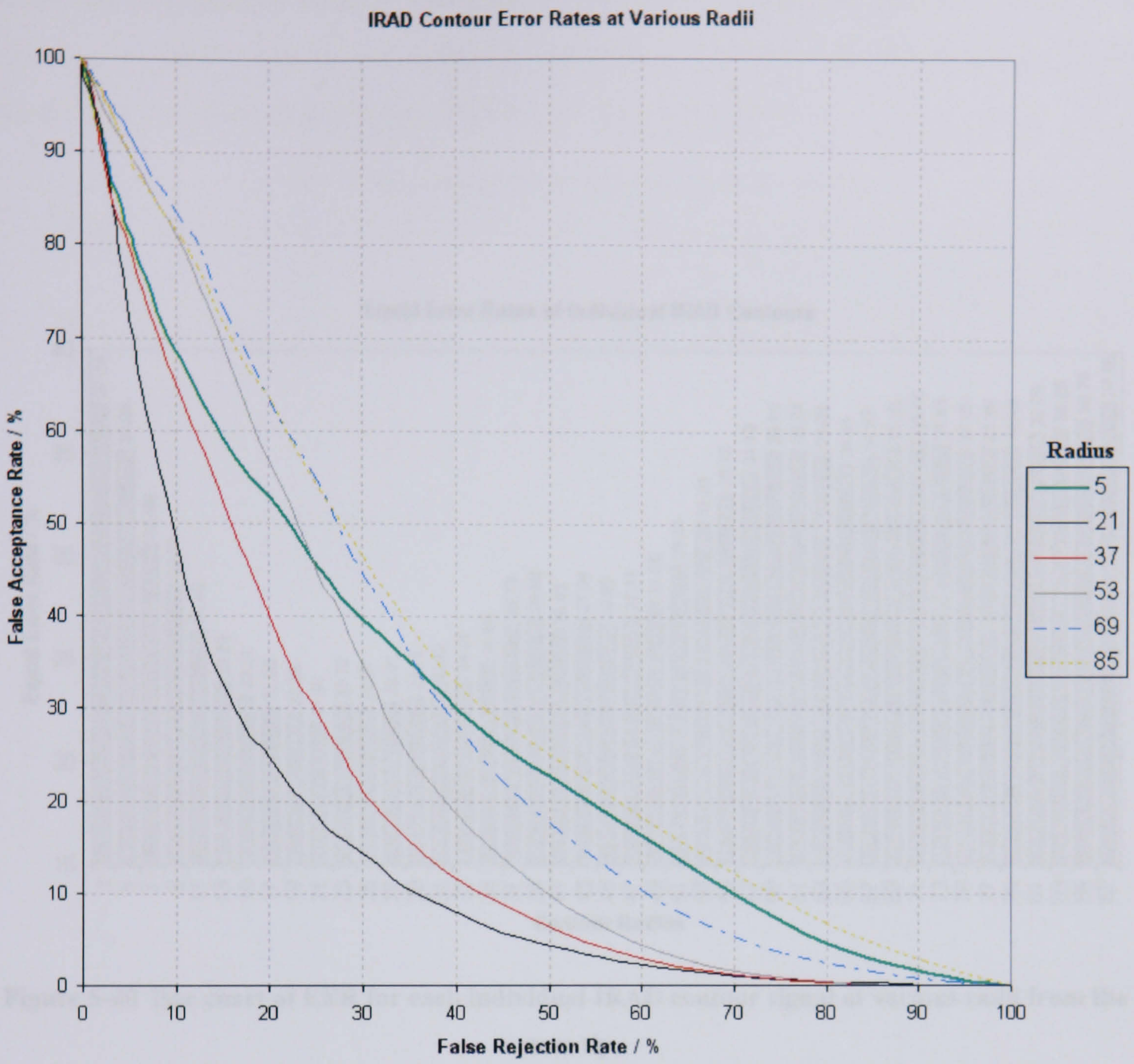

Figure 5-39 Error curves for six individual IRAD contour signals

It is clear from the bar chart below, that the smallest and largest radii are the worst performing. This is likely due to the very short length of the smaller IRADs and hence very little discriminatory information on which to base recognition, whereas the largest of the IRADs often extend beyond the boundaries of the side of the face and hence only represent a small segment of contour across the forehead (a relatively flat and non-distinctive part of the face). The most effective IRADs are those around the nose area, which tend to pass over the nose bridge, between 9 and 49 millimetres radius from the nose tip. The lowest EER achieved is 21.91%, which although substantially higher than some of the EERs produced by the Fishersurface systems, considering the method only utilises the shape information from a very small area of the face, it is surprisingly low i.e. 78% accurate from just one contour.

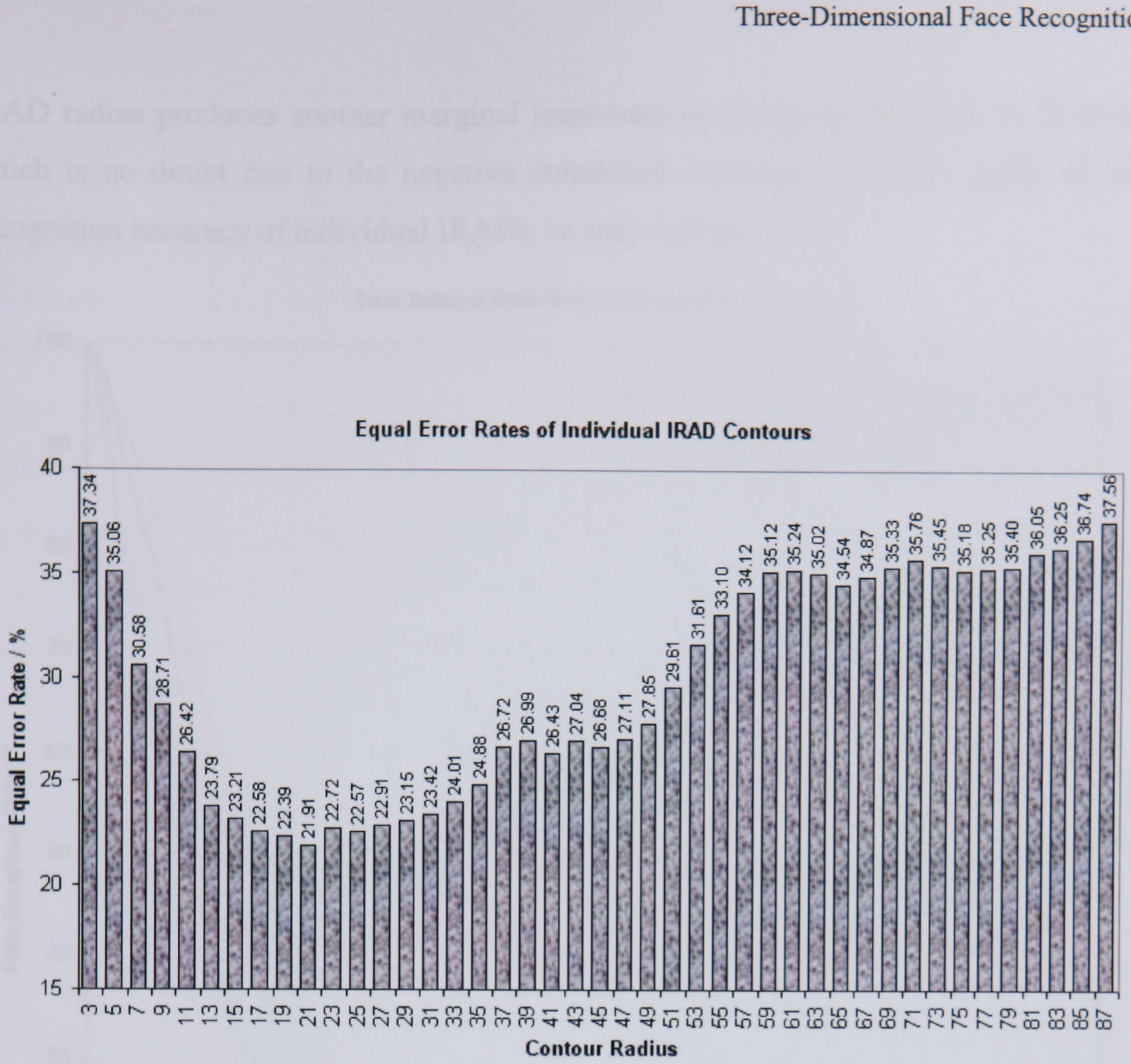

Figure 5-40 Bar chart of EER for each individual IRAD contour signal at various radii from the nose tip

The next step is to combine the scores using the four methods described earlier, to base the recognition on correlation of a signal ensemble (rather than a single IRAD). However, to produce the results shown in Figure 5-41, we have not implemented the rotational constraint that all IRADs must correlate 'in-phase'. That is, the rotational shift has been allowed to vary between signals i.e. the face is not considered as a rigid body.

We see that summing the correlation scores from all IRADs produced, results in a higher EER (25.40%) than using the best of the IRADs individually (21.91%). This result is only marginally improved (to an EER of 23.12%) by normalising the scores such that the average and standard deviation are equal for all signals prior to combination. However, we have been successful in improving the EER (down to 20.56%) by summing only those scores from the best performing IRADs (at radii between 9mm and 49mm). Finally, weighting the scores based on the inverse of the

IRAD radius produces another marginal improvement (dropping the EER to 20.02%), which is no doubt due to the negative correlation between the IRAD radius on the recognition accuracy of individual IRADs, as seen in Figure 5-41.

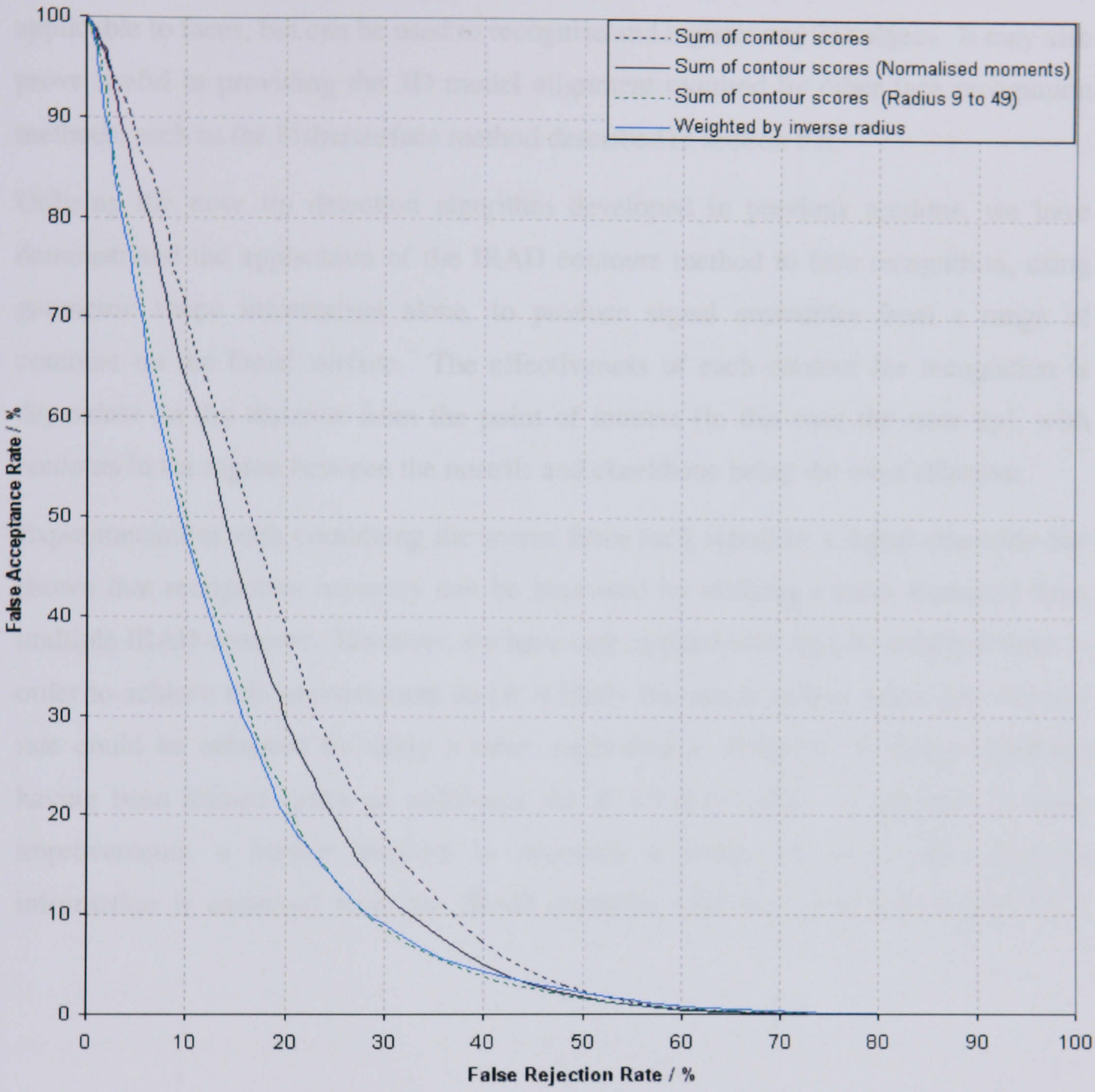

Figure 5-41 Error curve generated from combining multiple IRAD contour signals

5.7.9 Summary

We have developed a novel approach to 3D face recognition, capable of recognising faces based on cues extracted from both the colour and geometric shape data available in 3D face models. Unlike other face recognition algorithms, the IRAD contours method use relatively little registration in terms of feature detection and image alignment: requiring detection of a single point of interest, to which all extracted

features are relative. In particular, the method reduces the problem of head orientation to a one-dimensional shift in a simple cross-correlation process. The method is not only applicable to faces, but can be used to recognise and register any 3D object. It may also prove useful in providing the 3D model alignment required by other face recognition methods, such as the Fishersurface method described in section 5.6.

Utilising the nose tip detection algorithm developed in previous sections, we have demonstrated the application of the IRAD contours method to face recognition, using geometric shape information alone, to produce signal ensembles from a range of contours on the facial surface. The effectiveness of each contour for recognition is dependant on the distance from the point of interest (in this case the nose tip), with contours in the region between the nostrils and cheekbone being the most effective.

Experimentation with combining the scores from each signal in a signal ensemble has shown that recognition accuracy can be improved by utilising signals extracted from multiple IRAD contours. However, we have only applied very simple weighted sums in order to achieve this improvement and it is likely that much greater reductions in error rate could be achieved by using a more sophisticated weighting technique (perhaps having been trained using an additional set of 3D face data). In addition to these improvements, a further increase in accuracy is likely to occur when addition information is extracted from the IRAD contours, such as colour and texture data.

6 2D-3D Face Recognition

As we have seen in previous chapters the use of 3D face models for recognition can provide significant advantages over two-dimensional systems, in particular by reducing error rates in applications where head angle and lighting conditions are not easily controlled. However, we do not suggest that 3D face recognition will supplant two-dimensional face recognition systems completely, as two-dimensional systems do have a number of advantages over 3D systems for some specific applications. Not only are 3D cameras significantly more expensive than existing standard 2D cameras, but 2D images are already used in a great range of systems: they are captured by CCTV cameras; used on official identification documents such as passports and driving licenses; and they are acquired and stored in video and photograph for a variety of reasons. For these reasons there will always be a need to search and identify two-dimensional face images.

However, there are also many applications in which 3D face recognition would offer significant advantages, but the existing legacy databases contain two-dimensional images only. One such example is the UK police mug-shot databases. The UK police forces already use 2D face recognition to search these databases for potential matches to an image acquired as part of an investigation or when a suspect is held in custody his image may be searched for. It is easy to envisage the police swapping the 2D cameras for a 3D equivalent, allowing for a 3D face recognition system to be used with much greater accuracy (especially when the subjects are not very cooperative), however without the ability to search an existing 2D database. These circumstances give rise to the need for a 3D-2D matching capability. This would allow for the gradual introduction of a 3D recognition system, capturing 3D face models yet still allowing searching of an existing 2D database. As 3D face models are acquired and a new database of 3D face models begins to grow, this database can be searched at the same time as the legacy 2D databases. To match 3D face models against 2D images is a fairly simply procedure, although it requires a texture mapped 3D face model to undergo an orientation normalisation procedure before the 2D texture map is projected back into a two-dimensional plane. This 2D projection can then be scaled and aligned

according to the eye locations and matched against a standard 2D image using the techniques already discussed in section 4.

6.1 Recognition Using 3D Texture Map Projections

In this section we explore another approach to face recognition that falls somewhere between the two-dimensional and 3D approaches discussed so far, in that is uses the 3D face model in order to perform orientation normalisation, before performing recognition based on the two-dimensional texture data. Whereas the 3D systems explored in section 5 have all been intentionally applied to geometric structure alone (in order to become invariant to lighting conditions). It may be that if the lighting conditions can be controlled to some extent, then by ignoring the two-dimensional colour data held in the texture map we are discarding a wealth of highly discriminatory information that could be useful for recognition. We do address these issues in section 7.4, by reintroducing the 2D texture information in combining two-dimensional and 3D systems. However, if an existing 2D face recognition system is already in place, perhaps highly optimised for specific circumstances (for a certain race under specific lighting conditions for example), it may be preferential to continue using the two-dimensional system, rather than gathering the necessary training data to optimise a new 3D system. Under these circumstances it is still possible to gain some of the advantages offered by a 3D system by utilising the 3D camera, without necessarily performing recognition on the surface shape, but rely purely on the 2D texture map. Such a system would become more resistant to variations in head orientation, yet still use the underlying 2D recognition algorithm.

In order to implement such a system, the 3D camera would generate a texture mapped 3D face model, which would then undergo the orientation normalisation procedure described in section 5.2. The texture of the resultant fronto-parallel 3D face model can then be projected onto a 2D plane, creating a standard 2D image of the face. As well as having the advantage of normalising head orientation this system also introduces two other significant advantages. Firstly, the resultant image is to scale, meaning that the actual size of the head and distance between the eyes can be used as features for recognition. Secondly, because the orientation normalisation algorithm has already

aligned the image there is no need to align by the eye locations (providing it is being compared with other 2D projections and not standard 2D images).

Figure 6-1 Two-dimensional face images (left), the equivalent 3D texture mapped models before orientation normalisation (centre) and after normalisation (right)

Figure 6-1 shows how the 3D face model can be used to create a 2D projection suitable for recognition by a two-dimensional face recognition system, from an original image in which head orientation would have prevented a successful identification. Once the orientation normalised 2D image has been created it may be subjected to the same pre-processing techniques as used in the other two-dimensional systems. Hence we can create the range of face recognition systems as produced in section 4.4. Using the University of York 3D face database we train and test twenty-four 2D Projection face recognition systems using all pre-processing techniques (see section 4.5) applicable to grey-scale images. Testing these systems on test set A (as described in section 4.2.1), we produce the following EERs, shown below alongside the EERs for the corresponding 2D face recognition systems tested on the 2D images of the same data set.

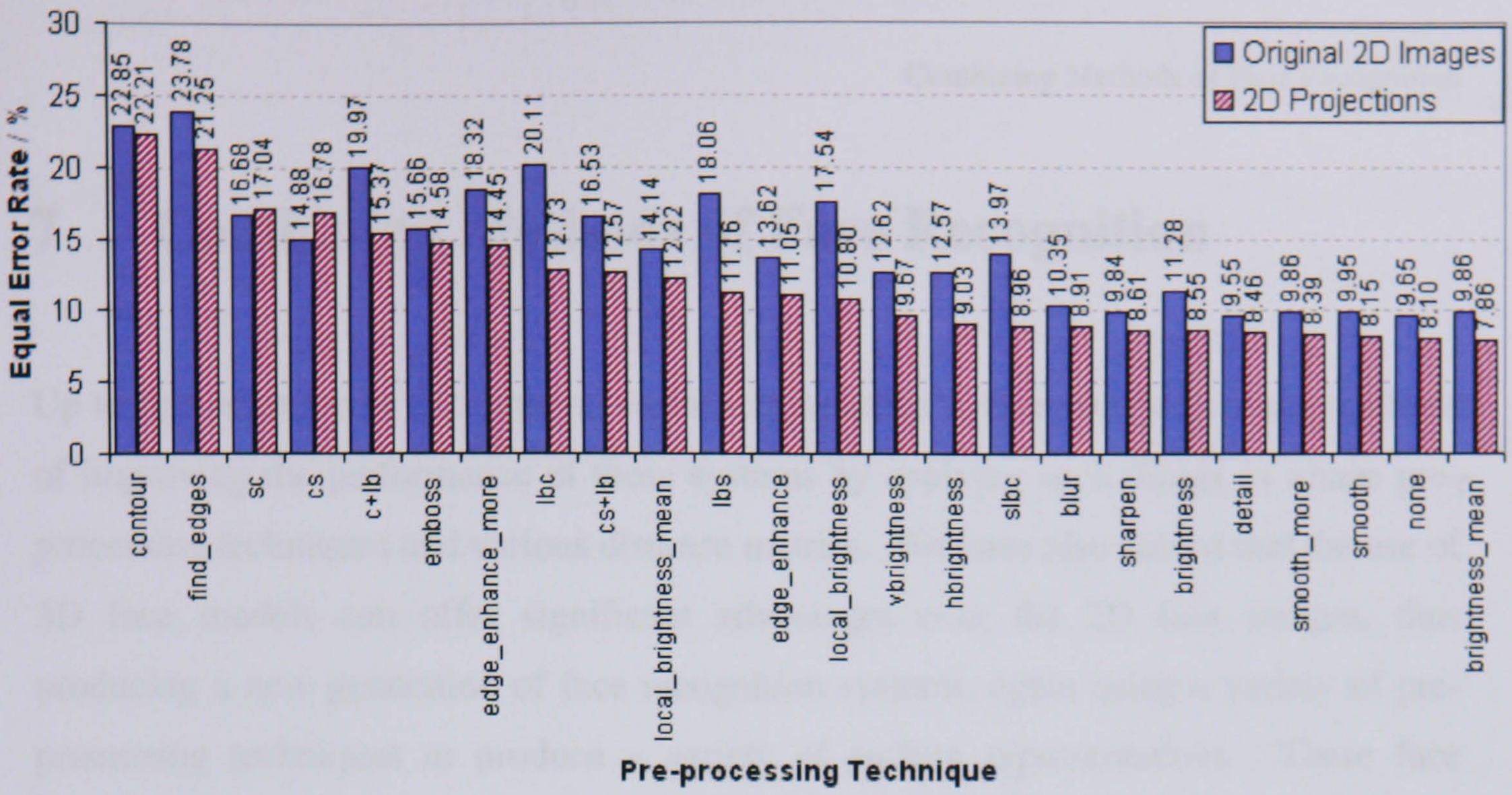

Figure 6-2 Bar chart of EERs produced by various 2D face recognitions systems and the equivalent 2D projection systems.

Clearly, the 2D projection systems have a significant advantage over the standard 2D systems. In almost all cases the error rates are significantly lower. As the test set contained faces of various orientations, this drop in error rate is most likely due to the orientation normalisation of these images. However, it is also likely that the slight adjustment of orientation, even for faces that appear to face directly forwards still aids recognition by producing a more robust angle of orientation. Finally, the use of absolute size as a feature for recognition will also have provided some additional discriminatory information. It is interesting to note that the system in which no image pre-processing is carried out ('none' in the figure above) performs significantly better in these experiments than in previous investigations. This is perhaps due to the fact that no lighting variation is included in this test set and hence lighting conditions may actually be providing some discriminatory information between multiple subjects in these experiments.

7 Combining Methods of Face Recognition

Up to this point we have discussed various approaches to face recognition and methods of improving the performance of these systems by applying such things as image pre-processing techniques and various distance metrics. We have also shown that the use of 3D face models can offer significant advantages over the 2D face images, thus producing a new generation of face recognition systems, again using a variety of pre-processing techniques to produce a variety of surface representations. These face recognition systems has each been evaluated by producing the EER for a given test set, resulting in a large range of error rates. What we have not considered, until this point, is that each system may have its own advantages under certain conditions, or that although one system may not perform well in terms of EERs, it may contain, within its extracted feature space, some discriminating factor not considered in other systems that use a different image (or surface) representation.

In this section we introduce methods of combining multiple face recognition systems, hoping to consolidate the advantages of numerous systems into a single unified system that outperforms any of its individual components. We begin by combining two-dimensional face recognition systems in section 7.1, computing the best combinations of eigenface and Fisherface systems, when applied to the AR face database of 2D images. We then apply a similar strategy to 3D Fishersurface systems, testing both the cosine and Euclidean distance measures in section 7.2. These two investigations lead naturally to the combining of two-dimensional and 3D systems, creating a unified face recognition method that utilises both 3D geometric structure as well as colour and texture information. Such a system is presented in section 7.4.

We introduce some new terminology in this section that deserves some clarification. We describe the method of amalgamating multiple face recognition systems as 'subspace combination' and the resultant combined subspace as a 'composite subspace.' When referring to a complete face recognition system that utilises a composite subspace it is often termed a 'multi-subspace system' in contrast with the 'single-subspace systems' described in previous chapters. Note that in many of the charts and figures we use the abbreviation 'combo X' to denote a multi-subspace system in which

combination has been applied across systems of type X (3D, 2D or 2D Projections). Unless a method is not explicitly stated to be a multi-subspace system it is assumed to be a single-subspace system.

7.1 Combining 2D Face Recognition

It has been shown that the application of image processing techniques as a pre-processing step to methods of face recognition, such as the eigenface and Fisherface methods, can significantly improve recognition accuracy (sections 4.3 and 4.4 and published in [14][15]). Such image processing techniques work on several principles, such as reducing noise, enhancing features or normalising environmental conditions. Therefore, each technique provides unique advantages, specifically suited to different conditions. For example, colour normalisation techniques may aid recognition by making such features as skin-tone and hair colour consistent despite the effect of lighting conditions. Another system may incorporate edge detection filters, focusing purely on facial structure, while a third may blur an image, reducing inaccuracies introduced by the feature alignment stage. Unfortunately, often incorporated with these beneficial characteristics are surplus side effects, which can actually degrade system performance: normalising colour and removing the effect of lighting conditions will reduce the geometric information encapsulated within the facial surface shading; edge-detection or gradient based filters preserve structural cues, but remove skin-tone information.

We analyse and evaluate a range of face recognition systems, each utilising a different image processing technique, in an attempt to identify and isolate the advantages offered by each system. Focusing on appearance based methods of face recognition we propose a means of selecting and extracting components from the image subspace produced by each system, such that they may be combined into a unified face space. We apply this method of combination to the eigenface approach (section 4.3) and Fisherface approach (section 4.4). The benefit of using multiple eigenspaces has previously been examined by Pentland et al [40], in which specialist eigenspaces were constructed for various facial orientations and local facial regions, from which cumulative match scores were able to reduce error rates. Our approach differs in that we extract and combine individual dimensions, creating a single unified face space.

In section 7.1.1 we begin with a brief explanation of the eigenface and Fisherface methods. We describe the database of face images used for testing and training in section 7.1.2, which are then analysed in section 7.1.3, discussing the image processing techniques evaluated in sections 4.3.3 and 4.6, the rationale for combining multiple systems and the criteria used to identify the most discriminatory components of each system. The algorithm used for combining these components is then described in section 7.1.4. After applying this combination process to the eigenface and Fisherface methods, we compare the effectiveness of the resultant face space combinations with the best systems produced in our earlier work (section 4.6). The evaluation procedure is described in section 7.1.5, by which we perform verification operations on a large test set of facial images that present typical difficulties when performing recognition, such as variations in illumination direction and facial expression. We present the results in the form of error rate curves in section 7.1.6, generated by varying a decision threshold in the verification operations.

7.1.1 The Eigenface and Fisherface Methods

In this section we give a brief explanation of the eigenface and Fisherface methods of face recognition, while referring the reader to sections 4.3 and 4.4 for more detailed explanations. Both approaches work on the same principle of analysing the image space of a given training set of face images Γ_{ni}, of c different people, attempting to reduce image space dimensionality down to the most discriminating components. This is accomplished by computing eigenvectors of one or more scatter matrices (Equ. 4-2 and Equ. 4-5) using standard linear methods, ultimately producing subspace projection matrices, U_{ef} and U_{ff}, of the top c-1 components with the highest eigenvalues for the eigenface and Fisherface systems respectively.

The two approaches differ in the scatter matrices from which the eigenvectors are calculated. The eigenface method applies principal component analysis (PCA) using the covariance matrix S_C, constructed from single examples of each person in the training set, whereas the Fisherface method is able to take advantage of multiple examples of each person, minimising within-class scatter (S_W), yet maintaining high between-class scatter (S_B). In addition, the Fisherface approach applies PCA to the total scatter matrix S_T, producing a preliminary projection matrix U_{pca}, used to reduce the

dimensionality of the scatter matrices S_B and S_W, ensuring they are non-singular, before computing the eigenvectors (U_{fld}) of the reduced scatter matrix ratio (Equ. 4-6, Equ. 4-7 and Equ. 4-8).

Figure 7-1 The average face (*left*) and first four eigenfaces (*right*) computed with no image pre-processing.

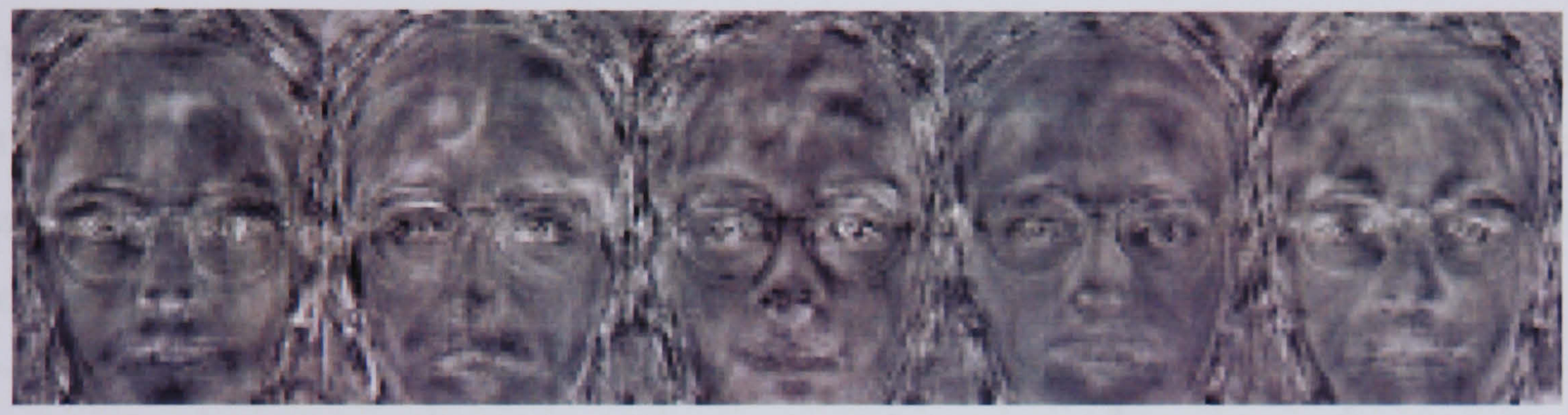

Figure 7-2 The first five Fisherfaces, defining a face space with no image pre-processing.

7.1.2 Test Data

We conduct experiments using a database of 960 bitmap images of 120 individuals (60 male, 60 female) of various race and age, extracted from the AR Face Database provided by Martinez and Benavente [39]. From this database we take a training set of 240 images (60 people under a range of lighting conditions and facial expressions), used to compute the scatter matrices described in section 2 and ultimately produce the face space projection matrices. The remaining 720 images (60 people, 12 images each) are then separated into two disjoint sets of equal size (test set A and test set B). We use test set A to analyse the face-key variance throughout face space, calculate discriminant weightings (see section 7.1.3) and compute the optimum face space combinations. This leaves test set B as an unseen set of data to evaluate the final multi-subspace system.

This use of dual data sets for training followed by analysis and combination may initially seem to needlessly use two different sets of data in the preliminary training

processes. Why not compute scatter matrices and system combinations on the same set of data? After testing this approach, producing disappointing results (error rates increase after combining systems), we hypothesise that significant over-training in the first PCA stage prevents any further optimisation by combination, as the resulting projection typically results in perfect classification of the training set. The reason for two training sets is effectively a scheme to prevent over-training. Because it is often necessary to use far fewer training images than the dimensionality (number of pixels) of the images themselves, it is often the case that PCA achieves perfect class separation on the training set. Hence discriminant values become artificially high, criteria for combination becomes biased towards very few dimensions and combination does not reflect an improvement outside of the initial training data.

Table 7-1 shows six examples of the images used for training and test sets, repeated on two days, making up the 12 images of each subject in the test sets. All images are pre-aligned with the eye centres 25 pixels apart, before being cropped to a width and height of 65 and 82 pixels respectively.

Lighting	Natural	From left	From right	Left & right	Natural	Natural
Expression	Neutral	Neutral	Neutral	Neutral	Happy	Angry
Example						

Table 7-1. Image capture conditions included in the database training and test sets.

7.1.3 Analysis of face recognition systems

In this section we analyse image subspaces produced when various image pre-processing techniques are applied to both the eigenface and Fisherface methods. We begin by reproducing the results obtained in previous investigations (see section 4.3), shown in Figure 7-3, showing the range of error rates produced when using various image processing techniques. Continuing this line of research we persist with these same image processing techniques, referring the reader to section 4.5 for

implementation details, while here we focus on the effect and methodologies of combining multiple systems, rather than the image processing techniques themselves.

Figure 7-3 clearly shows that the choice of image processing technique has a significant effect on the performance of both the eigenface and Fisherface approaches, with detail enhancement filters providing the lowest EER when used in conjunction with the Fisherface approach. However, we find it surprising that some image processing techniques give such poor performance, especially when designed specifically to compensate for conditions known to be a source of error in face recognition systems. For example, we see that intensity normalisation increases error rates for Fisherface-based systems, despite being the best performing image processing technique for eigenface-based recognition. Hence, it is apparent that this processing technique is able to preserve discriminatory information, while normalising lighting effects, yet is unsuitable for Fisherface-based recognition. We now carry out further investigation into the discriminating ability of each face recognition system by applying Fisher's Linear Discriminant (FLD), as used by Gordon [4] to analyse 3D face features, to individual components (single dimensions) of each face space. Focusing on a single face space dimension we calculate the discriminant d, describing the discriminating power of that dimension, between c people in test set A.

$$d = \frac{\sum_{i=1}^{c} (m_i - m)^2}{\sum_{i=1}^{c} \frac{1}{|\Phi_i|} \sum_{x \in \Phi_i} (x - m_i)^2}$$

Equ. 7-1

Where m is the mean value of that dimension in the face-keys of test set A, m_i the within-class mean of class i and Φ_i the set of vector elements taken from the face-keys of class i.

Figure 7-3 EERs of eigenface and Fisherface systems using a range of image processing techniques.

Applying Equ. 7-1 to each dimension of the eigenface face space (using no image pre-processing), provides a set of discriminant values as shown in Figure 7-4. Looking at the range of discriminant values, we note that the higher discriminants appear at the lower end of the face space. This is exactly as we would expect, showing that the order of principal components, in terms of eigenvalues, is broadly related to that dimensions discriminating ability.

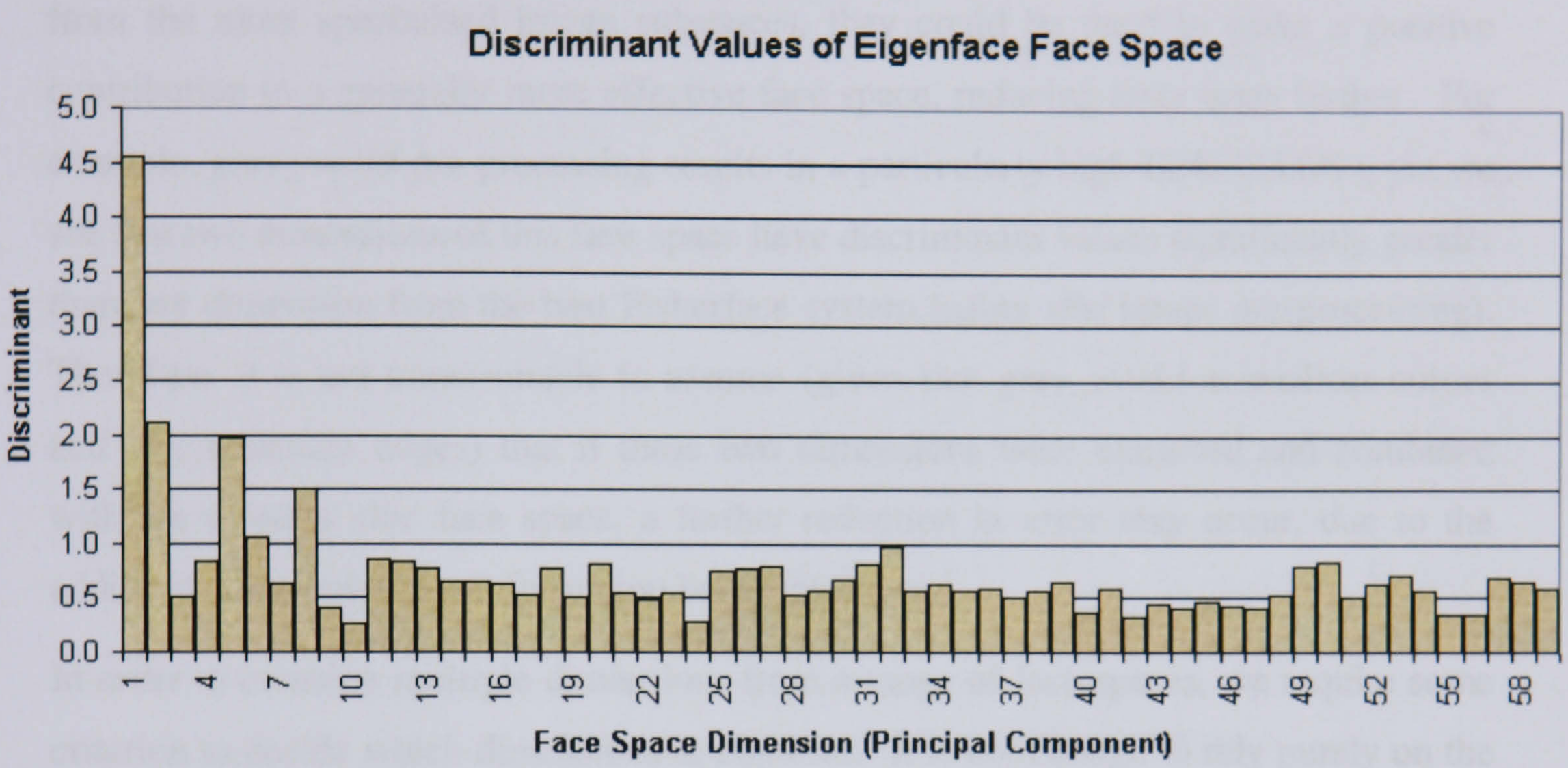

Figure 7-4 Discriminant values of the eigenface face space dimensions using no image pre-processing.

However, it can also be seen that certain dimensions produce very low discriminant values. In Figure 7-4 we see that the third principal component in particular has a very low discriminating ability, despite its relatively high eigenvalue. This highlights some problems in the eigenface training method, in that the third dimension obviously represents something of high variance in the training set that has little or no use in discriminating between different people. In other words, it is a feature of the environmental capture conditions. Applying Equ. 7-1 to each dimension in the assortment of Fisherface systems, we see similar results to those of the eigenface systems, with a wide range of discriminant values across the different image processing techniques. Figure 7-5 shows the top ten dimensions with the highest discriminant value from each Fisherface system.

It is clear that although some image processing techniques do not perform well in the face recognition tests, producing high EERs as seen in Figure 7-3 some of their face-key components do contain highly discriminatory information. We hypothesise that the

reason for these highly discriminating anomalies, in an otherwise ineffective subspace, is that a certain image processing technique may be particularly suited to a single discriminating factor, such as skin tone or hair colour, but is not effective when used as a more general classifier. Therefore, if we were able to isolate these few useful qualities from the more specialised image subspaces, they could be used to make a positive contribution to a generally more effective face space, reducing error rates further. For example, *grey_world* pre-processing results in a particularly high EER (23.0%), yet we see that two dimensions of this face space have discriminant values significantly greater than any dimension from the best Fisherface system (using *slbc* image pre-processing). Therefore, it is not unreasonable to assume (given that *grey_world* normalises colour and *slbc* enhances edges) that if these two dimensions were extracted and combined with the existing *slbc* face space, a further reduction in error may occur, due to the additional discriminatory information being introduced.

In order to combine multiple dimensions from a range of face spaces, we require some criterion to decide which dimensions to combine. It is not enough to rely purely on the discriminant value itself, as this only gives us an indication of the discriminating ability of that dimension alone, without any indication of whether the inclusion of this dimension would benefit the existing set of dimensions. If an existing face space already provides a certain amount of discriminatory ability, it would be of little benefit (or could even be detrimental) if we were to introduce an additional dimension describing a feature already present within the existing set, unless it was of a discriminant significantly high as to provide a valued contribution. Ideally we would use the EER as this criterion, such that a new dimension would be incorporated into any existing system if it resulted in a reduced EER. However, such an approach is problematic in that the time taken to process a complete verification evaluation for all dimension combinations would be unfeasible, without substantial algorithm optimisations and an abundance of memory. Thankfully, with such optimisations in place and access to numerous high specification PCs, we were able to test this approach in section 7.3.

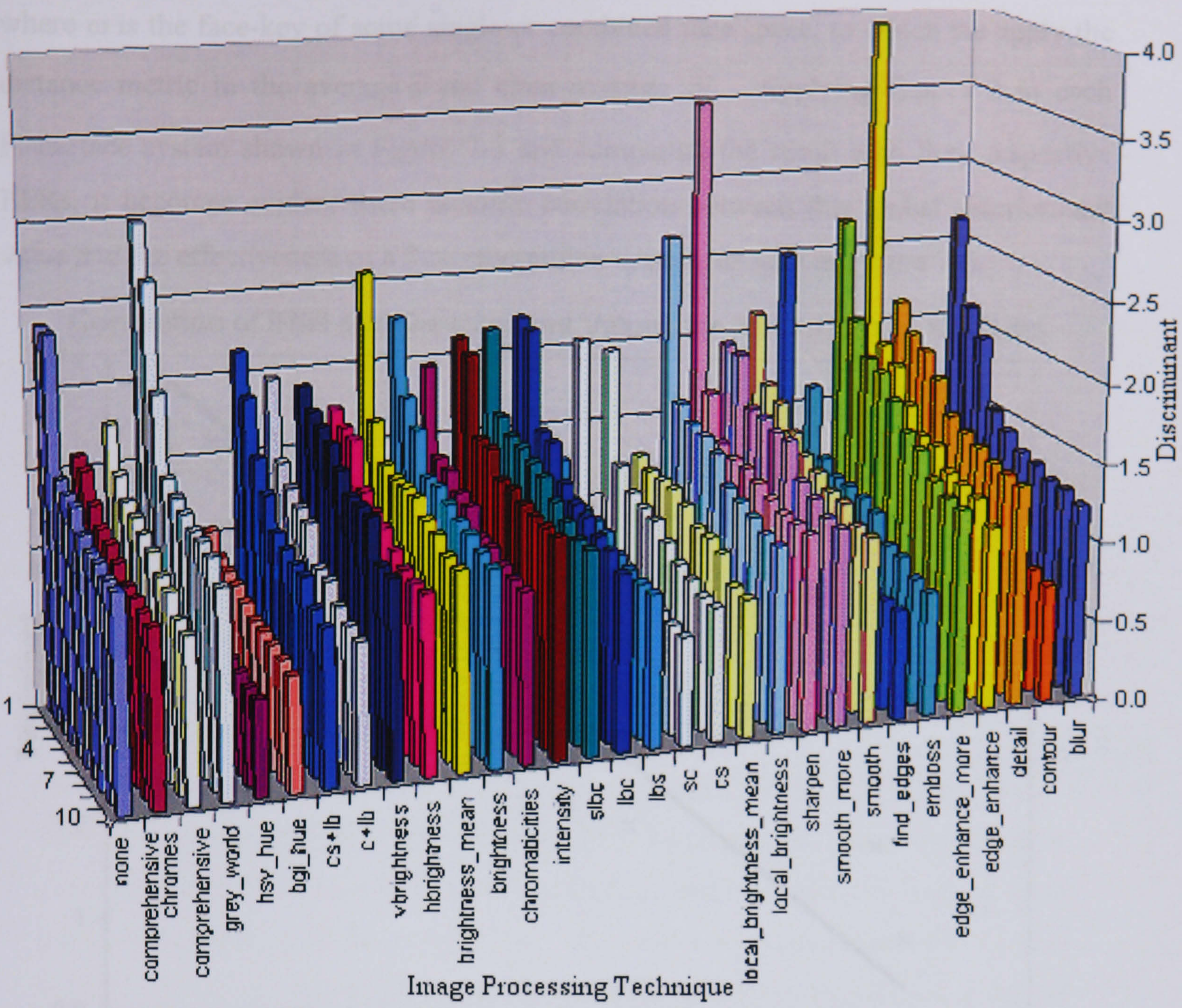

Figure 7-5 Ten greatest discriminant values of dimensions from Fisherface face spaces using a range of image pre-processing techniques.

What we require is some method of providing an indication of how effective a given combination of face space dimensions is likely to be, without the need of processing a complete evaluation of all verification operations. An obvious solution, already used to analyse individual face space dimensions is that of FLD, which with a small amount of adaptation can be applied to whole face-key vectors, rather than individual vector elements, providing a global discriminant value *d* for the entire face space,

$$d = \frac{\sum_{i=1}^{c} \left\| \overline{\omega}_i - \overline{\omega} \right\|}{\sum_{i=1}^{c} \frac{1}{|\Phi_i|} \sum_{\omega \in \Phi_i} \left\| \omega - \overline{\omega}_i \right\|}$$

Equ. 7-2

where ω is the face-key of some single or combined face space, to which we apply the distance metric to the average $\overline{\omega}$ and class average $\overline{\omega}_i$. Applying Equ. 7-2 to each Fisherface system shown in Figure 7-3 and comparing the result with their respective EERs, it becomes evident there is some correlation between this global discriminant value and the effectiveness of a face recognition system, as seen in Figure 7-6.

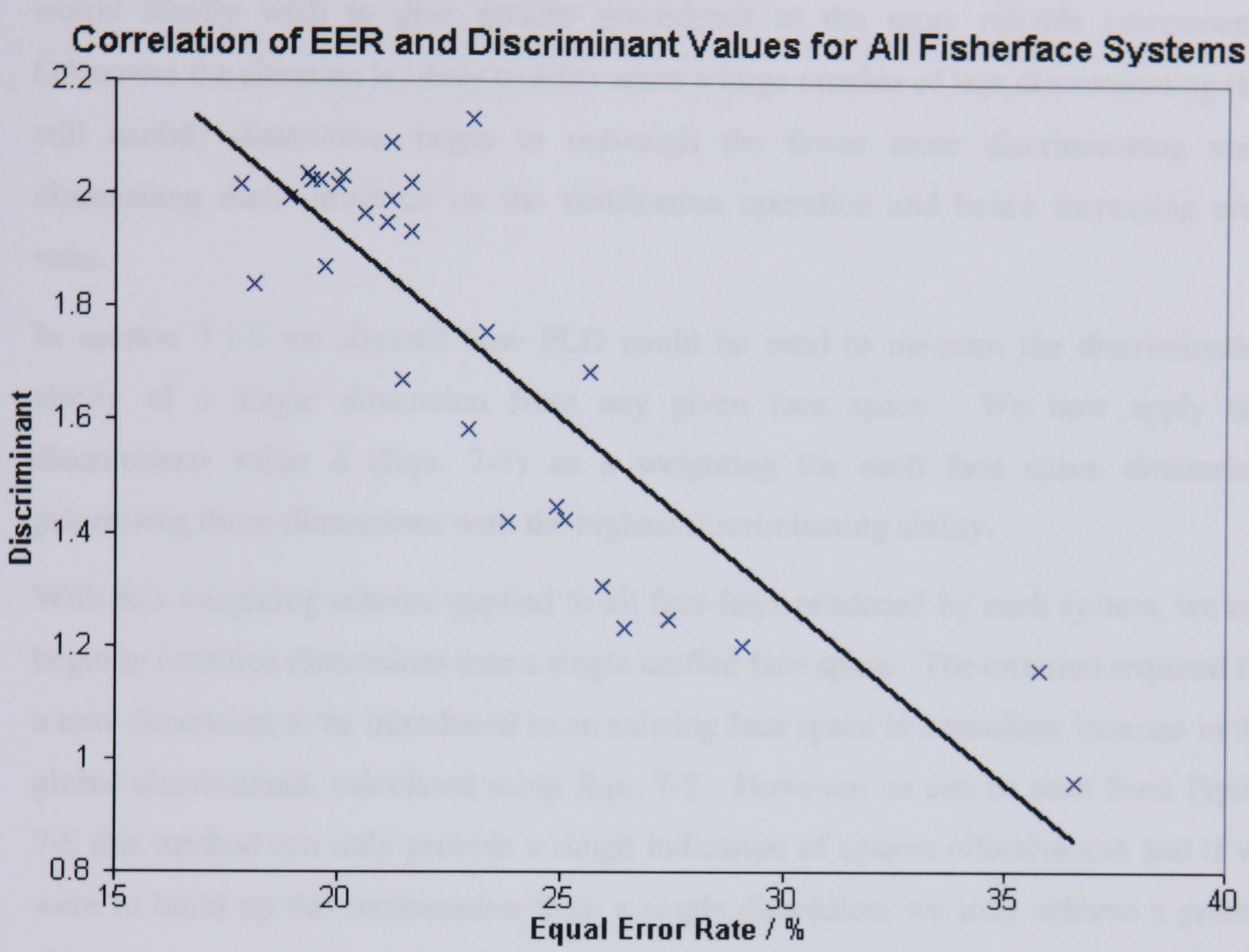

Figure 7-6 Scatter graph showing the correlation between the global discriminant value and EER of Fisherface systems.

7.1.4 Combining Systems

In this section we describe how the analysis methods discussed in section 7.1.3 are used to combine multiple face recognition systems. Firstly, we need to address the problem of prioritising face space dimensions. Because the average magnitude and deviation of face-key vectors from a range of systems are likely to differ by some orders of magnitude, certain dimensions will have a greater influence than others, even if the discriminating abilities are evenly matched. To compensate for this effect, we normalise moments by dividing each face-key element by its within-class standard

deviation. However, in normalising these dimensions we have also removed any prioritisation, such that all face space components are considered equal. Although not a problem when applied to a single face space, when combining multiple dimensions we would ideally wish to give greater precedence to the more reliable components. Otherwise the situation is likely to arise when a large number of less discriminating (but still useful) dimensions begin to outweigh the fewer more discriminating ones, diminishing their influence on the verification operation and hence increasing error rates.

In section 7.1.3 we showed how FLD could be used to measure the discriminating ability of a single dimension from any given face space. We now apply this discriminant value d (Equ. 7-1) as a weighting for each face space dimension, prioritising those dimensions with the highest discriminating ability.

With this weighting scheme applied to all face-keys produced by each system, we can begin to combine dimensions into a single unified face space. The criterion required for a new dimension to be introduced to an existing face space is a resultant increase in the global discriminant, calculated using Equ. 7-2. However, as can be seen from Figure 7-6 this method can only provide a rough indication of system effectiveness and if we were to build up the combination from a single dimension, we may achieve a greater discriminant but not necessarily the lowest EER. Therefore, in order to provide the combination with the best head start, we initialise the dimension set with the best face space achieved so far (*intensity* and *slbc* for eigenface and Fisherface systems respectively). Beginning with this small preliminary set of dimensions (the face space of the best eigenface or Fisherface system), we then iteratively test each additional dimension from other face spaces for combination with the existing dimension set as shown in the 'combination by accumulation' algorithm below.

The result is a new face space consisting of the dimensions taken from the best single subspace system, plus a selection of additional dimensions from other systems. Each new dimension will have increased the global discriminant, such that the final combination has a significantly higher discriminant value and will therefore also have reduced the EER when evaluated on test set B.

```
Composite face space = face space dimensions of best single system
Calculate global FLD of composite face space
For each face space system:
      For each dimension of face space system:
            Concatenate new dimension onto composite face space
            Calculate global FLD of composite face space
            If global FLD has not increased:
                  Remove new dimension from composite face space
Save composite face space ready for evaluation
```

Figure 7-7 Face space dimensional combination by accumulation algorithm, based on an FLD fitness criteria.

7.1.5 The Test Procedure

The effectiveness of the face recognition systems is evaluated by means of error rate curves (FRR vs. FAR) generated by performing a large number of verification operations on the database test sets. The images in the test set are verified against every other image, producing a distance value. No image is compared with itself and each pair is compared only once (the relationship is symmetric). This provides 64,620 verification operations when performed on all images in test set B or 258,840 operations if both test sets A and B are combined. After calculating the distance values for each comparison, a threshold is applied in order to derive the rejection/acceptance decision for each image pair. FAR is calculated as the percentage of acceptance decisions when images of different people are compared and FRR is the percentage of rejection decisions when images of the same person are compared. By varying the threshold we produce a set of FRR FAR plots, forming the error rate curve, as shown in Figure 7-9.

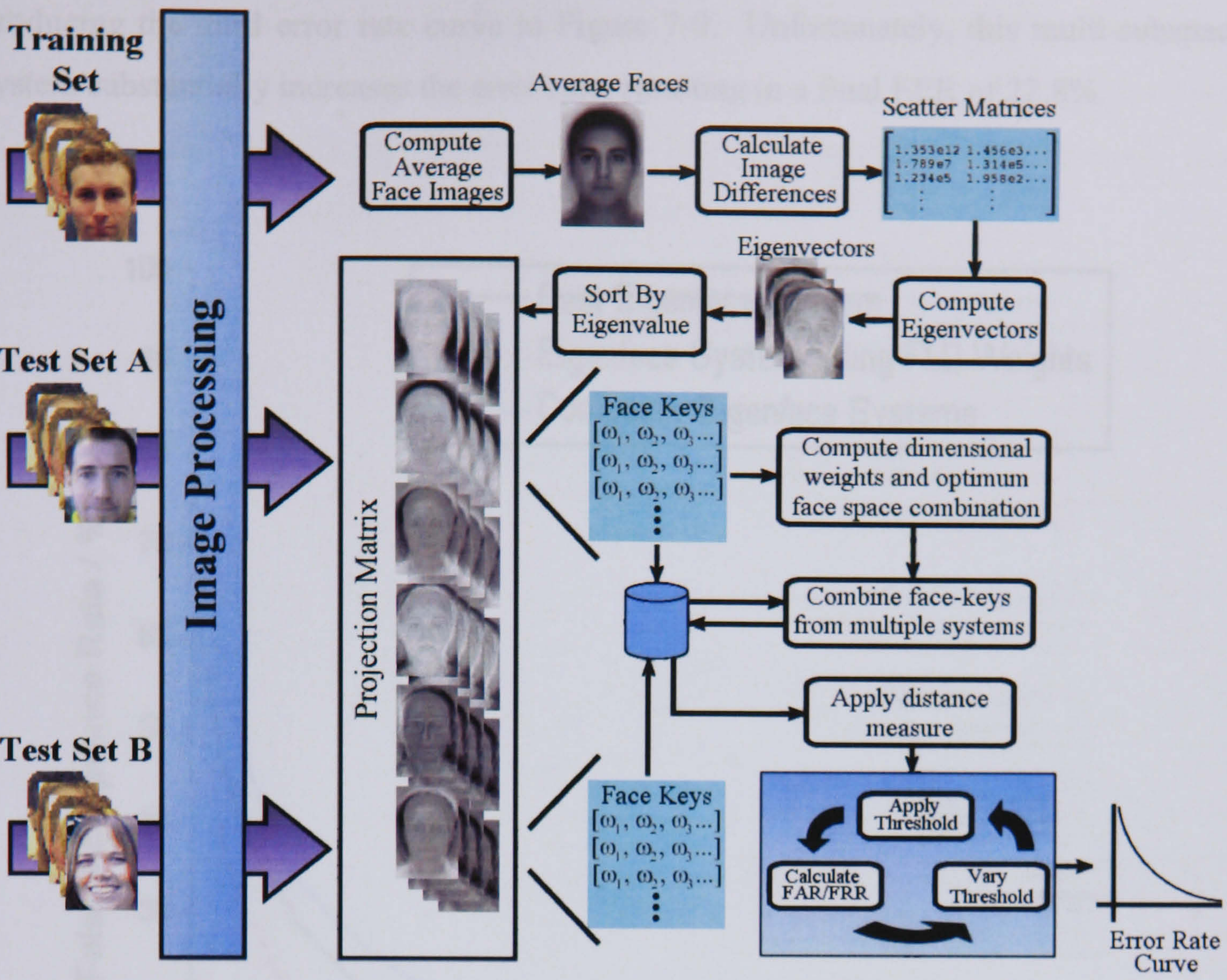

Figure 7-8 Flow chart of face recognition evaluation procedure.

7.1.6 Results

In this section we present results obtained from evaluating the best performing single-subspace systems and combined face recognition systems formed using the eigenface and Fisherface methods. The results are presented in the form of error rate curves (FAR vs. FRR) generated using the procedure described in section 6, taking the EER as a single comparative value.

Figure 7-9 shows the error rates obtained using the eigenface approach, when applied to test set B (the previously unseen test set). We see that applying the optimum eigenface system (incorporating the best image pre-processing technique discovered in section 4.3.3) to test set B, produces an EER of 19.7%. A significant improvement is witnessed when the discriminant values (calculated using test set A) are applied as a weighting scheme (described in section 5), prioritising the most discriminating principal components, reducing the EER to 15.4%. With this weighting scheme in place for all eigenface systems, we then apply the combination by accumulation algorithm,

producing the third error rate curve in Figure 7-9. Unfortunately, this multi-subspace system substantially increases the error rate, resulting in a final EER of 22.8%.

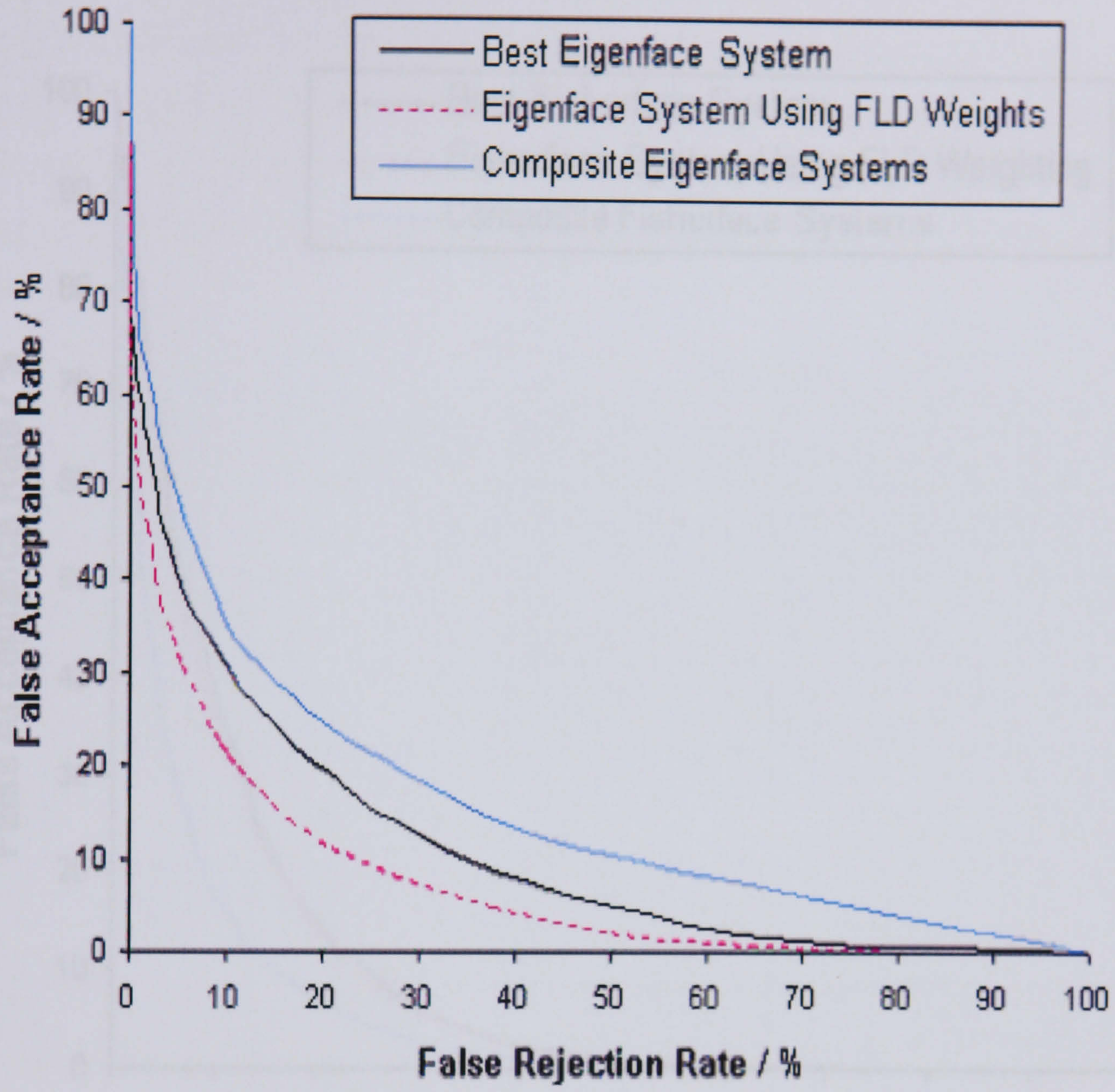

Figure 7-9 Error rate curves of the best single, weighted and multi-subspace eigenface systems

Figure 7-10 shows the results obtained when performing the same evaluation experiments using the Fisherface approach. The initial EER, using the optimum image pre-processing technique is 17.9%. Weighting the components according to discriminant values, unlike the eigenface system, has very little effect on system performance and although it provides marginal improvement at some points along the error curve, actually results in the same EER of 17.9%.

We conjecture that this interesting contrast between the eigenface and Fisherface methods is due to the application of LDA in the Fisherface training process. It is likely that Fisherface dimensions are effectively already weighted according to their

discriminant values. Obviously this is not a mathematical equivalence, otherwise the results would be identical, but it would seem that weighting dimensions by between-class to within-class ratios has little effect if those dimensions have already been constructed to maximise between-class to within-class ratios.

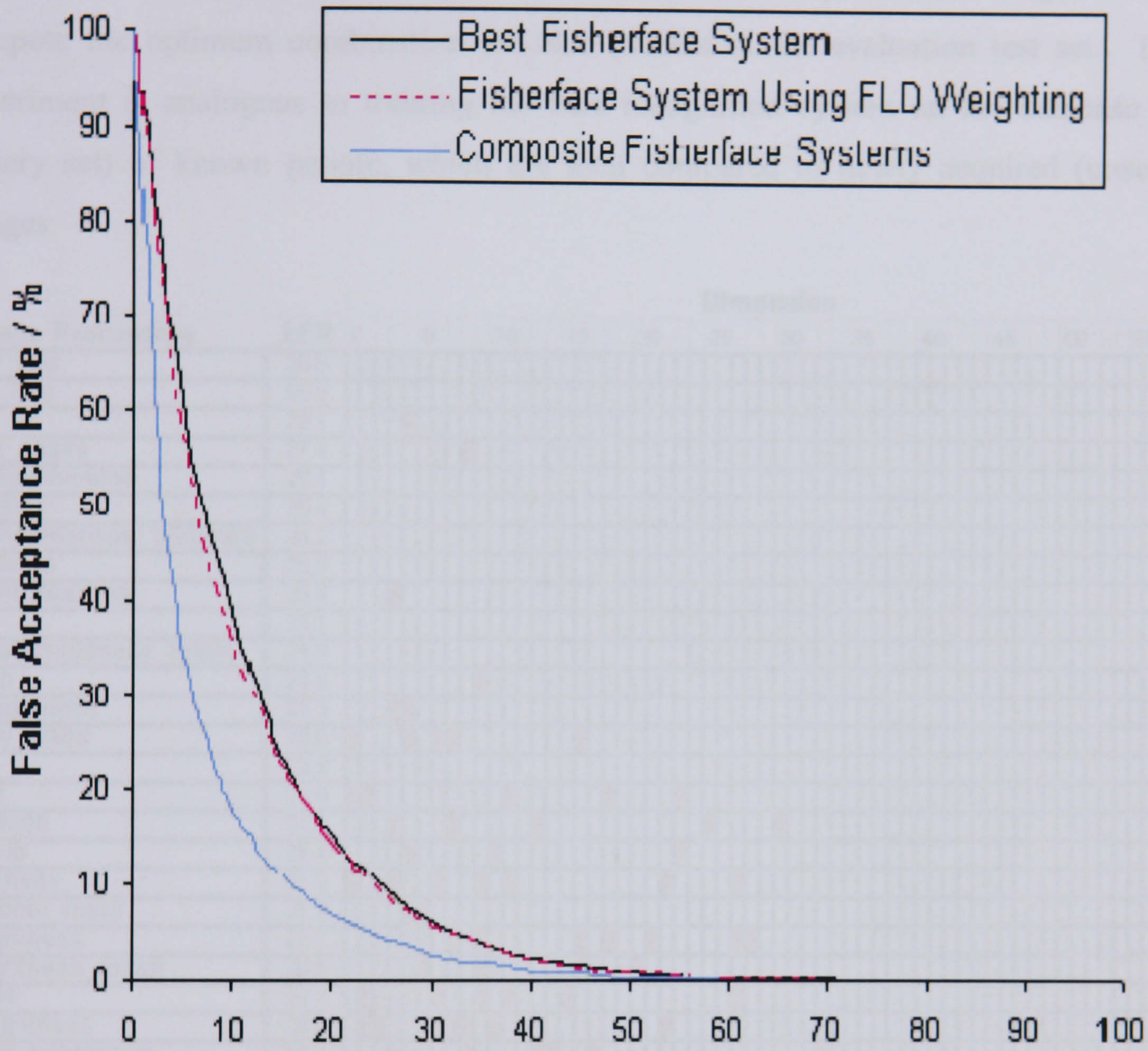

Figure 7-10 Error rate curves of Fisherface systems, produced when applied to test set B.

Combining the weighted dimensions, from all Fisherface systems, produces a significant error reduction to 13.0% EER. Displaying the face space dimensions selected for inclusion in this final multi-subspace Fisherface system in Figure 7-11 shows that those systems with lower EERs generally provide more highly discriminating dimensions for inclusion in the final system than systems with higher EERs. It is also evident that dimensions with higher eigenvalues provide the most discriminating information, as expected. However, it is interesting to note that even a

few of the least effective systems provide some contribution to the final composite face space.

Having evaluated the initial single-subspace systems and multi-subspace systems on the unseen test set B, demonstrating the improvement gained by combining multiple Fisherface dimensions, we now explore how these results vary when the images used to compute the optimum combination are also present in the evaluation test set. This experiment is analogous to training the face recognition system on the database (or gallery set) of known people, which are then compared to newly acquired (unseen) images.

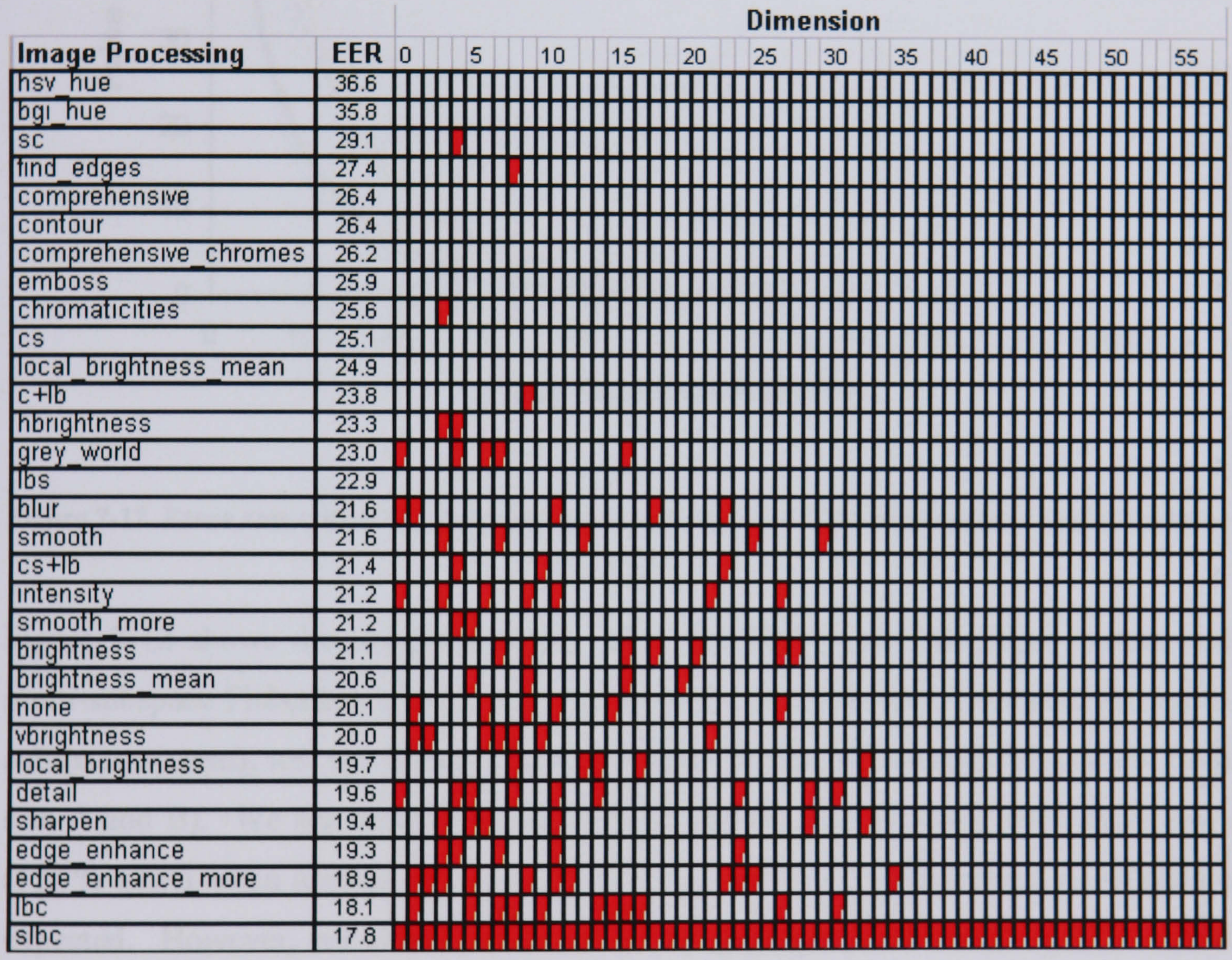

Figure 7-11 Face space dimensions included (■) in the final multi-subspace Fisherface face space used to produce the results shown in Figure 7-9.

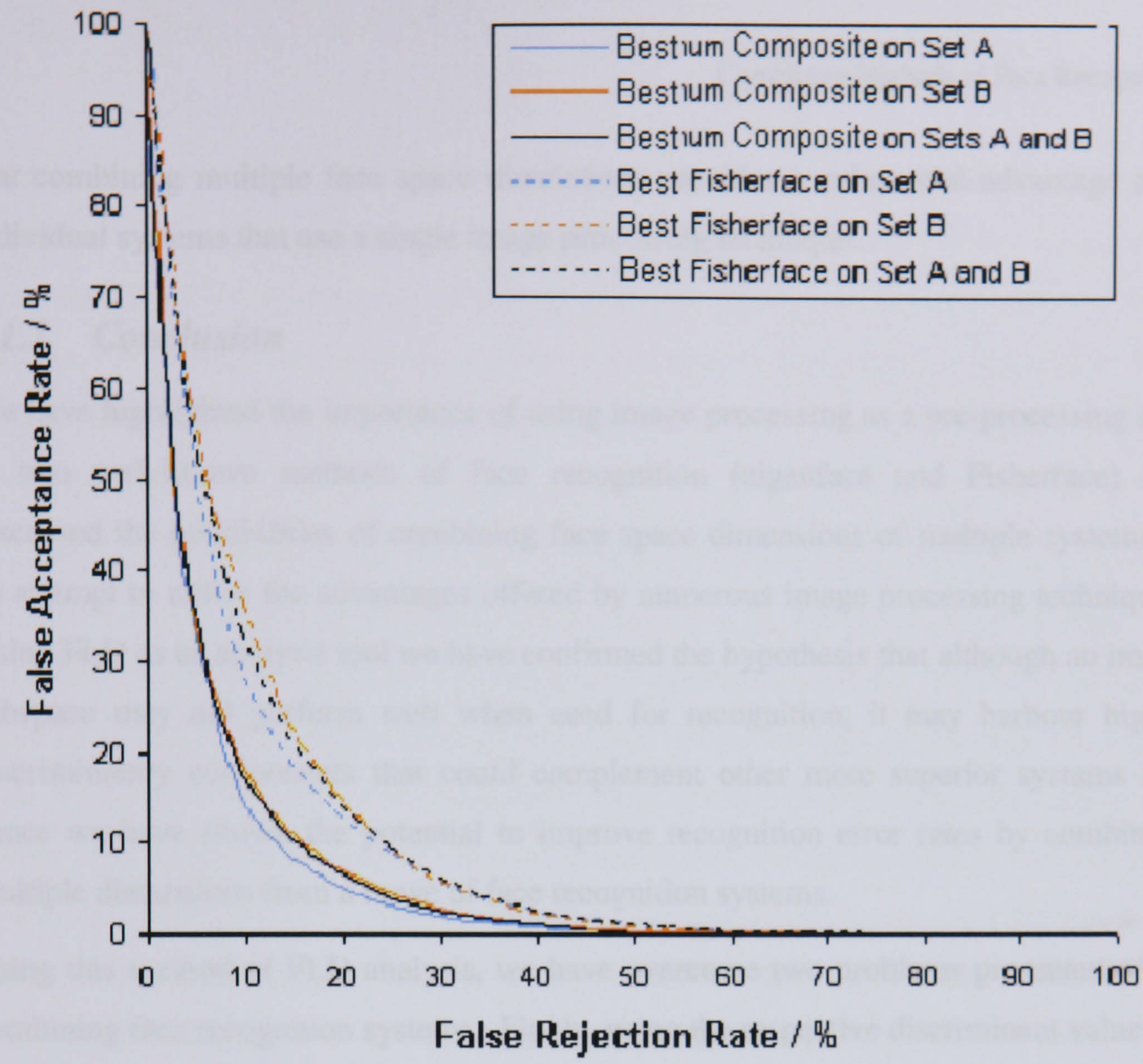

Figure 7-12 Error rate curves of best single and multi-subspace Fisherface systems applied to three test sets.

Figure 7-12 shows the results obtained when the best single Fisherface system and multi-subspace Fisherface system are applied to test set A (used to construct the multi-subspace system), test set B (the unseen test set) and the full test set (all images from sets A and B). We see that the multi-subspace system does produce lower error rates (11.7% EER) when applied to images used to construct the combination, as would be expected. However, we also see that test set A produces better results (16.6% EER) than test set B for the single Fisherface system, suggesting that it is actually a slightly easier test set anyway. Performing the evaluation on the larger set, providing 258,840 verification operations, the error rate drops slightly to 12.8% EER, showing that a small improvement is introduced if some test images are available for training, as well as suggesting that the method scales well, considering the large increase in image comparisons. The distinct separation between the error curves of the best single Fisherface system and those using the multi-subspace system further enforces the fact

that combining multiple face space dimensions provides a substantial advantage over individual systems that use a single image processing technique.

7.1.7 Conclusion

We have highlighted the importance of using image processing as a pre-processing step to two well-known methods of face recognition (eigenface and Fisherface) and discussed the possibilities of combining face space dimensions of multiple systems in an attempt to utilise the advantages offered by numerous image processing techniques. Using FLD as an analysis tool we have confirmed the hypothesis that although an image subspace may not perform well when used for recognition, it may harbour highly discriminatory components that could complement other more superior systems and hence we have shown the potential to improve recognition error rates by combining multiple dimensions from a range of face recognition systems.

Using this method of FLD analysis, we have overcome two problems presented when combining face recognition systems. Firstly, using the respective discriminant values to weight face space dimensions, according to their discriminating ability, has allowed us to combine multiple dimensions yet maintain a bias towards those that present the most distinguishing features. We have shown this weighting scheme to be highly beneficial when used with the best single eigenface system, reducing the EER from 19.7% to 15.4%, but have little influence on the effectiveness of individual Fisherface systems (probably because the subspace computation process has already accounted for between-class to within-class ratios). Secondly, applying FLD to entire face-keys and comparing these global discriminant values with the EERs of existing systems has demonstrated how this analysis can be used to provide a rough indication of the effectiveness of a given face recognition system, requiring significantly less processing time than completing a full set of verification operations on the same data. Using this global discriminant as criteria for selecting face space dimensions as potential sources of additional discriminatory information to an existing system has enabled an iterative approach of appending new face space dimensions to existing combinations, increasing the global discriminant value and hence improving the performance of the multi-subspace face recognition system.

Testing this method of combination on face space representations produced using the eigenface approach has shown it to be ineffective for this method of face recognition, increasing the EER significantly from 15.4% to 22.8%. However, applying the same combination process to Fisherface systems has shown that combining multiple face spaces can improve system performance substantially, reducing the EER from 17.9% down to 13.0%.

This key difference between the eigenface and Fisherface approaches is of particular interest and at first thought perhaps quite surprising. In order to understand this phenomenon, we must consider the method of combination used. We have created a criterion in which face space dimensions are incorporated into an existing set if they increase the discriminant of the composite face space. This criterion only takes into account the discriminating ability of the new dimension when compared with the level of discrimination already achieved within the existing combination. It does not allow for the inter-dependency of features or the possibility that features represented in the additional dimension may already be present in the existing combination face space. For example, consider a composite face space, in which its current set of dimensions encapsulates such features as the nose base width, bridge curvature and nose length. Now suppose we identify a new dimension for inclusion in the face space, representing the more general feature of nose shape, which due to its high between-class variance will increases the global discriminant. However, this new dimension represents a feature that is largely dependent on those already represented in the face space. Therefore the discriminatory information available in this new dimension is predominantly redundant, meaning that the only real contribution to the multi-subspace system is the additional noise of within-class variance.

This reasoning begins to uncover the grounds for failing to successfully combine multiple eigenface systems. The eigenface approach creates a face space that maximises image distribution, but uses no examples of within-class variance, therefore doing nothing to reduce noise or environmental features. Any dimension combined with an existing face space not only introduces the primary discriminating feature (which may have been present beforehand anyway) but also incorporates substantial within-class variance. Adini et al [26] have shown that differences due to lighting conditions and facial expression are greater than the differences between images of

different people, suggesting that the noise introduced when combining dimensions will be more diverse and cumulative than the discriminating features, which will often reoccur and hence be redundant. The Fisherface approach differs in its ability to formulate face space such that within-class variation is minimised relative to between-class variation, hence reducing environmental influence, allowing multiple dimensions to combine with relatively little increase in noise content. Therefore, even if the dimension contribution is redundant, little degradation is introduced.

The criterion used to select dimensions is obviously an important factor in the combination process. In this section we develop a method of using FLD to predict system effectiveness, which due to its short processing time allows many combinations to be tested in a relatively small amount of time, yet we see from Figure 7-6 that the system with the greatest discriminant value does not necessarily have the lowest EER. Therefore it is highly likely that other face space combinations exist that will produce a lower EER than the best combination presented so far in the thesis. Such a face space combination could easily be found if a more accurate representation of system effectiveness was used in the combination selection criteria. One obvious choice is the EER itself. Although this would take an extremely long time to process, once the dimensions have been identified, the multi-subspace projection matrix can be stored for latter use and providing the training set is sufficiently large and varied, re-training and re-combining would not be required.

We have already shown that image processing improves the Fisherface method of face recognition from an EER of 20.1% using no image processing, to 17.8% using the best processing technique. We have extended this line of research to show that creating a face space combination, incorporating multiple Fisherface systems reduces the EER further, down to 12.8% when tested on a large amount of data presenting typical difficulties when performing recognition. Evaluating this system at its fundamental level, using 258,840 verification operations between face images, demonstrates that combining multiple face space dimensions improves the effectiveness of the core face recognition engine. We have not applied any additional heuristics, typically incorporated into fully functional commercial and industrial systems. For example, we have not experimented with different distance metrics, multiple facial alignments, optimising crop regions or storing multiple gallery images. All of which are known to

improve error rates and can easily be applied to the multi-subspace face recognition systems presented here. With these additional measures in place, it is likely that the improvements made to the core recognition engine will bring the error rates of fully functional commercial and industrial systems substantially closer to those required for the application scenarios in mind.

7.2 Combining 3D Face Recognition

In section 5.3 we demonstrated how the use of various surface representations affects the performance of 3D face recognition systems and in analysing these various filtering techniques we have seen how the discriminating abilities vary. What we have not considered, until now, is how these various representations may be combined to further advantage.

In this section we expand on earlier investigations involving the use of facial surface data, derived from 3D face models (generated using a stereo vision 3D camera), as a substitute for the more familiar two-dimensional images. Previous investigations (section 5.5 and published in [16]), have shown how different surface representations and distance measures affect recognition, reducing the EER from 19.1% to 12.7% when applied to a difficult test set of 290 face models. However, the focus of this research has been on identifying optimum surface representations, with little regard for the advantages offered by each individual representation.

We suggest that different surface representations may be specifically suited to different capture conditions or certain facial characteristics, despite a general weakness for overall recognition. For example, curvature representations may aid recognition by making the system more robust to inaccuracies in 3D orientation but are highly sensitive to noise. Another representation may enhance nose shape, but lose information regarding jaw structure.

We now carry out similar investigations as those applied to two-dimensional recognition in section 7.1 and published by Heseltine et al [35]. We analyse and evaluate a variety of 3D Fishersurface [17] face recognition systems, each incorporating a different surface representation of facial structure. We propose a means of identifying and extracting components from the 3D surface subspace produced by each system, such that they may be combined into a single unified subspace. Pentland et al [40] have previously examined the benefit of using multiple eigenspaces, in which specialist subspaces were constructed for various facial orientations, from which cumulative match scores were able to reduce error rates. Our approach differs in that we extract and combine individual dimensions, creating a single unified surface space, as applied to two-dimensional images in previous investigations [35].

7.2.1 Test Data

For the purpose of these experiments we select a sample of 1770 face models (280 people) captured under the conditions in Figure 7-13, taken from the University of York 3D Face Database [50]. During data acquisition no effort was made to control lighting conditions. In order to generate face models at various head orientations, subjects were asked to face reference points positioned roughly 45° above and below the camera, but no effort was made to enforce precise orientation.

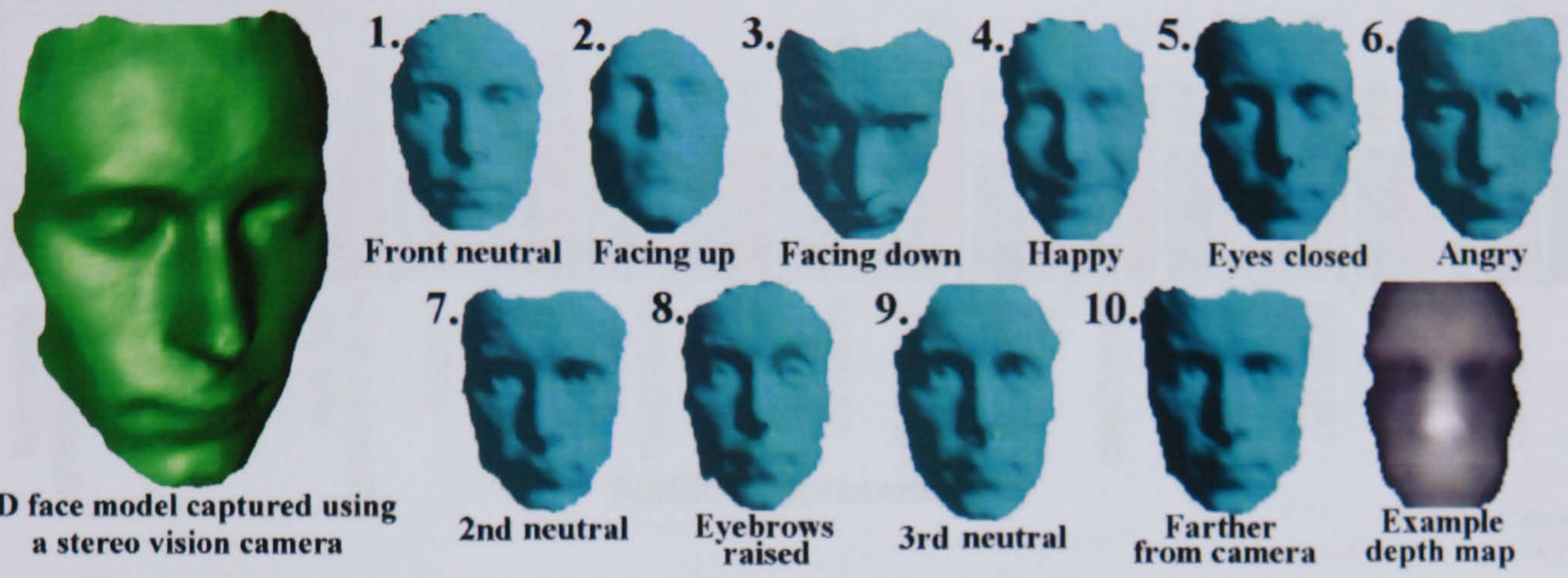

Figure 7-13 Example face models taken from the University of York 3D Face Database

3D models are aligned to face directly forwards before conversion into 60 by 90 pixel depth map representation. We then take a training set of 300 depth maps (50 people), used to compute the scatter matrices described in section 3. The remaining 1470 depth maps (230 people) are then separated into two disjoint sets of equal size (test set A and test set B). We use test set A to analyse the face-key variance throughout surface space, calculate discriminant weightings (see section 4) and compute the optimum surface space combinations. This leaves set B as an unseen test set to evaluate the final multi-subspace system. Both training and test sets contain subjects of various race, age and gender and nobody is present in both the training and test sets.

7.2.2 Surface Space Analysis

In this section we analyse the surface spaces produced when various facial surface representations are used with the Fishersurface method. We begin by testing the variety of Fishersurface systems (introduced in section 5.6) on test set A, showing the range of error rates produced when using various surface representations (Figure 7-14). Continuing this line of research we persist with the same surface representations,

referring the reader to section 5.3 for implementation details, while here we focus on the effect and methodologies of combining multiple systems, rather than the surface representations themselves.

Figure 7-14 clearly shows the choice of surface representation has a significant impact on the effectiveness of the Fishersurface approach, with horizontal gradient representations providing the lowest EER (point at which false acceptance rate equals false rejection rate).

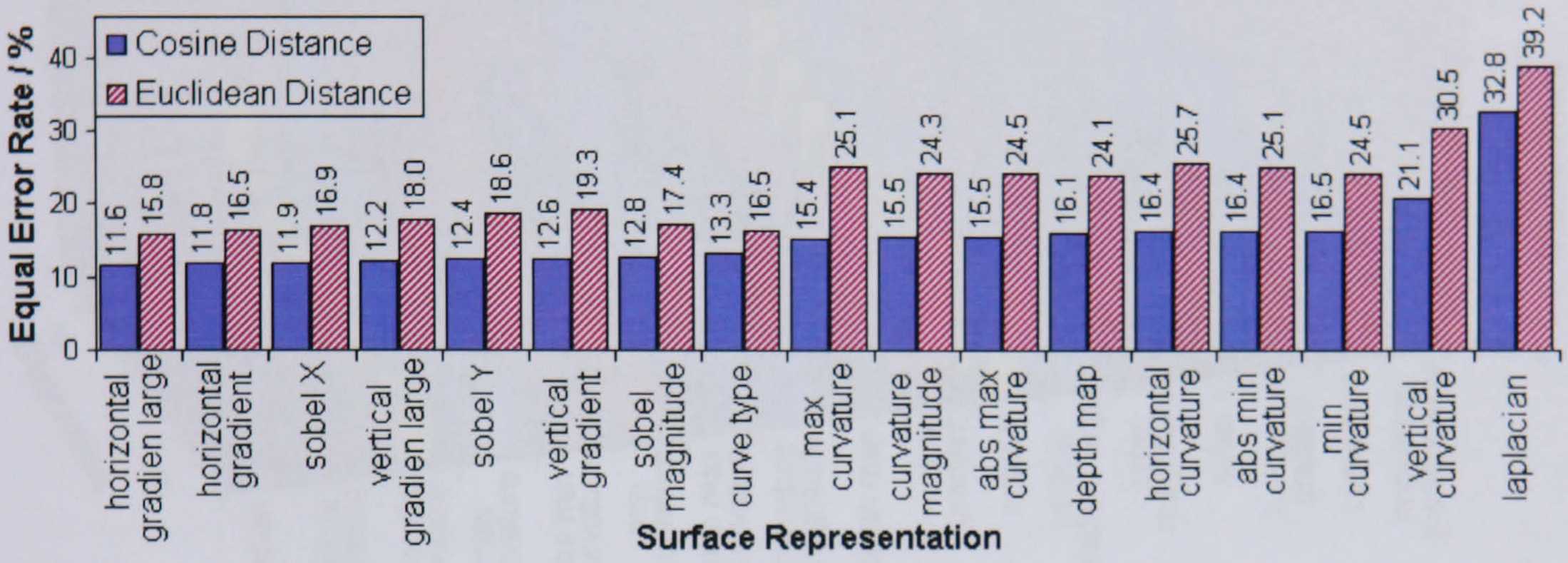

Figure 7-14 - Equal error rates of Fishersurface systems applied to test set A.

However, the superiority of the horizontal gradient representations does not suggest that the vertical gradient and curvature representations are no use whatsoever. Although discriminatory information provided by these representations may not be as robust and distinguishing, they may contain a degree of information not available in horizontal gradients and could therefore still make a positive contribution to a composite surface space. We measure the discriminating ability of surface space dimensions by applying Fisher's Linear Discriminant (FLD) (as used by Gordon [4]) to individual components (single dimensions) of each surface space. We calculate the discriminant d_n, describing the discriminating power of a given dimension n, between c people in test set A.

$$d_n = \frac{\sum_{i=1}^{C}(m_i - m)^2}{\sum_{i=1}^{C}\frac{1}{|\Phi_i|}\sum_{x\in\Phi_i}(m_i - m)^2}, \qquad \text{where} \quad m_i = \frac{1}{|\Phi_i|}\sum_{x\in\Phi_i} x,$$

$$m = \frac{1}{\sum_{i=1}^{C}|\Phi_i|}\sum_{i=1}^{C}\sum_{x\in\Phi_i} x$$

Equ. 7-3

Where Φ_i is the set of all class i face-key vector elements in dimension n, and m and m_i are the mean and class mean of nth dimension elements in test set A. Applying Equ. 7-3 to the assortment of surface space systems listed in Appendix A, we see a wide range of discriminant values across the individual surface space dimensions (Figure 7-15).

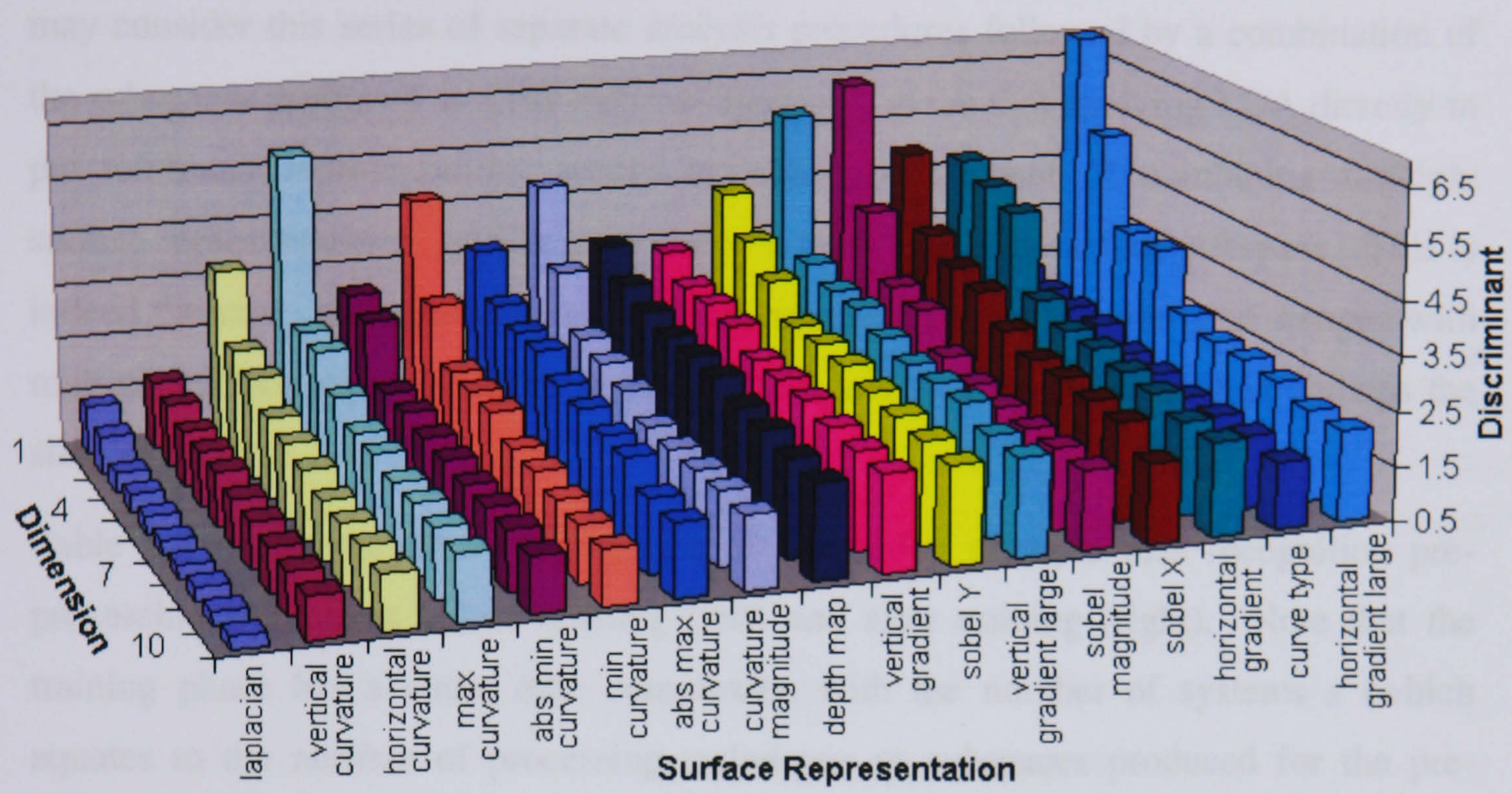

Figure 7-15 - Top ten discriminant values of all Fishersurface dimensions.

It is clear that although some surface representations do not perform well in the face recognition tests, producing high EERs, some face-key components do contain highly discriminatory information. For example, we see that the min and max curvature representations contain one dimension with a higher discriminant than any horizontal gradient and curve type dimension, yet the EERs are significantly higher. We hypothesise that the reason for these highly discriminating anomalies, in an otherwise ineffective subspace, is that a certain surface representation may be particularly suited to a single discriminating factor, such as nose shape or jaw structure, but is not effective when used as a more general classifier. Therefore, if we were able to isolate these few useful qualities from the more specialised subspaces, they could be used to make a positive contribution to a generally more effective surface space, reducing error rates further.

7.2.3 Combining Systems

In this section we describe how the analysis methods discussed in section 7.2.2 are used to combine multiple face recognition systems, where each face recognition system is

based on a different feature type (using a different surface representation). Note that this approach requires each face recognition system to be created individually, applying LDA to a training set pre-processed to produce a specific surface representation. One may consider this series of separate analysis procedures followed by a combination of the subspaces produced as a sub-optimal approach, given that applying LDA directly to pre-combined representations would maintain the concept of combining multiple surface representations, yet likely produced a more highly optimised subspace. This is indeed the case, and concatenating surface representations to create large images with multiple surface representations in each image, and then applying LDA is perhaps the simpler method.

Table 7-2 shows the time complexities of combining multiple face recognition pre-processing techniques before training (left) and after training (right). Note that the training phase has a cubic time complexity, with the number of systems s (which equates to the number of processing techniques or subspaces produced for the pre-training and post-training methods respectively) included in the base of each term. However, in the post-training method s is merely a coefficient of the polynomial terms, so despite the added time for projection (comparably negligible) and combination (easily varied by altering t) post-training combination is much more tractable within the timescales of this project.

Pre-Training Combination	**Post-Training Combination**
$Training = \mathrm{O}\left(M\,(sn)^2 + (sn)^3\right)$	$Training = \mathrm{O}\left(Msn^2 + sn^3\right)$ $\mathrm{Projection} = \mathrm{O}(snt)$ $Combination = \mathrm{O}\left(st^2 - st\right)$
Where: M is the number of images in the training set. s is the number of systems to be combined. n is the number of pixels in a single face image. t is the number of images in test set A (the combination set).	

Table 7-2 Time complexities of pre-training and post-training combination algorithms

Bearing in mind the time complexity of pre-training combination, concatenating just the 16 representations described in this thesis would create a large composite image of 86,400 pixels. Performing LDA on such an image would be a process to challenge the resources of a reasonably powerful desktop computer, even by today's standards. If we were to include a greater number of surface representations, the problem would soon become intractable, whereas the method described here provides a much more flexible process of combination, continually producing an improved system on each iteration. Once a multi-subspace system is produced, because of the progressive nature of the algorithm another surface representation can easily be included in the combination without the need to restart the process. In addition, the processing time can be controlled by the size of test set A, allowing a decrease in computation time at the expense of the statistical significance of the test set.

To begin combining multiple features we must first address the problem of prioritising surface space dimensions. We normalise moments by dividing each face-key element by its within-class standard deviation (calculated from test set A face-keys). In section 7.1.3 we showed how FLD could be used to measure the discriminating ability of a single dimension from any given face space. We now apply this discriminant value d_n as weighting for each surface space dimension n, prioritising those dimensions with the highest discriminating ability.

Our investigations in this thesis (published [35]) have used FLD, applied to a composite subspace in order to predict effectiveness when used for recognition. Additional dimensions are introduced if they result in an increase in discriminant value. This method has been shown to produce face space combinations achieving significantly lower error rates than individual two-dimensional systems, although we do note that an EER-based criterion is likely to produce a better combination, at the expense of greatly increased training time. However, with a more efficient program and greater computational resources, we now take that approach: the criterion required for introduction of a new dimension to an existing surface space is a resultant decrease in EER (computed using test set A). Thus creating an algorithm that implements a hill climbing technique to a locally optimum combination.

```
Composite surface space = first dimension of best current system
Compute EER of composite surface space
For each surface representation system:
      For each dimension of surface space:
            Concatenate dimension onto composite surface space
Compute EER of composite surface space
            If EER has not decreased:
Remove dimension from composite surface space
Save composite subspace ready for evaluation
```

Figure 7-16 Face space combination by dimensional accumulation algorithm, using the EER as a fitness criteria

7.2.4 The Test Procedure

In order to evaluate the effectiveness of a surface space, we project and compare each facial surface with every other surface in the test set, no surface is compared with itself and each pair is compared only once. The false acceptance rate (FAR) and false rejection rate (FRR) are then calculated as the percentage of incorrect acceptances and incorrect rejections after applying a threshold. By varying the threshold, we produce a series of FAR FRR pairs, which plotted on a graph produce an error curve as seen in Figure 7-19. The equal error rate (EER, the point at which FAR equals FRR) can then be taken as a single comparative value.

Using this test format we consider three separate data sets. The training set (τ) is used solely to compute the scatter matrices and ultimately the projection matrix that defines our surface subspace. The remaining data is separated into two disjoint test sets A and B. Test set A is used to compute a FAR and FRR curves for each iteration of the combination algorithm described above. The EER extracted from these graphs is then used as the decision criterion as to whether a dimension is utilised or discarded. The final test set B is used once the final combination has been computed, to provide a FAR, FRR curve calculated using previously unseen test data.

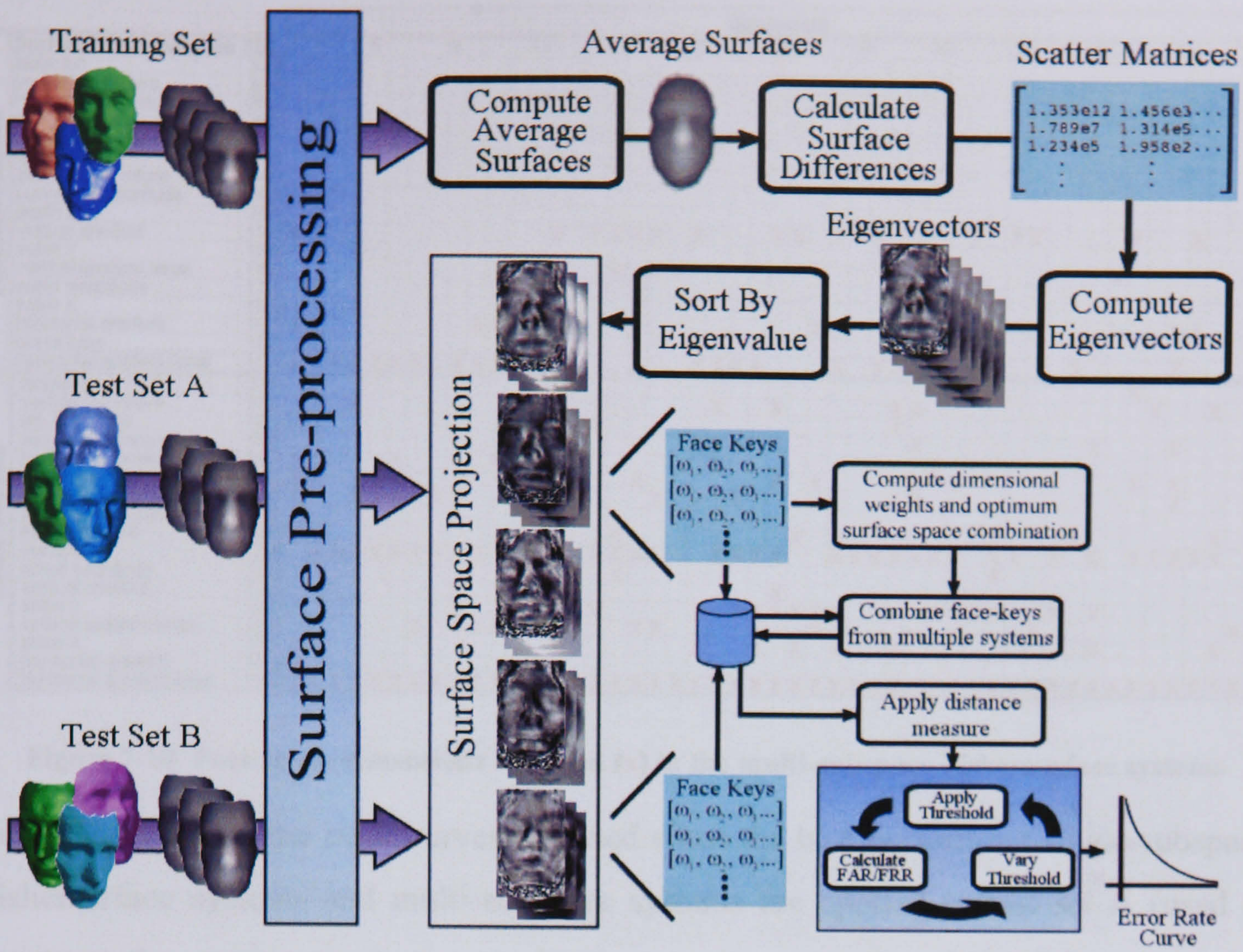

Figure 7-17 Flow chart of system evaluation procedure

7.2.5 Results

In this section we present the dimensions selected to form the multi-subspace Fishersurface systems (Figure 7-18) and the error rates obtained from a range of tests sets, making a comparison to best single-subspace systems in Figure 7-19.

We see that systems with lower EERs generally make the most contribution to the multi-subspace system, as would be expected. However, it is also interesting to note that even systems with particularly high EERs do contain some dimensions that make a positive contribution, although this is much more prominent for the cosine distance, showing that this metric is more suited to combing multiple surface spaces.

Having selected and combined the range of dimensions shown in Figure 7-18, we now apply these multi-subspace systems to test sets A and B using both the cosine and Euclidean distance metric. We also perform an evaluation on the union of test sets A and B: an experiment analogous to training on a database (or gallery set) of known people, which are then compared with newly acquired (unseen) images.

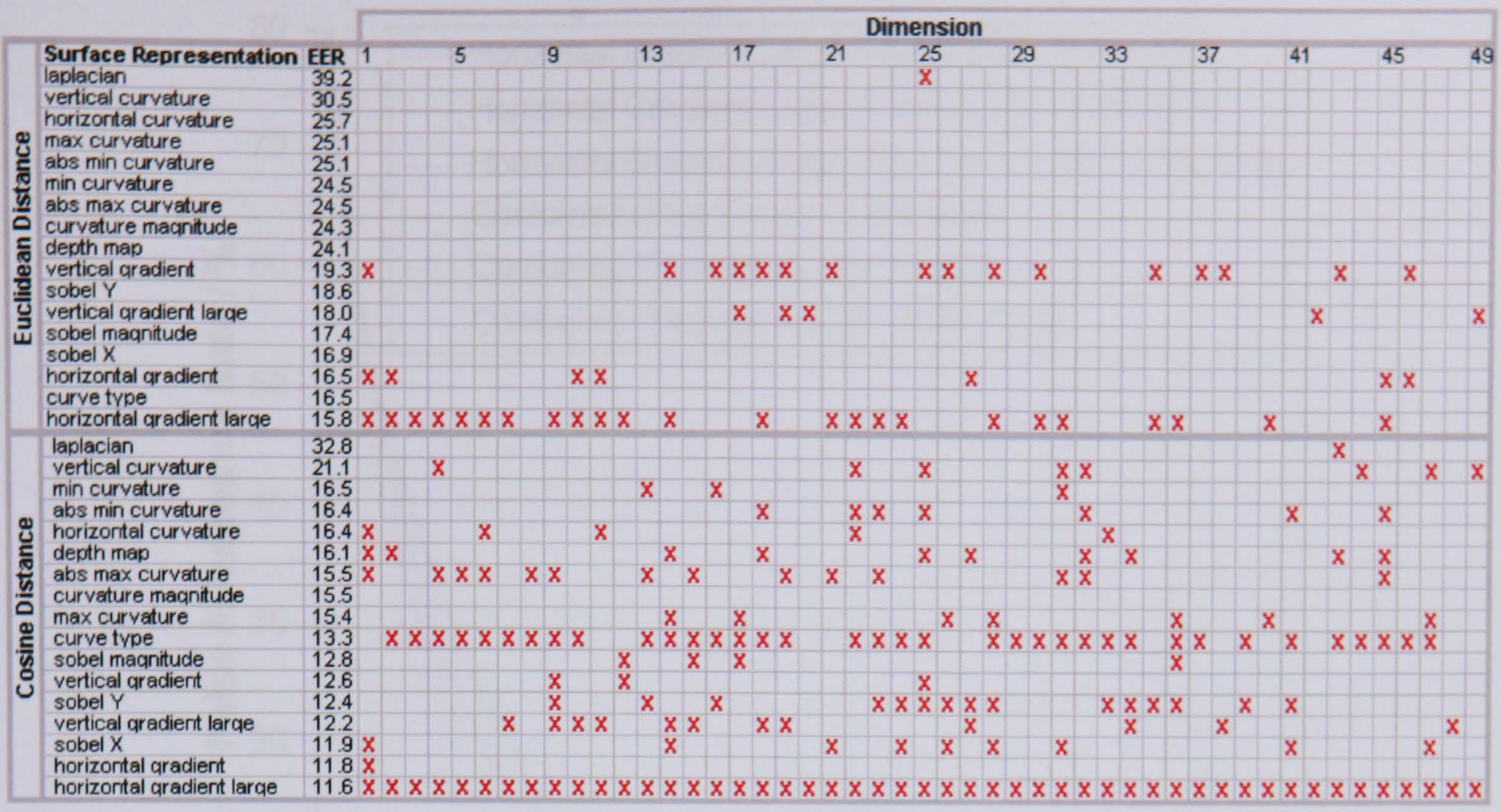

Figure 7-18 Face space dimensions included (x) in the multi-subspace Fishersurface systems

Figure 7-19 shows the error curves obtained when the best performing single-subspace Fishersurface systems and multi-subspace systems are applied to test set A (used to construct the combination), test set B (the unseen test set) and the full test set (all surfaces from sets A and B), using the cosine and Euclidean distance metrics. We see that the multi-subspace systems produce lower error rates than the best single-subspace systems for all six experiments. As would be expected, the lowest error rates are achieved when tested on the surfaces used to construct the combination (7.2% and 12.8% EER respectively). However an improvement is also seen when applied to the unseen test set B, from 11.5% and 17.3% using the best single systems to 9.3% and 16.3% EER for the multi-subspace systems. Performing the evaluation on the larger set, providing 1,079,715 verification operations (completed in 14 minutes 23 seconds on a Pentium III 1.2GHz processor at a rate of 1251 verifications per second), the error drops slightly to 8.2% and 14.4% EER, showing that a small improvement is introduced if some test data is available for training, as well as suggesting that the method scales well, considering the large increase in verification operations.

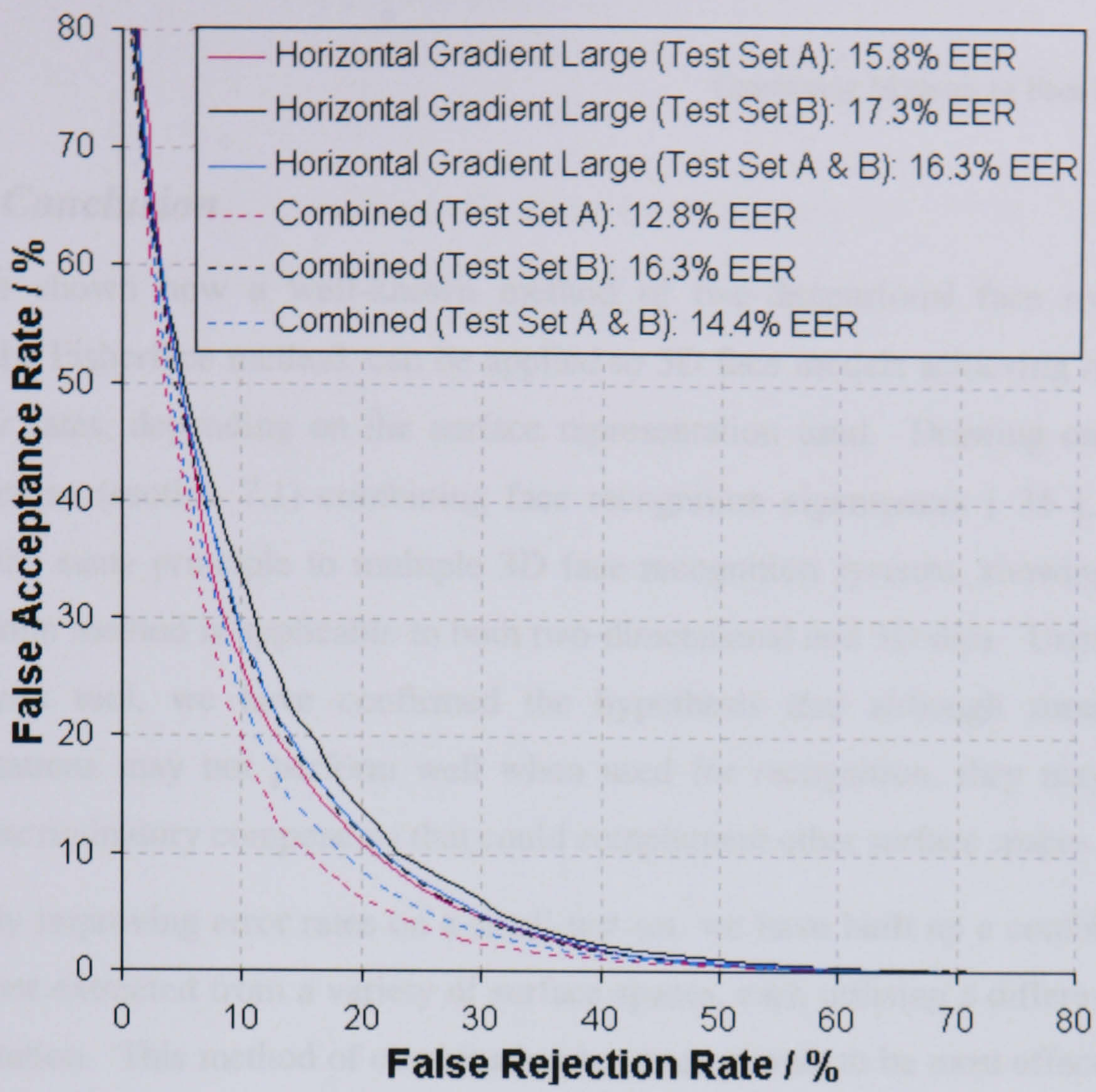

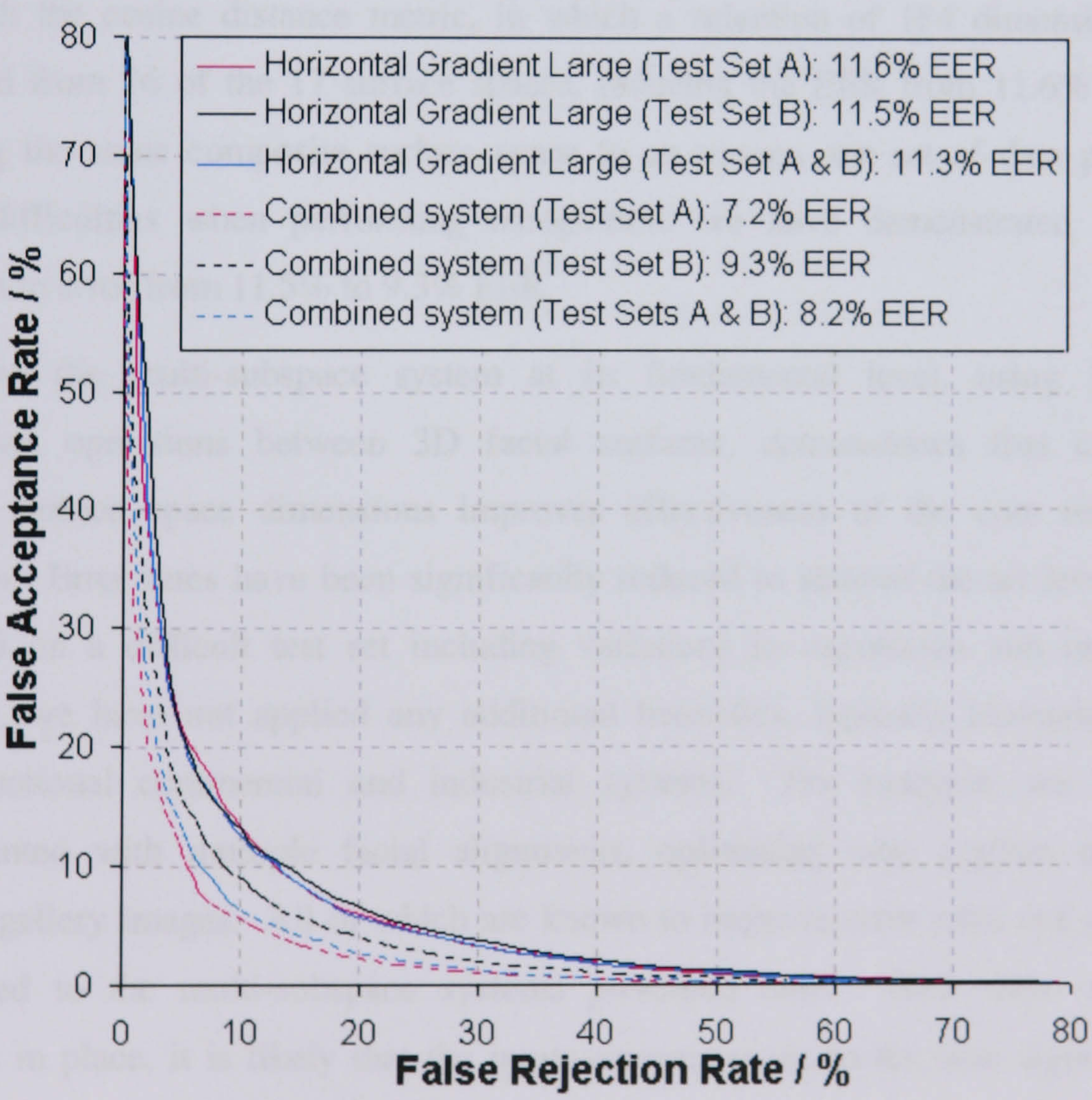

Figure 7-19 Error curves comparing multi-subspace (*dashed lines*) and individual (*solid lines*) systems using the Euclidean (*top*) and cosine (bottom) distance measures.

7.2.6 Conclusion

We have shown how a well-known method of two-dimensional face recognition, namely the Fisherface method, can be applied to 3D face models achieving reasonably low error rates, depending on the surface representation used. Drawing on previous investigations (section 7.1) combining face recognition eigenspaces [35], we have applied the same principle to multiple 3D face recognition systems, showing that the combination method is applicable to both two-dimensional and 3D data. Using FLD as an analysis tool, we have confirmed the hypothesis that although some surface representations may not perform well when used for recognition, they may harbour highly discriminatory components that could complement other surface spaces.

Iteratively improving error rates on a small test set, we have built up a combination of dimensions extracted from a variety of surface spaces, each utilising a different surface representation. This method of combination has been shown to be most effective when used with the cosine distance metric, in which a selection of 184 dimensions were combined from 16 of the 17 surface spaces, reducing the EER from 11.6% to 8.2%. Applying the same composite surface space to an unseen test set of data presenting typical difficulties when performing recognition, we have demonstrated a similar reduction in error from 11.5% to 9.3% EER.

Evaluating the multi-subspace system at its fundamental level, using 1,079,715 verification operations between 3D facial surfaces, demonstrates that combining multiple surface space dimensions improves effectiveness of the core recognition algorithm. Error rates have been significantly reduced to state-of-the-art levels, when evaluated on a difficult test set including variations in expression and orientation. However, we have not applied any additional heuristics, typically incorporated into fully functional commercial and industrial systems. For example, we have not experimented with multiple facial alignments, optimising crop regions or storing multiple gallery images. All of which are known to improve error rates and can easily be applied to the multi-subspace systems presented here. With these additional measures in place, it is likely that the improvements made to the core algorithm will propagate through to producing a highly effective face recognition system. Given the fast 3D capture method, small face-keys of 184 vector elements (allowing extremely

fast comparisons), invariance to lighting conditions and facial orientation. this system is particularly suited to security and surveillance applications.

7.3 Methods of Combination Optimisation

In the previous section we discussed two methods of selecting a set of dimensions from the complete collection of available face space and surface space systems and combining them to produce a augmented feature space that produces lower error rates than any of the individual systems alone. Some brief analysis and experimentation demonstrates that although the global discriminant value can be used as a fast approximation of system effectiveness, performing a complete evaluation and subsequently using the EER as the selection criteria is a significantly more effective selection criterion for the combination algorithm. Another aspect of the combination algorithm, which we have not yet addressed, is the order in which each dimension is selected and tested. Initial experimentation has indicated that this may be important, as the value of contribution of any candidate dimension is dependant on those dimensions already included in the existing composite subspace i.e. the optimisation is local, not global.

Actually, we have already begun to touch upon this issue, although somewhat indirectly, in the combination methods already discussed: it is precisely the reason we begin our combination with all dimensions from the current best performing system. Consider the case in which our composite face space consists of a single dimension, selected by chance from the worst of the face space systems. The next dimension tested for incorporation is almost certain to succeed (regardless of how discriminating it is), as such few features are currently utilised and even the smallest amount of additional discriminatory information would improve the system. On the other hand, once a combination incorporates a large number of dimensions is becomes increasingly unlikely that the next dimension will be of any benefit. These effects are witnessed in that more dimensions nearer the start of the list are included than those towards the end, as can be seen in section 7.1.6 and 7.2.5 (in which face space systems were considered for combination in order of ascending EER).

Some additional experimentation has uncovered another phenomenon that we must also consider here. It is possible that the incorporation of numerous dimensions into an existing subspace will significantly improve results; yet incorporating any one of those same dimensions individually can actually increase error rates. The combination

algorithms introduced so far only consider the addition of other dimensions on an individual basis and hence would miss any group of dimensions that require incorporation en masse. This effect is particularly well highlighted if we take the converse approach to subspace combination, by initialising the combined selection with all dimensions from all subspaces and iteratively discarding dimensions if the resultant combination reduces the EER. We see in section 7.3.1 that such an approach maintains a much greater number of dimensions than the 'combination by addition' method presented in sections 7.3.2 and 7.1.4.

We believe that this effect is due to the necessity of a coarse level classification having been applied (by incorporation of one dimension) before a fine detail lower-level classification becomes useful. In other words, some features are only capable of classifying sub-sets of faces. It is clear that the combinations computed by the methods discussed so far do not achieve the optimal combinations. Therefore we now explore three methods of subspace combination: combination by dimensional elimination; combination by dimensional accumulation; and combinatorial optimisation by genetic selection.

7.3.1 Combination by Dimensional Elimination

In this approach of dimensional combination we begin by combining all dimensions from every subspace produced, weighted by the inverse of the within-class standard deviation as explained in section 7.1. The EER is then calculated before iteratively eliminating each individual dimension (by reducing the corresponding weight to zero) in turn and testing for an improvement in error rate. If no increase in EER occurs the dimension is permanently discarded, otherwise the original weighting is reinstated.

```
Composite subspace = all dimensions of all systems
Compute EER of composite subspace
For each dimension:
        Remove dimension from composite subspace
        Compute EER of composite subspace
        If EER has increased:
Reinstate dimension into composite space
Save composite subspace ready for evaluation
```

Figure 7-20 Face space combination by dimensional elimination algorithm, using the EER as a fitness criteria.

By applying the algorithm above to a set of two-dimensional face recognition systems, we see that almost all dimensions are retained, as shown in Figure 7-21. This is in stark contrast to the combination by accumulation algorithm, in which very few dimensions are accumulated, a shown in Figure 7-22. It is also interesting to note that no dimensions are eliminated that were produced using the successful 'slbc' pre-processing technique, although seemingly contradictorily, no dimensions are eliminated from the 'hbrightness' system (which has one of the highest error rates), yet several dimensions are eliminated from the 'detail' system, which has the lowest error rates on this data set.

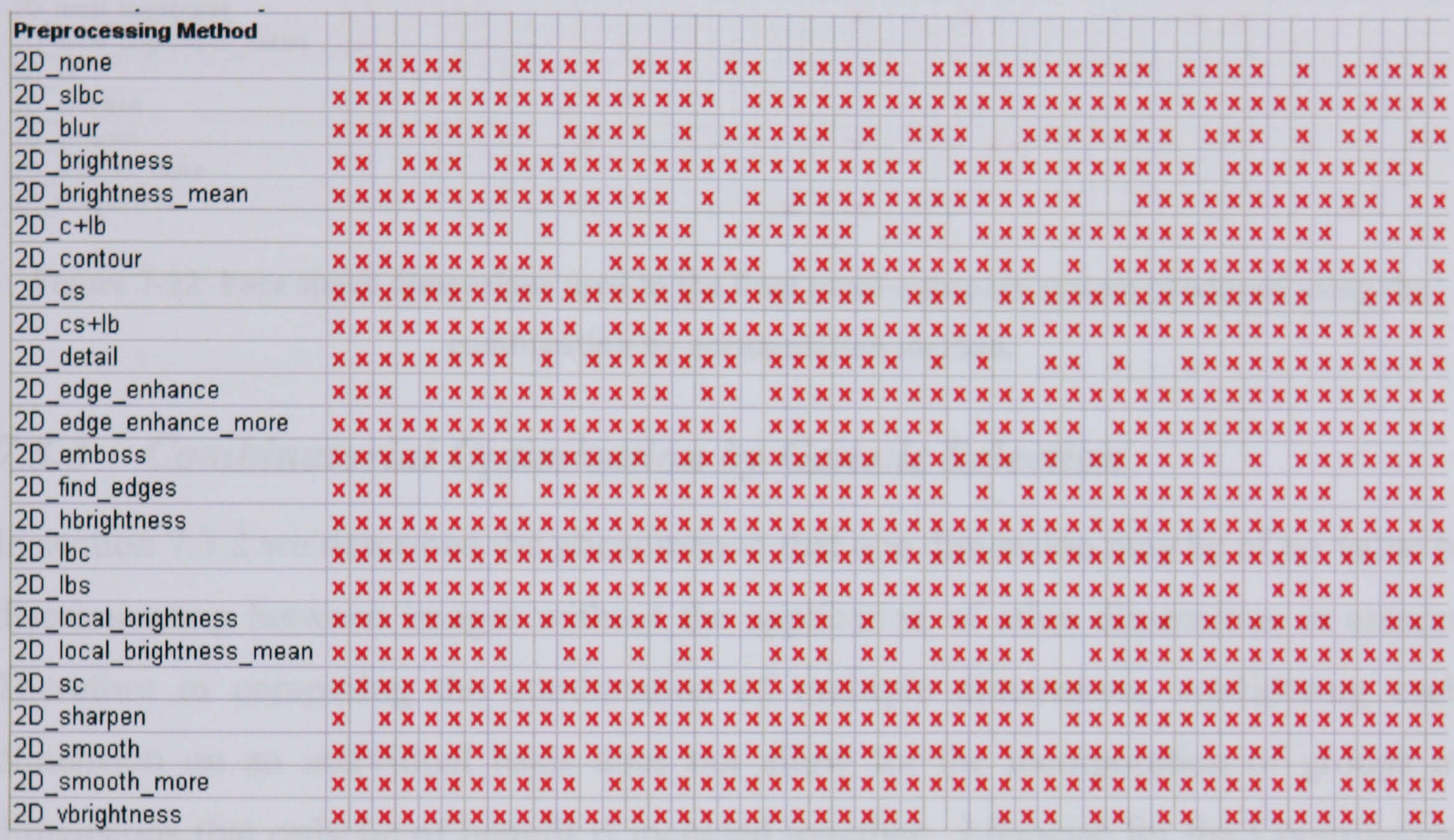

Figure 7-21 Face space dimensions used in the final multi-subspace system produced using the combination by elimination method.

7.3.2 Combination by Dimensional Accumulation

This is the combination algorithm used in previous sections to combine both two-dimensional face recognition systems and 3D face recognition systems. Although we now define the selection criteria as a reduction in EER, rather than the faster (but less successful) criterion of an increase in global discriminant. We apply the algorithm shown in section 7.1.4, to the same set of data used by the Combination by Dimensional Elimination algorithm described in the previous section. The combination produced can be seen in Figure 7-22.

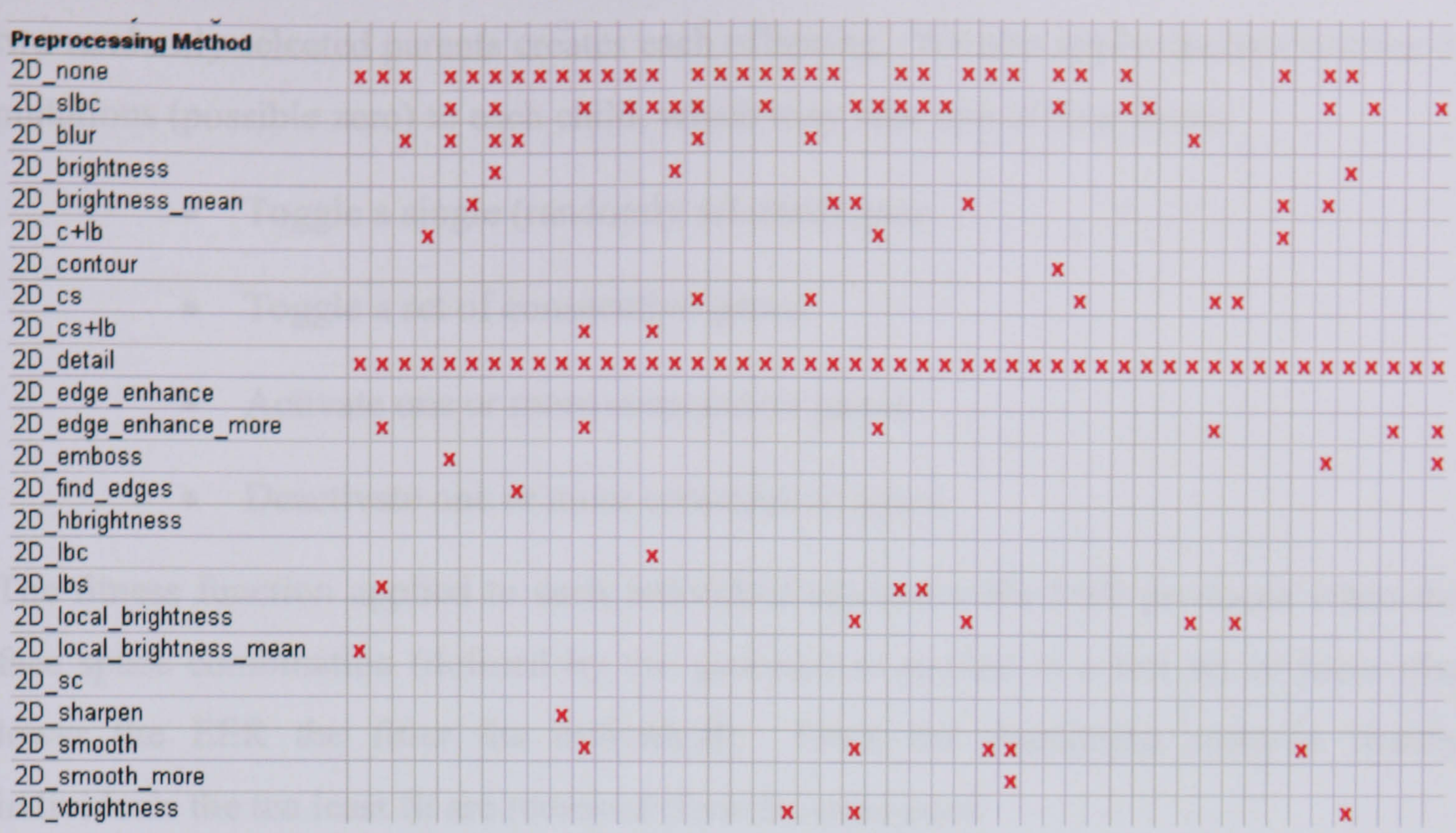

Figure 7-22 Face space dimensions used in the final multi-subspace system produced using the combination by accumulation method.

7.3.3 Combinatorial Optimisation by Genetic Selection

In section 7.3.2 we described the phenomenon that one dimension may be of no value in discriminating between images without the application of other dimensions in unison. Therefore in computing the combination of multiple dimensions, considering each dimension on an individual basis does not allow for the incorporation of groups of dimensions that only be of benefit if included together. Likewise for the Combination by Elimination algorithm it may be that removing a single dimension may increase error rates (because the removal of a high-level classification is causing several other dimensions to have a negative impact on recognition accuracy), yet removing a group of dimensions together will reduce error rates. For these reasons we now introduce a genetic algorithm to compute a more optimal combination of subspace dimensions. It is hoped that the nature of genetic algorithms, allowing traversal of many areas of the search space at the same time, will aid combination by avoiding the problem of local minima and incorporate elements that may have been of no use on earlier iterations.

We define our genome as a Boolean vector: each element indicating whether or not a dimension is included in the combination. The initial population shall consist of nine randomly generated vectors plus one additional vector in which only the dimensions from the most successful system are active. Combining randomly selected genes from

two randomly selected parents creates each offspring. We also apply random number of mutations (possible zero) to each child, which may take one of four forms:

- Toggle a single (randomly selected) gene.
- Toggle a set of consecutive genes.
- Activate one or more consecutive genes.
- Deactivate one or more consecutive genes.

The fitness function applied to each individual calculates the EER produced when the face space combination (defined by the genome) is applied to a test set of faces (the lower the EER the fitter the individual). Once the population contains twenty individuals the ten least fit are removed from the gene pool.

Applying the genetic algorithm to the same data set as used for the two combination algorithms described above, we produce the combination of dimensions shown in Figure 7-23.

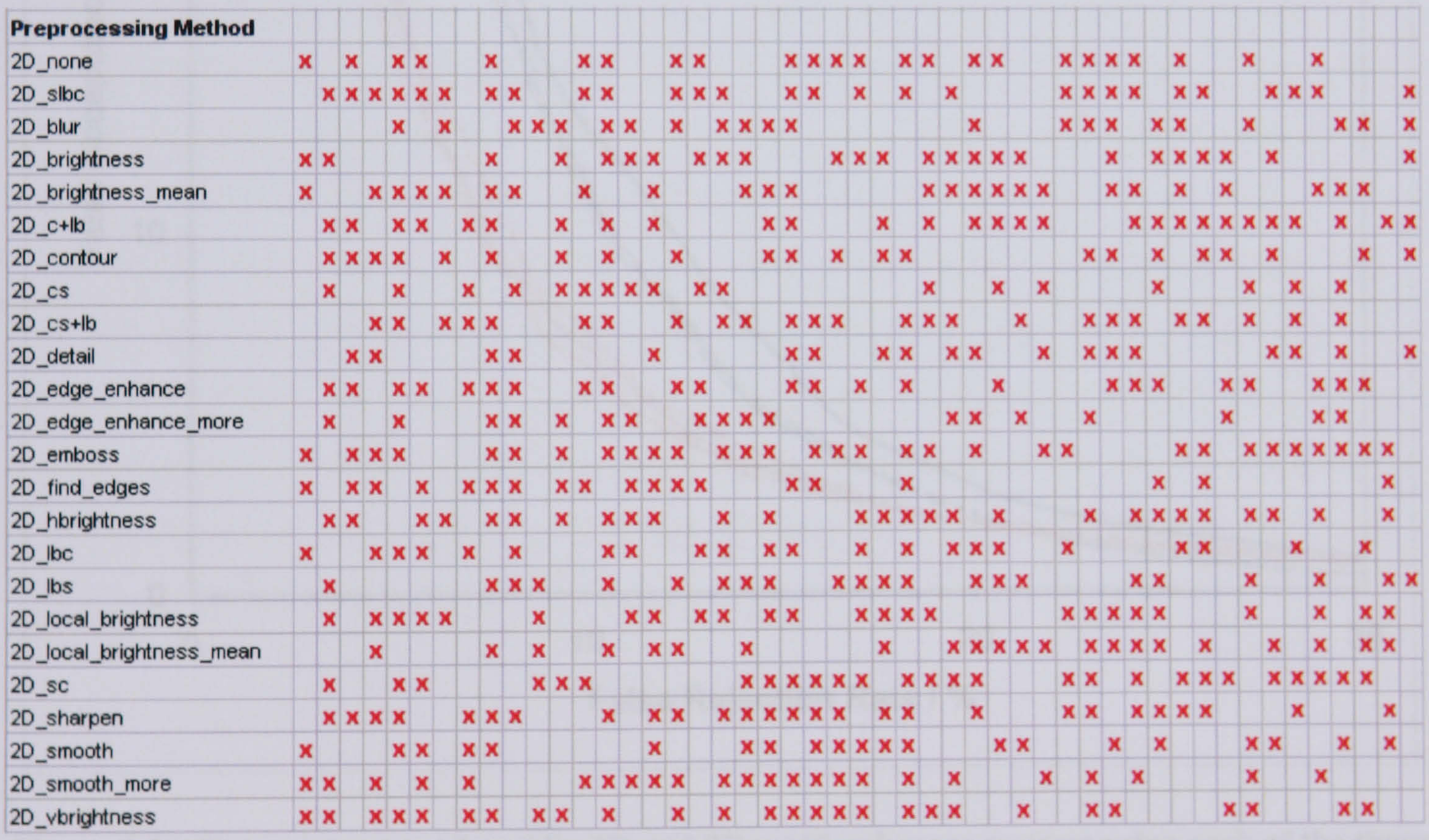

Figure 7-23 Face space dimensions used in the final multi-subspace system produced using the combination by genetic selection method.

7.3.4 Results Comparison

It is clear the three combination algorithms produce a very different combination of dimensions. In this section we apply each combination algorithm to the two-dimensional face recognition systems and the 3D systems.

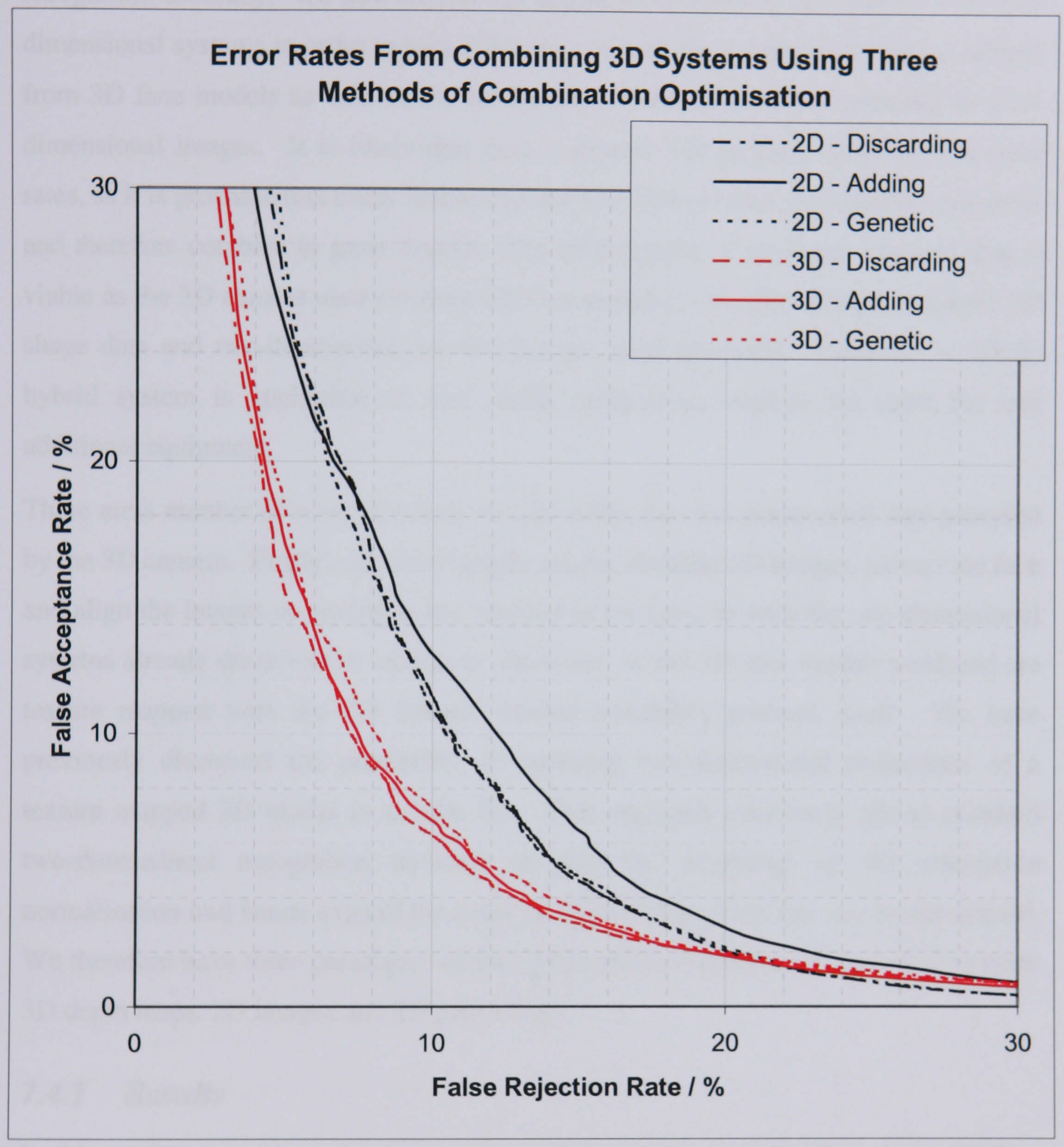

Figure 7-24 Error curves produced by 2D and 3D multi-subspace systems using each of the three methods of dimensional combination.

7.4 Combining 2D and 3D Face Recognition

Until this point we have concentrated on the combination of multiple two-dimensional face recognition systems and multiple 3D face recognition systems, considering the two

data types separately in the hope that different representations of the same data may encapsulation different features, which can subsequently be combined to improve recognition accuracy. We now extend this approach to combine 3D systems with two-dimensional systems in order to take advantage of both the geometrical shape available from 3D face models as well as the colour and texture information provided by two-dimensional images. It is likely that such a system will produce reductions in error rates, as it is probable that many features of the two types of data are mutually exclusive and therefore combine to great benefit. The combination of these two types of data is viable as the 3D camera used to create 3D face models is capable of capturing both 3D shape data and two-dimensional texture images simultaneously. Therefore, a 2D/3D hybrid system is applicable to real world applications without the need for any additional equipment.

There are a number of ways in which we can utilise the two-dimensional data provided by the 3D camera. Firstly, we could simply use the standard 2D images, extract the face and align the images according to the position of the eyes, as with the two-dimensional systems already described in section 4. However, as the 3D face models produced are texture mapped with the 2D images another possibility presents itself. We have previously discussed the possibility of matching two-dimensional projections of a texture mapped 3D model in section 6.1. This approach effectively allows standard two-dimensional recognition methods to gain the advantage of 3D orientation normalisation and hence expand the range of facial orientations that can be recognised. We therefore have three paradigms of data that may be combined into a unified system: 3D depth maps, 2D images and 2D projections.

7.4.1 Results

In this section we present the error rates produced when two-dimensional and 3D face recognition systems are combined and tested on the same data set as described in 7.3 (test set B). We apply the three combination algorithms to all pre-processing techniques and surface representations using test set A as the combination analysis data, before computing the error curve using test set B.

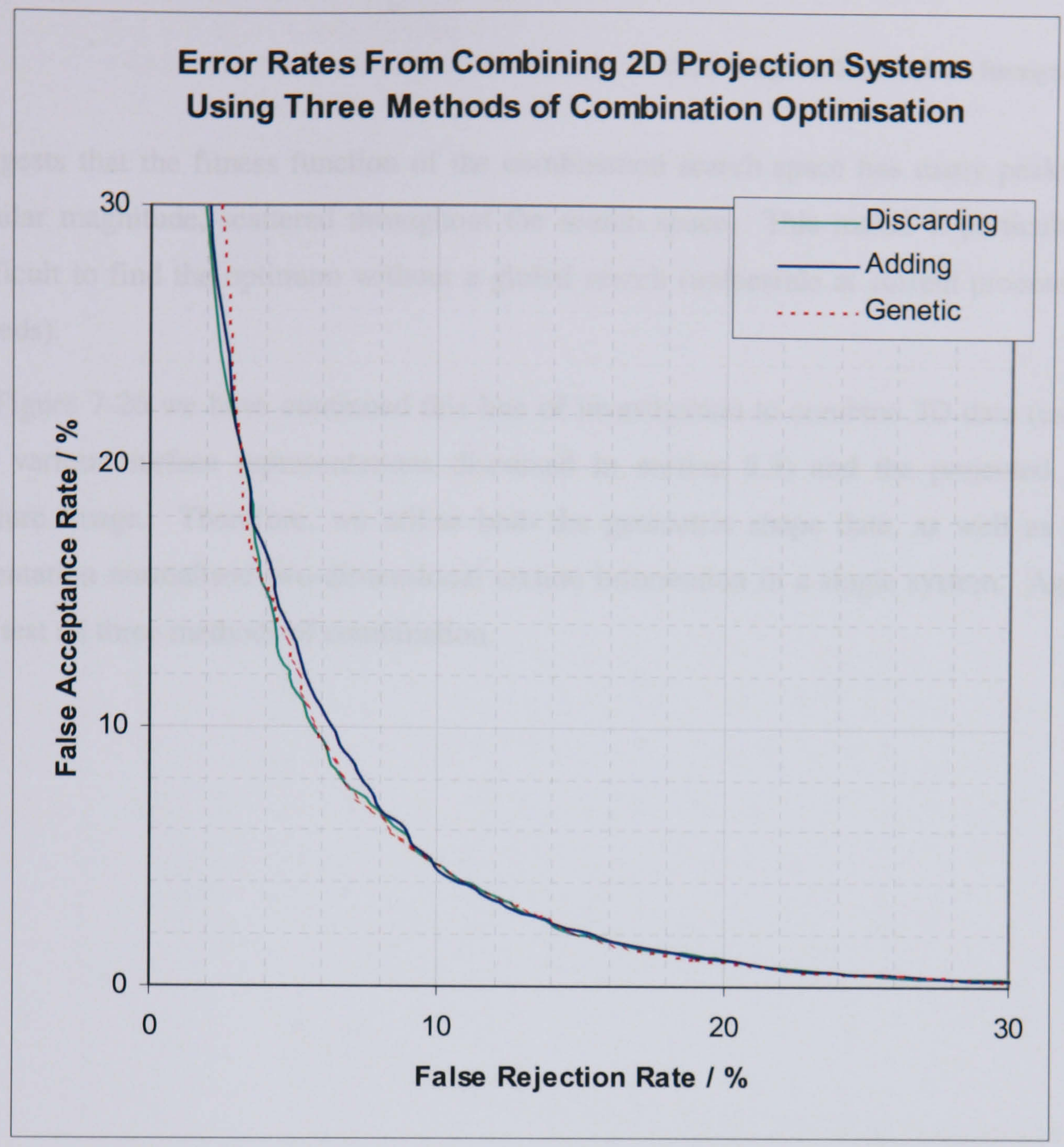

Figure 7-25 Error rate curves of 2D projection multi-subspace systems produced using the three methods of dimensional combination.

Figure 7-25 shows the error curves produced from three multi-subspace systems comprised of all pre-processing techniques applied to two-dimensional image projections (produced from a texture mapped 3D model). All three combination methods produce very similar error rates, although the discarding (7.33% EER) and genetic (7.21% EER) method do have a slight advantage of the addition method (7.58% EER) of system combination, which follows the same pattern of results produced in previous combination experiments with 2D and 3D systems, adding further evidence to support the genetic algorithm as the superior method of combination.

Looking at the patterns of dimensions included (Figure 7-21, Figure 7-22 and Figure 7-23) by the various combination techniques, it is interesting to note the great difference in selected components, but relatively little difference in the error rates produced. This

suggests that the fitness function of the combination search space has many peaks of similar magnitude, scattered throughout the search space. This makes it particularly difficult to find the optimum without a global search (unfeasible at current processing speeds).

In Figure 7-26 we have continued this line of investigation to combine 3D data (using the various surface representations discussed in section 5.3) and the projected 2D texture image. Therefore, we utilise both the geometric shape data, as well as the orientation normalised two-dimensional texture information in a single system. Again we test all three methods of combination.

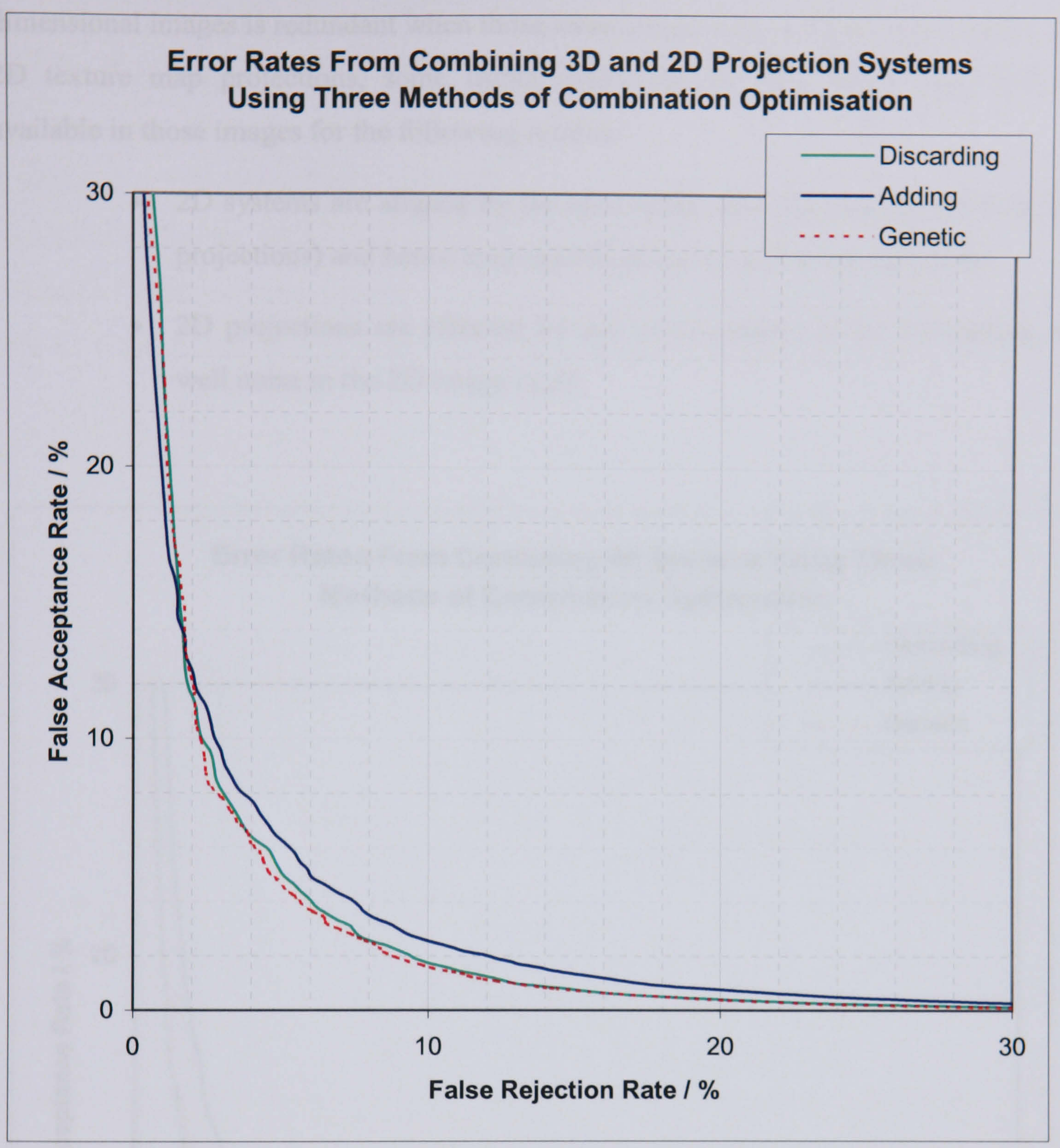

Figure 7-26 Comparison of error rate curves of multi-subspace 3D and 2D projection systems produced using the three methods of dimensional combination.

Clearly the use of both categories of information provides significant advantages, reducing the EER from 7.21% (using the genetic combination of 2D projections) down to 5.58%, 5.04% and 4.84% EER using the adding, discarding and genetic methods of combination respectively (once again the genetic method is shown to produce the most effective combination).

We now present results gained by increasing the number of multi-subspace systems to include 3D depth maps, 2D projections and those that use standard 2D images. Although at first thought it may seem that the information provided by standard two-

dimensional images is redundant when those same images have already been used in the 2D texture map projections, some useful discriminatory information may still be available in those images for the following reasons:

- 2D systems are aligned by the eyes rather than the nose tip (as with 2D projections) and hence may expose different cues in the face space.
- 2D projections are effected by any noise present in the 3D surface, as well noise in the 2D image itself.

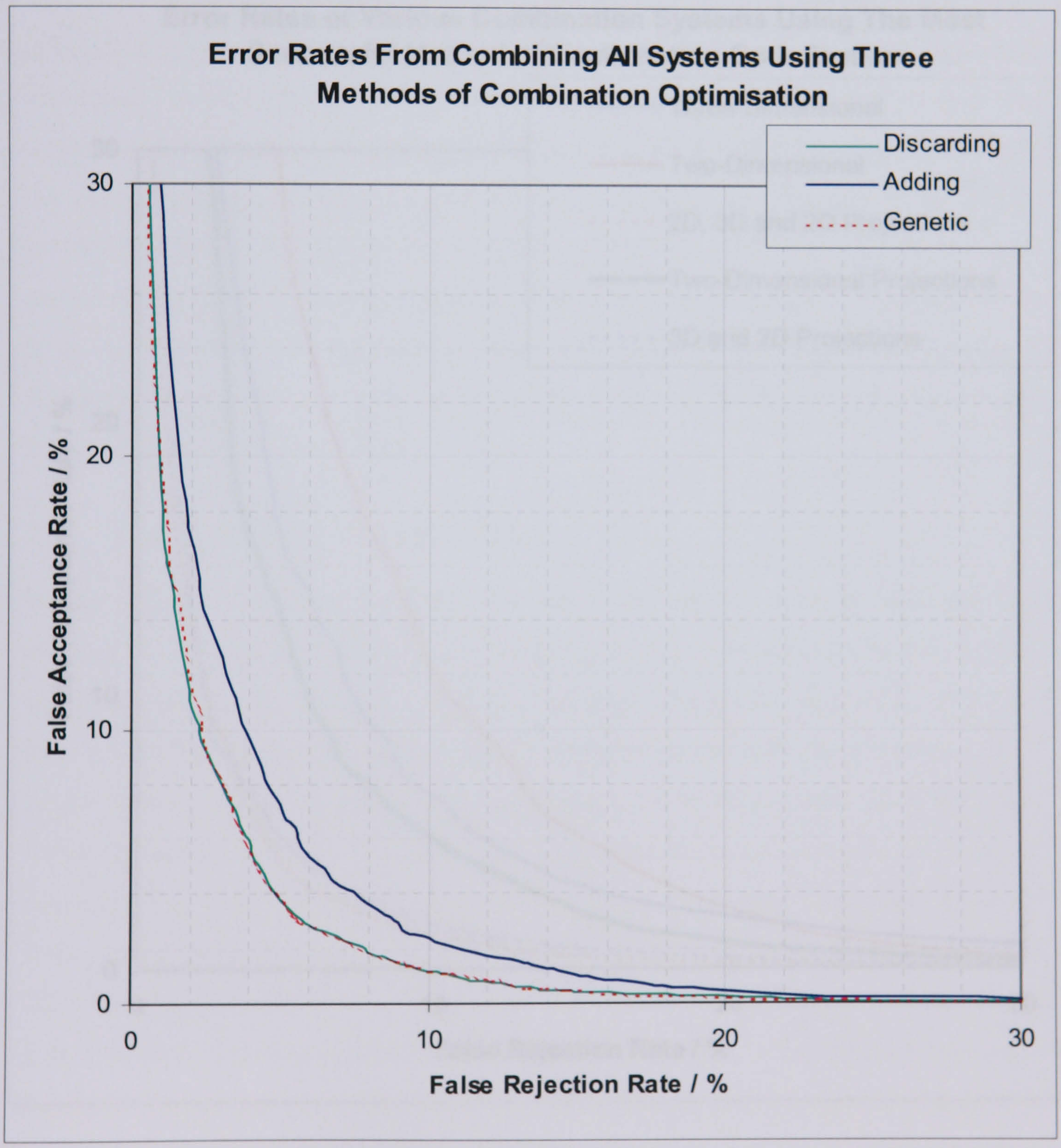

Figure 7-27 Error rate curves of multi-subspace systems produced using the three methods of dimensional combination across all face data types.

Once again, by introducing yet more information in the form of standard 2D images we are able to reduce error rates further. As witnessed in previous experiments the genetic and discarding methods of combination generate the best results, producing EERs of 4.50% and 4.55% respectively. The adding method of genetic combination produces a significantly higher EER of 5.72%. If we now compare the results of the most successful methods of combining each category of data, we get a good overview of the effectiveness of each type of facial representation for recognition.

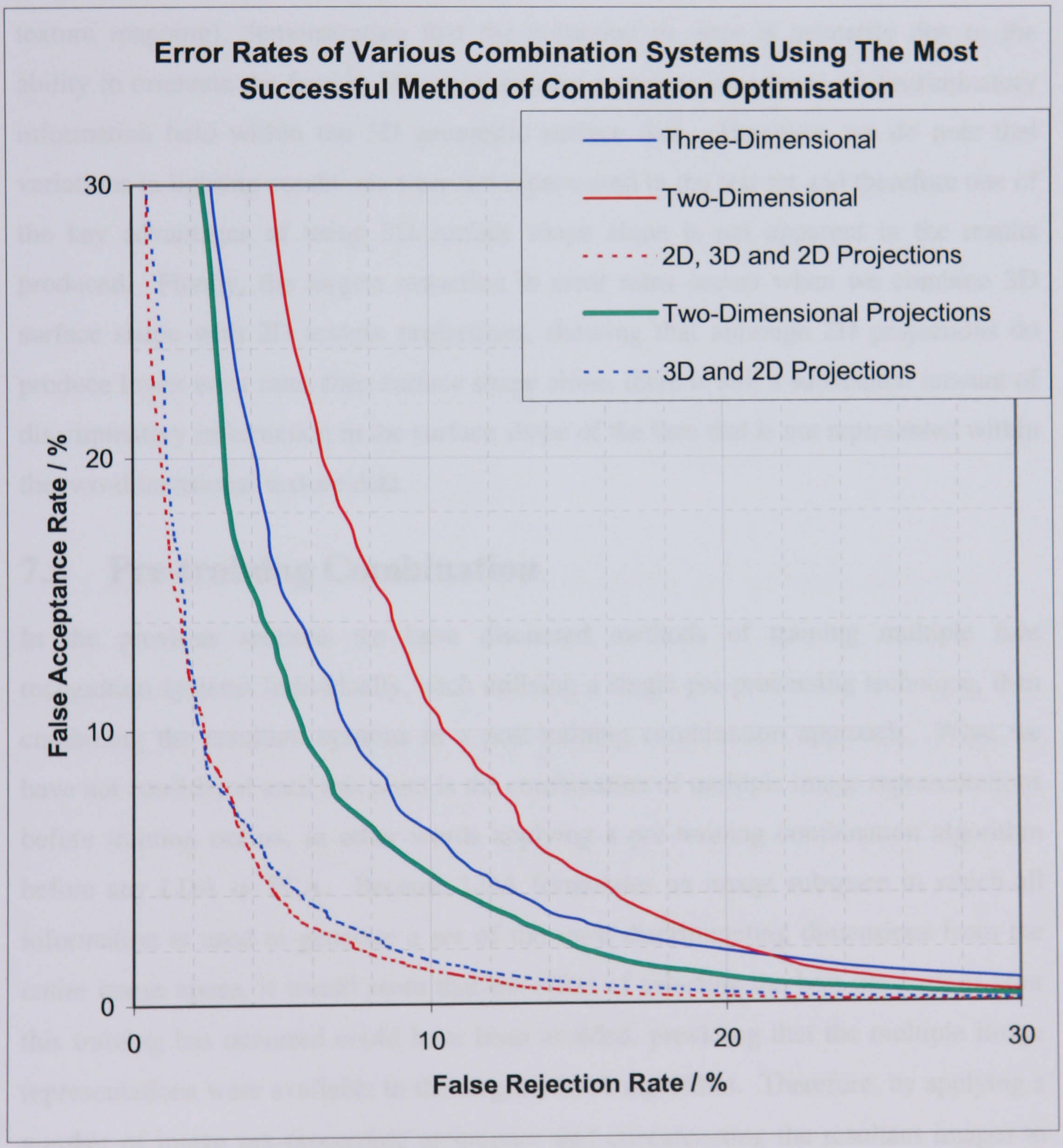

Figure 7-28 Comparison of error rate curves of the most effective of each type of multi-subspace system.

Figure 7-28, shows the error curves of combining all two-dimensional systems (red), three dimensional systems (blue), 2D projections (green) and 3D with 2D data (dashed). We see that standard two dimensional systems produce the highest EER, as would be expected due to the varying facial orientations in the test data. The use of 3D models overcomes this alignment problem by allowing 3D orientation normalisation and hence we witness a substantial drop in error rates. However, we then see that using the 2D image projections actually produces lower error rates than the 3D surfaces (without texture mapping), demonstrating that the reduction in error is primarily due to the ability to orientate the face in 3D space and not a greater abundance of discriminatory information held within the 3D geometric surface data. However, we do note that variations in lighting conditions were not represented in the test set and therefore one of the key advantages of using 3D surface shape alone is not apparent in the results produced. Finally, the largest reduction in error rates occurs when we combine 3D surface shape with 2D texture projections, showing that although 2D projections do produce lower error rates than surface shape alone, there is still a substantial amount of discriminatory information in the surface shape of the face that is not represented within the two-dimensional texture data.

7.5 Pre-training Combination

In the previous sections we have discussed methods of training multiple face recognition systems individually, each utilising a single pre-processing technique, then combining the resultant systems in a post-training combination approach. What we have not considered until this point is the combination of multiple image representations before training occurs, in other words applying a pre-training combination algorithm before any LDA or PCA. Because LDA formulates an image subspace in which all information is used to generate a set of the most discriminating dimensions from the entire image space, it would seem that the effort of selecting the best dimensions after this training has occurred could have been avoided, providing that the multiple image representations were available to the original LDA algorithm. Therefore, by applying a number of image pre-processing techniques and concatenating the resultant images to create a larger image, which can than be used for LDA we provide the training process with all the information that would have been combined in the post-training combination methods.

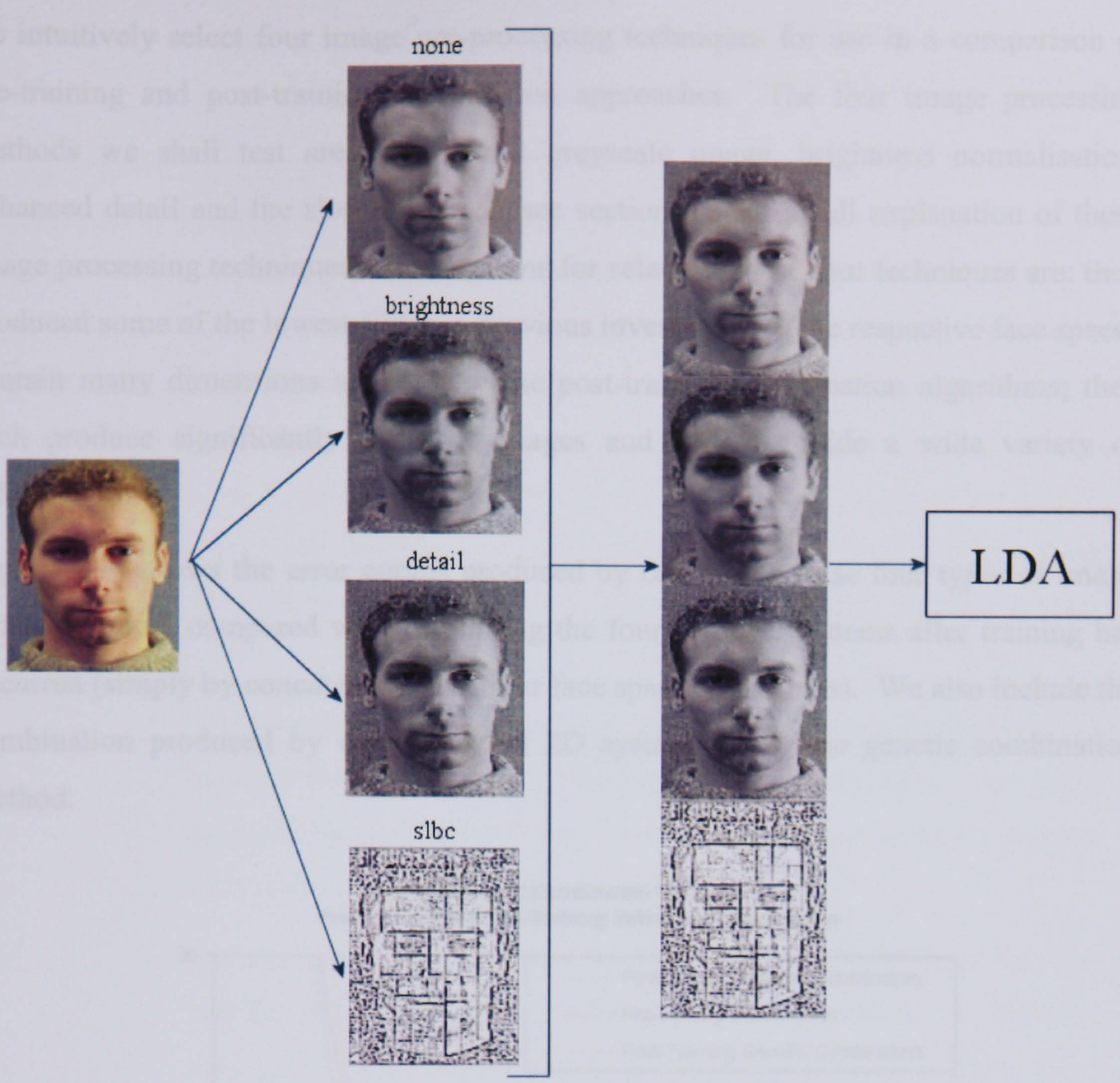

Figure 7-29 Illustration of the process used to carry out pre-training combination.

The main drawback of this method is the high computational time complexity. As the computation time of creating an image subspace has a polynomial dependence on the size of the images, $O(Mn^2+n^3)$, where M is the number of items in the training set and n the dimensionality (pixels) of the face images. Computing an optimum combination would become an intractable problem as a new subspace would have to be computed at every iteration (whereas the post-training combination method just concatenates image subspace projections). Despite this, just combining a small number of images would still allow generation of a face space with the potential to make more efficient use of the available information. By concatenating just four pre-processed images the training time will be increased by a factor of 61 (taking approximately 15 hours to complete, rather than including all 31 image-processing techniques increasing computation time to nearly 10 months). Therefore, in order to test this pre-training combination approach

we intuitively select four image pre-processing techniques for use in a comparison of pre-training and post-training combination approaches. The four image processing methods we shall test are the original greyscale image, brightness normalisation, enhanced detail and the slbc technique (see section 4.5 for a full explanation of these image processing techniques). The reasons for selecting these four techniques are: they produced some of the lowest EERs in previous investigations; the respective face spaces contain many dimensions selected by the post-training combination algorithms; they each produce significantly different images and hence provide a wide variety of information.

Figure 7-30 shows the error curves produced by combining these four types of image before training, compared with combining the four separate systems after training has occurred (simply by concatenating the four face space projections). We also include the combination produced by combining all 2D systems using the genetic combination method.

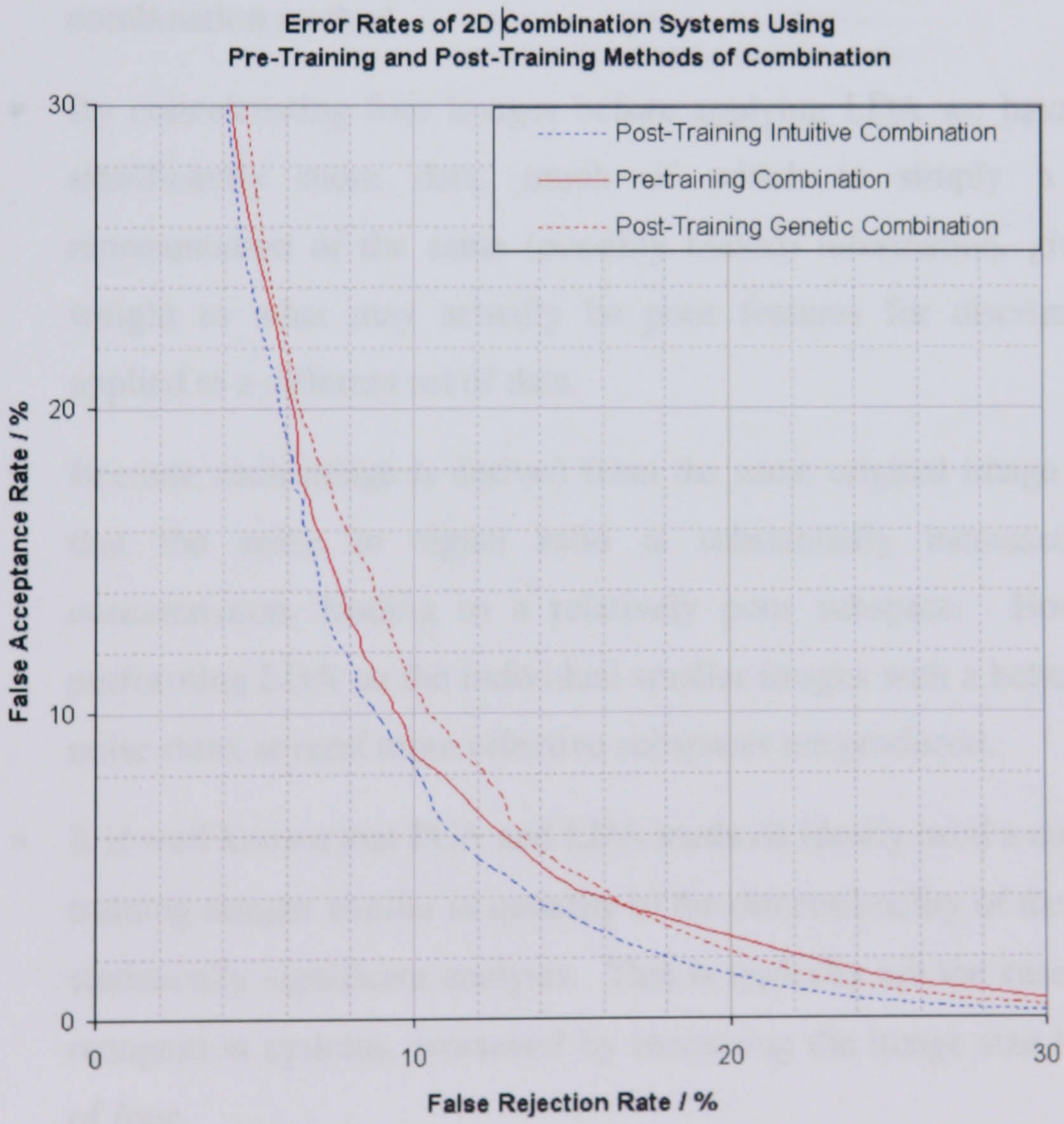

Figure 7-30 Comparison of error rate curves produced by post-training and pre-training combination systems.

This experiment has produced some interesting results. Firstly, we see that the combination computed by the genetic combination algorithm is not optimal. Even though the genetic combination contains various dimensions from all twenty-four 2D systems (10.33% EER), a simple intuitive selection of just four systems produces a lower EER of 9.26%, suggesting that the evolution methods used in the genetic algorithm could be improved by toggling all dimensions from a entire face space in a single mutation. More surprisingly we see that the error rates produced by combining the four systems before training are higher (with an EER of 9.66%) than those produced by combining the four systems after training. There are a number of possible reasons for this outcome:

- The two-stage training process of the post-training combination method acts as a filtering mechanism for any features that have been over-trained on the test data, whereas any such features will remain in the pre-training combination method.

- By concatenating four images before applying LDA we have supplied significantly more data, much of which is simply a different representation of the same (possibly biased) information, giving extra weight to what may actually be poor features for discrimination if applied to a different set of data.

- Because each image is derived from the same original image it may be that the noise to signal ratio is substantially increased through concatenation, leading to a relatively poor subspace. However, by performing LDA on the individual smaller images with a better signal to noise ratio, several more effective subspaces are produced.

- It is well known that PCA and LDA methods ideally need a collection of training images similar in quantity to the dimensionality of the data for a statistically significant analysis. This is typically not the case with face recognition systems, worsened by increasing the image size by a factor of four.

- The combination process accumulates dimensions based on the same criteria used to evaluate performance (the EER). This combination

process may therefore be more suited to producing a better subspace (according to the evaluation criteria) than PCA and LDA, which merely attempt to produce greatest between-class scatter. Such representations are not necessarily optimal for classification due to subspace manifolds and local clustering.

8 Final Comparative Evaluation

Throughout this thesis we have presented a range of results from numerous investigations carried out during the course of this PhD research. We began by exploring two-dimensional face recognition methods using a database of 2D face images provided by Martines and Benvente [39]. As our direction of research began to focus on 3D techniques we required a database of 3D face models. As no suitable database was available we managed to obtain access to a prototype state-of-the-art 3D camera and began to populate a preliminary database for development of 3D face recognition algorithms. Initial investigations indicated that this direction of research was promising, but 3D imaging technology progressed substantially over that period and a superior 3D camera soon emerged which was capable of capturing high quality 3D models with high-resolution 2D texture maps. At this point we began to populate a new 3D face database that would provide the capability to test and develop 3D face recognition technologies, incorporate 2D texture maps and compare 3D face recognition directly to 2D approaches using images captured at the same instant.

This selection of databases available have continually evolved throughout the course of these investigations, which means that we cannot directly compare the results of those systems tested on one database to those computed from another. Having reached the end of the development stage in this research, we now address this issue by defining a standard dataset, containing 2D and 3D images acquired simultaneously and hence under the same environmental conditions.

In section 8.1 we specify the image capture conditions and present the results gathered in section 8.2 and 8.3. We apply two methods of face recognition analysis to the standard dataset, reflecting the two primary applications of face recognition technology: verification and identification. Verification is performed by comparing two face images (either 2D, 3D or 2D projections), calculating False Acceptance Rates and False Rejection Rates for a range of threshold values. The resultant error curve is plotted as in previous sections. Again the EER is taken as a single comparative value, for direct comparison of multiple systems. In addition to the verification tests we also produce cumulative match curves for each face recognition system, indicating the system

effectiveness in searching a large database of facial images to identify the correct subject.

8.1 Database Specification

For the purpose of these experiments we select a sample of 1770 faces (280 people) captured under the conditions in Figure 8-1, taken from the University of York 3D Face Database [50]. Each face is represented by a standard two-dimensional greyscale bitmap image, a 3D face model and a texture map projection of the orientation normalised 3D model (also stored as a 2D greyscale bitmap). Figure 8-1 shows the range of capture conditions present in the database, but we refer the reader to section 5.1 for a detailed explanation of how the data was acquired and the specific data formats.

A test set of 735 faces (115 people) is selected at random to compute error rates and cumulative match rates, leaving the remaining 1035 faces (165 people) to use in training the various face recognition systems. Typically, 300 of these faces are used to compute the face space projection matrices, while the face space combination methods require the additional faces in order to compute the best system combinations. The training and test sets are completely disjoint, so that none of the faces (or the people) in the training sets are present in the unseen test set.

Front facing, neutral expression, optimum distance from camera (1.7m from unit to nose tip)

Neutral expression, facing roughly **45 degrees up**.

Neutral expression, facing roughly **45 degrees down**.

Front facing, **smiling**.

Front facing, **eyes closed.**

Front facing, **angry expression**.

Front facing, **neutral expression**.

Front facing, **eyebrows raised.**

Front facing, neutral expression, **no glasses**.

Front facing, neutral expression, no glasses, **further away** from the camera (1.9m from unit to nose tip).

Figure 8-1 Example image capture conditions and data types present in the database used for the final comparative evaluation.

8.2 Verification Results

Error rate curves are produced as described in section 4.2.1, using the 735 faces of the test set, such that each error rate is based on 269,745 verification operations. We begin by comparing the EERs of all the multi-subspace systems (see section 7), as shown in Figure 8-2.

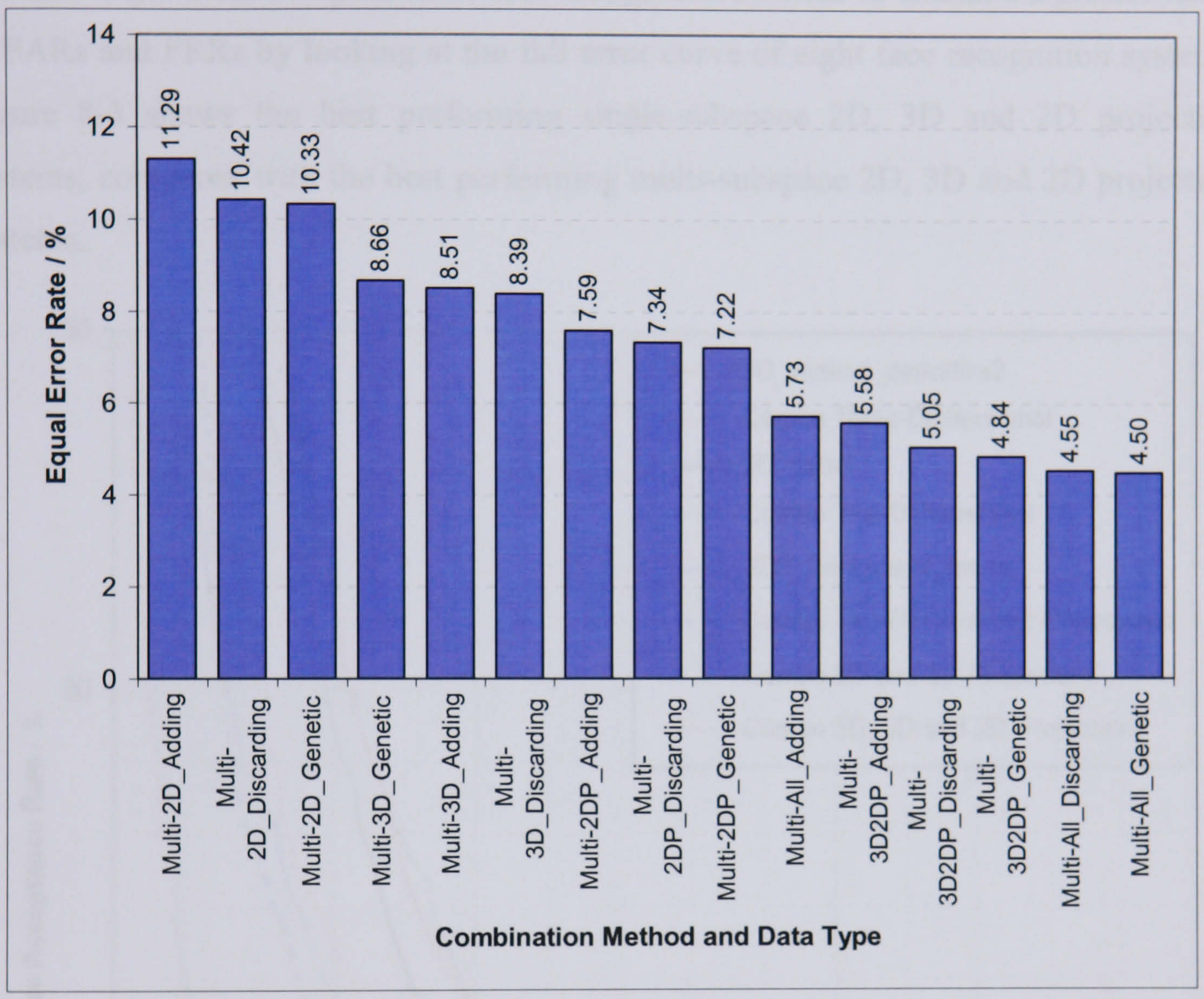

Figure 8-2 EERs of each multi-subspace system applied to the final evaluation test set.

We see that the two best performing face recognition systems use a combination of 2D images, 3D models and 2D projections, producing EERs of 4.55% and 4.50%. The genetic method (4.50% EER) of combination shows a slight improvement over the discarding method (4.55% EER), whereas the adding method has a significantly higher EER of 5.73%. The multi-subspace systems with the highest EERs are the 2D multi-subspace systems (11.29%, 10.42% and 10.33% EER). No doubt this is a reflection of the systems inability to cope with variations in head orientation, as all 2D projection systems (using orientation normalised projections of the same faces) achieve much lower EERs of 7.59%, 7.34% and 7.22%. Perhaps surprisingly, the 2D projection

systems outperform the systems that use 3D face models, demonstrating that the colour and texture of the face is more discriminating than the face shape alone. However, as variations in lighting condition were not included in the test set, we do expect to see lower error rates from the 2D systems than if strong variations in lighting conditions were included in the test data.

We now expand our comparison of face recognition systems to examine a greater range of FARs and FRRs by looking at the full error curve of eight face recognition systems. Figure 8-3 shows the best performing single-subspace 2D, 3D and 2D projection systems, compared with the best performing multi-subspace 2D, 3D and 2D projection systems.

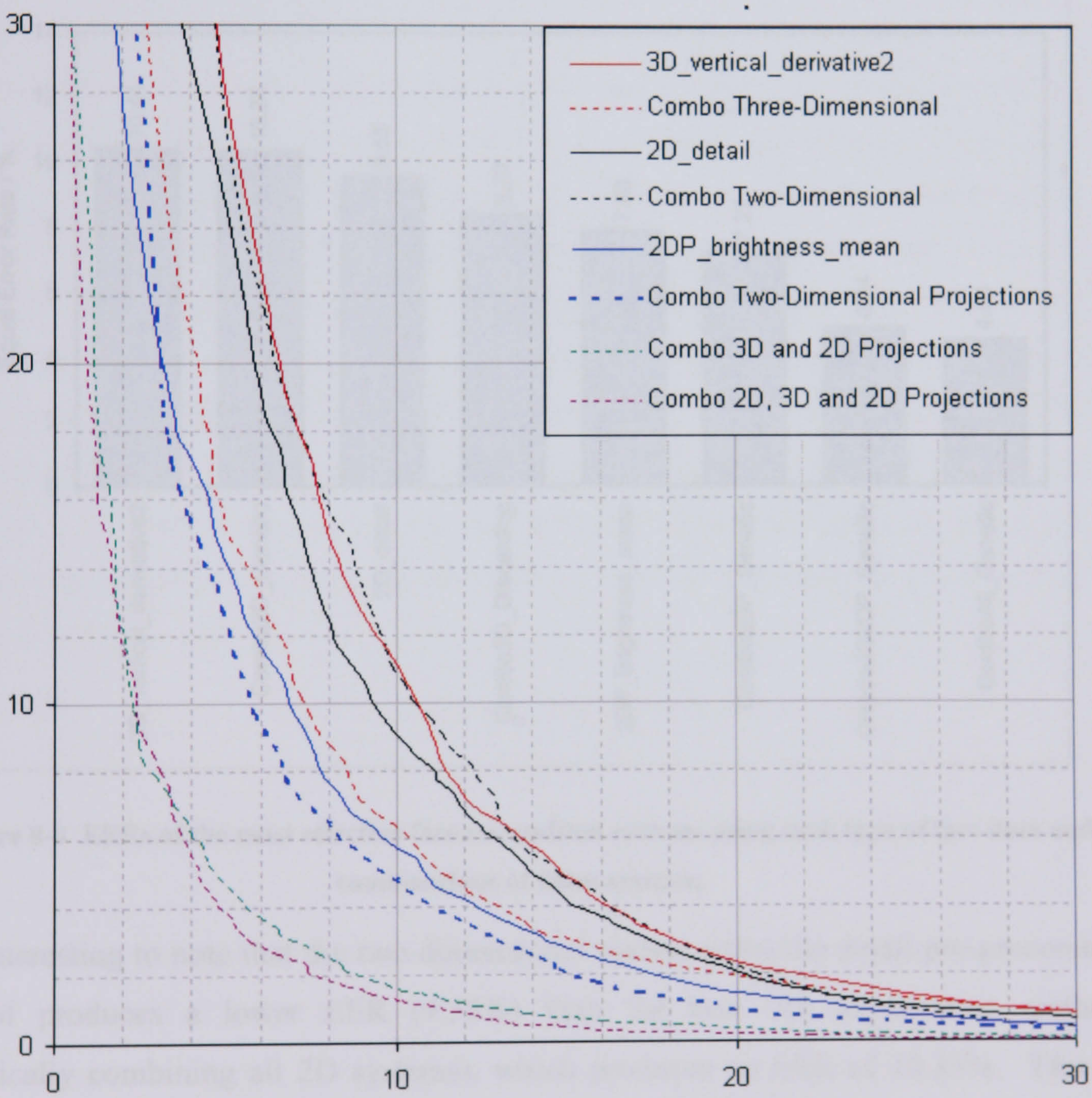

Figure 8-3 Error rate curves of the most effective face recognition systems using each type of face data and combinations of those systems.

Figure 8-3 shows the performance of the face recognition systems with FAR and FRR ranging from zero to thirty percent. On the right side of the graph we see the circumstances under which a high security system would operate: tolerating a higher rate of false rejection to achieve a lower possibility of an intruder gaining access. On the left hand side of the graph the plots show the characteristics of such systems operating in a system that require high subject throughput, at the expense of a higher rate of false acceptances. Again we see the same pattern of error rates, with the full multi-subspace systems achieving the lowest error rates, followed by 2D projections, 3D models and finally 2D systems. Taking the EER from each of these plots, we can compare the range of systems using a single error rate, as shown in Figure 8-4.

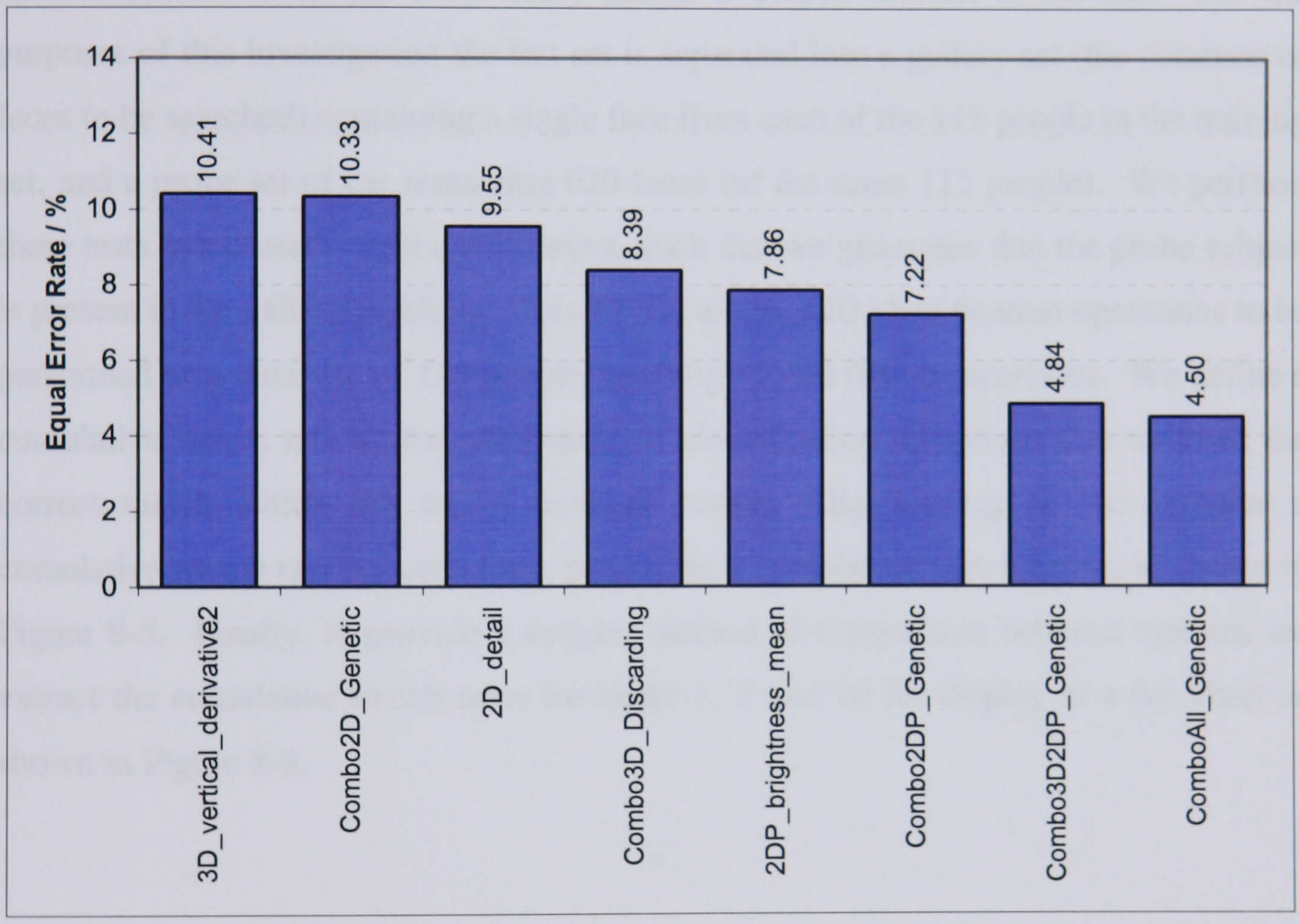

Figure 8-4 EERs of the most effective face recognition systems using each type of face data and combinations of those systems.

It is interesting to note that the two-dimensional system using the detail pre-processing method produces a lower EER (9.55%) than the best 2D combination method (genetically combining all 2D systems), which produces an EER of 10.33%. This is particularly surprising, as the fitness function for combining multiple systems requires an improvement in the EER for any two systems to combine. However, because this analysis is computed using a different data set, these results seem to indicate substantial

over-training on the combination set, which means that when the system is then applied to the unseen test set, the error rates are significantly higher.

8.3 Identification Results

The identification test evaluates the ability of a face recognition system to search a database of faces and select the most likely matches to a given probe face. This method of evaluation differs from the verification tests in that we are not interested in gaining a definite acceptance/rejection decision for a pair of faces, but rather in producing an ordered list in which the most likely match is placed highest in the list. For the purposes of this investigation the test set is separated into a gallery set (the database of faces to be searched) containing a single face from each of the 115 people in the training set, and a probe set of the remaining 620 faces (of the same 115 people). We perform these tests in a closed-world environment, such that we guarantee that the probe subject is present in the gallery database. This format allows 620 identification operations to be performed on a database of 115 people, totalling 71,300 face comparisons. We define a cumulative match rate as the percentage of identification operations that returned the correct match within the top N returned results. By varying N, we compute a cumulative match rate for each rank, producing a cumulative match curve, as shown in Figure 8-5. Finally, to provide a simpler method of comparison between systems we extract the cumulative match rates for ranks 1, 5 and 10 for display in a bar chart as shown in Figure 8-6.

8.3.1 Two-Dimensional Systems

Figure 8-5 shows the cumulative match curve for the three most effective 2D face recognition systems. We see the cumulative match rate trail off as it becomes less and less likely that the correct match will be returned in the top N rank. In particular a sharp decrease in cumulative match rate is seen for ranks of less than 10. In general the best performing 2D system uses the detail pre-processing method, until the correct match is expected in the top 5 ranks, in which case the highest match score is achieved by a 2D system using no pre-processing.

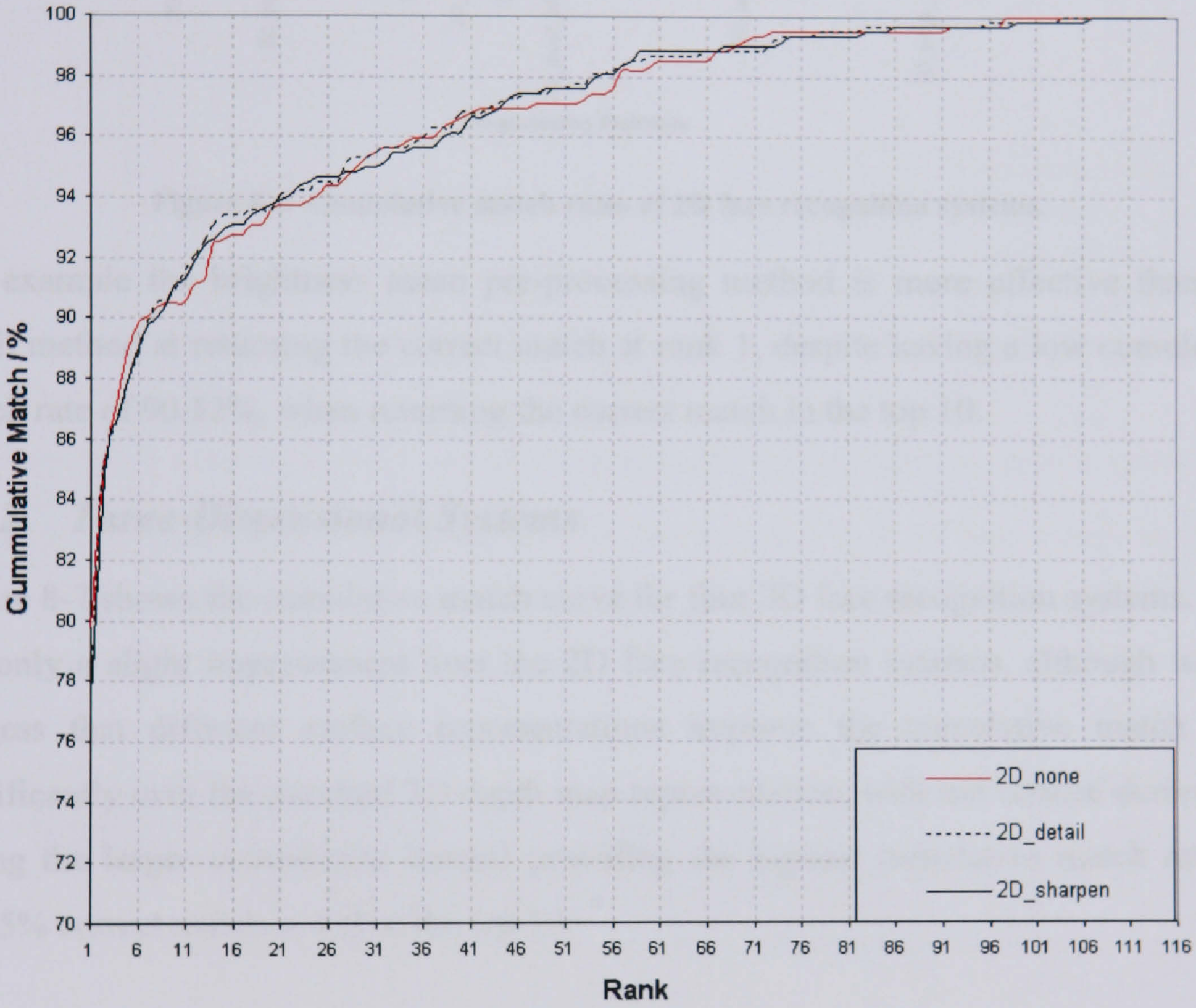

Figure 8-5 Cumulative match curves of the three most effective 2D face recognition systems.

Figure 8-6 shows the cumulative match rates for ranks of one, five and ten for all 2D face recognition systems. Again we see that the detail pre-processing method returns the correct match in the top ten most often (91.13%), although the most effective system depends on the required placement of the correct match within the rank.

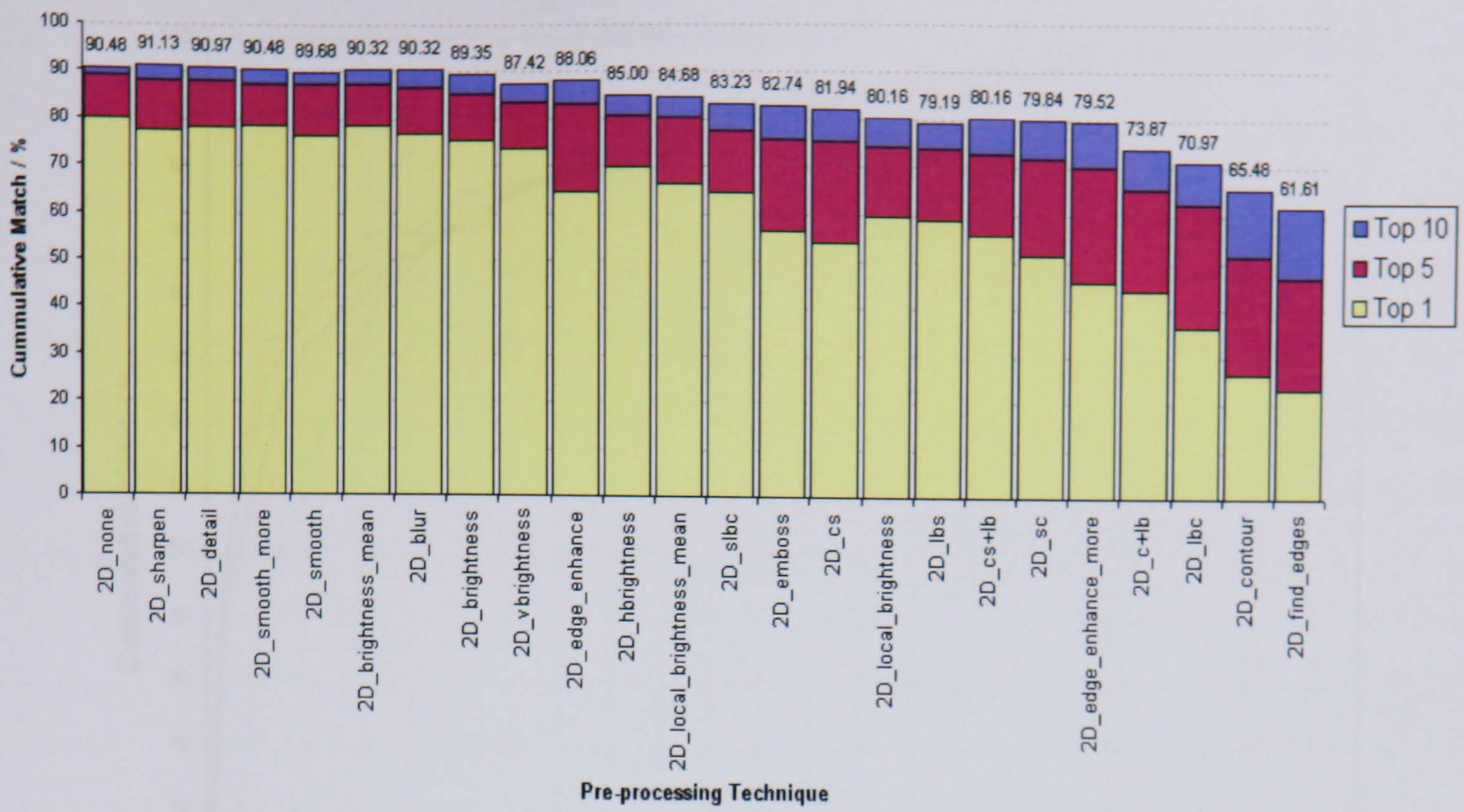

Figure 8-6 Cumulative match rates of 2D face recognition systems.

For example the brightness mean pre-processing method is more effective than the detail method at returning the correct match at rank 1, despite having a low cumulative match rate of 90.32%, when returning the correct match in the top 10.

8.3.2 Three-Dimensional Systems

Figure 8-7 shows the cumulative match curve for four 3D face recognition systems. We see only a slight improvement over the 2D face recognition systems, although we do witness that different surface representations improve the cumulative match rate significantly over the standard 3D depth map representation, with the vertical derivative (using the larger convolution kernel) providing the highest cumulative match rate of 91.45% correct matches within the top 10.

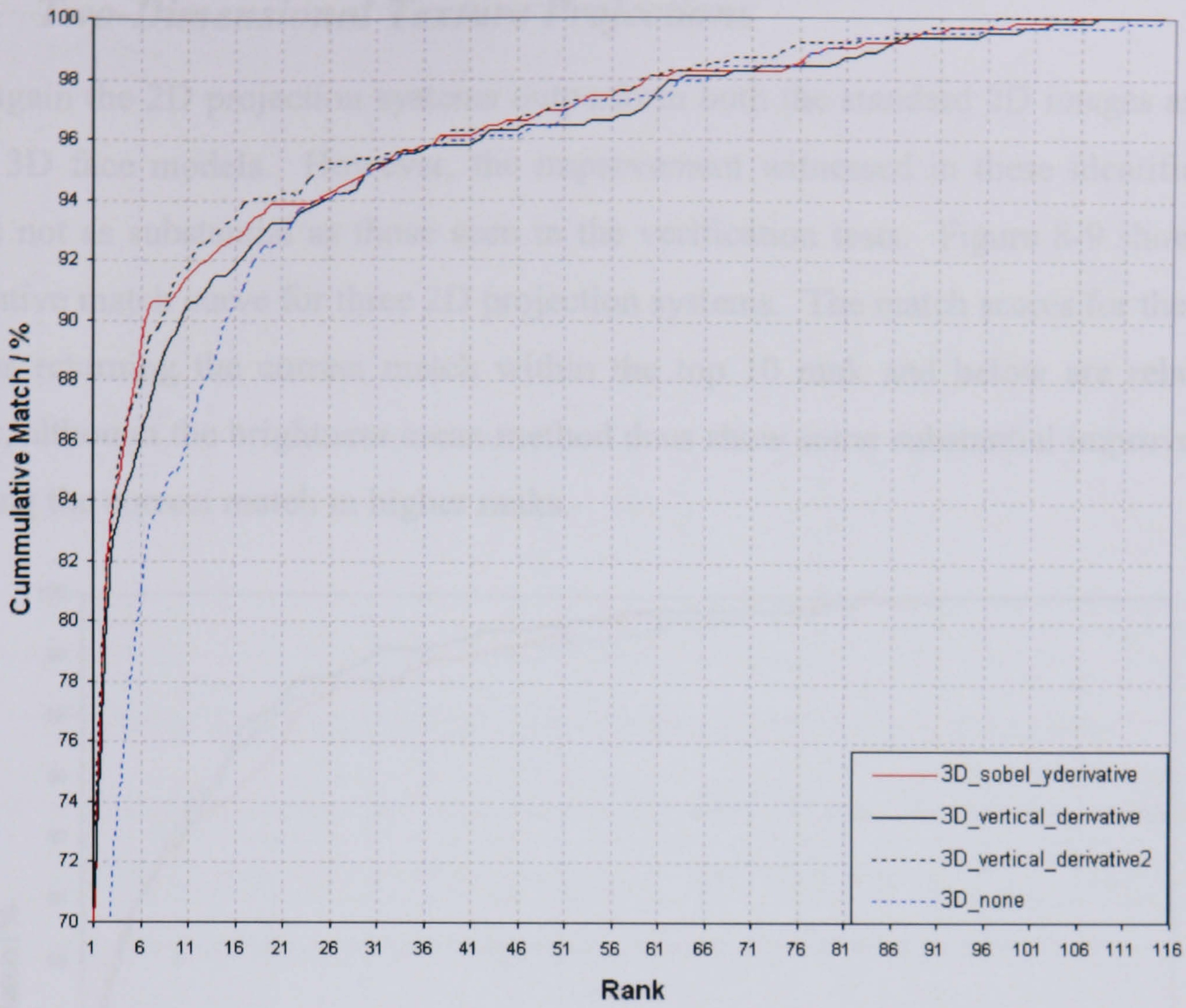

Figure 8-7 Cumulative match curves of the three most effective 3D face recognition systems.

Looking at the bar chart of match scores shown in Figure 8-8 we see a wide range of results for the various surface representations. As for verification, the most effective systems are those using the gradient representations.

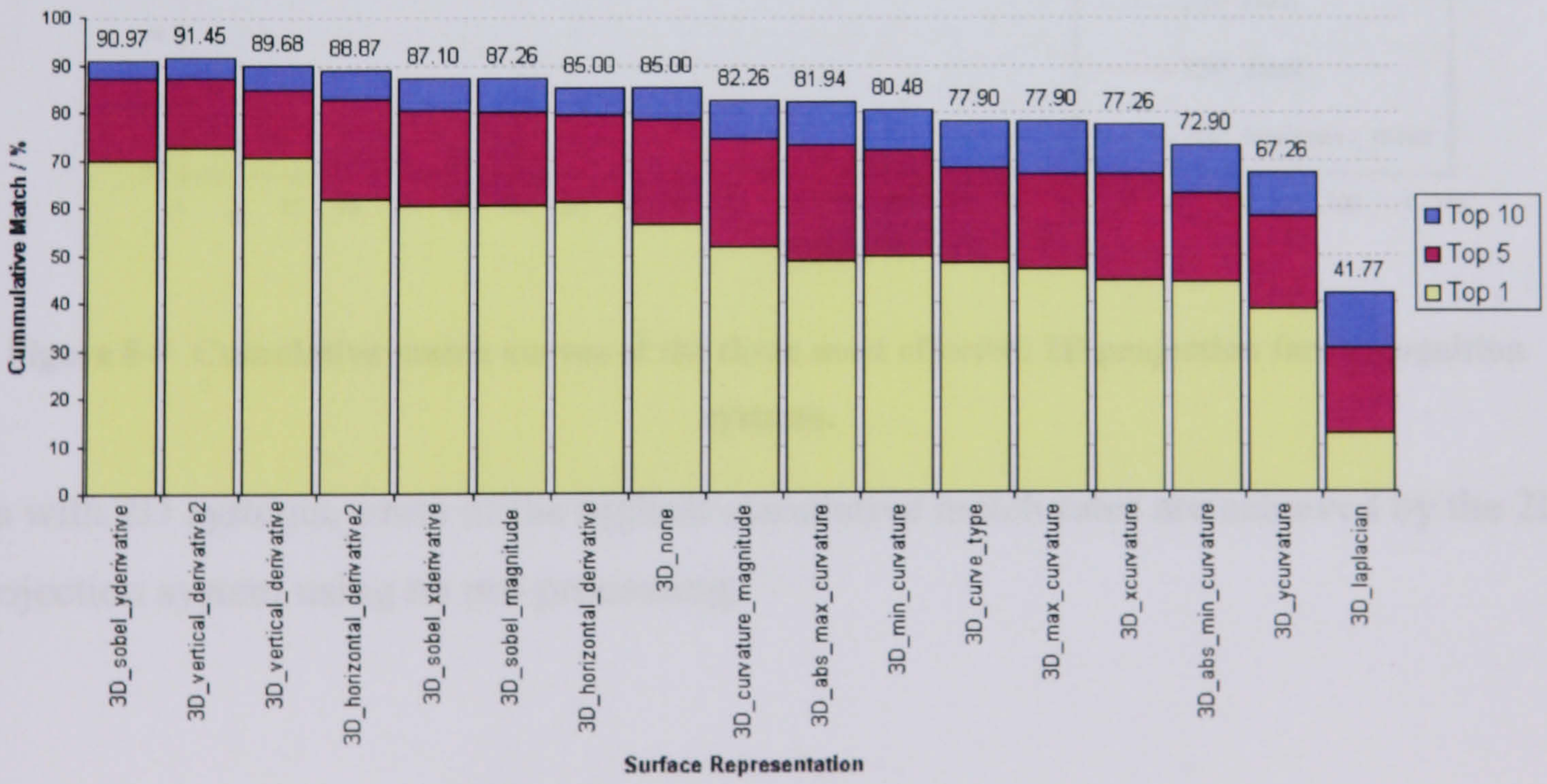

Figure 8-8 Cumulative match rates of 3D face recognition systems.

8.3.3 Two-Dimensional Texture Projections

Once again the 2D projection systems outperform both the standard 2D images as well as the 3D face models. However, the improvement witnessed in these identification tests is not as substantial as those seen in the verification tests. Figure 8-9 shows the cumulative match curve for three 2D projection systems. The match scores for the three systems returning the correct match within the top 10 rank and below are relatively similar, although the brightness mean method does show some substantial improvement returning the correct match in higher ranks.

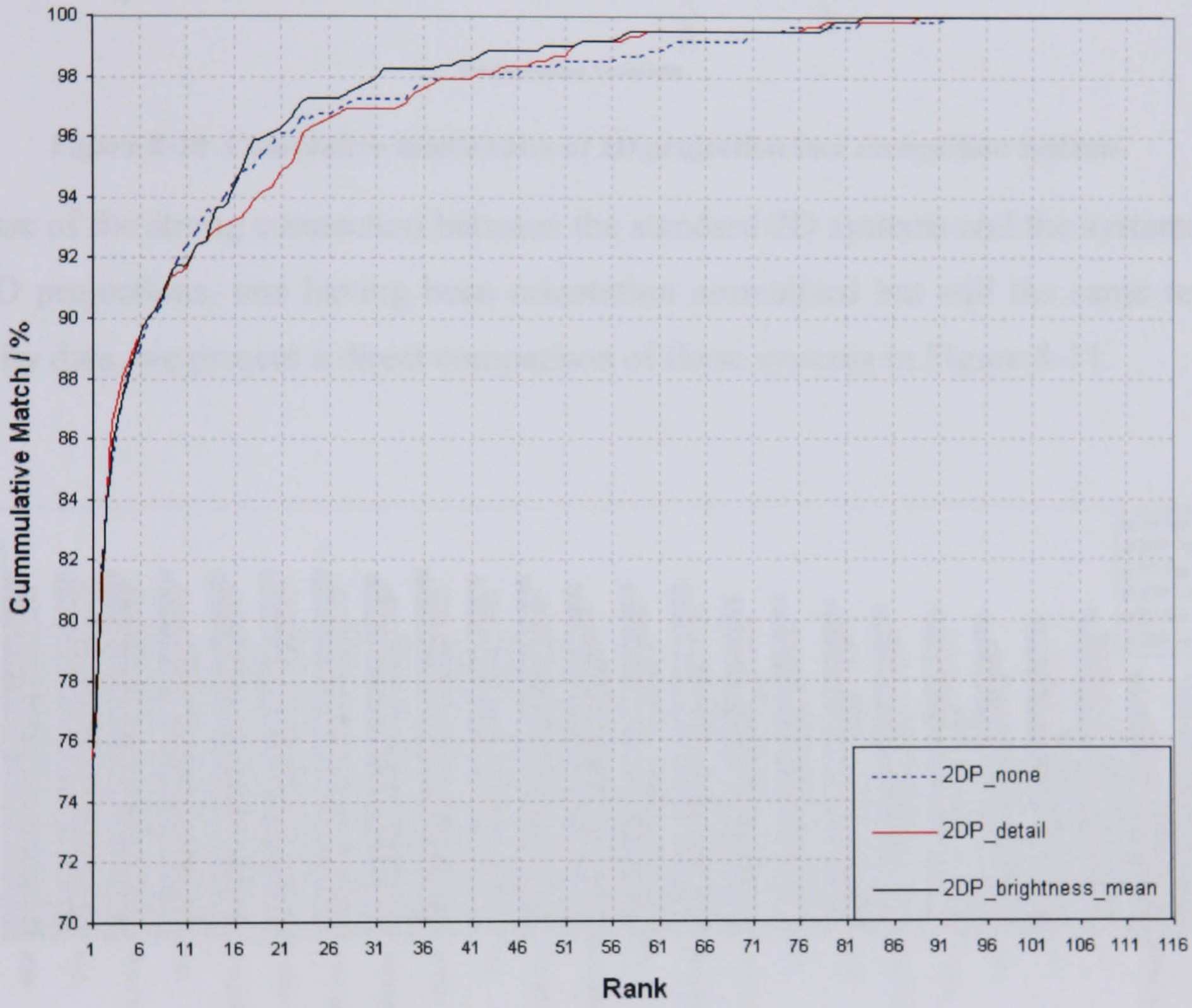

Figure 8-9 Cumulative match curves of the three most effective 2D projection face recognition systems.

As with 2D systems, some of the highest cumulative match rates are achieved by the 2D projection system using no pre-processing.

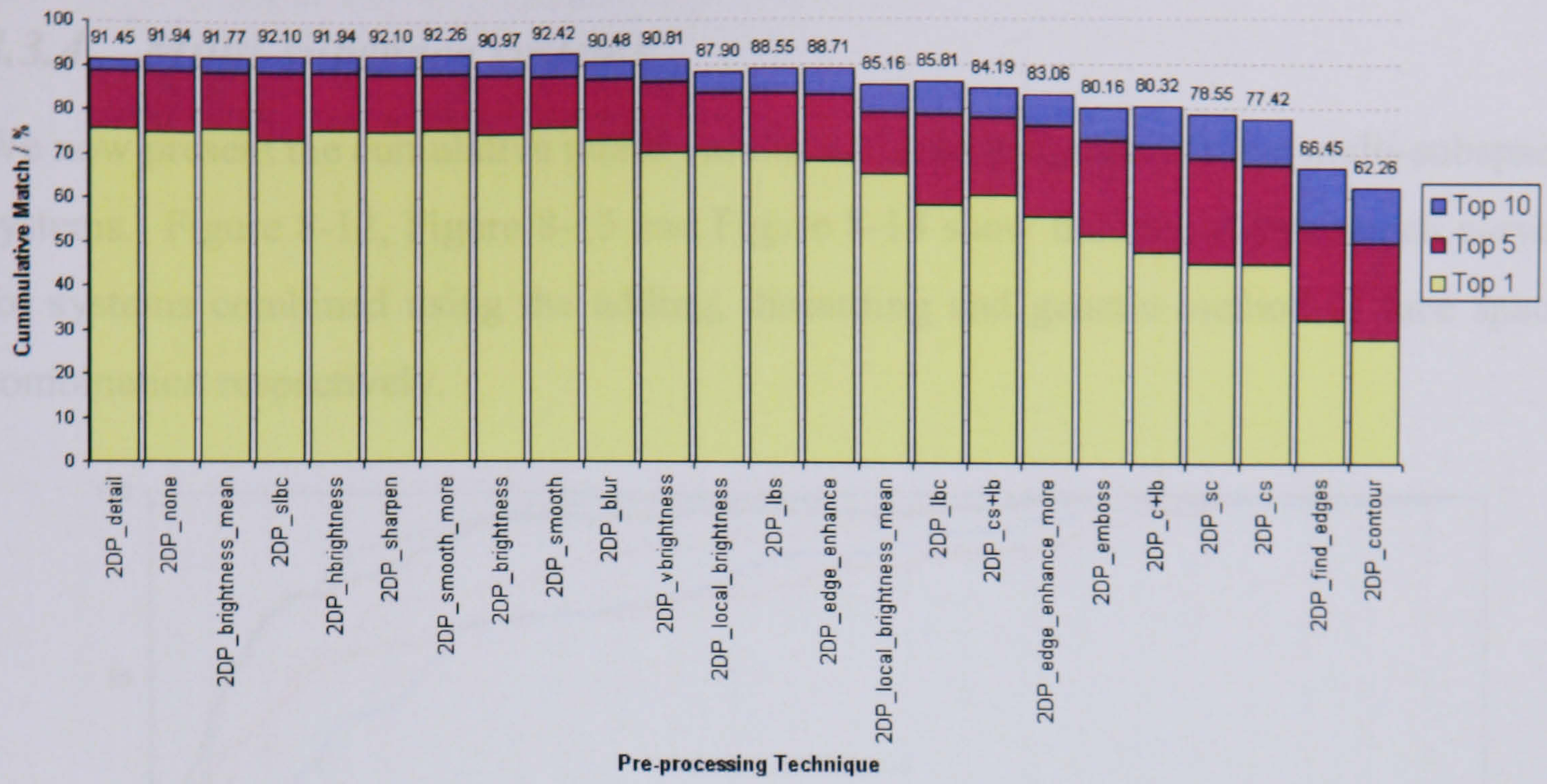

Figure 8-10 Cumulative match rates of 2D projection face recognition systems.

Because of the strong connection between the standard 2D systems and the systems that use 2D projections, one having been orientation normalised but still the same texture intensity data, we present a direct comparison of these systems in Figure 8-11.

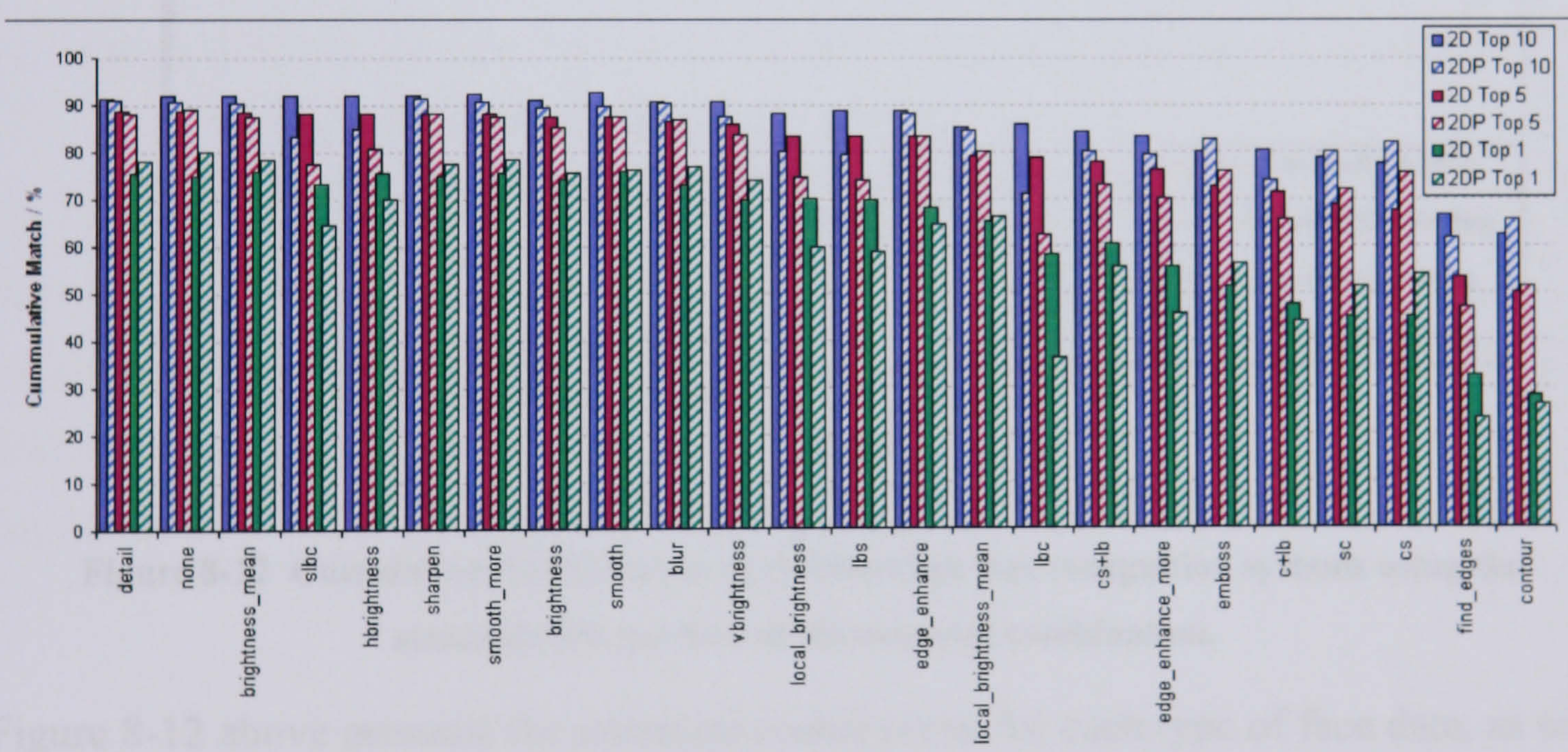

Figure 8-11 Comparison of cumulative match rates of 2D and 2D projection face recognition systems.

8.3.4 Multi-subspace systems

We now present the cumulative match results achieved using the various multi-subspace systems. Figure 8-12, Figure 8-13 and Figure 8-14 show the cumulative match curves for systems combined using the adding, discarding and genetic method of face space combination respectively.

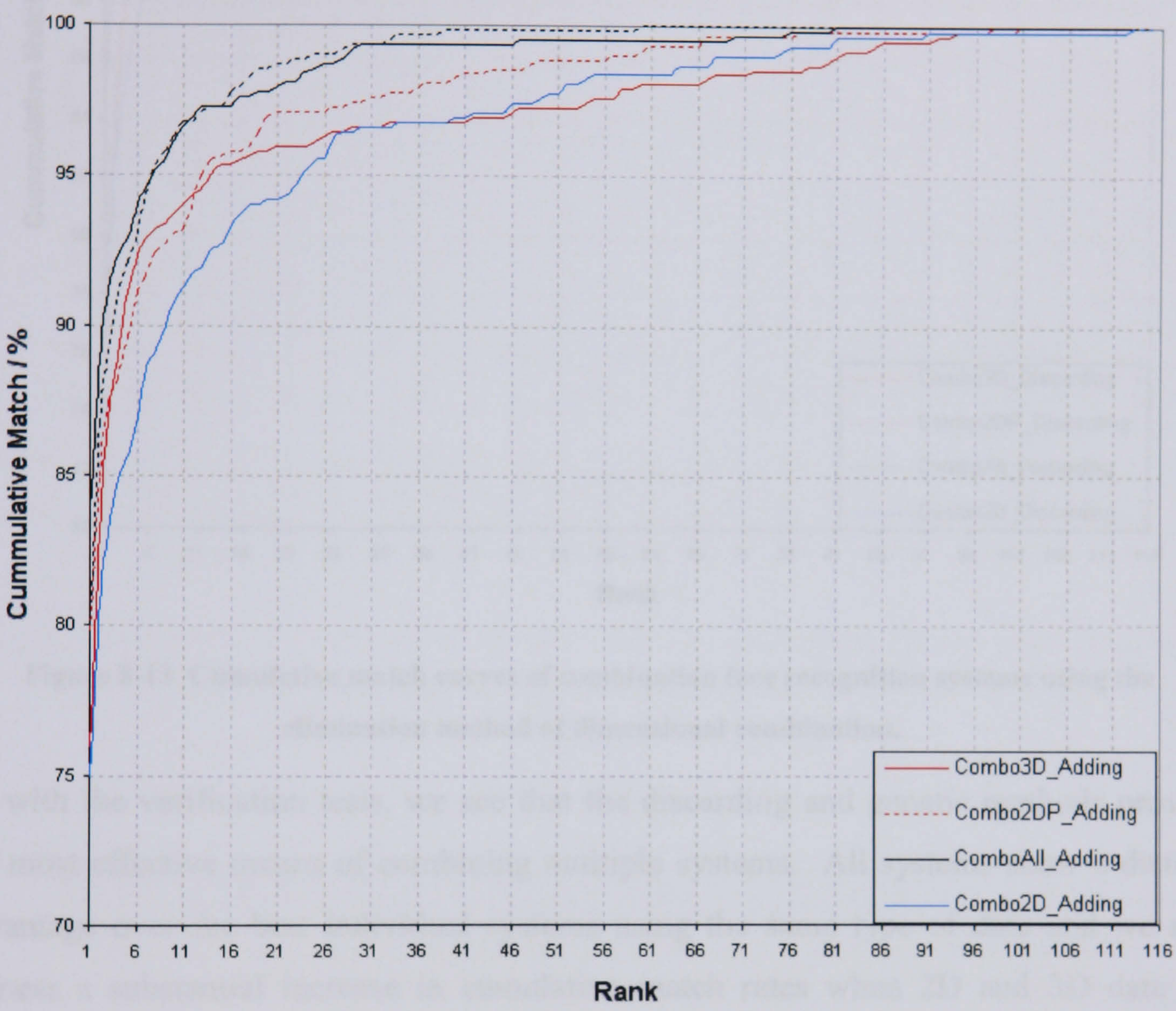

Figure 8-12 Cumulative match curves of combination face recognition systems using the accumulation method of dimensional combination.

Figure 8-12 above presents the cumulate match curve for each type of face data, as well as the full multi-subspace systems. Once again we see the greatest improvement when 3D and 2D data are combined into a single system.

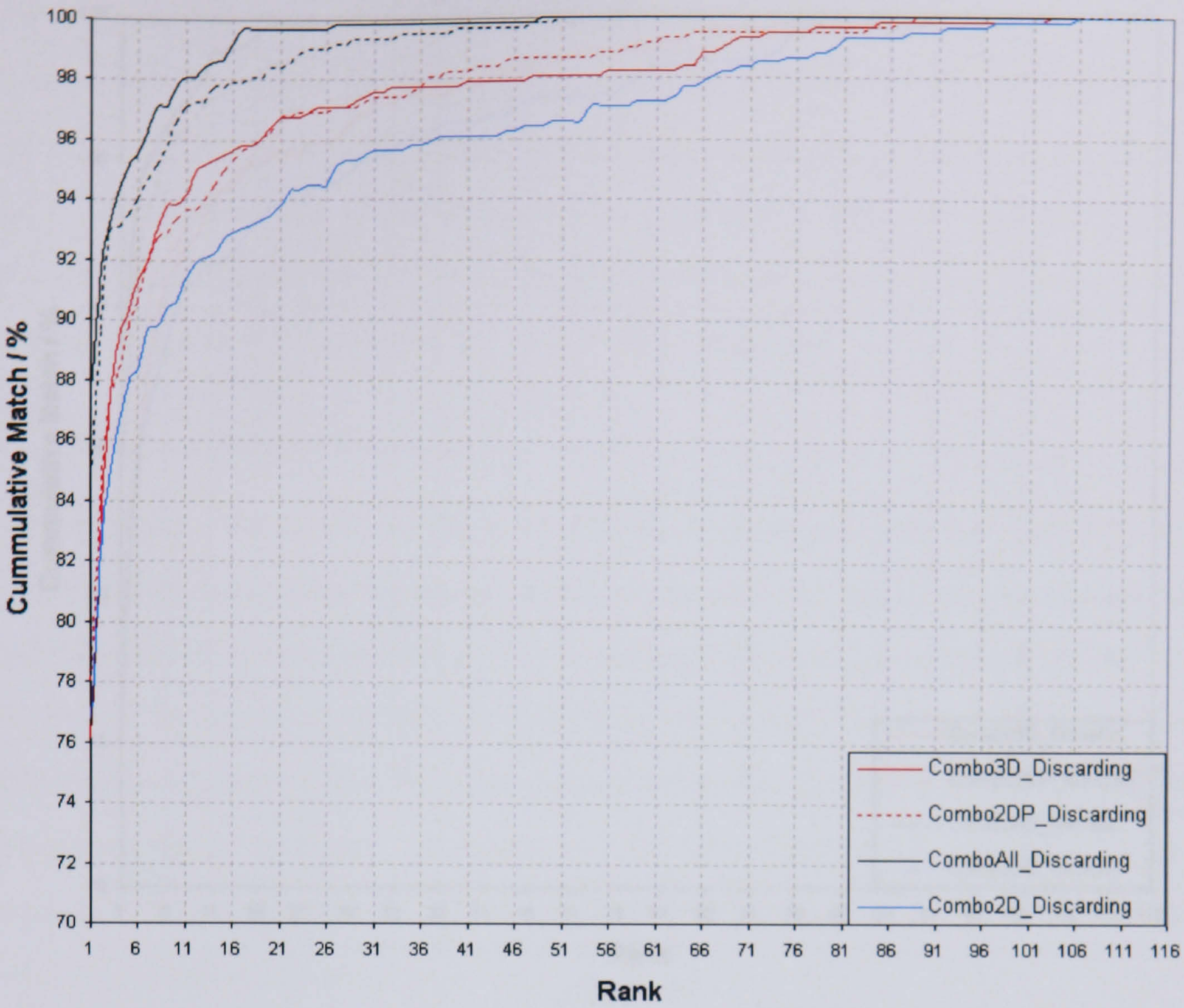

Figure 8-13 Cumulative match curves of combination face recognition systems using the elimination method of dimensional combination.

As with the verification tests, we see that the discarding and genetic methods provide the most effective means of combining multiple systems. All systems show a distinct advantage over the best individual systems using the same type of data and we also witness a substantial increase in cumulative match rates when 2D and 3D data are combined.

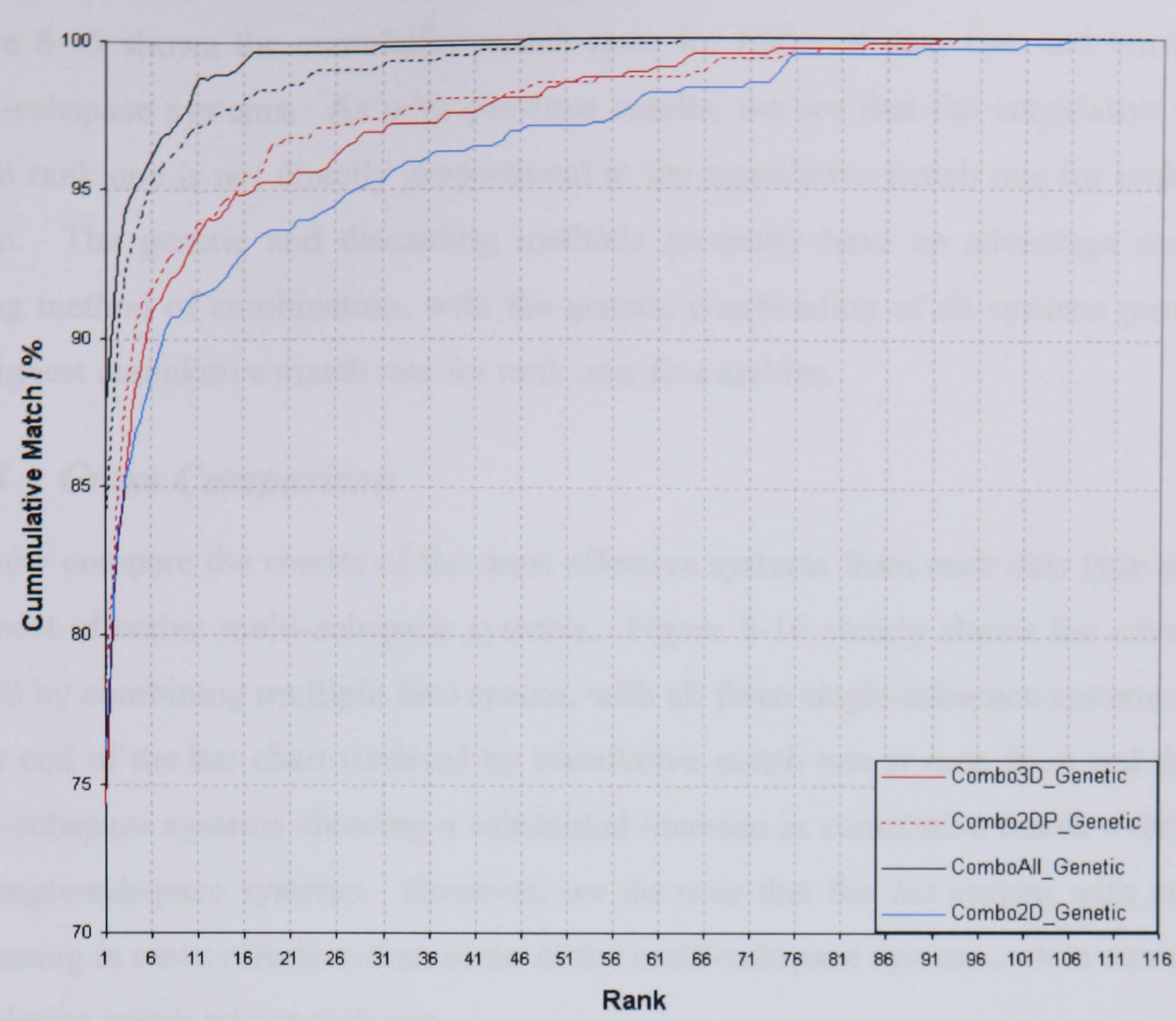

Figure 8-14 Cumulative match curves of combination face recognition systems using the genetic method of dimensional combination.

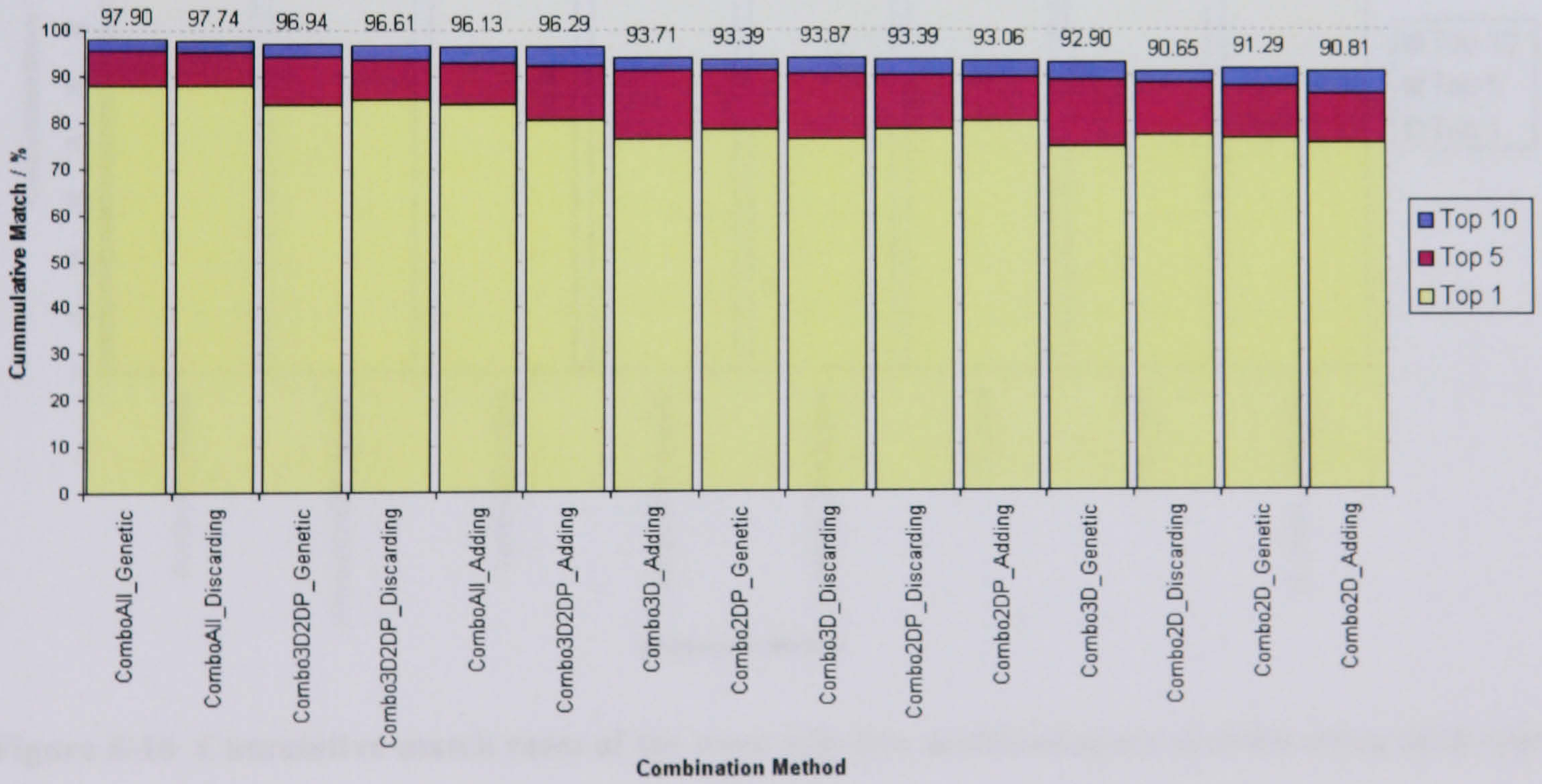

Figure 8-15 Cumulative match rates of face recognition system combinations.

Figure 8-15 shows the cumulative match rates for ranks of one, five and ten for all multi-subspace systems. As with previous results, we see that the cumulative match rate at rank one is not directly proportional to the cumulative match rate for ranks five or ten. The genetic and discarding methods generally have an advantage over the adding method of combination, with the genetic combination of all systems providing the highest cumulative match rate for rank one, five and ten.

8.3.5 Cross Comparison

We now compare the results of the most effective systems from each data type against the most effective multi-subspace systems. Figure 8-16 clearly shows the advantage gained by combining multiple face spaces, with all three single-subspace systems at the lower end of the bar chart (ordered by cumulative match rate at rank five) and the full multi-subspace systems showing a substantial increase in cumulative match over all of the single-subspace systems. However, we do note that the 2D system with no pre-processing is more effective than some of the multi-subspace systems, when comparing cumulative match rate at rank one.

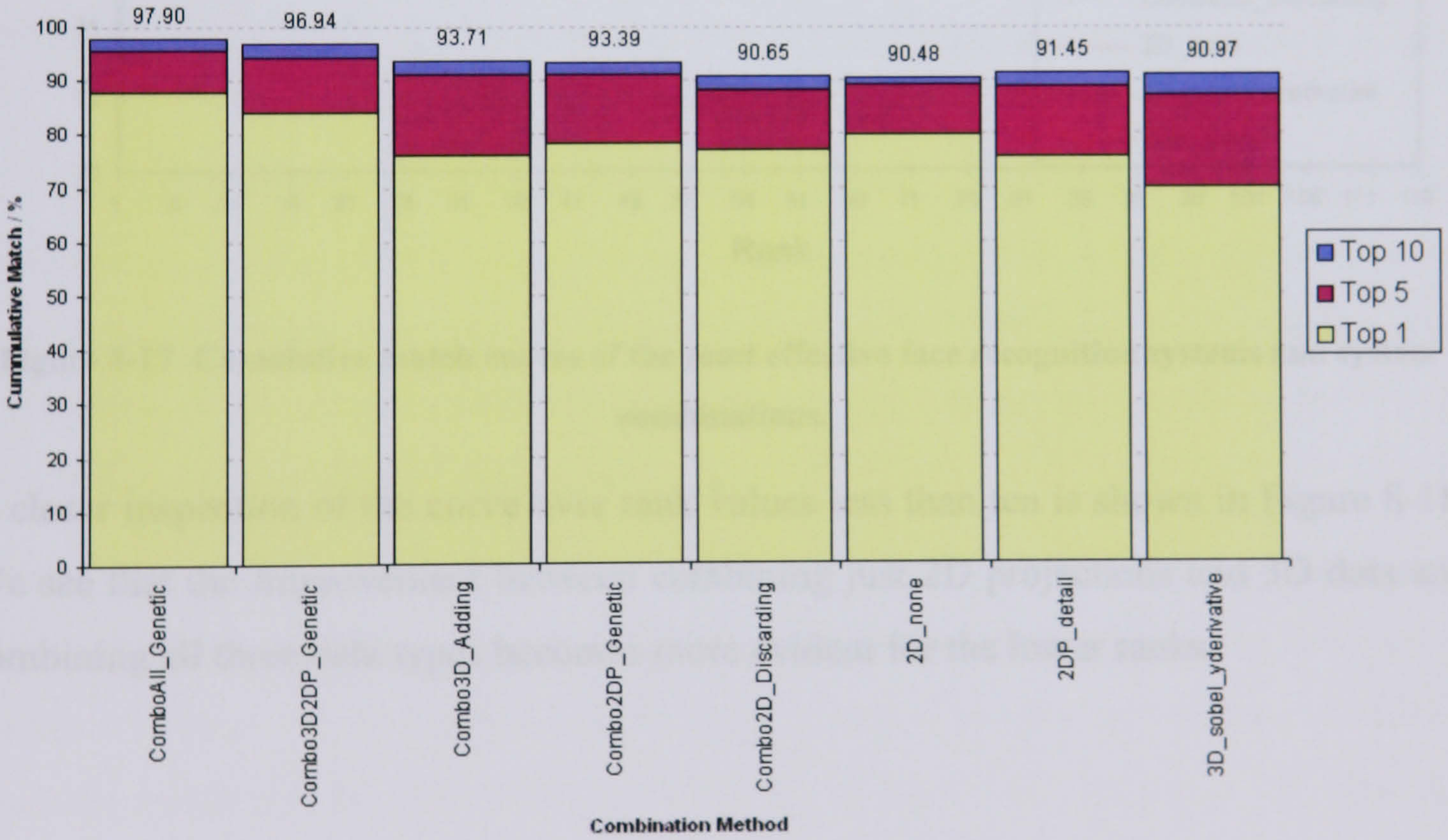

Figure 8-16 Cumulative match rates of the most effective multi-subspace systems using each type of face data.

Looking at the cumulative match curve used to generate the chart above in Figure 8-16, we see how each system performs over the full range of rank values and the distinct

improvement of the two most effective multi-subspace systems becomes more apparent, seeing that close to one hundred percent of searches will return the correct match within the top thirty.

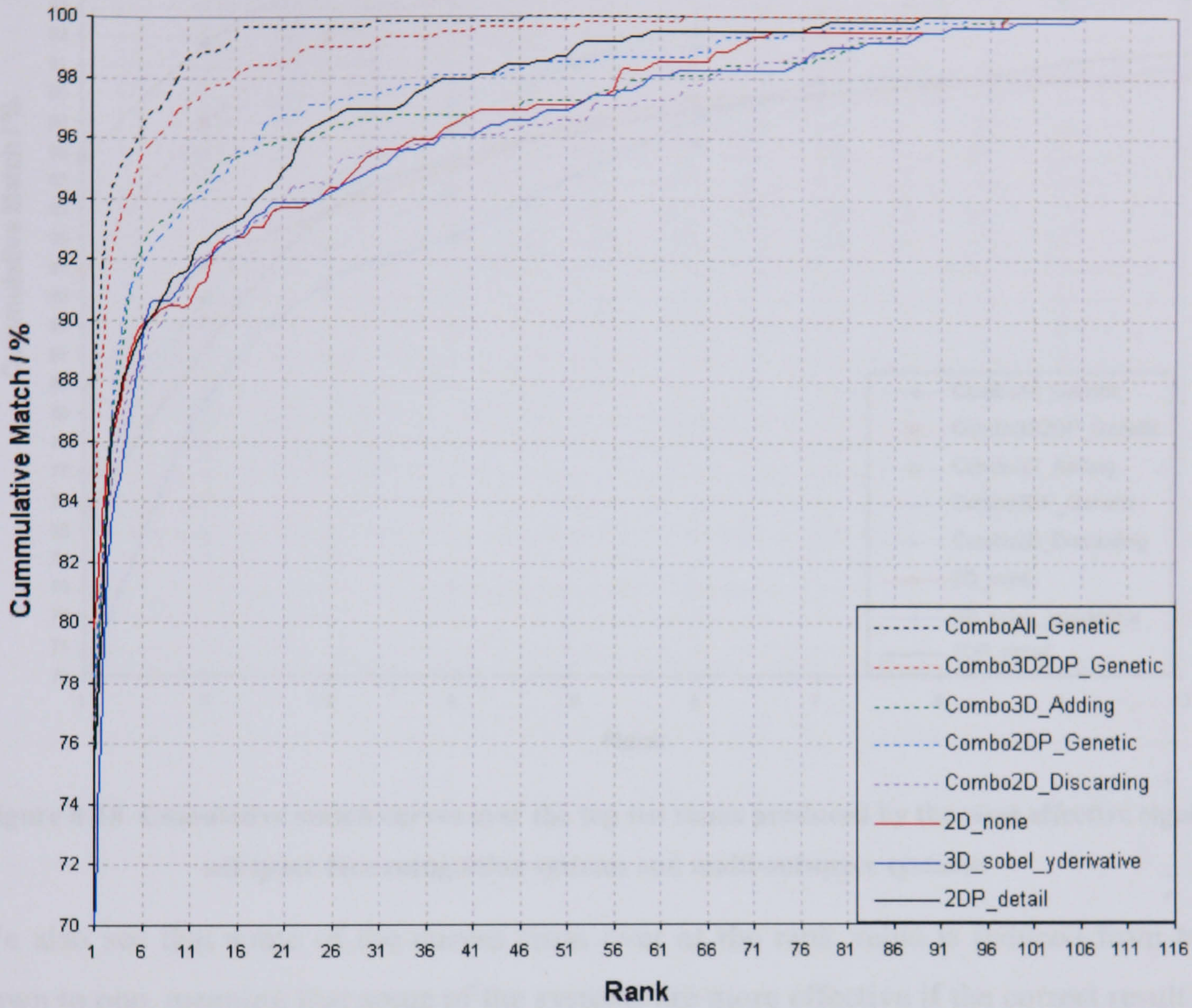

Figure 8-17 Cumulative match curves of the most effective face recognition systems and system combinations.

A closer inspection of the curve over rank values less than ten is shown in Figure 8-18. We see that the improvement between combining just 2D projections and 3D data and combining all three data types becomes more evident for the lower ranks.

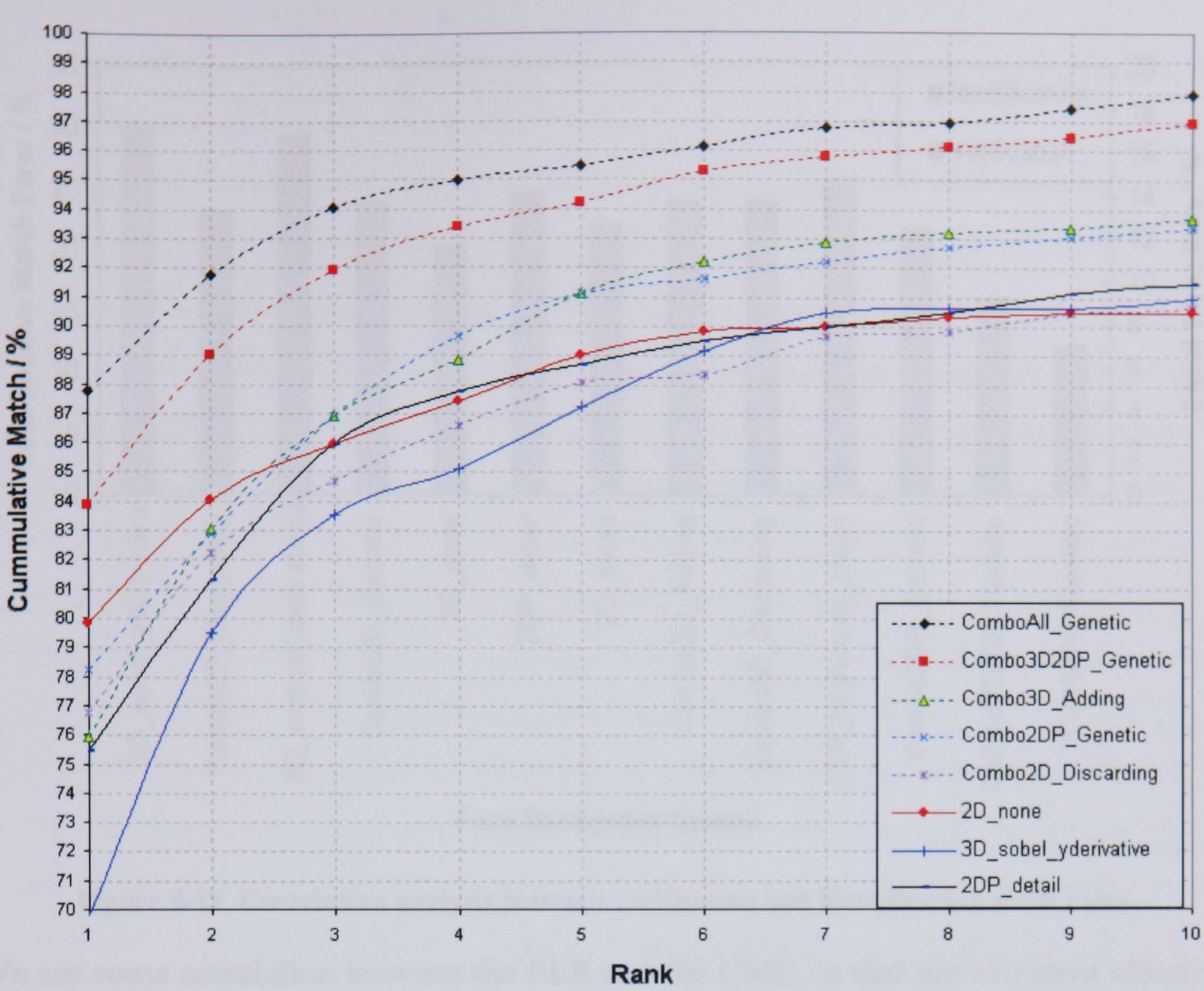

Figure 8-18 Cumulative match curves over the top ten ranks produced by the most effective signle subspace face recognition systems and multi-subspace systems.

We also see that some of the curves cross over as the rank value is reduced from ten down to one, meaning that some of the systems are more effective if the correct result is only required in some top *N* returned matches, whereas a different system may be more appropriate if we only consider the number one match returned (which would be the case if the system was fully automated).

Finally, we compare the EER produced from the verification tests against the results produced in the identification tests. To do this, we represent the cumulative match results in terms of cumulative match error, defined as the percentage of search operations that fail to return the correct match at rank one. Figure 8-19, uses two vertical scales, such that these values may be compared.

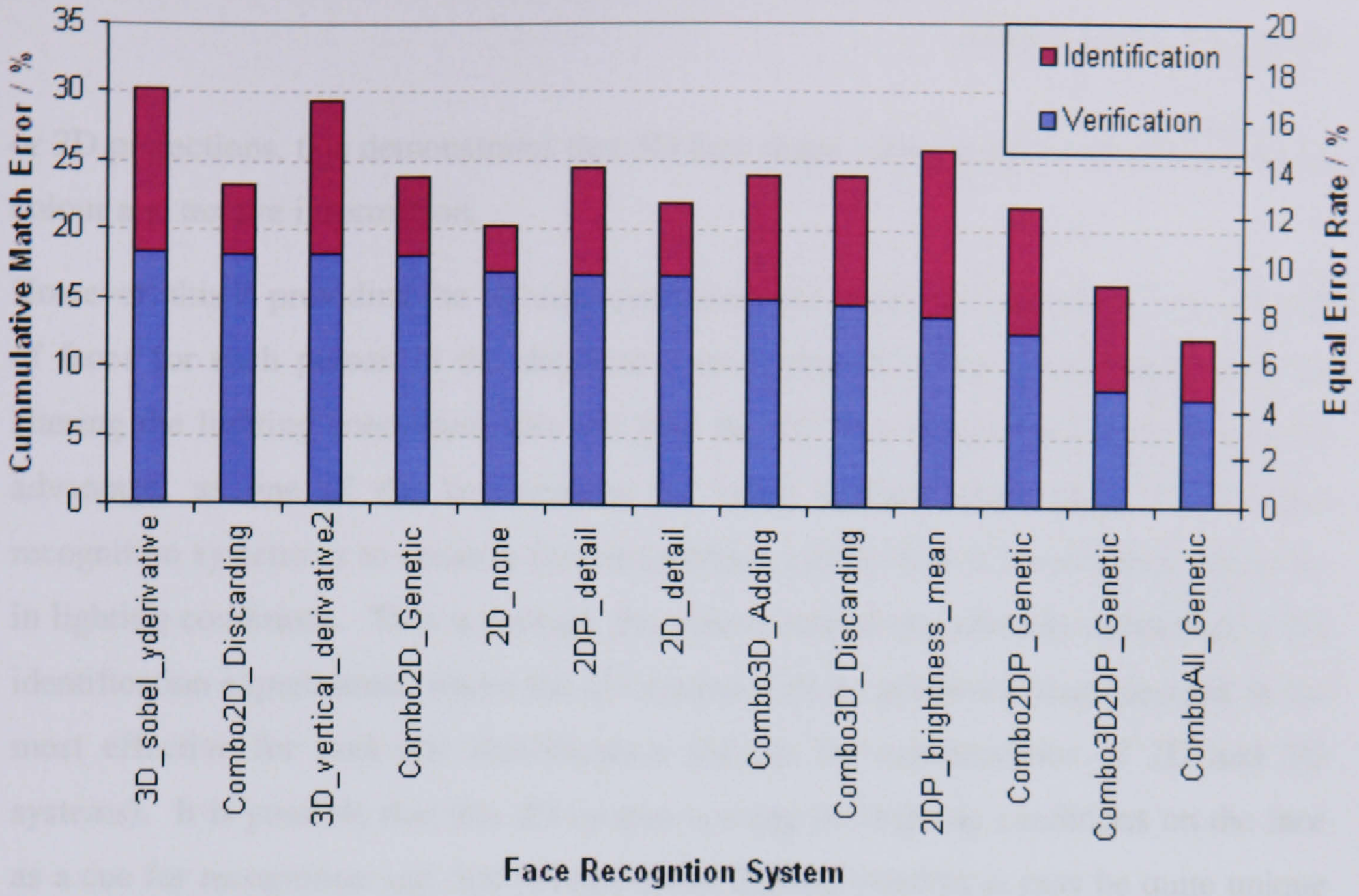

Figure 8-19 Correlation analysis between verification and identification error rates.

We see some correlation between the EER and the CME, in that the two most effective verification systems also produce the lowest CME. However, for the other systems this correlation is less apparent.

8.4 Conclusion

By providing a database of faces stored in three data types (3D, 2D and 2D Projections), in which each of the data types were acquired at the same instant in time, under exactly the same capture conditions, we have provided the means to test and compare numerous face recognition systems on an equal level. By applying 2D, 3D and 2D projection face recognition systems to this data set, we have shown that the 2D projection systems are significantly more effective that any of the 2D or 3D systems for one-to-one verification. As the 2D and 2D projection systems use the same greyscale intensity data, the improvement in recognition accuracy must be attributed to the ability to perform orientation normalisation prior to recognition and the fact that the 2D projection images are all to the same scale.

As the 3D face models are orientation normalised and all to the same scale (as with the 2D projections) and the 3D face recognition systems did not perform as well as the 2D

or 2D projections, this demonstrates that 3D face shape alone is not as discriminating as colour and texture information.

However, this is providing the lighting conditions are relatively controlled. As each set of faces for each person in the database were captured in the same session without altering the lighting conditions, this did give the 2D face recognition systems a slight advantage, as one of the key reasons for using surface shape alone in 3D face recognition systems is to create a face recognition system that is invariant to variations in lighting conditions. This is perhaps the reason behind the anomaly witnessed in the identification experiments, where the 2D system with no pre-processing emerged as the most effective for rank-one identification (except for combinations of 2D and 3D systems). It is possible that this 2D system is using the lighting conditions on the face as a cue for recognition and that because these lighting conditions may be quite unique (due to the slow progressive changes in lighting throughout the captures sessions and the height of the person meaning overhead lighting is reflected differently) they are very useful for selecting a rank-one match. Whereas in order to achieve the higher cumulative match rates for larger rank values, the system must be less reliant on the chance that the lighting has remained constant and therefore other systems take the lead, as seen when considering matches in the top ten: the 2D none system becomes the least effective.

We have shown that combining multiple systems provides substantial benefits in terms of verification and identification capabilities. In almost all cases combining multiple systems provides a reduction in EER and CME, when compared to all individual systems using the same type of data. A much greater improvement is then provided when we bridge the gap between 2D and 3D data, by combining systems across these data types. Combining 2D projection systems with 3D systems reduced the EER to 4.84% and improves the CMR-10 to 96.94%. The further improvement introduced when standard 2D systems are included in the combination could be due to an increased robustness to small inaccuracies in orientation normalisation (2D images are aligned by the eyes rather than the nose tip), by effectively providing an alternative method of alignment. Secondly, the orientations at which different people naturally position their head may also be used as a cue for recognition. It may also be that variations in lighting from one data collection location to another (represented in 2D images by small areas of

background in the corners of the image) could aid recognition, as no subject was present in more than one capture location.

9 Final Conclusions and Future Work

We now bring a close to this thesis by summarising the discoveries and achievements made throughout our research. In chapter 1 we outlined a number of goals that we hoped to achieve and we now begin this chapter by considering our progress towards each of these goals in relation to the relevant sections of this thesis. We then discuss each of the technologies explored, again referring to individual chapters, summarising the progress made. Finally, we draw overall conclusions from the results obtained and predict their impact on the research field, before suggesting the most promising avenues of future research.

9.1 Progress Achieved

Give an overview of existing face recognition systems and the current state of research in this field.

In section 3 we reviewed the current literature regarding face recognition technology and identified a number of promising methods worthy of further investigation. In particular we focused on PCA and LDA approaches, such as the Eigenface and Fisherface methods as discussed in sections 4.3 and 4.4 respectively. We carried out experiments similar to those of other researches, reconfirming results on a standard dataset and began to explore some ways of improving these systems.

Identify the problems associated with existing face recognition systems and possible avenues of research that may help to address these issues.

Among the available literature it was clear that several issues had become well known as primary hindrances to face recognition systems, namely variations in lighting conditions, facial expressions and head orientation. Although there are several other problems that will eventually need to be addressed, such as facial occlusion, disguises (beards, glasses, headwear) and aging, these are generally considered secondary (perhaps because they are more difficult). Obviously, it is accepted that a face cannot be recognised if it cannot be seen, but an ideal surveillance application should be able to cope with these secondary problems. However, a great deal of improvement was

needed in terms of coping with lighting, facial expression and head orientation before these more difficult problems could be addressed.

Improve the effectiveness of existing face recognition algorithms, by introduction of additional processing steps or adaptation of the method.

In order to improve a systems ability to cope with variations in lighting we explored the area of image pre-processing in section 4.5, in an attempt to normalise lighting conditions while maximising between-class variation. We identified a number of pre-processing methods that reduced error rates for the eigenface system, presented in section 4.6. We then addressed the problem of expression by further developing the statistical analysis used in producing the model for discrimination. Approaches such as the Fisherface method allowed for multiple representations of the same face in order to capture such within-class variation, which we explored in detail in section 4.4, again showing how image pre-processing can reduce error rates.

Design and implement novel face recognition approaches, taking advantage of the newly emerging 3D-capture technology.

In order to address the problem of head orientation, we began an investigation into the use of 3D capture technology to aid face recognition in section 5. Using 3D face models we were able to normalise facial orientation using the techniques described in section 5.2. to perform recognition on face depth maps as explained in section 5.3.1. We continued this research direction using the experience gained in 2D face recognition investigations: we applied various pre-processing methods to produce numerous 3D surface representations, again producing a reduction in error rates. The resultant system was able to perform face recognition to a high level of accuracy, with much improved robustness to head orientation, as presented in section 5.3.

The 3D face database also allowed for projection of the 2D texture from an orientation normalised 3D model. This facilitated creation of a third novel type of face recognition system, using 2D techniques applied to an orientation normalised 2D image, created using some of the advantages offered in 3D systems, as shown in section 6.1. In an attempt to utilise multiple approaches to improve error rates, we developed new methods of combining systems (section 7), taking advantages of 3D and 2D data and a range of pre-processing methods in a single system.

Finally, returning to the first principles of 3D face recognition to develop a new recognition algorithm aside from the subspace PCA and LDA approaches used in previous chapters, we developed the novel IRAD contours methods of face recognition (see section 5.7).

Analyse and evaluate a range of face recognition systems applied to both two-dimensional and three-dimensional data.

Because 3D face recognition was relatively unexplored we collected a large database of 3D face models to train and test 3D face recognition systems. This database will provide a great resource for research into the areas of 3D and 2D face recognition. As the database includes 2D images, captured alongside the 3D face models it allows a direct comparison of the two types of face data. We carried out investigations using the same PCA and LDA approaches applied to 3D face data and the corresponding 2D face data and presented the results in section 8.

Determine the most effective method of combining the range of face recognition techniques, in order to achieve a more effective face recognition system.

It became clear in section 7.2 that although combining multiple face recognition systems could reduce error rates, the degree of this improvement was dependent on the method of criteria used for combination. In section 7.3 we developed and tested three methods of combination. The results presented demonstrated that the most effective method of the three was to use a genetic algorithm to optimise the combination. However, in section 7.5 we were able to demonstrate that even this improvement could be surpassed by some human intuition and that a more effective genetic algorithm would likely be discovered with some additional investigation.

Evaluate this final face recognition system and present results in a standard format.

In chapter 8 we defined standard training and test sets from the 3D face database, in which each image was represented by a 3D face model, 2D image and 2D texture projection. We then selected numerous face recognition systems and compared the performance on this triple modal database. The results are presented in such formats as to be easily compared to the majority of face recognition publications.

Identify limitations of the final face recognition system and propose a line of further research to combat these limitations.

In section 9 we describe some of the difficulties still faced by face recognition systems. We suggest points at which our own research may be extended to explore these problems and what other technologies are required in order to increase the capabilities of face recognition systems.

9.2 2D Face Recognition

We began by exploring the eigenface method of face recognition, implementing a standard system using no image pre-processing to produce an EER of 34.0%. Further investigation showed that some pre-processing techniques could greatly reduce error rates and without any alterations to the eigenface technique itself, an EER of 22.4% percent can be achieved (a reduction of 11.6%). We published these findings in the conference proceedings of the International Conference on Image and Graphics. Although the test set used in these experiments contained a majority of extremely difficult images (20% of the images are partially obscured and 40% of the images have extreme lighting conditions), an error rate in which one in five verifications produces an incorrect decision is not suitable for most potential face recognition applications. However, this investigation did prove that selecting a suitable image pre-processing technique is vital to the performance of a face recognition system.

Continuing research focused on appearance based approaches leading towards the Fisherface method, which is widely reported to produce superior recognition accuracy than the eigenface method when multiple examples of the same subject are available for training. However, our initial experiments did not comply with these findings. Further investigation showed that by altering the training and test sets such that they both represented the same capture conditions produced significantly better results. Therefore, if the Fisherface method is to be used in a real world scenario, it is vital that the training set is an adequate representation of the expected application data. Providing such a training set is available, the Fisherface method has significantly lower error rates (20.1%) than both the eigenface (25.5%) and direct correlation methods (25.1%) applied to the same test set. Hypothesising that the Fisherface method would be as dependent on the image pre-processing techniques as the eigenface method, we tested the same

processing techniques as in previous experiments, reducing the EER to 17.8%. We compared the Fisherface and eigenface methods in detail in section 4.6 (also published in 'Face Recognition: A Comparison of Appearance-Based Approached' [15] and presented at the International Conference on Digital Image Computing: Techniques and Applications. These investigations supported the consensus that Fisherface systems typically produce lower error rates than eigenface. Although an additional key finding was that lighting correction techniques (colour normalisation etc.) have less affect than application of LDA to model such variations.

9.3 3D Face Recognition

Because of the success of PCA and LDA appearance-based approaches to two-dimensional face recognition, we adapted these methods for application to 3D face data. This required implementation of an orientation normalisation routine, to localise the nose of the 3D face model and orientate the facial surface to a fronto-parallel orientation, before producing a depth map of the 3D face model. Applying PCA to these depth maps we introduced the eigensurface method of face recognition, which was capable of recognising faces with substantially lower error rates (12.7% EER) than the best two-dimensional systems (20.4% EER and 17.8% EER). These promising results (published in [16]) demonstrated that geometric face structure is useful for recognition when used independently from colour and texture and capable of achieving high levels of accuracy, suggesting that 3D face recognition has distinct advantages over conventional two-dimensional approaches.

To follow on the success of applying PCA to facial surface representations we continued along the same course of research as applied to two-dimensional systems by examining the application of LDA to 3D surface representations. The EER produced using the best surface representations was 11.3% EER, again demonstrating the superior performance of LDA when compared with PCA approaches, as well as reinforcing earlier findings that 3D face recognition could produce better results than corresponding two-dimensional Fisherface systems (17.8% EER). The experiments carried out to produce these results are documented in detail in section 5 (also published in [17]). Given that the 3D capture method produces face models invariant to lighting conditions

and provides the ability to recognise faces regardless of pose, this system is particularly suited for use in security and surveillance applications.

Rather than focus purely on subspace-based approaches to 3D face recognition we also developed a novel method capable of recognising faces based on cues extracted from both the colour and geometric shape data available in 3D face models. One of the key advantages of our IRAD contours method is that it uses relatively little registration in terms of feature detection and image alignment. Once this single feature localisation operation has been performed all variances due to head orientation are reduced to a one-dimensional shift in a simple cross-correlation process. Using this technique we were able to show that a single contour around the tip of the nose contained enough discriminatory information to perform recognition with an EER of just 21.91%. Although we were restricted by time limitations to explore this method in great detail, we were able to apply a simple weighted sum across signal ensemble correlation scores, reducing the EER to 20.02%, although much greater reductions are expected if colour and texture information were included and additional constraints applied.

Finally, we investigated a method that perhaps lies at a midpoint between two-dimensional and 3D face recognition. By using a texture mapped 3D face model we produced system that was able to orientate the face to a fronto-parallel orientation before projecting the texture back into the 2D image plane. This 2D image could then be used for recognition as with standard two-dimensional face recognition methods. We have demonstrated that such 2D projection systems have significant advantages over standard 2D systems: in almost all cases the error rates are significantly lower than the equivalent system without 3D orientation. This emphasises the importance of orientation normalisation for recognition and that the use of absolute size (2D projections are real-size) as a feature for recognition can provide additional discriminatory information.

However, an additional side-effect of 2D projection systems, which may also have improved results, is that surface noise in terms of depth precision errors are effectively compressed onto a 2D plane. Because no virtual lighting or surface shading effects are used, any error in surface depth is not visible in the 2D image projection. Perhaps with a better method of dealing with surface noise in 3D methods we would see substantial improvements.

9.4 Multiple Subspace Combinations

By applying FLD as an analysis tool to individual face space dimensions we were able to confirm that although an image subspace may not perform well when used for recognition, it may still contain discriminatory components that could complement other face space systems. Hence we uncovered the potential to improve recognition error rates by combining multiple dimensions from a range of face recognition systems. Combining multiple systems in this way has been shown to be highly beneficial when used with the best single-subspace eigenface system, reducing the EER from 19.7% to 15.4%. Although when the same method was applied to the Fisherface systems, little influence was witnessed. These initially confusing results lead to further investigation into the methods of combination and weighting schemes applied. By using the EER as combination criteria, we were able to demonstrate that a Fisherface system could also be improved in the same way, reducing the EER from 17.8% using the best processing technique down to 12.8% for the multi-subspace. We submitted the findings from this investigation to BMVC 2004, which were later published in the conference proceedings [21].

Naturally, this method of system combination could also be extended to the appearance-based 3D systems, which we tested using a variety of distance metrics, to discover that the cosine distance metric was the most suitable for dimensional combination. Out of the seventeen surface spaces (with forty-nine dimensions in each one) sixteen subspaces were shown to provide at least one useful dimension, totalling 184 dimensions in the final composite surface space. This combination process was able to reduce the EER from 11.5% to 9.3% EER, which is explained in more detail in section 7.2.

The final application of combining multiple subspaces was to combine 3D and 2D systems in order to create a face recognition method that utilises both 3D geometric shape and 2D texture information together with the ability to perform orientation normalisation. This combination managed to reduce the EER to 4.84%. These error rates are state-of-the-art, particularly when considering that this is applied to test sets with variations in head orientation and the increased robustness to lighting variation due to the use of geometric shape data. However, it is likely that further reductions are still possible using a similar method of dimensional combination. This prediction is extrapolated from the realisation that the combination of two-dimensional systems is not

optimal. Even though the combination contains various dimensions from all twenty-four 2D systems (producing 10.33% EER), a simple intuitive selection of all dimensions from just four systems produces a lower EER of 9.26%. This suggests that an improved combination process could be derived from the principles used in the intuitive selection (four of the best systems using very different pre-processing techniques). Because this improved combination, utilising only four face spaces performs so well, it raises the question as to whether these four image types could be combined prior to LDA. This would not be possible using all pre-processing techniques as the high time space complexity makes the process intractable, but it may produce a more efficient subspace for recognition than combining the dimensions after training.

Surprisingly, this is not the case. We see that pre-training combination produces a higher EER of 9.66% than those produced by combining the four systems after training. We hypothesise that the reason for the improved results of the post-training combination is due to the use of two disjoint training sets: one to compute the projection matrices and the second as a double check before combining only the most discriminatory dimensions. Perhaps by concatenating four images before applying LDA we supplied so much information that the system effectively over-trains on the single training set, but forcing four separate systems to rely on less information and then combining on a separate secondary training set reduces any over-training that may have occurred in the preliminary LDA.

9.5 Comparative Evaluation

The penultimate chapter of our thesis provided a final evaluation across three data types (3D, 2D and 2D Projections), in which each of the data types were acquired at the same instant in time, providing the means to test and compare numerous face recognition systems on an equal level. This was done to recompense the inability to directly compare some of the results from the various experiments throughout our research. We included an additional measure of system effectiveness in the form of a cumulative match curve, in order to demonstrate a systems ability to perform at the task of identification when searching through a database of known faces.

The ability to directly compare the results from numerous systems has allowed for some interesting conclusions. We see that the 2D projection systems are significantly more

effective than any of the 2D or 3D systems for one-to-one verification. Because these two types of system are actually using the same greyscale intensity data, the improvement in recognition accuracy can only be attributed to the orientation normalisation procedure and the consistent scale of 2D projections. Conversely, because the 3D systems are also privy to these same advantages, but do not perform as well as the 2D projections this demonstrates that 3D face shape alone is not as discriminating as colour and texture information (providing the lighting conditions remain constant).

The final evaluation also reconfirmed that combining multiple systems provides substantial benefits for both verification and identification operations. The multi-subspace using 2D, 3D and 2D projection data achieved a CMR of 96.94% correct matches returned in the top ten.

9.6 Future Research

The most effective face recognition system produced from our research has been the multiple subspace combinations that combine Fisherface and Fishersurface systems using 3D face models, 2D images and 2D texture projections into a single composite subspace. Although we explored three methods of combination and identified the genetic algorithm method as marginally the most effective, there is still a great deal of development that may be done in this area. One brief experiment has already demonstrated that an intuitive selection of just four subspaces can produce lower error rates than the best combination produced by the GA, when applied to two-dimensional systems. This suggests that altering the evolution functions used in the GA may produce more effective combinations.

We would suggest that a coarse to fine evolution cycle might be more effective. Such a system would begin by combining entire subspaces, rather than individual dimensions; a single mutation would accumulate or discard all dimensions from an entire subspace and crossover would select random subspaces as a whole from each parent. As the fitness of the population reaches a plateau the mutation and crossover functions would begin operating on a finer level, selecting smaller and smaller fractions of the subspaces until individual dimensions were being selected or discarded.

Another area in which this combination approach may be expanded would be to create subspace systems using partial sections of the original face image (or 3D surface). Pentland et al [40] found that this approach was beneficial in their paper on modular eigenface approaches, although they were not using the same criteria based dimensional combination approach as described here. We have witnessed the same phenomena (although from a different perspective) when we discovered that concatenating four images before applying LDA, produced higher error rates than performing LDA on each individual image and then combining the dimensions after the training phase. The same may apply to an image of a single face: perhaps splitting the image into two parts and then combining the resultant subspaces of each after LDA will produce a more effective system. This approach could be performed on a large scale using the GA combination algorithm. For example, supposing we applied all the same image pre-processing techniques and 3D surface representations to images of the nose area alone (having cropped out the cheeks, forehead and chin) producing a variety of nose-recognition systems. These subspaces could then be included in the combination genome, doubling the number of subspaces available and providing much larger scope for improvement. We believe that such an approach could prove to be highly effective for the following reasons:

- Different image pre-processing techniques and surface representations are likely to be particularly well suited to specific areas of the face (edge detectors around the eyes, colour normalisation for the cheeks, gradient representations for the nose for example).
- By reducing the size of the image to focus on a smaller area of the face but maintaining the size of the training set, we improve the ratio between true discriminatory information and noise.
- By using multiple subspaces concentrated on partial regions of the face we increase robustness against partial occlusion of one area, such as glasses, hats or beards.

Another exciting area that we have not explored in this thesis is the possibility of using multiple face recognition systems in series. This is a different approach to combining multiple systems to make a single definitive decision, but rather to make an initial

screening step, before making the final accept/reject decision. Such an approach would allow each face recognition system to concentrate on one aspect of the decision problem. For instance, the primary face recognition system may be used to remove any certain rejections, before the secondary system makes the final acceptance decision. The threshold of the primary system would be configured such that the false rejection rate was near zero and then used to prune the training set for the secondary system, leaving only comparisons that looked similar. Using this two stage technique the resultant secondary system would be specifically designed to determine the likeness of two similar faces, knowing that it would never have to compare any drastically different faces the subspace could be a more effective representation of the between class differences.

One of the most interesting findings of our research was that the 2D projection systems were the most effective means of recognising faces. However, the test set on which these results were based did not contain any controlled variations in lighting conditions. Therefore, lighting typically remained constant for each person and might also have contributed as cues for recognition. One of the key advantages of using 3D face models is that basing the recognition on shape rather than colour and texture means that the system becomes invariant to lighting conditions (providing the 3D camera is still capable of constructing a 3D model), but this advantage is lost when reverting back to texture data of 2D projections. One method of combating this problem would be to use the 3D model shape to facilitate lighting correction. As any two-dimensional image pre-processing technique can only adjust colour and intensity levels without taking into account the shadow and shading due to the surface shape of the face, it becomes very difficult to reproduce or compensate for specific lighting conditions. However, by using the 3D face model to generate virtual lighting on the textured surface it becomes possible to normalise lighting across the 3D surface or simulate the same lighting conditions from one face onto another.

The IRAD contours method as described in section 5.7 has only been touched upon in this thesis. Unfortunately, the technique was only conceived towards the end of our research project and we now leave the full potential of this method to be exposed by another researcher. There are two immediate topics that must be addressed. Firstly, to test the effect of constraining correlation of multiple contour signals to have the same

rotational phase. The process described in section 5.7.5 allowed each individual signal to correlate independently, meaning that the highest correlations of two signals may compete with different phase shifts, hence allowing greater flexibility for incorrect matches to achieve a higher correlation score. Secondly, no colour or texture information was extracted for use in the signal correlation stage. Since this information has been shown to be of great benefit when combining 2D and 3D subspaces it is highly likely that similar improvements will be seen for this method.

Further improvements to the IRAD contours method would be expected by performing some statistical analysis on the discriminatory nature of the various facial contours and the relative dependence on such features as curvature, symmetry, texture and facial location. We have already witnessed that weighting contours signals according to the distance from the contour origin has a beneficial effect, but there are likely to be other such dependencies. The systems ability to cope with changes in expression must also be investigated. Whereas with LDA approaches we are able to represent and model within-class variation (including expression to some extent), this is currently not featured in the IRAD contours method. There are numerous possibilities that may contain some potential to overcome these difficulties, such as correlating on partial signals extracted from rigid facial areas whilst ignoring those from malleable regions, or modelling signal variation due to expression by LDA or some other statistical method.

10 Appendices

I - 3D FACE DATABASE STORAGE

Master copies of the database will be held by Cybula Ltd. and made available by secure download (access via username and password) and/or DVD library, agreed with Cybula beforehand. No information revealing the subject identity will be stored with the data. Agreement signatures will be held separately by Cybula Ltd. and not distributed to any other party. No data may be redistributed by anybody other than Cybula Ltd.

Each 3D face model will be stored under a filename using the naming convention shown in Appendix II. For example, a file stored under the name '00021-10-mww24bnncy.obj' is a Wavefront OBJ file containing a 3D model of a 24 year old (24) white (ww) male (m), who does have a beard, but is not wearing glasses or headwear (bnn) and facing forwards with a neutral expression (-10-). Colour texture is available (c) for the model (stored under filename 00021-10-mww24bnncy.bmp) and permission has been given for his image to be published (y). All other files in the database containing "00021-" contain models of the same person. A text file will be stored with the model under filename 00021-10-mww25bnncy.txt, containing the following information.

```
Subject ID  00021
Model ID    10
Capture Conditions      Front facing, neutral expression.
Sex   m
Ethnicity   White
Age   24 years
Subject was wearing:
No Beard
No hat
No glasses
Height:     5'10"
Weight:     75 Kg
More....
Subject has given permission to publish his/her image in
scientific papers and journals
Colour texture is not available
```

II - 3D FACE DB METADATA

Filename	nnnnn-xx-srraaeeetp.ext	
nnnnn	Five digit unique subject identifier.	
Xx	Two digit capture condition identifier as specified in Table 5-1.	
S	Single character indicating gender. m = male, f = female	
Rr	Two character label indicating ethnicity: ww White ap Asian Pakistani ab Asian Bangladeshi ai Asian Indian ac Asian Chinese aj Asian Japanese ao Asian Other na American Indian ng Aboriginal bb Black British	bc Black Caribbean ba Black African bo Black Other hs Hispanic Spanish hm Hispanic Mexican hp Hispanic Puerto Rican hc Hispanic Cuban ho Hispanic Other mm Mixed oo Other / Abstain
Aa	Two digit number indicating age, calculated from the DOB entry.	
eee	Three character label indicating presence of external features: b = beard present, n = not present g = glasses present, n = not present h = headwear present, n = not present	
t	Single character indicating the type of texture available for that model: g = greyscale texture, c = colour texture, n = no texture	
p	Single character flag indicating whether permission for publication has been granted. y = publication permissions granted. n = publication permissions not granted.	
ext	Three character extension, indicating the file type. obj = The 3D Face Mode file. bmp = The 2D bitmap texture file. sp1 = Intermediate 3D reconstruction file. sp2 = Intermediate 3D reconstruction file. txt = The questionnaire information file.	

Table 10-1 File storage convention used for the UOY 3D Face Database.

III - AURA GRAPH MATCHER RESULTS

Proof-of-concept tests were carried out using a small database of facial surfaces, comprising 4 models of one person (A1, A2, A3, A4) and four models of other people (B1, C1, D1, E1) [46][47]. Graph nodes are selected from the vertices of the facial surfaces (no feature detection is attempted). For training, the graphs are fully connected and the edges labelled with the distances between nodes. The AURA graph matcher is then trained to recognise the 8 facial surfaces.

Identification tests are carried out by performing identification operations using four models of one subject from the database (A1, A2, A3, A4), at various levels of quantisation.

Quantisation	Query	Matches (Strength)
0.001	A1	A1(100%), A2(100%)
	A2	A2(100%)
	A3	A3(100%)
	A4	Out of memory
0.01	A1	A1(100%), A2(100%), A3(100%), B1(100%)
	A2	A2(100%)
	A3	Out of memory
	A4	Out of memory
0.05	A1	A1(100%), A2(100%), A3(100%), A4(100%), B1(100%)
	A2	Out of memory
	A3	Out of memory
	A4	Out of memory

Table 10-2 – Results of proof-of-concept identification tests using the AURA graph matcher taken from Turner [47].

We see in many cases that the algorithm halted due to insufficient memory before completing the identification: this is due to instability in the current stage of AURA development. Other results show that the query model matches perfectly with itself in all cases, as would be expected. Three queries also return correct matches with other face models of the same person, while two false matches are also witnessed.

IV – VERIFICATION ERROR RATES OF 2D MULTI-SUBSPACE SYSTEM

Multi-subspace 2D
Date: Fri, 23 Jul 2004 06:50:23
Test Set B

EER	10.4215
Minimum	0.0864
Maximum	1.4969

Threshold	FRR	FAR	Threshold	FRR	FAR	Threshold	FRR	FAR
0.0864	99.9604	0.0000	0.6882	14.7606	4.7280	1.0549	0.5144	78.4101
0.1006	99.8813	0.0000	0.6929	14.4044	5.0285	1.0690	0.3166	81.3830
0.1147	99.6438	0.0000	0.6976	14.0879	5.3372	1.0831	0.2374	84.0583
0.1288	99.4856	0.0000	0.7023	13.8504	5.6748	1.0972	0.0791	86.4844
0.1429	98.9315	0.0000	0.7070	13.6526	6.0071	1.1113	0.0000	88.6950
0.1570	98.0214	0.0000	0.7117	13.3755	6.3446	1.1254	0.0000	90.6443
0.1711	96.8738	0.0000	0.7164	13.0985	6.6994	1.1396	0.0000	92.2887
0.1852	95.2909	0.0000	0.7211	12.7820	7.1073	1.1537	0.0000	93.7388
0.1993	93.5892	0.0000	0.7258	12.3467	7.5223	1.1678	0.0000	94.9382
0.2134	90.8192	0.0000	0.7305	12.1884	7.9452	1.1819	0.0000	95.9797
0.2275	88.2074	0.0000	0.7352	11.7531	8.3872	1.1960	0.0000	96.8277
0.2416	86.0704	0.0000	0.7399	11.3573	8.8594	1.2101	0.0000	97.5144
0.2557	83.6565	0.0000	0.7446	10.8033	9.3366	1.2242	0.0000	98.0716
0.2698	80.8073	0.0000	0.7493	10.7638	9.8380	1.2383	0.0000	98.5241
0.2839	77.5623	0.0000	0.7540	10.4472	10.3642	1.2524	0.0000	98.8766
0.2980	74.5548	0.0007	0.7587	10.2097	10.8952	1.2665	0.0000	99.1621
0.3121	71.9430	0.0007	0.7634	9.9723	11.4386	1.2806	0.0000	99.3814
0.3262	67.8670	0.0015	0.7681	9.6953	12.0213	1.2947	0.0000	99.5330
0.3403	64.7012	0.0022	0.7728	9.3391	12.6552	1.3088	0.0000	99.6568
0.3544	60.7835	0.0041	0.7775	8.9830	13.2701	1.3229	0.0000	99.7519
0.3685	57.7760	0.0086	0.7822	8.5873	13.9197	1.3370	0.0000	99.8264
0.3826	54.6498	0.0120	0.7869	8.4685	14.5780	1.3511	0.0000	99.8814
0.3967	51.6423	0.0210	0.7917	8.2707	15.2774	1.3652	0.0000	99.9165
0.4108	48.9513	0.0318	0.7964	8.0332	15.9922	1.3793	0.0000	99.9446
0.4249	46.8935	0.0445	0.8011	7.8750	16.7433	1.3934	0.0000	99.9663
0.4390	44.5192	0.0610	0.8058	7.7562	17.5022	1.4075	0.0000	99.9794
0.4532	42.3427	0.0846	0.8105	7.4792	18.2978	1.4216	0.0000	99.9873
0.4673	40.0475	0.1141	0.8152	7.3209	19.0983	1.4357	0.0000	99.9940
0.4814	37.6336	0.1564	0.8199	6.8856	19.9481	1.4498	0.0000	99.9963
0.4955	35.8924	0.2002	0.8246	6.4899	20.8373	1.4639	0.0000	99.9981
0.5096	33.5180	0.2679	0.8293	6.2920	21.6920	1.4780	0.0000	99.9993
0.5237	31.6977	0.3604	0.8434	5.2632	24.5066	1.4922	0.0000	99.9996
0.5378	29.2046	0.4659	0.8575	4.8279	27.4574			
0.5519	27.4238	0.5950	0.8716	4.3926	30.6671			
0.5660	25.9596	0.7571	0.8857	4.2343	34.0482			
0.5801	24.4954	0.9794	0.8998	3.9968	37.5712			
0.5942	22.8334	1.2454	0.9139	3.4824	41.2311			
0.6083	21.6462	1.5497	0.9280	3.1262	45.0089			
0.6224	20.3403	1.9183	0.9421	2.8097	48.8496			
0.6365	19.1927	2.3513	0.9562	2.4139	52.8179			
0.6506	18.1243	2.8711	0.9703	1.8599	56.8064			
0.6647	16.8579	3.5020	0.9844	1.5433	60.6741			
0.6694	16.4622	3.7202	0.9985	1.3455	64.5398			
0.6741	16.0269	3.9578	1.0126	1.0289	68.2997			
0.6788	15.5916	4.2097	1.0267	0.7519	71.8746			
0.6835	15.2750	4.4578	1.0408	0.5936	75.2640			

V – VERIFICATION ERROR RATES OF 3D MULTI-SUBSPACE SYSTEM

Multi-subspace 3D
Date: Sun, 11 Jul 2004 07:38:50
Test Set B

EER	8.3869
Minimum	0.1000
Maximum	1.3873

Threshold	FRR	FAR	Threshold	FRR	FAR	Threshold	FRR	FAR
0.1000	99.9604	0.0000	0.6921	20.2216	1.8749	0.9410	2.5326	32.8675
0.1129	99.8417	0.0000	0.7050	18.1243	2.2083	0.9539	2.1765	36.7992
0.1257	99.8417	0.0000	0.7179	16.3435	2.5889	0.9667	2.0578	40.9770
0.1386	99.6834	0.0000	0.7222	15.9478	2.7266	0.9796	1.7808	45.2556
0.1515	99.5251	0.0000	0.7265	15.3542	2.8890	0.9925	1.4246	49.8073
0.1643	99.4460	0.0000	0.7307	15.0376	3.0496	1.0054	1.1080	54.4765
0.1772	99.0107	0.0000	0.7350	14.2857	3.2187	1.0182	0.8706	59.1611
0.1901	98.8128	0.0000	0.7393	13.8900	3.4114	1.0311	0.6727	63.7199
0.2030	98.4567	0.0000	0.7436	13.6526	3.5926	1.0440	0.4749	68.2649
0.2158	97.9818	0.0000	0.7479	13.3360	3.7816	1.0569	0.1583	72.6590
0.2287	97.2695	0.0000	0.7522	12.9402	3.9814	1.0697	0.1583	76.7018
0.2416	96.5968	0.0000	0.7565	12.5841	4.1928	1.0826	0.0791	80.3670
0.2545	95.7657	0.0000	0.7608	12.1092	4.4133	1.0955	0.0791	83.8080
0.2673	94.4994	0.0000	0.7651	11.9114	4.6498	1.1083	0.0791	86.8579
0.2802	92.9165	0.0000	0.7694	11.4365	4.8878	1.1212	0.0396	89.5419
0.2931	91.4127	0.0000	0.7737	11.1595	5.1336	1.1341	0.0000	91.7681
0.3059	90.1860	0.0007	0.7779	10.8429	5.4102	1.1470	0.0000	93.6692
0.3188	88.7218	0.0019	0.7822	10.6055	5.7182	1.1598	0.0000	95.2447
0.3317	86.7036	0.0022	0.7865	10.3680	6.0254	1.1727	0.0000	96.4598
0.3446	84.7250	0.0034	0.7908	9.9327	6.3607	1.1856	0.0000	97.4354
0.3574	82.8651	0.0045	0.7951	9.3787	6.7323	1.1985	0.0000	98.1921
0.3703	80.9260	0.0064	0.7994	8.9434	7.1069	1.2113	0.0000	98.7463
0.3832	78.8287	0.0097	0.8037	8.7455	7.4972	1.2242	0.0000	99.1557
0.3961	76.3356	0.0138	0.8080	8.5873	7.8936	1.2371	0.0000	99.4548
0.4089	73.7238	0.0183	0.8123	8.4685	8.2958	1.2499	0.0000	99.6456
0.4218	71.7056	0.0243	0.8166	8.0728	8.7371	1.2628	0.0000	99.7841
0.4347	69.0146	0.0307	0.8209	7.6771	9.1977	1.2757	0.0000	99.8642
0.4475	66.4424	0.0393	0.8251	7.4397	9.7011	1.2886	0.0000	99.9121
0.4604	63.7911	0.0543	0.8294	7.1626	10.1902	1.3014	0.0000	99.9517
0.4733	61.1397	0.0696	0.8337	6.9252	10.7294	1.3143	0.0000	99.9734
0.4862	58.3696	0.0898	0.8380	6.8065	11.3013	1.3272	0.0000	99.9869
0.4990	56.3910	0.1175	0.8423	6.6482	11.8832	1.3401	0.0000	99.9948
0.5119	52.9482	0.1486	0.8466	6.2525	12.4584	1.3529	0.0000	99.9970
0.5248	50.3759	0.1920	0.8509	5.9755	13.0938	1.3658	0.0000	99.9993
0.5377	47.5267	0.2305	0.8552	5.7776	13.7154	1.3787	0.0000	99.9996
0.5505	44.8753	0.2766	0.8595	5.3819	14.4070			
0.5634	42.5406	0.3271	0.8638	5.0257	15.1180			
0.5763	40.2849	0.3963	0.8681	4.8674	15.7920			
0.5891	37.2774	0.4809	0.8723	4.6300	16.5662			
0.6020	35.3383	0.5752	0.8766	4.5904	17.3622			
0.6149	32.6474	0.6875	0.8809	4.4321	18.1743			
0.6278	30.5501	0.8248	0.8852	4.2738	18.9998			
0.6406	28.3340	0.9711	0.8895	4.1947	19.8856			
0.6535	25.9992	1.1459	0.9024	3.6011	22.6998			
0.6664	23.9019	1.3498	0.9153	3.2054	25.7733			
0.6793	22.1607	1.5979	0.9281	2.7701	29.1788			

VI – VERIFICATION ERROR RATES OF 2D PROJECTION MULTI-SUBSPACE SYSTEM

Multi-subspace 2DP
Date: Wed, 14 Jul 2004 09:14:45
Test Set B

EER	7.3385
Minimum	0.0699
Maximum	1.4772

Threshold	FRR	FAR	Threshold	FRR	FAR	Threshold	FRR	FAR
0.0699	99.9604	0.0000	0.6704	13.4943	2.7120	0.9988	0.4749	61.9468
0.0840	99.8813	0.0000	0.6751	12.9007	2.9115	1.0128	0.2770	65.8964
0.0981	99.6834	0.0000	0.6798	12.7028	3.1207	1.0269	0.2374	69.7124
0.1121	99.4460	0.0000	0.6845	12.3467	3.3355	1.0410	0.1979	73.3124
0.1262	98.7732	0.0000	0.6891	11.9905	3.5499	1.0550	0.0396	76.6962
0.1403	97.8631	0.0000	0.6938	11.5156	3.7797	1.0691	0.0396	79.8475
0.1544	96.9925	0.0000	0.6985	11.0803	4.0259	1.0832	0.0000	82.8361
0.1684	95.7657	0.0000	0.7032	10.6055	4.2935	1.0973	0.0000	85.4965
0.1825	94.3807	0.0000	0.7079	10.2097	4.5757	1.1113	0.0000	87.9207
0.1966	93.0748	0.0000	0.7126	9.7349	4.8986	1.1254	0.0000	90.0718
0.2106	91.2545	0.0000	0.7173	9.2996	5.2085	1.1395	0.0000	91.9676
0.2247	89.3945	0.0000	0.7220	9.1017	5.5303	1.1536	0.0000	93.5921
0.2388	87.3763	0.0000	0.7267	8.9038	5.8798	1.1676	0.0000	94.9569
0.2529	85.6351	0.0000	0.7314	8.4685	6.2425	1.1817	0.0000	96.0762
0.2669	83.2608	0.0000	0.7361	8.1124	6.6238	1.1958	0.0000	97.0335
0.2810	81.0447	0.0000	0.7407	7.6375	7.0197	1.2099	0.0000	97.7573
0.2951	78.2746	0.0000	0.7454	7.2418	7.4415	1.2239	0.0000	98.3336
0.3092	76.0190	0.0000	0.7501	6.7273	7.8906	1.2380	0.0000	98.7725
0.3232	73.3676	0.0007	0.7548	6.4108	8.3490	1.2521	0.0000	99.1228
0.3373	70.8746	0.0007	0.7595	6.1733	8.8366	1.2661	0.0000	99.3807
0.3514	67.9858	0.0015	0.7642	6.0546	9.3441	1.2802	0.0000	99.5622
0.3655	64.7804	0.0019	0.7689	5.7380	9.8444	1.2943	0.0000	99.7002
0.3795	61.8916	0.0037	0.7736	5.4610	10.3874	1.3084	0.0000	99.8020
0.3936	59.0028	0.0075	0.7783	5.2632	10.9581	1.3224	0.0000	99.8668
0.4077	55.7974	0.0116	0.7830	4.9466	11.5460	1.3365	0.0000	99.9184
0.4217	52.7899	0.0165	0.7877	4.8674	12.1717	1.3506	0.0000	99.9476
0.4358	50.2176	0.0187	0.7923	4.4321	12.7675	1.3647	0.0000	99.9719
0.4499	47.7246	0.0288	0.7970	4.3926	13.4272	1.3787	0.0000	99.9828
0.4640	45.2711	0.0460	0.8017	4.3134	14.1072	1.3928	0.0000	99.9891
0.4780	43.0550	0.0726	0.8064	4.1551	14.8246	1.4069	0.0000	99.9944
0.4921	40.1662	0.1010	0.8111	3.8781	15.5760	1.4210	0.0000	99.9970
0.5062	36.8817	0.1415	0.8158	3.7990	16.3503	1.4350	0.0000	99.9989
0.5203	34.1907	0.1946	0.8205	3.6407	17.1340	1.4491	0.0000	99.9996
0.5343	31.2624	0.2578	0.8252	3.5615	17.9576	1.4632	0.0000	99.9996
0.5484	28.0966	0.3484	0.8299	3.4824	18.8191			
0.5625	25.8805	0.4554	0.8439	2.9284	21.5087			
0.5766	23.8227	0.5842	0.8580	2.4139	24.4089			
0.5906	22.1607	0.7481	0.8721	2.0973	27.5105			
0.6047	20.4195	0.9644	0.8862	1.8203	30.8493			
0.6188	19.0344	1.2260	0.9002	1.5829	34.4307			
0.6328	16.9767	1.5373	0.9143	1.4642	38.1408			
0.6469	15.4333	1.8940	0.9284	1.2268	41.9612			
0.6516	14.9189	2.0257	0.9425	0.8310	45.9026			
0.6563	14.4440	2.1780	0.9565	0.7519	49.9132			
0.6610	14.0879	2.3479	0.9706	0.6332	53.8998			
0.6657	13.9296	2.5230	0.9847	0.4749	57.9751			

VII – VERIFICATION ERROR RATES OF 3D AND 2D PROJECTION MULTI-SUBSPACE SYSTEM

Multi-subspace 3D+2DP
Date: Thu, 19 Aug 2004 18:11:39
Test Set B

EER	5.0458
Minimum	0.0983
Maximum	1.3708

Threshold	FRR	FAR	Threshold	FRR	FAR	Threshold	FRR	FAR
0.0983	99.9604	0.0000	0.6667	14.2066	0.8731	0.8618	1.4642	16.4285
0.1110	99.9604	0.0000	0.6709	13.6526	0.9341	0.8661	1.3850	17.3046
0.1237	99.9209	0.0000	0.6752	12.9798	1.0123	0.8788	1.2268	20.1031
0.1365	99.8813	0.0000	0.6794	12.7028	1.0912	0.8915	1.0289	23.2447
0.1492	99.7230	0.0000	0.6837	12.3467	1.1878	0.9042	0.9102	26.7269
0.1619	99.3668	0.0000	0.6879	12.0301	1.2716	0.9170	0.6332	30.5054
0.1746	99.2085	0.0000	0.6922	11.5948	1.3633	0.9297	0.4749	34.6103
0.1874	98.8128	0.0000	0.6964	11.1199	1.4629	0.9424	0.3562	38.9285
0.2001	98.1401	0.0000	0.7006	10.7638	1.5695	0.9551	0.2374	43.4851
0.2128	97.5465	0.0000	0.7049	10.3285	1.6829	0.9679	0.1979	48.2741
0.2256	96.6363	0.0000	0.7091	9.8932	1.8079	0.9806	0.1583	53.0705
0.2383	95.5679	0.0000	0.7134	9.5370	1.9404	0.9933	0.1187	57.9763
0.2510	94.3807	0.0000	0.7176	9.2996	2.0878	1.0060	0.0396	62.8326
0.2637	93.3518	0.0000	0.7218	8.9434	2.2469	1.0188	0.0000	67.4947
0.2765	91.6502	0.0000	0.7261	8.5873	2.4059	1.0315	0.0000	72.0180
0.2892	89.7903	0.0000	0.7303	8.0332	2.5799	1.0442	0.0000	76.2344
0.3019	87.9699	0.0000	0.7346	7.6771	2.7539	1.0569	0.0000	80.1503
0.3146	86.2683	0.0000	0.7388	7.4792	2.9519	1.0697	0.0000	83.6968
0.3274	84.0127	0.0000	0.7431	7.3209	3.1547	1.0824	0.0000	86.8856
0.3401	81.8362	0.0000	0.7473	6.8856	3.3643	1.0951	0.0000	89.6126
0.3528	79.8180	0.0000	0.7515	6.5295	3.5881	1.1079	0.0000	91.9946
0.3655	77.7998	0.0000	0.7558	6.1733	3.8433	1.1206	0.0000	93.8836
0.3783	75.0693	0.0004	0.7600	5.9755	4.0903	1.1333	0.0000	95.4778
0.3910	72.4179	0.0007	0.7643	5.6985	4.3691	1.1460	0.0000	96.6986
0.4037	69.2125	0.0015	0.7685	5.4214	4.6696	1.1588	0.0000	97.6491
0.4164	66.1258	0.0015	0.7727	5.1049	4.9521	1.1715	0.0000	98.3403
0.4292	63.0392	0.0034	0.7770	4.9070	5.2661	1.1842	0.0000	98.8638
0.4419	60.1108	0.0041	0.7812	4.7487	5.5999	1.1969	0.0000	99.2471
0.4546	56.8658	0.0060	0.7855	4.5509	5.9584	1.2097	0.0000	99.5068
0.4673	53.7396	0.0101	0.7897	4.0760	6.3188	1.2224	0.0000	99.6913
0.4801	50.9300	0.0135	0.7940	3.7594	6.7050	1.2351	0.0000	99.8144
0.4928	47.5267	0.0172	0.7982	3.5615	7.1073	1.2478	0.0000	99.8926
0.5055	44.4796	0.0236	0.8024	3.3241	7.5369	1.2606	0.0000	99.9409
0.5182	41.6304	0.0329	0.8067	3.0471	7.9871	1.2733	0.0000	99.9704
0.5310	39.2956	0.0460	0.8109	2.8097	8.4699	1.2860	0.0000	99.9824
0.5437	36.2485	0.0632	0.8152	2.7305	8.9687	1.2987	0.0000	99.9903
0.5564	33.3993	0.0861	0.8194	2.6118	9.5136	1.3115	0.0000	99.9951
0.5691	30.9854	0.1216	0.8236	2.2952	10.0491	1.3242	0.0000	99.9981
0.5819	28.6506	0.1613	0.8279	2.1765	10.6464	1.3369	0.0000	99.9993
0.5946	26.3949	0.2043	0.8321	2.0973	11.2608	1.3496	0.0000	99.9996
0.6073	23.4666	0.2706	0.8364	1.8599	11.9127	1.3624	0.0000	99.9996
0.6200	21.2901	0.3574	0.8406	1.7412	12.6069			
0.6328	19.0740	0.4607	0.8449	1.7016	13.3356			
0.6455	16.6996	0.5958	0.8491	1.6620	14.0788			
0.6582	15.2355	0.7522	0.8533	1.5829	14.8216			
0.6625	14.8002	0.8121	0.8576	1.5433	15.5888			

VIII – VERIFICATION ERROR RATES OF 3D, 2D AND 2D PROJECTION MULTI-SUBSPACE SYSTEM

Multi-subspace 3D+2D+2DP
Date: Fri, 23 Jul 2004 06:02:37
Test Set B

EER	4.5539
Minimum	0.1174
Maximum	1.3713

Threshold	FRR	FAR	Threshold	FRR	FAR	Threshold	FRR	FAR
0.1174	99.9604	0.0000	0.6608	13.3755	0.6197	0.8530	1.3455	15.3298
0.1299	99.9604	0.0000	0.6649	13.0590	0.6676	0.8572	1.1476	16.1651
0.1424	99.9604	0.0000	0.6691	12.6237	0.7309	0.8698	0.9497	18.9141
0.1550	99.8021	0.0000	0.6733	12.1884	0.8050	0.8823	0.8310	22.0797
0.1675	99.6438	0.0000	0.6775	11.5948	0.8723	0.8948	0.7123	25.5866
0.1801	99.4064	0.0000	0.6817	11.2782	0.9550	0.9074	0.5936	29.4759
0.1926	99.0107	0.0000	0.6858	10.7638	1.0359	0.9199	0.5144	33.6022
0.2051	98.3775	0.0000	0.6900	10.4076	1.1186	0.9325	0.3562	37.9907
0.2177	98.0609	0.0000	0.6942	10.1702	1.2009	0.9450	0.2374	42.7729
0.2302	96.9133	0.0000	0.6984	9.6953	1.2978	0.9575	0.1583	47.6319
0.2428	95.5679	0.0000	0.7026	9.3391	1.3985	0.9701	0.0791	52.6563
0.2553	94.2620	0.0000	0.7067	9.0621	1.5029	0.9826	0.0791	57.7989
0.2678	92.9165	0.0000	0.7109	8.7455	1.6197	0.9952	0.0396	62.9168
0.2804	91.2940	0.0000	0.7151	8.4685	1.7428	1.0077	0.0000	67.8139
0.2929	89.2758	0.0000	0.7193	8.0728	1.8745	1.0202	0.0000	72.4925
0.3055	87.4555	0.0000	0.7235	7.8750	2.0219	1.0328	0.0000	76.8653
0.3180	85.3186	0.0000	0.7276	7.5188	2.1859	1.0453	0.0000	80.9017
0.3305	82.0736	0.0000	0.7318	7.1626	2.3617	1.0579	0.0000	84.5018
0.3431	79.3431	0.0000	0.7360	6.8461	2.5328	1.0704	0.0000	87.6307
0.3556	76.5334	0.0000	0.7402	6.4503	2.7128	1.0829	0.0000	90.3461
0.3682	72.6553	0.0000	0.7444	5.9755	2.9081	1.0955	0.0000	92.5937
0.3807	69.8852	0.0000	0.7485	5.7380	3.1323	1.1080	0.0000	94.4207
0.3932	67.6296	0.0004	0.7527	5.3819	3.3707	1.1206	0.0000	95.8629
0.4058	64.2659	0.0004	0.7569	5.1840	3.6027	1.1331	0.0000	96.9938
0.4183	61.0210	0.0004	0.7611	4.9861	3.8508	1.1456	0.0000	97.8680
0.4309	57.6573	0.0019	0.7653	4.7883	4.1270	1.1582	0.0000	98.5229
0.4434	54.5706	0.0034	0.7694	4.6300	4.4069	1.1707	0.0000	98.9660
0.4559	51.1674	0.0041	0.7736	4.4717	4.7126	1.1832	0.0000	99.2908
0.4685	48.8326	0.0056	0.7778	4.2738	5.0610	1.1958	0.0000	99.5101
0.4810	45.2711	0.0071	0.7820	4.1156	5.4124	1.2083	0.0000	99.6770
0.4936	42.6989	0.0090	0.7862	4.0364	5.8106	1.2209	0.0000	99.7863
0.5061	39.1373	0.0112	0.7903	3.8385	6.1905	1.2334	0.0000	99.8642
0.5186	36.4068	0.0191	0.7945	3.6407	6.6122	1.2459	0.0000	99.9143
0.5312	34.1907	0.0262	0.7987	3.5220	7.0403	1.2585	0.0000	99.9439
0.5437	31.6977	0.0348	0.8029	3.2450	7.5152	1.2710	0.0000	99.9630
0.5563	29.2046	0.0516	0.8071	3.0471	8.0298	1.2836	0.0000	99.9783
0.5688	26.3949	0.0737	0.8112	2.7701	8.5312	1.2961	0.0000	99.9899
0.5813	24.7329	0.1014	0.8154	2.5722	9.0600	1.3086	0.0000	99.9944
0.5939	22.4377	0.1411	0.8196	2.3744	9.6307	1.3212	0.0000	99.9978
0.6064	20.6965	0.1938	0.8238	2.2556	10.2119	1.3337	0.0000	99.9993
0.6190	18.8366	0.2526	0.8280	2.0182	10.8264	1.3463	0.0000	99.9996
0.6315	17.1745	0.3417	0.8321	1.9391	11.4659	1.3588	0.0000	99.9996

11 Definitions

AURA	Advanced Uncertain Reasoning Architecture
EER	Equal Error Rate
FAR	False Acceptance Rate
FRR	False Rejection Rate
FMTD	Fast Marching on Triangulated Domains (FMTD)
FLD	Fisher's linear discriminant
FRVT	Face Recognition Vendor Tests
IRAD Contour	Isoradius contour
LDA	Linear Discriminant Analysis
PCA	Principal Component Analysis
SOM	Self Organising Map
ICA	Independent Component Analysis
CME	Cumulative Match Error
CMR	Cumulative Match Rate

12 References

[1] Phillips, P., Grother, P., Micheals, R., Blackburn, D., Tabassi, E., Bone, J. "FRVT 2002 Overview and Summary." www.frvt.org/FRVT2002, March, 2003.

[2] "The Face Recognition Grand Challenge." http//frvt.org/FRGC/

[3] C. Beumier, M. Acheroy, "Automatic 3D Face Authentication" Image and Vision Computing, vol. 18, no. 4, pp. 315-321, 2000.

[4] G. Gordon, "Face Recognition Based on Depth and Curvature Features." Proc. of the IEEE Computer Society Conference on Computer Vision and Pattern Recognition, pp. 108-110, 1992.

[5] Beumier, C., Acheroy, M. "Automatic Face Verification from 3D And Grey Level Clues." In Proc. Of the 11th Portuguese Conference on Pattern Recognition, pp. 95-101, 2000.

[6] C. Hesher, A. Srivastava, and G. Erlebacher, "A novel technique for face recognition using range imaging," in Proc. IEEE Int. Symposium on Signal Processing and Its Applications, pp. 201–204, July 2003.

[7] R. Cutler. "Face Recognition Using Infrared Images and Eigenfaces." Technical Report. UMI Order Number: CSC 989, University of Maryland at College Park, USA 1996.

[8] C. Chua, F. Han, T. Ho, "3D Human Face Recognition Using Point Signature" Proc. 4th IEEE Int. Conf. on Automatic Face and Gesture Recognition, pp. 233-238, 2000.

[9] W. Zhao, R. Chellappa, "3D Model Enhanced Face Recognition" Proc. Int. Conf. on Image Processing, Vol. 3, pp. 50-53, 2000.

[10] S. Romdhani, V. Blanz, T. Vetter, "Face Identification by Fitting a 3D Morphable Model using Linear Shape and Texture Error Functions" The European Conf. on Computer Vision, LNCS 2353, pp. 3-19, 2002.

[11] Blanz, V., Romdhani, S., Vetter, T. "Face Identification across Different Poses and Illuminations with a 3D Morphable Model." In Proc. of the 5th IEEE Conference on Automatic Face and Gender Recognition, pp. 202-207, 2002.

[12] P. Hancock, V. Bruce, A. M. Burton. "Testing Principal Component Representations for Faces." 4th Neural Computation and Psychology Workshop, London, England, Springer pp. 84-97, 1998.

[13] P. Hancock, A. M Burton, V. Bruce. "Preprocessing Images of Faces Correlations with Human Perceptions of Distinctiveness and Familiarity." Proceedings of IEE Fifth International Conference on Image Processing, pp. 727-731.

[14] T. Heseltine, N. Pears, J. Austin, "Evaluation of image pre-processing techniques for eigenface-based face recognition" Proc. 2nd Int. Conf. on Image and Graphics, SPIE vol. 4875 pp. 677-685, 2002.

[15] T. Heseltine, N. Pears, J. Austin, "Face Recognition A Comparison of Appearance-based Approaches" Proc. 7th Int. Conf. on Digital Image Computing Techniques and Applications, vol. 1 pp. 59-69, 2003.

[16] Heseltine, T., Pears, N., Austin, J. "Three-Dimensional Face Recognition An Eigensurface Approach." In Proc. of the International Conference on Image Processing, pp. 1421-1424, 2004.

[17] Heseltine, T., Pears, N., Austin, J. "Three-Dimensional Face Recognition A Fishersurface Approach." In Proc. of the International Conference on Image Analysis and Recognition, pp. 684-691, 2004.

[18] W. W. Bledsoe, "The model method in facial recognition," Panoramic Research Inc., Technical Report PRI15, Palo Alto, CA, 1964.

[19] T. Kanade, "*Computer Recognition of Human Faces.*" Basel and Stuttgart Birkhauser, 1977.

[20] W. Zhao, R. Chellappa, A. Rosenfeld, P.J. Phillips, "Face Recognition A Literature Survey." ACM Computing Surveys, pp. 399-458, 2003.

[21] T. Heseltine, N. Pears, J. Austin "Three-Dimensional Face Recognition Using Surface Space Combinations." The British Machine Vision Conference, Vol 2. pp. 1527-536, 2004.

[22] G. Guo, S.Z. Li, K. Chan, "Face Recognition by Support Vector Machines." Proc. of the IEEE International Conference on Automatic Face and Gesture Recognition, pp. 196-201, 2000.

[23] K. Jonsson, J. Matas, J. Kittler, Y.P. Li, "Learning Support Vectors for Face Verification and Recognition." Proc. of the IEEE International Conference on Automatic Face and Gesture Recognition, Grenoble, France, pp. 208-213, 2000

[24] B. Moghaddam, T. Jebara, A. Pentland, "Bayesian Face Recognition." Pattern Recognition, Vol. 33, Issue 11, pp. 1771-1782, November 2000.

[25] C. Liu, H. Wechsler, "A Unified Bayesian Framework for Face Recognition." Proc. of the 1998 IEEE International Conference on Image Processing, Chicago, Illinois, USA, pp. 151-155, October 1998.

[26] Y. Adini, Y. Moses, S. Ullman, "Face Recognition the Problem of Compensating for Changes in Illumination Direction." IEEE Trans. on Pattern Analysis and Machine Intelligence, Vol. 19 No. 7, pp. 721-732, 1997.

[27] P. Belhumeur, J. Hespanha, D. Kriegman. "Eigenfaces vs. Fisherfaces Recognition Using Class Specific Linear Projection." IEEE Transactions on Pattern Analysis and Machine Intelligence, PAMI19 (7), pp. 711-720, 1997.

[28] P. Belhumeur, J. Hespanha, D. Kriegman, "Eigenfaces vs. Fisherfaces Face Recognition using class specific linear projection." Proc. of the European Conference on Computer Vision, pp. 45-58, 1996.

[29] Brunelli, R., Poggio, T. "Face Recognition Features versus Templates." IEEE Transactions on Pattern Analysis and Machine Intelligence 15, pp. 1042-1052, 1993.

[30] R. Brunelli, T. Poggio. "Face Recognition through Geometrical Features." Proceedings ECCV92, pp. 792-800, 1992

[31] Chin-Seng Chua and Ray Jarvis. "Point signatures A new representation for 3d object recognition." Int. Journal of Computer Vision, 25(1), pp. 63-85, 1997.

[32] A. M. Coombes, R. Richards, A. Linney, V. Bruce, R. Fright. "Description and recognition of faces from 3D data." Proceedings-of-the-SPIE --The-International-Society-for-Optical-Engineering. Vol. 1766, pp. 307-319, 1992.

[33] G. Finlayson, G. Schaefer, "Hue that is Invariant to Brightness and Gamma." In Proc. of the British Machine Vision Conference, pp. 303–312. 2001.

[34] G. Finlayson, B. Schiele, J. L. Crowley, "Comprehensive Colour Image Normalisation." Proc. of the European Conference on Computer Vision, LNCS 1406. Springer, pp. 475-490, 1998.

[35] Heseltine, T., Pears, N., Austin, J. "Combining multiple face recognition systems using Fisher's linear discriminant." In Proc. of the SPIE Defense and Security Symposium, Biometric Technology for Human Identification, Vol. 5404. pp. 470-481, 2004.

[36] S. Lawrence, C. L. Giles, A. C. Tsoi, A. D. Back. "Face Recognition A Convolutional Neural Network Approach." IEEE Trans. on Neural Networks, vol. 8, pp. 98--113, 1997.

[37] Laurenz Wiskott, Jean-Marc Fellous, Norbert Kruger, Christoph von der Malsburg. "Face Recognition by Elastic Bunch Graph Matching." Proc. 7th Intern. Conf. on Computer Analysis of Images and Patterns, pp. 456-463, 1997.

[38] Marcialis, G., Roli, F. "Fusion of LDA and PCA for Face Recognition." in Biometric Authentication, Vol. LNCS 2359, pp. 30-37, Jun. 2002.

[39] Martinez, A., Benavente, R. "The AR Face Database." Computer Vision Centre Technical Report #24, 1998.

[40] A. Pentland, B. Moghaddom, T. Starner, "View-Based and Modular Eigenfaces for Face Recognition." Proc. of IEEE Conf. on Computer Vision and Pattern Recognition, pp. 84-91, 1994.

[41] S. Rizvi, P. J. Phillips and H. Moon, "The FERET Verification Testing Protocol for Face Recognition Algorithms" In Proc. of International Conference on Automatic Face and Gesture Recognition, pp. 48-53, 1998.

[42] P. J. Phillips, H. Moon, P. J. Rauss, and S. Rizvi, "The FERET evaluation methodology for face recognition algorithms In Proc. of IEEE Computer Vision and Pattern Recognition, pp. 137-143, June 1997.

[43] P. J. Phillips, P. J. Rauss, and S. Z. Der, "FERET (Face Recognition Technology) Recognition Algorithm Development and Test Results" Army Research Lab technical report 995, 1996.

[44] P. J. Phillips, H. Wechsler, J. Huang, P. Rauss, "The FERET database and evaluation procedure for face recognition algorithms" Image and Vision Computing J, Vol. 16, No. 5, pp 295-306, 1998.

[45] H. Rowley, S. Baluja, T. Kanade. "Neural Network-Based Face Detection." In IEEE Pattern Analysis and Machine Intelligence, Vol. 20, pp. 22-38, 1998.

[46] A. Turner, J. Austin. "AURA Graph Matcher Applied To Faces". www.cs.york.ac.uk/arch/NeuralNetworks/AURA/aura.html, University of York, 2001.

[47] A. Turner. "AURA Graph Matcher: 2nd Investigation into Face Recognition", www.cs.york.ac.uk/arch/NeuralNetworks/AURA/aura.html, University of York, 2001.

[48] Turk, M., Pentland, A. "Eignefaces for Recognition." Journal of Cognitive Neuroscience, Vol. 3, pp. 72-86, 1991.

[49] M. Turk, A. Pentland. "Face Recognition Using Eignefaces." In Proc. IEEE Conf. on Computer Vision and Pattern Recognition, pp. 586-591, 1991.

[50] "The UOY 3D Face Database." The University of York. www.cs.york.ac.uk/~tomh

[51] Ho Y Wang Y, Chua C and Ren Y. "Integrated 2d and 3d images for face recognition." In 11th Int. Conf. on Image Analysis and Processing, pages 48-53, 2001.

[52] W.Y. Zhao, R. Chellappa, "Image-based Face Recognition Issues and Methods." Image Recognition and Classification , Ed. B. Javidi, M. Dekker, pp. 375-402, 2002.

[53] P. Navarrete, J. Ruiz-Del-Solar, "Analysis and Comparison of Eigenspace-Based Face Recognition Approaches." International Journal of Pattern Recognition and Artifficial Intelligence, Vol. 16, No. 7, pp. 817-830, 2002.

[54] W.S. Yambor, "Analysis of PCA-based and Fisher Discriminant-Based Image Recognition Algorithms." M.S. Thesis, Technical Report CS-00-103, Computer Science Department, Colorado State University, July 2000.

[55] A.M. Martinez, A.C. Kak, "PCA versus LDA." IEEE Trans. on Pattern Analysis and Machine Intelligence, Vol. 23, No. 2, pp. 228-233, 2001.

[56] J. Huang, B. Heisele, V. Blanz, "Component-based Face Recognition with 3D Morphable Models." Proc. of the 4th International Conference on Audio- and Video-Based Biometric Person Authentication, pp. 27-34, 2003.

[57] V. Blanz and T. Vetter. A morphable model for synthesis of 3D faces. In Computer Graphics Proceedings SIGGRAPH, pp. 187-194, Los Angeles, 1999.

[58] B. Heisele, P. Ho, and T. Poggio. "Face recognition with support vector machinesglobal versus component-based approach." In Proc. 8th International Conference on Computer Vision, volume 2, pp. 688-694, Vancouver, 2001.

[59] A. Bronstein, M. Bronstein, R. Kimmel, and A. Spira. "3D face recognition without facial surface reconstruction." In Proc. of European Conference on Computer Vision, CIS-2003-05, www.cs.technion.ac.il/tech-reports/ 2004.

[60] M.S. Bartlett, J.R. Movellan, T.J. Sejnowski, "Face Recognition by Independent Component Analysis." IEEE Trans. on Neural Networks, Vol. 13, No. 6, pp. 1450-1464, November 2002.

[61] A. Bronstein, M. Bronstein, and R. Kimmel, "Expression-invariant 3D face recognition." Proc. Audio & Video-based Biometric Person Authentication (AVBPA), Lecture Notes in Comp. Science 2688, Springer, pp. 62-69, 2003.

[62] "The Advanced Uncertain Reasoning Architecture." The University of York, www.cs.york.ac.uk/arch/neural/research/aura.

[63] "The Wavefront OBJ File Format for 3D Graphics and Objects Visualisation" www.fileformat.info/format/wavefrontobj.

[64] "The Psychological Image Collection at Stirling." The University of Stirling Psychology Department, http//pics.psych.stir.ac.uk.

[65] "The UMIST Face Database." The University of Manchester Institute of Science and Technology, http//images.ee.umist.ac.uk/danny/database.html.

[66] "The Extended Multi Modal Verification for Teleservices and Security Database (XM2VTSDB)." The University of Surrey, http//www.ee.surrey.ac.uk/Research/VSSP/xm2vtsdb.

[67] "The Yale Face Database." The Centre for Computational Vision and Control, Yale University, http//cvc.yale.edu/projects/yalefaces/yalefaces.html.

[68] F. Stein and G. Medioni, "Structural Indexing Efficient 3-D Object Recognition," IEEE Trans. Pattern Analysis and Machine Intelligence, vol. 14, no. 2, pp. 125-145, February 1992.

[69] A.M. Burton, V. Bruce, P.J.B. Hancock, "From Pixels to People A Model of Familiar Face Recognition." Cognitive Science, Vol. 23, No. 1, pp. 1-31, 1999.

[70] A.M. Burton, S. Wilson, M. Cowan, V. Bruce, "Face recognition in poor-quality video Evidence From Security Surveillance." Psychological Science, Vol. 10, No. 3, pp. 243-248, May 1999.

[71] G. Shakhnarovich, B. Moghaddam, "Face Recognition in Subspaces." Handbook of Face Recognition, Eds. Stan Z. Li and Anil K. Jain, Springer-Verlag, December 2004.

[72] T.F. Cootes, K. Walker, C.J. Taylor, "View-Based Active Appearance Models." Proc. of the IEEE International Conference on Automatic Face and Gesture Recognition, Grenoble, France, pp. 227-23, March 2000.

[73] K. Chang, K. Bowyer, P. Flynn. "Face Recognition Using 2D and 3D Facial Data." In ACM Workshop on Multimodal User Authentication, pp. 25-32, Santa Barbara, California, 2003.

[74] Arun, K.S., Huang, T.S., Blostein, S.D., Least-squares fitting of two 3D point sets. IEEE Pattern Analysis and Machine Intelligence, 9 (5), pp. 698-700, 1987.

[75] Zhang, Z., Iterative point matching for registration of free-form curves and surfaces. International Journal of Computer Vision, 13 (2), pp. 119-152, 1994.

[76] Williams, J.A., Bennamoun, M., Latham, S., Multiple view 3D registration: A review and a new technique. IEEE Int. Conf. on Systems, Man, and Cybernetics, Tokyo, pp. 497-502, 1999.

[77] Godin, G., Rioux, M., Baribeau, R., Three-dimensional registration using range and intensity information. SPIE vol.2350, Videometrics III, pp. 279-290, 1994.

[78] Chua, C., and Jarvis, R., 3D free form surface registration and object recognition. International Journal of Computer Vision, 17 (1), pp. 77-99, 1996.

[79] A. D. J. Cross & E. R. Hancock. Convergence of a hill climbing genetic algorithm for graph matching. In Lecture Notes in Computer Science 1654. pp. 220–236. E. R. Hancock, M. Pelillo (Eds.), York, UK, 1999.

[80] E. R. Hancock & J. Kittler. Edge-labeling using dictionary-based relaxation. IEEE Transactions on Pattern Analysis and Machine Intelligence 12(2), pp. 165–181, 1990.

[81] Barrow, H. G., Burstall, R. M., Subgraph Isomorphism, Matching Relational Structures and Maximal Cliques, University of Edinburgh. Department of Artificial Intelligence, Working Paper 4(4): pp 83-84, Nov 1974.